2025

The neural control of gait switching in larval zebrafish

Elena Maria Daniela Collins

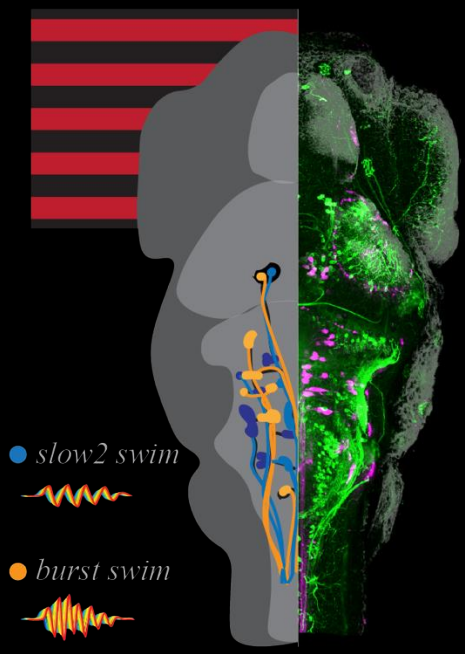

Dissertation presented to obtain the **Ph.D degree in Neuroscience**

International Neuroscience Doctoral Program

Oeiras, February 2025

INSTITUTO DE TECNOLOGIA QUÍMICA E BIOLÓGICA ANTÓNIO XAVIER | UNIVERSIDADE NOVA DE LISBOA

The neural control of gait switching in larval zebrafish

Elena Maria Daniela Collins

Dissertation presented to obtain the
Ph.D. degree in Neuroscience

Instituto de Tecnologia Quimica e Biologica | Universidade Nova de Lisboa

Research work coordinated by:

Champalimaud Foundation

FCT
Fundação para a Ciência e a Tecnologia
MINISTÉRIO DA CIÊNCIA, TECNOLOGIA E ENSINO SUPERIOR

Oeiras,
February 2025

The neural control of gait switching in larval zebrafish.

Elena Maria Daniela Collins

A Dissertation presented to obtain the Doutoramento (Ph.D.) degree in Neuroscience at the Instituto de Tecnologia Química e Biológica da Universidade Nova de Lisboa

Supervised by Dr Michael B. Orger

Oeiras, February 2025

"We have a brain for one reason and one reason only — and that's to produce adaptable and complex movements."

— Daniel Wolpert [1]

Acknowledgments

First and foremost, I would like to thank my supervisor Mike for inviting me into your lab and guiding me through this project throughout the years. Things were not always (or rarely...) as "easy" as you made them sound, but your sheer enthusiasm for all things fish brains and unwavering optimism despite technical challenges provided a much needed light at the end of the tunnel. Towards the end of my PhD journey, Aaron stepped up as a sort of day-to-day mentor. Always offering a helping hand, lending an ear or a gentle push when needed - Aaron is the glue that holds this lab together. I am immensely grateful for the support you have given me in these last 2 years! I would also like to thank my lab mates for their companionship, help and insightful discussions throughout these years - THANK YOU ALL!

A big thank you to the Fish Platform for setting up countless crosses, my work would not have been possible without your continuous support. Thanks also to the ABBE microscopy platform for your help with confocal imaging and creativity for the juvenile brain mounting. Thank you to Raquel from the Molecular Tools platform for cloning and assisting with transgenic line development. Thank you to the graduate office, in particular Simone and Teresa from the early days, for helping me find my feet in Lisbon, and navigate bureaucratic matters.

A huge thank you to the CCU community for being so vibrant, enthusiastic, curious and fun. From the retreats to happy hours to cafeteria chats, it's been a pleasure. To my INDP class of 2017/18 thanks for being such a friendly, curious and supportive bunch. We've done it all, from the early days in the class room to the self-help group with all things thesis submission. A shout-out also to the Green Team; Inês, Anna and Catarina, for your perseverance, creativity and friendship trying to make CCU a greener place. Caroline, Laura, Oihane, Joana and Francesca - founding the Women and Allies group with you has been a privilege. Your like-mindedness, thoughtfulness and positivity were so comforting.

Now comes the hard part. Danke to my wonderful parents Joe and Heidi, thank you for your continuous support and generosity. As per tradition your visits

provided a much needed respite from the lab and the city, exploring Portugal together has been a joy. You have instilled a strong work ethic in me from a young age and that has come in really handy. I also really enjoyed our daily chats on the way home from the lab. Always willing to listen to how my day went, thank you so much for your time and unconditional love. Ich hab euch lieb!

To my wonderful husband Sam. My rock, personal cheerleader, best friend. You've been there every step of the way, from joining me on this crazy adventure to Portugal, becoming cat parents, duping ourselves into believing we speak Portuguese, learning all things coeliac, to practising my presentations with me, keeping your fingers crossed for code compiling and cheering me on when my fish were behaving. Thank you for holding the fort down when I came home from the lab late, again... (sorry). You are amazing and I can't wait to see what the future holds for us!

Thank you to my friends in Lisbon and abroad for all the wonderful times together and reminding me of the sunshine in life.

Last but not least thank you and big cuddles to my cats Jura and Islay for being so cute and supportive.

Abstract

Animals need to perform a diverse range of behaviours to navigate their environment successfully. A central question in neuroethology has long been whether different behaviours are controlled by distinct or overlapping supraspinal circuits. To address this, I investigated the mechanism of transition between different movements in larval zebrafish, particularly in the context of forward swimming, on both a behavioural and neural level.

To characterise gait-switching behaviour, larval zebrafish were presented with gratings moving from tail to head at different speeds eliciting forward swimming, known as the optomotor response. Collecting various kinematic parameters, through tracking fish position and tail angle, allowed swims to be classified into different categories of movement. In response to slow gratings, larval zebrafish predominantly exhibited slow swims, whereas fast gratings elicited a rapid transition from slow to sustained trains of fast swims.

To identify the neural correlates of slow and fast swims, I first characterised 7 transgenic lines with genetically labelled neural populations in the brainstem. By retrogradely labelling reticulospinal neurons in each line I was able to demonstrate transgenic access to different subpopulations within the reticulospinal system. Next, I recorded calcium activity in the brainstem of head-fixed larval zebrafish while they performed the optomotor response in a closed-loop configuration, utilising a light-sheet microscope. Head-fixed fish showed differences in bout kinematics from freely swimming fish, with longer movements that included switches in frequency within a single bout. I therefore used convolutional sparse coding to decompose bouts into slow, fast, turn and struggle movement motifs to identify neuronal populations associated with different modes of swimming. This revealed a recruitment of reticulospinal cells in the nMLF, RoL, MiV2, MiDs and CaD/CaV cells during forward swimming, with a marked increase in excitation from slow to fast swims. Turning was associated with ventromedial cells, while almost the entire reticulospinal population was recruited during struggles. My findings demonstrate how the brain selects dynamically between two distinct motor outputs, providing insight into fundamental principles in the supra-spinal control of locomotion.

Titulo e Resumo

O controlo neural da transição entre modos de locomoção da larva de peixe-zebra.

Os animais precisam de realizar uma ampla gama de comportamentos para navegar com sucesso no seu ambiente. Uma questão central na neuroetologia tem sido se comportamentos diferentes são controlados por circuitos supraespinhais distintos ou sobrepostos. As larvas do peixe-zebra nadam através de episódios discretos de movimento, classificáveis em 13 categorias. Para compreender os princípios fundamentais do controlo supraespinal da locomoção em animais, eu investiguei o mecanismo de transição entre diferentes movimentos da larvas de peixe-zebra, particularmente no contexto da locomoção frontal, tanto a nível comportamental como neural.

Para caracterizar o comportamento de mudança de velocidade, as larvas do peixe-zebra foram expostas a listas em movimento a diferentes velocidades, na direcção da cauda para a cabeça, induzindo a larva a nadar para a frente, num comportamento denominado de resposta optomotora. A aquisição de diversos parâmetros cinemáticos, através da detecção da posição do peixe e do ângulo da cauda, permitiu a classificação dos dados em diferentes modos de movimento. As larvas do peixe-zebra exibiram predominantemente modos de locomoção lenta em resposta a listas de baixa velocidade, enquanto as listas de velocidade mais elevada provocaram uma transição rápida do uso movimentos lentos para uma utlização repetida de movimentos rápidos.

Para estabelecer correlações neurais dos movimentos lentos e rápidos e compreender a dinâmica populacional subjacente às transições de modo, eu comecei por caracterizar 7 linhas transgénicas com expressão de GCaMP no tronco cerebral. Ao marcar retrogradamente os neurónios reticuloespinais em cada linha, consegui demonstrar o acesso transgénico a subpopulações distintas dentro do sistema reticuloespinal.

Depois, observei a atividade de populações neurais geneticamente marcadas no tronco cerebral de larvas de peixe-zebra fixadas pela cabeça enquanto estas

executavam a resposta optomotora, utilizando um microscópio de folha de luz. Os peixes fixos pela cabeça apresentaram variações cinemáticas no movimento quando comparadas com peixes a nadar livremente, apresentando episódios de movimento mais longos e que incluíam mudanças de frequência dentro de um único episódio. Assim sendo, usei codificação esparsa convolucional para decompor os ataques em motivos de movimento lento, rápido, de virada e de luta para identificar populações neuronais associadas a diferentes modos de natação. Isso revelou um recrutamento de células reticulospinais nas células nMLF, RoL, MiV2, MiDs e CaD/CaV durante a natação para frente, com um aumento acentuado na excitação de nados lentos para rápidos. A virada foi associada a células ventromediais, enquanto quase toda a população reticulospinal foi recrutada durante as lutas.

Minhas descobertas revelam como o cérebro seleciona dinamicamente entre dois padrões motores distintos, e dão-nos informação sobre os princípios fundamentais do controlo supraespinal da locomoção animal.

Financial Support

This work was carried out as part of the International Neuroscience Doctoral Programme (INDP) class of 2017/2018 hosted by Champalimaud Foundation and funded by the Portuguese Foundation for Science and Technology (Fundação para a Ciência e a Tecnologia (FCT), Bolsa SFRH/BD/ 147089/2019) and the Champalimaud Foundation.

I am grateful for the financial support to the lab secured by Michael Orger through the ERC Consolidator Grant (Neurofish-DLV-773012), the Volkswagen Stiftung Life? Initiative (A126151) and Champalimaud Foundation.

Fish care was supported by the research infrastructure CONGENTO, co-financed by Lisboa Regional Operational Programme (Lisboa2020), under the PORTUGAL 2020 Partnership Agreement through the European Regional Development Fund (ERDF) and FCT under the project LISBOA-01-0145-FEDER-022170.

Author Contributions

This thesis was written by Elena Maria Daniela Collins with input and guidance from Michael B. Orger. All data were acquired and analysed by Elena Maria Daniela Collins. Detailed contributions are provided per chapter.

Overview

This thesis is structured into five chapters. Chapter 1 introduces the topics of supraspinal control of locomotion, the locomotor repertoire of the larval zebrafish and its suitability to reticulospinal studies, and presents the three aims of the project. Chapter 2 describes gait switching behaviour in larval zebrafish in a freely-swimming assay and a head-embedded preparation. Chapter 3 showcases several existing and new transgenic lines that label different sets of reticulospinal neurons at larval stages, as well as the neurotransmitters expressed in those lines across development. Chapter 4 focuses on neuronal activity during gait switching behaviour; combining the behavioural head-embedded assay from chapter 2, the transgenic lines from chapter 3 and finally, functional whole-brain imaging at cellular resolution together in a single experimental paradigm to elucidate the neural basis of different forward swims and the population activity underlying transitions between movements. Finally, Chapter 5 discusses the findings of this work in the wider context of supraspinal control of locomotion and provides an outlook on future studies.

Table of Contents

List of Figures

List of Tables

Nomenclature

ARTR anterior rhombencephalic turning region

AS approach swim

BS burst swim

CfN cuneiform nucleus

CiDs circumferential descending interneurons

CPG central pattern generator

dF/F change in fluorescence compared to baseline

DLR diencephalic locomotor region

dpf days post-fertilisation

EPSPs excitatory post-synaptic potentials

FDA fluorescin-coupled dextran amine

fps frames per second

GABA gamma-aminobutyric acid

HAT high-angle turn

INs interneurons

IPSPs inhibitory post-synaptic potentials

LLC long-latency C-start

LPGi lateral paragigantocellular nucleus

MCoDs multipolar commissural interneurons

MeS mesencephalic small cells [in the nMLF]

MLMN mesencephalic locomotion maintenance neurons

MLR mesencephalic locomotor region

MNs motoneurons

MRRN middle rhombencephalic reticular nucleus

nMLF nucleus of the medial longitudinal fasciculus

OMN oculomotor nucleus

OMR optomotor response

PAG peri-aqueductal gray

PCA principal component analysis

PPN pedunculopontine nucleus

PTU 1-phenyl 2-thiourea

RF reticular formation

ROI region of interest

RS reticulospinal [system]

RSNs reticulospinal neurons

RT routine turn

rTBA rostral tail-bend amplitude

SAT shadow-avoidance turn

SLC short-latency C-start

TBF tail-beat frequency

Tu Tubingen [wildtype zebrafish strain]

Chapter 1

General Introduction

1.1 The descending control of locomotion

Animals are constantly faced with the need to produce flexible and adaptable behaviour in response to a rapidly-changing environment. From foraging for food, finding a mate, to escaping from predators – movement is central to survival. As such, it is no surprise that a large portion of the central nervous system is dedicated to its production, with the spinal networks that are under the control of brainstem locomotor centres at the very core [1]. Different species of animals, including both vertebrates and invertebrates, share an extraordinarily similar organization of the neural networks responsible for the control of locomotion [2, 3]. From lamprey to cat, there are three main neural components that interact dynamically to produce movement [4, 5] (Figure 1.1):

Coordinated patterns of muscle activity are generated by neural networks in the spinal cord, including central pattern generators (**CPG**) [5]. CPGs receive motor commands via excitatory reticulospinal neurons (**RSNs**), situated in the reticular formation (**RF**) in the lower brainstem [6, 7]. RSNs, in turn, are activated and controlled by specific locomotor command areas situated upstream, which are responsible for the initiation and maintenance of locomotion [3, 6, 8]. These centres are called the diencephalic locomotor region (**DLR**) in the forebrain [9–11] and the mesencephalic locomotor region (**MLR**) in the midbrain [12]. Motor selection itself is believed to be mediated by higher centres in the brain, such as the basal ganglia [10, 13]. The latter provide continuous inhibition of the DLR and MLR, so only when that inhibition is removed via striatal excitation can the centre generate a chosen motor pattern [1]. At each stage, there is interaction with sensory signals enabling continuous, rapid sensorimotor integration [3, 14].[1]

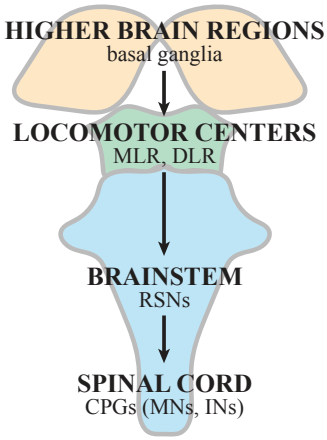

Figure 1.1: Descending control of locomotion.

[1] For an extensive review on the control of locomotion across vertebrates, see [1].

1.1.1 Spinal networks for movement production

Historical perspective A plethora of studies spanning from cat [15], rat [16], mice [17], to eel [18], dogfish [19], frog [20], salamander [21] and lamprey [22] have shown that the spinal cord can generate coordinated locomotor-like movement when deprived of any supraspinal control following partial or complete transection. The concept of the first CPG prototype was first postulated by Graham T. Brown in the early 1900s, in which he proposed that the generation of locomotor patterns was intrinsic [23, 24]. This was controversial, as the prevailing thought at the time was that locomotor patterns were generated in response to sensory feedback via a chain of reflexes [25–27]. Nearly 50 years later, this debate was settled by a seminal paper by Wilson demonstrating autonomous bursting activity in the locomotor CPG during locust flight [28], and subsequently applied to spinal organisation generating locomotion in cats [29, 30], lamprey [31], tadpoles [20] and zebrafish [32–34].

In mammals, Brown's findings inspired the half-centre hypothesis [23, 24], consisting of alternating flexor vs extensor muscle activation and reciprocal inhibition between the two sides. Different versions of the half-centre hypothesis have been put forward in the last decade, in particular concerning possible intrinsic bursting capabilities on the flexor [35–37] or both sides [38]. There have been recent attempts to unify the different hypotheses by considering the internal state of the animal [39]. However, the exact organisation of the CPG circuit within the spinal cord, the mechanisms responsible for rhythmogenesis and the overall control of locomotor pattern and frequency are not completely understood.

Lessons learned from aquatic vertebrates Considering organisms with fewer cells is instructive; so much so that in lamprey, Xenopus tadpole and zebrafish the intrinsic function of the CPG providing alternation in a given segment is in principle understood [1]. Swimming movements are generated by segmentally repeated CPGs. A rostro-caudal wave is transmitted along the length of the body and pushes the animal forward through the water. Studies in lamprey and salamander laid the groundwork for the basic principle of a CPG: excitatory glutamatergic

interneurons (**INs**) excite motoneurons (**MNs**) and provide reciprocal inhibition [31, 40]. The burst activity in segmental excitatory INs (termed E-neurons) is a result of supraspinal drive from RSNs via NMDA and AMPA receptors, their connectivity and intrinsic membrane properties [1].

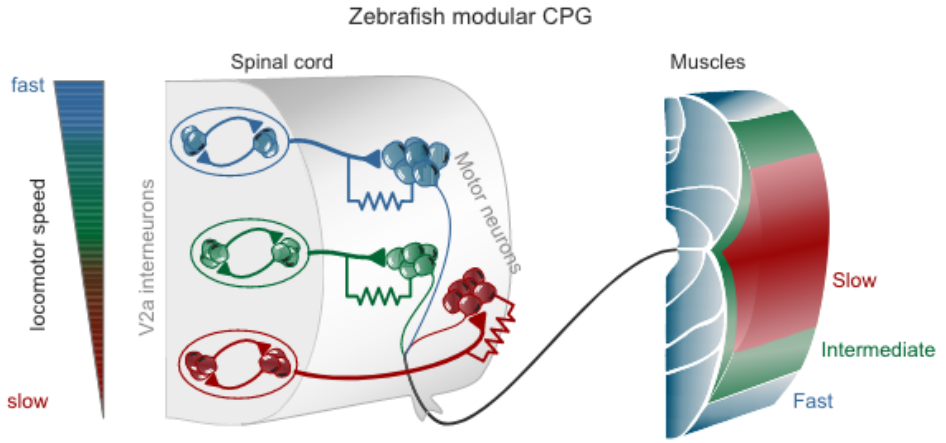

Figure 1.2: Overview of the modular CPG in zebrafish. Adapted from [5].

In zebrafish, rhythm generation is mediated by V2a INs, defined by expression of the transcription factor Chx10 [2] [34]. Detailed work from the El Manira lab in adult zebrafish has shown that these INs are necessary and sufficient for movement production [32]. There are three subtypes of glutamatergic excitatory INs (V2a-type) in the spinal CPG projecting directly to slow, intermediate and fast MNs [41, 42]. Slow INs project to slow MNs and have the lowest activation threshold as well as a tendency to oscillate when depolarised. In addition, there is mutual excitation that reinforces, and coordinates slow IN population activity. An increase in descending drive from supraspinal structures will recruit intermediate INs, which also receive input from slow INs for coordinated activity. The same applies to fast INs, where a further increase in descending drive recruits fast INs to generate swimming at the fastest speeds (Figure 1.2). At the same time, there are inhibitory INs, which receive input from excitatory INs and in turn inhibit premotor INs and MNs on the contralateral side [43]. Adult zebrafish swim continuously at low

[2]Note that the nomenclature of Chx10 has changed over the years, alternative names include *alx* and more recently *vsx2* in zebrafish

frequencies (peaking at 8-10 Hz, never exceeding 21 Hz) [44, 45]. They use 3 layers of muscles [45] and a combination of synaptic input computation and biophysical properties to regulate swimming speed [1].

Conversely, larval zebrafish swim in a burst-and-glide fashion at frequencies >20 Hz, using only a single layer of fast muscles. A recent paper in larval zebrafish revealed a spatial (lateral to medial) order of recruitment of fast muscle cells as a function of movement strength. In addition, muscle fibre size increases systematically along the same axis [46]. Insight into MN and IN recruitment with swimming speed in larval zebrafish comes from the Fetcho and McLean labs. Similar to the adult zebrafish, there is a topographic map of dorsoventral recruitment in the larvae: at lower swimming speeds, smaller, more ventral MNs and INs are recruited, whereas at higher swimming speeds larger, more dorsal MNs and INs are recruited [47]. According to the size principle, pools of active cells grow with increases in the force and speed of movement, following a gradient of increases in soma-size, axon conduction velocity and motor unit size [48, 49]. The size principle is a shared feature across vertebrates and invertebrates [50–52], including zebrafish, where MNs are recruited according to their size and remain active once recruited [47].

Interneuron recruitment in larval zebrafish, however, does not seem to follow the size principle. Instead, circumferential descending interneurons (**CiDs**), recruited at higher frequencies, silence multipolar commissural interneurons (**MCoDs**), recruited at lower frequencies [53]. MCoDs have ventral somata located laterally in the neuropil, with a commissural axon that descends in the ventral spinal cord and short, finger-like axon collaterals [54]. Ablation of MCoDs impairs slow swimming and they are subject to glycinergic inhibition during fast swimming speeds [47].

The switch from CiDs to MCoDs was observed in an experiment where touching the tail evokes a burst swim (**BS**) that eventually decays to a slow swim (around 40Hz) [55]. CiDs are active during and necessary for fast escapes and fast swims [53], as their ablation impairs those behaviours [56]. They are located more broadly along the dorso-ventral axis [57], with a corresponding recruitment pattern as a function of swimming speed [53]. They almost follow the size principle with a

general increase in size going from ventral to dorsal, except for a separate dorsally-located group of smaller CiD neurons that are active exclusively during fast escapes (but not fast swimming). There is a continuous shift in silencing of more ventral populations of CiDs as swimming frequency increases [53].

The dorso-ventral topographic organisation of MNs and INs has developmental relevance. The first movements that arise in larval zebrafish are powerful, high amplitude escape swims. Over time, the animal gradually adds exploratory behaviours to its repertoire, such as slow swimming or turns. At the same time, dorsal MNs and INs arise first in development, with more ventrally located INs being layered on over time [34, 58]. The dorsal cells drive escapes while the ventral cells are associated with slow swimming. The correlation of a growing behavioural repertoire and a gradually populated dorso-ventral axis of large to small MNs and INs demonstrates a temporal emergence of networks [58].

In summary, central pattern generators in the spinal cord are made up of rhythm-generating (bursting) interneurons that excite motoneurons, which provide excitatory drive to muscle fibres to produce locomotion, and inhibitory commissural interneurons, which inhibit both moto- and interneurons on the contralateral side. The exact mechanisms of rhythm generation are not yet fully understood. A large body of work in adult zebrafish has revealed a topographic (ventral to dorsal) organisation of spinal MNs, INs and muscle fibres to produce slow, intermediate and fast swimming. A similar, though more graded, topographic organisation exists in larval zebrafish, with more continuous shifts in active interneuron classes reported as a function of swimming speed [3]. Though there are many outstanding questions, recent efforts have made progress on understanding the functional organisation of spinal networks in limbed and non-limbed animals alike.

1.1.2 Supraspinal motor systems in vertebrates

The Mesencephalic Locomotor Region

In the 1960s Grigori Orlovskii and colleagues discovered that local stimulation at the junction between the mid- and hindbrain initiated controlled walking and

[3]For a comprehensive review on zebrafish spinal circuits see [59]

running in resting cats, and named it the mesencephalic locomotor region [12]. Subsequently, the MLR was physiologically identified in many other vertebrate species, including the rat [60], mouse [61, 62], guinea-pig [63], rabbit [64], monkey [65–67], lamprey [6, 68], salamander [69], stingray [70], goldfish [71–73] and recently zebrafish [74]. The key characteristic of the MLR is its graded control, where the intensity of stimulation scales with locomotor output [12]. This characteristic has so far been discovered in all animals investigated. In salamander, different stimulation intensities could even elicit two different modes of locomotion; walking and swimming [69]. MLR connectivity is bilateral, as unilateral stimulation of the MLR has been shown to produce symmetric locomotion in both salamander and lamprey [12, 68, 75, 76].

The MLR receives input from the basal ganglia and the medial and lateral hypothalamus through the peri-aqueductal gray (**PAG**) [77]. Sensory gating of the MLR occurs via muscarinic receptors [78]. The MLR has no direct projections to the spinal cord, but instead projects to reticulospinal cells in the RF. In addition to RSNs, it projects to a population of muscarino-receptive cells that provide additional excitation to RSNs, amplifying locomotor output [79, 80].

The mammalian MLR consists of two nuclei: the cuneiform nucleus (**CfN**) and the pedunculopontine nucleus (**PPN**). It is comprised of cholinergic, glutamatergic and GABAergic neurons [3, 7]. For a long time, it was unclear whether different subnuclei of the MLR controlled different motor functions. However, it had been proposed that locomotion generated during different behavioural contexts (e.g. hunting, escape, exploration) was initiated by different parts of the MLR [3, 81]. Recent advances in genetic tools, such as Cre-inducible viruses [82], have enabled optogenetic stimulation of the mouse MLR. In an effort to untangle subnucleus-specific contributions to locomotion, several recent studies have shown MLR-mediated initiation [62, 83–86] and cessation [86, 87] of locomotor bouts.

Several studies showed that glutamatergic cells in the MLR initiate or are sufficient to induce locomotion [62, 83, 84, 86]. Roseberry *et al.*, showed that glutamatergic cells in the MLR are sufficient for inducing locomotion and can be inhibited by locally projecting GABAergic cells, with cholinergic cells modulating

locomotion [62]. The study by Takasukaki *et al.* also supports these findings by showing that cholinergic cells in the MLR modulate locomotion by modifying descending inputs downstream at the level of RSNs and CPGs [88]. Caggiano *et al.* revealed that glutamatergic neurons in the CfN and PPN drive slow exploratory locomotion, while glutamatergic neurons in the CfN drive fast exploratory locomotion [83]. Josset *et al.* argue for a more spatially separated organisation, where glutamatergic and cholinergic cells in the PPN drive slow exploratory locomotion, while glutamatergic cells in the CfN drive fast escape responses [84].

A study by Goñi-Erro *et al.* revealed that activation of glutamatergic Chx10-neurons in the PPN arrests all ongoing movements while causing apnea and bradycardia in a 'pause-and-play' fashion [87]. This cessation of movement is different to amygdala- and ventrolateral PAG-mediated freezing [89–91]. A study by Grätsch *et al.* illustrates just how fine-tuned the graded control of the MLR really is. The authors show that electrical stimulation of the same MLR site in lamprey can either start or stop locomotion. When triggered, a second MLR stimulation stops locomotion if the intensity if lower than initially used to stimulate. If the second stimulation is higher than the first, then the locomotor bout is prolonged [2]. In summary, the ability to distinguish and manipulate cells depending on their neurotransmitter identity has proven to be a powerful tool to dissect the functional roles of sub-populations within the MLR.

The Diencephalic Locomotor Region

Historically, most research on the initiation and control of locomotion has focused on the MLR rather than the DLR. More than 30 years after Orlovskii and colleagues first reported their findings on a mesencephalic locomotor region [12], Sten Grillner's group described another locomotor region in the diencephalon of adult lamprey [9]. Using fluorescin-coupled dextran amine (**FDA**) labelling, they showed that neurons in the ventral thalamus project to the RF in the hindbrain but not directly to the spinal cord. FDA labelling also identified input to the ventral thalamus from the olfactory bulb, pallial areas, striatum, preoptic nucleus, hypothalamus, dorsal thalamus, optic tectum and dorsal isthmic gray. Extra-cellular stim-

ulation of the ventral thalamus elicited monosynaptic and polysynaptic excitatory post-synaptic potentials (**EPSPs**), mediated by glutamate, and inhibitory post-synaptic potentials (**IPSPs**), mediated by gamma-aminobutyric acid (**GABA**), in both middle and posterior RSNs [9].

The same group later showed that stimulating the DLR can not only lead to rhythmic ventral root activity in the spinal cord but actually produce locomotion [11]. DLR stimulation in head-fixed adult lamprey induced symmetric locomotor movements characterized by an undulatory wave travelling down the body. Local administration of GABA agonists inhibited movement, whereas antagonists facilitated movement initiation, suggesting tonic inhibition of movement by GABAergic projections that allow movement once turned off. This could represent output from the basal ganglia as the DLR receives GABAergic projections from both the pallium and striatum [11].

Reticulospinal organisation of locomotor control

The reticular formation is a collection of distributed, interconnected nuclei located in the brainstem that serves as a relay and integration site for several ascending and descending tracts [92]. It receives descending input from the telencephalon, diencephalon and cerebellum, ascending input from the the spinal cord and is integrated in local circuitry [14]. The RF can be divided into 3 columns along the medial to lateral axis: the raphe nuclei, the gigantocellular reticular nuclei and the parvocellular reticular nuclei, which are involved in mood regulation and arousal, motor coordination, and respiratory functions (particularly exhalation), respectively [92]. Neuronal cell types can be monoaminergic, cholinergic, GABA/glycinergic or glutamatergic, with glutamatergic reticulospinal neurons housed in the gigantocellular nuclei forming the key descending output driving locomotion [14, 93, 94].[4]

The reticulospinal (**RS**) system is formed by a distributed network of neurons that extends from the caudal midbrain through the pons to the medulla oblongata [95]. RSNs receive input from rostral motor centres [93]. This was first demon-

[4]In this thesis, the term reticulospinal neurons (**RSNs**) refers to the cells providing descending drive for the production of locomotion.

strated by Noga *et al* [96], where MLR stimulation with concurrent cooling of the medial RF abolished fictive locomotion in un-anaesthetised, decerebrate cats. This indicated that the MLR projects to the spinal cord via the medial RF to drive locomotion [96]. RSNs descend through the ventrolateral funiculus of the spinal cord to form synapses with spinal interneurons and motoneurons that participate in locomotion [93]. It was seen early on that within the gigantocellular nuclei exist multiple populations with distinct neurotransmitter expression [94]. Indeed, it was recently shown that the RS system is not exclusively excitatory: 20% of axons descending in the reticulospinal tract were shown to have GABAergic terminals [97] and 20% of reticulospinal synaptic contacts on commissural interneurons in the rat spinal cord are inhibitory. [98]. Despite increasing in number and complexity throughout evolution, RSNs are evolutionarily conserved across species and have the same fundamental architecture and role [99].

Given the fact that RSNs are situated in-between the rostral motor centres that mediate action selection, and the spinal circuits that produce locomotor patterns, RSNs are often referred to as command neurons [93]. To be considered as a command neuron, a candidate neuron needs to meet the criteria of sufficiency and necessity for initiating a given motor action [100]. Command neurons are a common principle across vertebrates and invertebrates.

One such example in early appearing agnathans, such as lamprey and hagfish, is the Müller cell. Situated bilaterally in the brainstem, their axons cross the midline and descend the length of the spinal cord to drive swimming [99]. Another example of a command neuron is the Mauthner cell, found in later-evolving fish and amphibians at the level of the 4th rhombomere near the midline of the medulla. Mauthner cells are a large, bilateral pair of cells, and are easily identifiable due to their similar location, morphology and synaptic connectivity across species [101–103]. Similar to the Müller cells, their axons decussate in the brainstem and project through the spinal cord, where they form excitatory glutamatergic connections with large, primary MNs and premotor excitatory INs [104–106]. They are also electrotonically coupled to glycinergic commissural INs that inhibit large MNs and INs on the contralateral side [106, 107]. Mauthner cells fire a single action

potential that causes a fast, powerful C-start escape away from the stimulus [71, 108]. The C-start escape response is often described as a stereotypical behaviour [108]. However, some modulation of the motor pattern is possible, depending on the stimulus location and intensity, and the combinations of RSNs involved [109, 110].[5] Considering that behavioural responses mediated by the reticulospinal system are adaptable illustrates that responses to command neuron activity are variable and state-dependent [93].

Considerable functional diversity exists within reticulospinal neurons. The two examples above showcase how the activity of single neurons elicits specific behaviours. Studies in lamprey have shown that RSNs from the middle rhombencephalic reticular nucleus (**MRRN**) are essential for the initiation and control of locomotion [111]. Designated as command neurons, they have also been described as key mediators of locomotor speed and swimming direction [80, 112]. Lamprey RSNs were subsequently divided into neuronal subpopulations that when stimulated, either initiate, initiate and maintain, or terminate locomotion [113].

Similar findings were reported in *Mus musculus*. Arber and colleagues identified functionally distinct subpopulations of RSNs in the caudal brainstem, distinguishable by their neurotransmitter identity, connectivity and location, that influence locomotion parameters [86]. Glutamatergic neurons within the lateral paragigantocellular nucleus (**LPGi**) are essential for high-speed locomotion and can tune locomotor speed via graded input from the MLR. 'Stop' commands are more widely distributed across the RF than their 'start'-counterparts: Activation of glycinergic neurons within the LPGi, and also in other nuclei within the RF, arrests locomotor behaviour [86]. This is supported by previous work from Kiehn and colleagues that showed that optogenetic activation of a subset of rostral glutamatergic V2a-neurons in the medulla leads to the cessation of ongoing locomotor activity [114]. Similarly to the MLR, together these findings illustrate the usefulness of being able to stimulate subpopulations of RSNs with different neurotransmitter expression patterns to decode the reticulospinal control of locomotion.

Evidence for the hypothesis that different behaviours are represented by dis-

[5] A more detailed description of this modulation and the contribution of Mauthner homologues is given in the next section.

tinct clusters of RSNs also stems from a recent study attributing distinct mouse forelimb actions to subpopulations in the lateral rostral medulla [115]. Stimulation of distinct subpopulations elicited reaching or food handling, whereas perturbations impaired both. These distinct subpopulations can be distinguished by their axonal targets and they act through differential recruitment of intra-brainstem and spinal circuits [115]. Command-level control of locomotion is not restricted to vertebrates. A recent study in *Drosophila melanogaster* has provided evidence for the concept of command-like neurons recruiting additional descending neurons to achieve population-level locomotor control to drive complete behaviours. Interestingly, activation of command-like neurons alone produced stereotyped movements, whereas joint activation of command-like neurons and additional descending neuronal networks produced complete behaviours [116].

In conclusion, while the reticulospinal system has prevailed throughout evolution, and has indeed flourished in terms of its size, complexity and diversity, the fundamental architecture remains largely the same [93]: RSNs are large cells situated bilaterally in the brainstem that receive motor selection information from higher centres. They have large fast-conducting axons that descend in the spinal cord and dense arborisations, forming synapses with MNs and INs across multiple segments to ultimately produce movement.

1.2 The Zebrafish Model System

Larval zebrafish, *Danio rerio*, are a small teleost with homologies in key genetic, physiological, and behavioural features to larger vertebrates. They are native to India and Myanmar and are commonly found in shallow waters in rivers [117]. Due to their large clutch size, fast generation time, ease of handling and ex-utero embryonic development, larval zebrafish have become a popular model organism in developmental biology over the last century [118].

Recent advances in genetically encoded calcium sensors have enabled recording of calcium activity in individual cells as a proxy for neuronal activity. In zebrafish, their small size and transparency at larval stages enable whole-brain imaging in a non-invasive manner, with a single-cell resolution of up to 80% of their 100.000

neurons [119]. This is a clear advantage compared to larger vertebrates, where simultaneous recordings of anatomically distant neurons are often difficult, if not impossible.

At only a few days post-fertilization (**dpf**) larval zebrafish already possess a comprehensive repertoire of innate behaviours, ranging from simple exploratory movements, such as forward swimming and turning, to more computationally demanding behaviours, such as hunting, prey capture, escaping from predators and social avoidance (Figure 1.3) [120]. A breadth of visual, auditory, tactile and social stimuli can be used to reliably elicit these behavioural responses, with examples ranging from moving gratings, looming discs, startling tones to prey and multi-fish interactions. Last but not least, larval zebrafish have recently become an attractive model for toxicological and pharmacological studies as agents can simply be added to the fish medium at different concentrations followed by behavioural observations. Together, optical accessibility at larval stages, an abundance of readily available genetic tools and a robust set of instinctive visually guided behaviours, have made larval zebrafish an attractive model organism in behavioural neuroscience.

1.2.1 The behavioural repertoire of larval zebrafish

From 3 dpf onwards, larval zebrafish move in a burst-and-glide fashion, called bouts, by bending the tail [121]. In addition to tail bending, larval zebrafish use their pectoral fins in an alternating fashion during slow, exploratory behaviour. At faster speeds and during escapes, these are tucked against the body to propel themselves forward [55]. In escape behaviours, which can be tested experimentally using looming shadows or auditory startles, larval zebrafish bend their tail in a characteristic C-shape, giving them the name C-starts. Starting at 5 dpf, larval zebrafish begin to hunt small prey, such as L-type rotifers or paramecia. In addition to studying naturalistic behaviours, experimenters can use visual stimuli to elicit specific behaviours, such as translating or rotating gratings for forward swimming, turning and eye saccades, respectively, dimming for phototaxis, or expanding spots for avoidance [122]. Utilising high-speed video recordings of the

animal's trajectory, heading direction and tail angle allows detailed characterisation of the locomotor repertoire of larval zebrafish using supervised or unsupervised classification methods [122, 123].

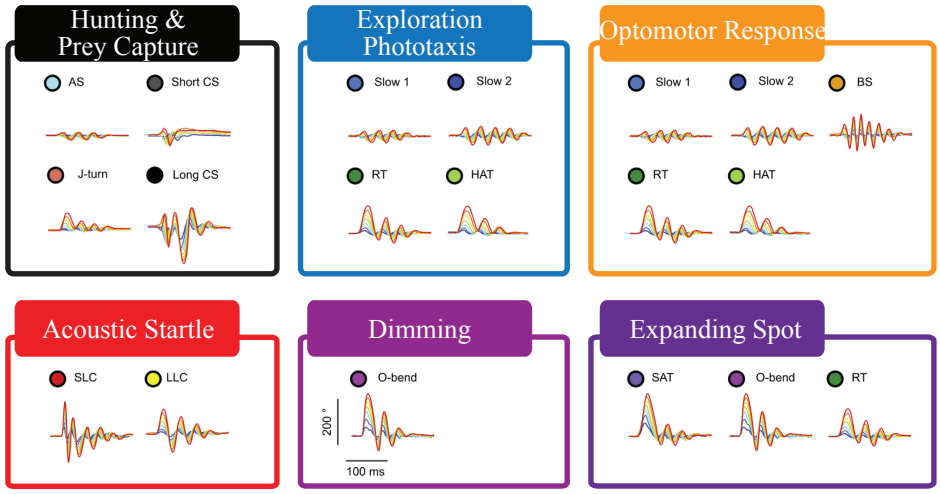

Figure 1.3: Behavioural repertoire of larval zebrafish. Adapted from [122].

1.2.2 Reticulospinal contributions to locomotion in larval zebrafish

Given their amenability to genetic tools, optical accessibility early in development and complex behavioural repertoire, larval zebrafish have been instrumental in shedding light on the fundamental question of how the reticulospinal system encodes commands to drive different behaviours [124–126].

The hindbrain of larval zebrafish is arranged according to a broad structural and functional ground plan [127–129]. Along the medial-lateral axis, neurons of a particular marker form alternating rostro-caudal glutamatergic-glycinergic stripes and differ in their morphology (Figure 1.4A). The most medial stripe of glutamatergic (*vglut2*) neurons overlaps with the transcription factor *chx10* and has ipsilaterally descending axons. This is followed by a glycinergic stripe of *engrailed1b*-positive neurons, with ipsilaterally ascending axons. Neurons expressing the transcription factor *dbx1b* span several stripes and exhibit contralateral

branching. Finally, the transcription factor *barhl2* overlaps with some neurons in the most lateral glutamatergic stripe. Neurons in the most lateral glycinergic stripe have both ipsi- and contralateral branches. There is also an age-related pattern along the dorso-ventral axis in the *chx10* stripe. In contrast to the spinal cord, in the hindbrain, first-born neurons are located ventrally and have low input resistance, whereas younger neurons are dorsally positioned and have higher input resistance. This corresponds to their recruitment at different swimming frequencies, with dorsal, younger cells recruited at lower swimming frequencies and ventral, older cells recruited at higher ones [128]. The next few paragraphs will go into more detail on the functional roles associated with different reticulospinal populations in zebrafish and other danionins (Figure 1.4B).

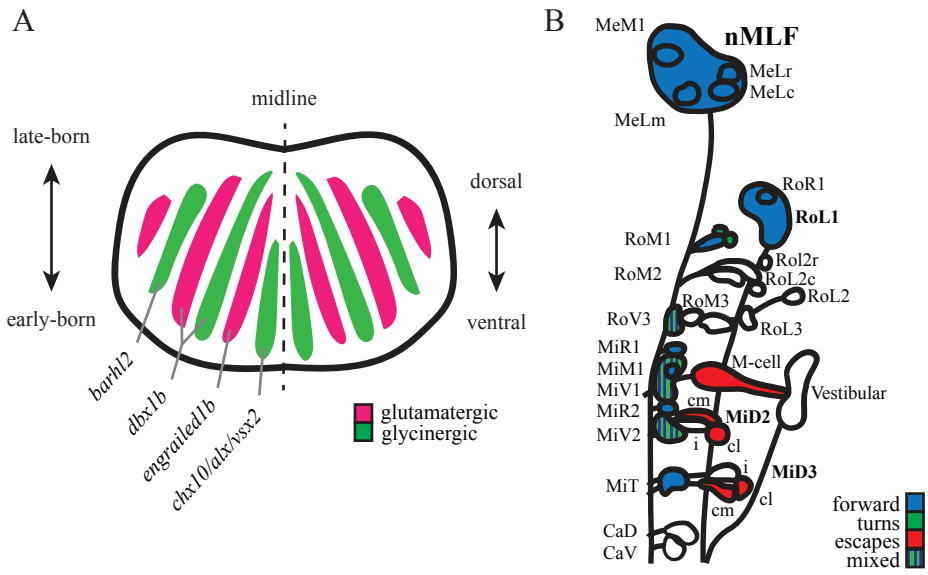

Figure 1.4: Larval zebrafish reticulospinal system, associated behaviours and hindbrain patterning. A) Labelled reticulospinal neurons, colour-coded with associated behaviours: forward swimming (blue), turns (green), escapes (red). B) Patterning of hindbrain, adapted from [128].

Initiation, maintenance and termination of swimming Studies on the reticulospinal system in mammals have predominantly focused on the initiation, maintenance and termination of locomotion. In larval zebrafish, calcium activity in

the medial stripe of glycinergic *engrailed1b* neurons was found to be highly correlated with the onset of swimming [130]. A comparative study of larval *Danio rerio* and adult *Danionella cerebrum* identified a common nucleus in the midbrain associated with swimming [131]. Termed the mesencephalic locomotion maintenance neurons (**MLMN**), their activity was shown to be correlated with initiation and maintenance of swimming in both species. Optogenetic activation of the MLMN in zebrafish resulted in a reliable increase in swimming following stimulation [6]. In *D. cerebrum* activity of different neurons distributed across the hindbrain was correlated with the cessation of swimming [131]. Future work is needed to clarify the neurotransmitter identity and projection pattern of these 'stop' neurons in *D. cerebrum* and whether they match the inhibitory *engrailed1b* neurons identified in larval zebrafish [130]. [7]

Escapes Escape responses are mediated by the Mauthner array, consisting of the Mauthner cell and its homologues (MiD2cm/cl, MiD3cm/cl and other descending RSNs). The Mauthner cells are a pair of large, bilateral cells located in the midbrain near rhombomere 4. They have large-diameter, fast-conducting, decussating axons that descend down the length of the spinal cord, forming excitatory glutamatergic connections to primary MNs and INs [104–106]. The Mauthner homologues are several smaller, bilateral pairs of cells arranged in two segments caudal to the Mauthner cell with contralaterally-projecting axons do [109]. The Mauthner network has been conserved across evolution, ranging from the early Müller cells in lamprey and hagfish, to the Mauthner and homologues in teleosts and mammals [93].

Unilateral activation of the Mauthner cell elicits the escape/startle response. A mere 3-5 ms after onset of an aversive acoustic stimulus, a single spike is fired by the Mauthner cell [71, 108]. This produces a short-latency C-start, where the fish makes a characteristic C-bend and swims away from the stimulus [106, 133]. A recent paper showed that complete Mauthner cell ablation, including its soma and axons, abolishes short-latency escapes [134].

[6] Note that this experiment was only carried out in zebrafish due to transgenic lines not being available for *D. cerebrum*

[7] For a review on locomotion termination in other animals see [132].

Bilateral, simultaneous activation of the Mauthner cells by touching the tail drives an S-start escape response. Here, the fish bends in an "S"-shape as a result of regional muscle activity on both left and right sides. Interestingly, simultaneous current injection into both Mauthner cells does not elicit an S-startle response. Instead, upon touching the tail, local sensory inputs inhibit caudal MNs via inhibitory INs. This pre-conditions the MNs so that when the spike arrives from the Mauthner cells, they are biased toward either the left or right side and this determines whether a C-start or S-start is performed [135].

The homologues have a higher firing threshold and thus respond a few milliseconds later by firing in bursts [136] and activating spinal circuits that cause the trunk to contract [106]. As activation of the Mauthner cell generates an escape behaviour, it was soon deemed command-like [110]. However, it was long believed that its ablation does not abolish escapes but merely delays them by a few milliseconds [137, 138]. This mystery was solved by a set of elegant experiments confirming that the homologues are involved depending on the stimulus direction. As proposed by the Foreman and Eaton model in goldfish [139], a stimulus presented to the tail elicits a Mauthner-cell-mediated escape behaviour alone, whereas a stimulus presented to the head activates both the Mauthner cell and its homologues [109, 140]. Causality of this was later demonstrated using photo-ablation [141]. It remains to be seen whether complete ablation of the whole Mauthner array abolishes both short- and long-latency escapes.

Turning Several studies have attributed turning-related behavioural responses to the ventromedial RSNs in the hindbrain [74, 142, 143]. In response to moving gratings, fish turn toward and follow the direction of perceived motion, called the optomotor response (**OMR**). Combining an OMR assay with 2-photon microscopy, Orger *et al.* were able to identify several RSNs linked to forward swimming and/or turning. Regarding routine turns, they demonstrated that the RoM1r and ventromedial cells of rhombomeres 3-5 (RoV3, MiV1, MiV2) were activated by visual stimuli that drive turning behaviour. Subsequent ablation of RoM1 cells did not affect turning behaviour. Unilateral ablation of the ventromedial cells, however, abolished stimulus-evoked turns toward the ablated side, while leaving forward

swimming and turning to the other side intact [142].

A subsequent study by the same group showed that ventromedial cells were necessary to drive multiple types of turns, elicited spontaneously or during phototaxis, in the OMR or in response to dark flashes [143]. Given that their ablation affected multiple turn types across different behavioural contexts suggests a universal role of ventromedial RSNs in controlling turning behaviour. To distinguish turning vs forward components, the authors hypothesised that 1) forward swims and turns are controlled by independent RSNs, 2) unilateral ventromedial cell activity drives turns while bilateral activity elicits forward swimming or 3) ventromedial cells can transform forward swims (controlled elsewhere) into turns by introducing an asymmetrical component. While ablation of ventromedial cells abolished turns in response to turn-evoking visual stimulation, there was an increase in forward swims. Considering that rhythmic tail undulations were unaffected, this supports the third hypothesis that ventromedial cells transform a symmetric (forward) into an asymmetric pattern (turn) [143]. Another recent study also decomposed spontaneous swims into a forward and turn/steering component. Using oblique light-sheet microscopy (SCAPE, [144, 145]) coupled with a head-fixed assay in enucleated fish, the authors associated steering-related neuronal activity with glutamatergic V2a-neurons in rhombomeres 2-6 as well as rhombomeres 7-8 in the medulla [74].

These studies clearly demonstrate the necessity and sufficiency of ventromedial cells to produce turning behaviour. Turns can be to the left or the right side, and studies have shown that over time, fish exhibit a bias to turn in the same direction multiple time in a row. By combining whole-brain volumetric imaging with recordings of fictive swim activity, Dunn and Mu *et al* identified a cluster of neurons in the anterior hindbrain that drives this long-term bias during exploratory behaviour. Naming it the anterior rhombencephalic turning region (**ARTR**), the authors showcase bilateral clusters in rhombomeres 2-3, consisting of a medial glutamatergic and a lateral GABAergic group, that form a mutually inhibitory circuit motif. Targeted manipulations showed that the ARTR is not responsible for sending the turning motor command itself, but instead connects to ventromedial cells and biases turn direction on a slower timescale [146].

Forward swimming Several RSNs across the brainstem have been linked to driving forward swimming in zebrafish: neurons in the nucleus of the medial longitudinal fasciculus (**nMLF**)[8] in the midbrain [142, 147–150], several rostral and ventromedial RSNs in the hindbrain [142], glutamatergic-V2a neurons [74, 129, 151] and medial glycinergic *engrailed1b* neurons in the pons and medulla [130].

Taking a closer look at the nMLF; its association with forward swimming is supported by evidence from several key studies [142, 147–149]. Orger *et al.*, in addition to identifying turning-related RSNs, reported calcium activity in small and large (MeM1, MeLr, MeLc, MeLm) nMLF cells during forward swimming elicited by the OMR. In addition to cells in the nMLF, forward-swimming-related activity was also reported in several other RSNs in the hindbrain (RoL1/RoR1, RoM1c, RoV3, MiR1, MiM1, MiV1, MiR2, MiV2, MiT). The same group later showed that ablation of large nMLF cells leads to a significant deficit in achieving fast swimming speeds in response to visual stimuli, whereas ablation of the RoM cells had no effect [147]. Electrical micro-stimulation of the nMLF revealed that the strength of stimulation correlates with an increase in swim duration and tail-beat frequency. To test whether this was also true in visually induced swimming, larvae were presented with moving gratings at different speeds while calcium activity and tail movements were recorded. The large nMLF cells were active all the time and small nMLF cells most of the time, meaning fast swimming occurs due to changes in activity in already active cells, not due to additional recruitment of cells. Using regression analysis revealed that the lateral MeLr and MeLc correlated significantly with bout duration and tail-beat frequency, whereas the medial MeLm and MeM1 did not.

In contrast to graded activity of the same cells, a recent paper in adult zebrafish argues for spatial separation of slow and fast swimming related neurons in the nMLF. Namely, the authors described medial neurons in the nMLF that are active during slow forward swimming, while lateral neurons drive fast forward swimming [149]. In addition, other studies have linked neuronal activity in the nMLF to touch-evoked escapes [152], turning and struggles in response to light head-taps [150], and postural control and navigation [148, 153, 154].

[8]The nMLF is now also sometimes referred to as the interstitial nucleus of Cajal [74]

Besides the nMLF, forward swimming-related neuronal responses have been observed in the caudal glutamatergic V2a-neurons in the hindbrain [74, 129, 151]. As aforementioned, by decomposing swims into forward and steering components, Carbo-Tano and Lapoix *et al.* revealed neurons in the medial V2a stripe spanning from rhombomeres 2-8 (except for rhombomere 6) active during spontaneous forward swimming [74], matching previously described glutamatergic V2a (*chx10*) neurons active with swimming onset [129].

While the association of forward swimming to different groups of RSNs appears contradictory, these studies can also be instructive to devise a wider framework for how movement commands are organised in the reticulospinal system. While escapes and turns have been linked to distinct, spatially separate groups of RSNs, forward swimming-related neurons identified to date are far more distributed across the brainstem. The question arises whether forward swimming should be represented as clearly as turns or escapes in the first place. For instance, forward swimming could be the base behavioural motif that can be changed by introducing a biased tail deflection in the first undulation cycle [74, 142, 143]. The question of whether different behaviours map onto distinct or overlapping sets of RSNs remains largely unanswered. The next section will outline different potential configurations.

1.3 Neural coding strategies in motor control

A central question in the control of locomotion has long been whether there are distinct motor commands for individual behaviours or whether behaviours are a combination of descending commands, integrated and adapted at the level of the spinal cord [124–126, 155].

Experimental support for distinct subpopulations of RSNs driving distinct behaviours comes from studies showing the Mauthner system driving escapes [109, 133, 134, 156–158], ventromedial RSNs mediating turns [142, 143, 146], and the nMLF and medullary V2a neurons having been linked to forward swimming [74, 129, 142, 147–149, 151]. Considering that there is functional, anatomical and molecular separation into slow, intermediate and fast motor neurons, interneurons

and muscles at the level of the spinal cord [39, 41, 42, 45], it would be plausible to assume a similar organisation further upstream in the reticulospinal system.

On the other hand, it is equally possible that RSNs simply relay sub-components of motor commands, such as the movement duration, speed, asymmetry or heading direction. Experimental support for this stems from studies attributing control of kinematic aspects across behavioural contexts to the same neurons [148], scaling of neuronal activity as a function of swimming speed [147], distributed recruitment of RSNs during touch-evoked escapes [152], the conversion of symmetrical forward swims to turns by biasing the first tail undulation [143] and the decomposition of swims into forward and steering components mediated by distributed, partially overlapping subdivisions of RSNs [74].

Finally, one can attempt to cluster movement motifs into groups of behaviours. Different groups could be driven by different sets of RSNs. For instance, forward swimming movements (approach swim, slow1, slow2, burst swim) could be spatially distinct from escape behaviours (short-latency C-start (**SLC**), long-latency C-start (**LLC**), shadow-avoidance turn (**SAT**), O-bend), and different to turns (J-turn, routine turn (**RT**), high-angle turn (**HAT**)). However, within a group there could be modulation of movement parameters such as degree of turning, or speed of swimming, duration, heading direction etc. The next question would be whether there are also anatomical or molecular markers for different behavioural groups or whether the distinction is purely functional. I have formulated three hypotheses for reticulospinal organisation at the functional level (Figure 1.5):

1. Distinct sets of RSNs encode commands for distinct behavioural motifs, with a graded or abrupt switch between those different populations.
2. Distinct behavioural motifs arise from the combinatorial population activity of all RSNs, for instance by changes in excitation.
3. Movement motifs can be grouped into sets of behaviours, for instance escapes vs exploration vs hunting, that are also distinctly organised in the RS system. Within those sets there is modulation, for instance progressive recruitment.

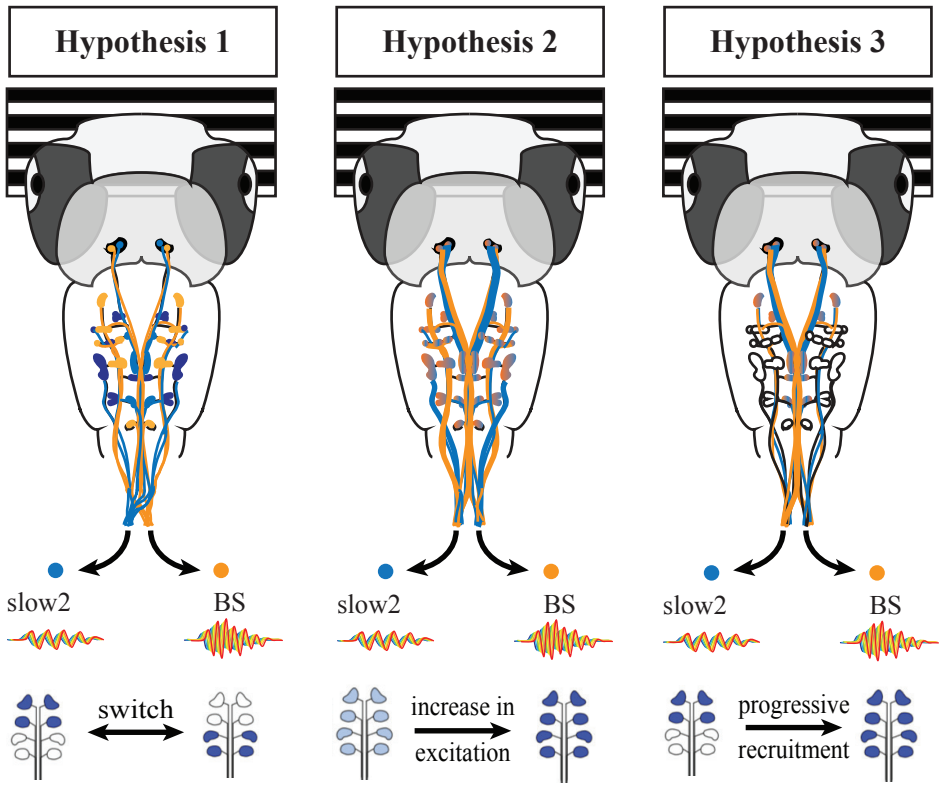

Figure 1.5: Three hypotheses of RSN organization to produce different movement motifs.

1.4 Objectives of this thesis

The overarching goal of this project was to investigate the neural control of gait switching in larval zebrafish. Specifically, I set out to identify the neural correlates of slow and fast bouts and elucidate the population dynamics underlying bout transitions during the optomotor response.

1.4.1 Aim 1

Elicit slow and fast bouts in response to optomotor gratings in freely-swimming and head-restrained assays, with a particular focus on the characterisation of gait transitions.

Hypothesis Larval zebrafish will predominantly employ slow bouts during slow optomotor gratings and fast bouts during fast optomotor gratings.

Method I will test several configurations in freely-swimming larval zebrafish to identify the ideal parameters driving gait switching behaviour. For detection and classification of swim bouts, a novel method will be used [122]. To facilitate subsequent imaging experiments, larval zebrafish will be embedded in low-melting point agarose in a head-restrained, tail-free preparation, while whole- field visual stimuli will be presented using a closed-loop virtual-reality system. For comparison to freely-swimming swim, analysis of tail kinematics will be performed.

1.4.2 Aim 2

Characterisation of transgenic lines labelling reticulospinal neurons in the hindbrain of the larval zebrafish.

Hypothesis Several established transgenic lines exist with cells labelled in the reticular formation, however, it is unknown if and which reticulospinal cells are included. I hypothesise that *nefma* labels all RSNs, *vsx2* labels only ipsilaterally-projecting RSNs in the hindbrain, *s1171Et* only labels RSNs in the midbrain and *tiam2a* labels the Mauthner cells and homologues.

Method I will characterise the degree of RSN labelling in each line using dextran-conjugated injections into the rostral spinal cord, back-labelling RSNs and performing immunohistochemistry and confocal imaging. This allows us to compare which RSNs are labelled in each transgenic line. Subsequently, I will perform in situ hybridisation chain reaction to confirm RSNs are glutamatergic, as well as characterise other cells of potential interest.

1.4.3 Aim 3

Identify the neural correlates of slow and fast bouts in the hindbrain and elucidate the mechanism of transition.

Hypothesis There are three possible hypotheses:

1. Distinct sets of RSNs encode commands for distinct behavioural motifs, with a graded or abrupt switch between those different populations.
2. Distinct behavioural motifs arise from the combinatorial population activity of all RSNs, for instance by changes in excitation.
3. Movement motifs can be grouped into sets of behaviours, for instance escapes vs exploration vs hunting, that are also distinctly organised in the RS system. Within those sets there is modulation, for instance progressive recruitment.

Method I will record whole-brain neural activity using fast volumetric calcium imaging in head-embedded behaving fish performing the OMR using a light-sheet microscope, combined with high-speed recordings of the tail to measure motor output.

1.5 References

1. Grillner, S. & El Manira, A. Current Principles of Motor Control, with Special Reference to Vertebrate Locomotion. *Physiological Reviews* **100,** 271–320. doi:10.1152/physrev.00015.2019 (2020).
2. Grätsch, S., Büschges, A. & Dubuc, R. Descending control of locomotor circuits. *Current Opinion in Physiology* **8,** 94–98. doi:10.1016/j.cophys.2019.01.007 (2019).
3. Le Ray, D., Juvin, L., Ryczko, D. & Dubuc, R. in *Progress in Brain Research* 51–70 (Elsevier, 2011). doi:10.1016/B978-0-444-53825-3.00009-7.
4. Orlovsky, G., Deliagina, T. G. & Grillner, S. *Neuronal Control of Locomotion:From Mollusc to Man* doi:10.1093/acprof:oso/9780198524052.001.0001 (Oxford University Press, 1999).
5. Grillner, S. & Kozlov, A. The CPGs for Limbed Locomotion–Facts and Fiction. *International Journal of Molecular Sciences* **22,** 5882. doi:10.3390/ijms22115882 (2021).
6. Dubuc, R. *et al.* Initiation of locomotion in lampreys. *Brain Research Reviews* **57,** 172–182. doi:10.1016/j.brainresrev.2007.07.016 (2008).
7. Ryczko, D. & Dubuc, R. The Multifunctional Mesencephalic Locomotor Region. *Current Pharmaceutical Design* **19,** 4448–4470. doi:10.2174/1381612811319240011 (2013).
8. Noga, B. R. & Whelan, P. J. The Mesencephalic Locomotor Region: Beyond Locomotor Control. *Frontiers in Neural Circuits* **16,** 884785. doi:10.3389/fncir.2022.884785 (2022).
9. El Manira, A., Pombal, M. & Grillner, S. Diencephalic projection to reticulospinal neurons involved in the initiation of locomotion in adult lampreysLampetra fluviatilis. *The Journal of Comparative Neurology* **389,** 603–616. doi:10.1002/(SICI)1096-9861(19971229)389:4<603::AID-CNE5>3.0.CO;2-4 (1997).
10. Grillner, S., Wallén, P., Saitoh, K., Kozlov, A. & Robertson, B. Neural bases of goal-directed locomotion in vertebrates—An overview. *Brain Research Reviews* **57,** 2–12. doi:10.1016/j.brainresrev.2007.06.027 (2008).
11. Ménard, A. & Grillner, S. Diencephalic Locomotor Region in the Lamprey—Afferents and Efferent Control. *Journal of Neurophysiology* **100,** 1343–1353. doi:10.1152/jn.01128.2007 (2008).
12. Shik, M. L., Severin, F. V. & Orlovskiĭ, G. N. Control of walking and running by means of electric stimulation of the midbrain. *Biofizika* **11,** 659–666 (1966).
13. Graybiel, A. M. The Basal Ganglia and Chunking of Action Repertoires. *Neurobiology of Learning and Memory* **70,** 119–136. doi:10.1006/nlme.1998.3843 (1998).
14. Perreault, M.-C. & Giorgi, A. Diversity of reticulospinal systems in mammals. *Current Opinion in Physiology* **8,** 161–169. doi:10.1016/j.cophys.2019.03.001 (2019).

15. Rossignol, S., Bouyer, L., Barthélemy, D., Langlet, C. & Leblond, H. Recovery of locomotion in the cat following spinal cord lesions. *Brain Research Reviews* **40,** 257–266. doi:10.1016/S0165-0173(02)00208-4 (2002).

16. Alluin, O., Delivet-Mongrain, H. & Rossignol, S. Inducing hindlimb locomotor recovery in adult rat after complete thoracic spinal cord section using repeated treadmill training with perineal stimulation only. *Journal of Neurophysiology* **114,** 1931–1946. doi:10.1152/jn.00416.2015 (2015).

17. Leblond, H., L'Espérance, M., Orsal, D. & Rossignol, S. Treadmill Locomotion in the Intact and Spinal Mouse. *The Journal of Neuroscience* **23,** 11411–11419. doi:10.1523/JNEUROSCI.23-36-11411.2003 (2003).

18. Bickel, A. Beiträge zur Rückenmarksphysiologie des Aales. *Pflüger, Archiv für die Gesammte Physiologie des Menschen und der Thiere* **68,** 110–119. doi:10.1007/BF01662728 (1897).

19. Grillner, S. On the generation of locomotion in the spinal dogfish. *Experimental Brain Research* **20.** doi:10.1007/BF00238013 (1974).

20. Kahn, J. A. & Roberts, A. Experiments on the central pattern generator for swimming in amphibian embryos. *Philosophical Transactions of the Royal Society of London. B, Biological Sciences* **296,** 229–243. doi:10.1098/rstb.1982.0004 (1982).

21. Ryczko, D., Charrier, V., Ijspeert, A. & Cabelguen, J.-M. Segmental Oscillators in Axial Motor Circuits of the Salamander: Distribution and Bursting Mechanisms. *Journal of Neurophysiology* **104,** 2677–2692. doi:10.1152/jn.00479.2010 (2010).

22. Wallén, P. & Williams, T. L. Fictive locomotion in the lamprey spinal cord in vitro compared with swimming in the intact and spinal animal. *The Journal of Physiology* **347,** 225–239. doi:10.1113/jphysiol.1984.sp015063 (1984).

23. Brown, T. G. The intrinsic factors in the act of progression in the mammal. *Proceedings of the Royal Society of London. Series B, Containing Papers of a Biological Character* **84,** 308–319. doi:10.1098/rspb.1911.0077 (1911).

24. Brown, T. G. On the nature of the fundamental activity of the nervous centres; together with an analysis of the conditioning of rhythmic activity in progression, and a theory of the evolution of function in the nervous system. *The Journal of Physiology* **48,** 18–46. doi:10.1113/jphysiol.1914.sp001646 (1914).

25. Philippson, M. L'autonomie et la centralisation dans le système nerveux des animaux. 1–208 (1905).

26. Sherrington, C. S. Flexion-reflex of the limb, crossed extension-reflex, and reflex stepping and standing. *The Journal of Physiology* **40,** 28–121. doi:10.1113/jphysiol.1910.sp001362 (1910).

27. Sherrington, C. S. REMARKS ON THE REFLEX MECHANISM OF THE STEP. *Brain* **33,** 1–25. doi:10.1093/brain/33.1.1 (1910).

28. Wilson, D. M. The Central Nervous Control of Flight in A Locust. *Journal of Experimental Biology* **38,** 471–490. doi:10.1242/jeb.38.2.471 (1961).

29. Grillner, S. & Zangger, P. How detailed is the central pattern generation for locomotion? *Brain Research* **88,** 367–371. doi:10.1016/0006-8993(75)90401-1 (1975).

30. Grillner, S. & Zangger, P. On the central generation of locomotion in the low spinal cat. *Experimental Brain Research* **34.** doi:10.1007/BF00235671 (1979).

31. Buchanan, J. T. & Grillner, S. Newly Identified 'Glutamate Interneurons' and Their Role in Locomotion in the Lamprey Spinal Cord. *Science* **236,** 312–314. doi:10.1126/science.3563512 (1987).

32. Eklöf-Ljunggren, E. *et al.* Origin of excitation underlying locomotion in the spinal circuit of zebrafish. *Proceedings of the National Academy of Sciences* **109,** 5511–5516. doi:10.1073/pnas.1115377109 (2012).

33. Ljunggren, E. E., Haupt, S., Ausborn, J., Ampatzis, K. & El Manira, A. Optogenetic Activation of Excitatory Premotor Interneurons Is Sufficient to Generate Coordinated Locomotor Activity in Larval Zebrafish. *The Journal of Neuroscience* **34,** 134–139. doi:10.1523/JNEUROSCI.4087-13.2014 (2014).

34. Kimura, Y., Okamura, Y. & Higashijima, S.-i. *alx* , a Zebrafish Homolog of *Chx10* , Marks Ipsilateral Descending Excitatory Interneurons That Participate in the Regulation of Spinal Locomotor Circuits. *The Journal of Neuroscience* **26,** 5684–5697. doi:10.1523/JNEUROSCI.4993-05.2006 (2006).

35. Pearson, K. G. & Duysens, J. in *Neural Control of Locomotion* (eds Herman, R. M., Grillner, S., Stein, P. S. G. & Stuart, D. G.) Series Title: Advances in Behavioral Biology, 519–537 (Springer US, Boston, MA, 1976). doi:10.1007/978-1-4757-0964-3_21.

36. Duysens, J. *How deletions in a model could help explain deletions in the laboratory. Journal of Neurophysiology* **95,** 562–565. doi:10.1152/jn.00888.2005 (2006).

37. Duysens, J., De Groote, F. & Jonkers, I. The flexion synergy, mother of all synergies and father of new models of gait. *Frontiers in Computational Neuroscience* **7.** doi:10.3389/fncom.2013.00014 (2013).

38. Hägglund, M. *et al.* Optogenetic dissection reveals multiple rhythmogenic modules underlying locomotion. *Proceedings of the National Academy of Sciences* **110,** 11589–11594. doi:10.1073/pnas.1304365110 (2013).

39. Ausborn, J., Snyder, A. C., Shevtsova, N. A., Rybak, I. A. & Rubin, J. E. State-dependent rhythmogenesis and frequency control in a half-center locomotor CPG. *Journal of Neurophysiology* **119,** 96–117. doi:10.1152/jn.00550.2017 (2018).

40. Roberts. How neurons generate behaviour in a hatchling amphibian tadpole: an outline. *Frontiers in Behavioral Neuroscience.* doi:10.3389/fnbeh.2010.00016 (2010).

41. Ampatzis, K., Song, J., Ausborn, J. & El Manira, A. Separate Microcircuit Modules of Distinct V2a Interneurons and Motoneurons Control the Speed of Locomotion. *Neuron* **83,** 934–943. doi:10.1016/j.neuron.2014.07.018 (2014).

42. Ausborn, J., Shevtsova, N. A., Caggiano, V., Danner, S. M. & Rybak, I. A. Computational modeling of brainstem circuits controlling locomotor frequency and gait. *eLife* **8,** e43587. doi:10.7554/eLife.43587 (2019).

43. Higashijima, S.-i., Masino, M. A., Mandel, G. & Fetcho, J. R. Engrailed-1 Expression Marks a Primitive Class of Inhibitory Spinal Interneuron. *The Journal of Neuroscience* **24,** 5827–5839. doi:10.1523/JNEUROSCI.5342-03.2004 (2004).

44. Kyriakatos, A. *et al.* Initiation of Locomotion in Adult Zebrafish. *Journal of Neuroscience* **31,** 8422–8431. doi:10.1523/JNEUROSCI.1012-11.2011 (2011).

45. Ampatzis, K., Song, J., Ausborn, J. & El Manira, A. Pattern of Innervation and Recruitment of Different Classes of Motoneurons in Adult Zebrafish. *Journal of Neuroscience* **33,** 10875–10886. doi:10.1523/JNEUROSCI.0896-13.2013 (2013).

46. Shimizu, S. *et al.* Spatially ordered recruitment of fast muscles in accordance with movement strengths in larval zebrafish. *Zoological Letters* **11,** 1. doi:10.1186/s40851-024-00247-8 (2025).

47. McLean, D. L., Fan, J., Higashijima, S.-i., Hale, M. E. & Fetcho, J. R. A topographic map of recruitment in spinal cord. *Nature* **446,** 71–75. doi:10.1038/nature05588 (2007).

48. Henneman, E., Somjen, G. & Carpenter, D. O. FUNCTIONAL SIGNIFICANCE OF CELL SIZE IN SPINAL MOTONEURONS. *Journal of Neurophysiology* **28,** 560–580. doi:10.1152/jn.1965.28.3.560 (1965).

49. Zajac, F. E. & Faden, J. S. Relationship among recruitment order, axonal conduction velocity, and muscle-unit properties of type-identified motor units in cat plantaris muscle. *Journal of Neurophysiology* **53,** 1303–1322. doi:10.1152/jn.1985.53.5.1303 (1985).

50. Hill, A. A. V. & Cattaert, D. Recruitment in a heterogeneous population of motor neurons that innervates the depressor muscle of the crayfish walking leg muscle. *The Journal of Experimental Biology* **211,** 613–629. doi:10.1242/jeb.006270 (Pt 4 2008).

51. Davis, W. J. Functional significance of motorneuron size and soma position in swimmeret system of the lobster. *Journal of Neurophysiology* **34,** 274–288. doi:10.1152/jn.1971.34.2.274 (1971).

52. Gabriel, J. P., Scharstein, H., Schmidt, J. & Büschges, A. Control of flexor motoneuron activity during single leg walking of the stick insect on an electronically controlled treadwheel. *Journal of Neurobiology* **56,** 237–251. doi:10.1002/neu.10237 (2003).

53. McLean, D. L., Masino, M. A., Koh, I. Y. Y., Lindquist, W. B. & Fetcho, J. R. Continuous shifts in the active set of spinal interneurons during changes in locomotor speed. *Nature Neuroscience* **11,** 1419–1429. doi:10.1038/nn.2225 (2008).

54. Hale, M. E., Ritter, D. A. & Fetcho, J. R. A confocal study of spinal interneurons in living larval zebrafish. *The Journal of Comparative Neurology* **437,** 1–16. doi:10.1002/cne.1266 (2001).

55. Thorsen, D. H., Cassidy, J. J. & Hale, M. E. Swimming of larval zebrafish: fin–axis coordination and implications for function and neural control. *Journal of Experimental Biology* **207,** 4175–4183. doi:10.1242/jeb.01285 (2004).

56. Fan, J. & Hale, M. E. *Excitatory descending spinal interneurons influence the degree of axial bending during startles of larval zebrafish.* in. Soc Neurosci Abstr 31:751.14. (2005).

57. Bhatt, D. H., McLean, D. L., Hale, M. E. & Fetcho, J. R. Grading movement strength by changes in firing intensity versus recruitment of spinal interneurons. *Neuron* **53,** 91–102. doi:10.1016/j.neuron.2006.11.011 (2007).

58. McLean, D. L. & Fetcho, J. R. Spinal Interneurons Differentiate Sequentially from Those Driving the Fastest Swimming Movements in Larval Zebrafish to Those Driving the Slowest Ones. *The Journal of Neuroscience* **29,** 13566–13577. doi:10.1523/JNEUROSCI.3277-09.2009 (2009).

59. Berg, E. M., Björnfors, E. R., Pallucchi, I., Picton, L. D. & El Manira, A. Principles Governing Locomotion in Vertebrates: Lessons From Zebrafish. *Frontiers in Neural Circuits* **12,** 73. doi:10.3389/fncir.2018.00073 (2018).

60. Skinner, R. & Garcia-Rill, E. The mesencephalic locomotor region (MLR) in the rat. *Brain Research* **323,** 385–389. doi:10.1016/0006-8993(84)90319-6 (1984).

61. Lee, A. M. *et al.* Identification of a Brainstem Circuit Regulating Visual Cortical State in Parallel with Locomotion. *Neuron* **83,** 455–466. doi:10.1016/j.neuron.2014.06.031 (2014).

62. Roseberry, T. K. *et al.* Cell-Type-Specific Control of Brainstem Locomotor Circuits by Basal Ganglia. *Cell* **164,** 526–537. doi:10.1016/j.cell.2015.12.037 (2016).

63. Marlinsky, V. & Voitenko, L. The effect of procaine injection into the medullary reticular formation on forelimb muscle activity evoked by mesencephalic locomotor region and vestibular stimulation in the decerebrated guinea-pig. *Neuroscience* **45,** 753–759. doi:10.1016/0306-4522(91)90287-X (1991).

64. Musienko, P., Zelenin, P., Lyalka, V., Orlovsky, G. & Deliagina, T. Postural performance in decerebrated rabbit. *Behavioural Brain Research* **190,** 124–134. doi:10.1016/j.bbr.2008.02.011 (2008).

65. Gay, M. *et al.* Anatomo-Functional Mapping of the Primate Mesencephalic Locomotor Region Using Stereotactic Lesions. *Movement Disorders* **35,** 789–799. doi:10.1002/mds.27983 (2020).

66. Karachi, C. *et al.* Cholinergic mesencephalic neurons are involved in gait and postural disorders in Parkinson disease. *Journal of Clinical Investigation* **120,** 2745–2754. doi:10.1172/JCI42642 (2010).

67. Rolland, A.-S., Karachi, C., Muriel, M.-P., Hirsch, E. C. & François, C. Internal pallidum and substantia nigra control different parts of the mesopontine reticular formation in primate: Descending Basal Ganglia Pathways. *Movement Disorders* **26,** 1648–1656. doi:10.1002/mds.23705 (2011).

68. Sirota, M. G., Di Prisco, G. V. & Dubuc, R. Stimulation of the mesencephalic locomotor region elicits controlled swimming in semi-intact lampreys: Brainstem-induced swimming. *European Journal of Neuroscience* **12,** 4081–4092. doi:10.1046/j.1460-9568.2000.00301.x (2000).

69. Cabelguen, J.-M., Bourcier-Lucas, C. & Dubuc, R. Bimodal Locomotion Elicited by Electrical Stimulation of the Midbrain in the Salamander *Notophthalmus viridescens*. *The Journal of Neuroscience* **23,** 2434–2439. doi:10.1523/JNEUROSCI.23-06-02434.2003 (2003).

70. Bernau, N. A., Puzdrowki, R. L. & Leonard, R. B. Identification of the midbrain locomotor region and its relation to descending locomotor pathways in the Atlantic stingray,Dasyatis sabina. *Brain Research* **557,** 83–94. doi:10.1016/0006-8993(91)90119-G (1991).

71. Fetcho, J. R. The Spinal Motor System in Early Vertebrates and Some of Its Evolutionary Changes. *Brain, Behavior and Evolution* **40,** 82–97. doi:10.1159/000113905 (1992).

72. Fetcho, J. R. & Svoboda, K. R. Fictive swimming elicited by electrical stimulation of the midbrain in goldfish. *Journal of Neurophysiology* **70,** 765–780. doi:10.1152/jn.1993.70.2.765 (1993).

73. Kashin, S., Feldman, A. & Orlovsky, G. Locomotion of fish evoked by electrical stimulation of the brain. *Brain Research* **82,** 41–47. doi:10.1016/0006-8993(74)90891-9 (1974).

74. Carbo-Tano, M. *et al.* The mesencephalic locomotor region recruits V2a reticulospinal neurons to drive forward locomotion in larval zebrafish. *Nature Neuroscience*. doi:10.1038/s41593-023-01418-0 (2023).

75. Shik, M. L. & Orlovsky, G. N. Neurophysiology of locomotor automatism. *Physiological Reviews* **56,** 465–501. doi:10.1152/physrev.1976.56.3.465 (1976).

76. Ryczko, D., Auclair, F., Cabelguen, J.-M. & Dubuc, R. The mesencephalic locomotor region sends a bilateral glutamatergic drive to hindbrain reticulospinal neurons in a tetrapod. *Journal of Comparative Neurology* **524,** 1361–1383. doi:10.1002/cne.23911 (2016).

77. Jordan, L. M. Initiation of Locomotion in Mammals. *Annals of the New York Academy of Sciences* **860,** 83–93. doi:10.1111/j.1749-6632.1998.tb09040.x (1998).

78. Ray, D. L., Juvin, L., Boutin, T., Auclair, F. & Dubuc, R. A neuronal substrate for a state-dependent modulation of sensory inputs in the brainstem: MLR-induced depression of sensory inputs. *European Journal of Neuroscience* **32,** 53–59. doi:10.1111/j.1460-9568.2010.07276.x (2010).

79. Smetana, R. W., Alford, S. & Dubuc, R. Muscarinic Receptor Activation Elicits Sustained, Recurring Depolarizations in Reticulospinal Neurons. *Journal of Neurophysiology* **97,** 3181–3192. doi:10.1152/jn.00954.2006 (2007).

80. Smetana, R., Juvin, L., Dubuc, R. & Alford, S. A parallel cholinergic brainstem pathway for enhancing locomotor drive. *Nature Neuroscience* **13,** 731–738. doi:10.1038/nn.2548 (2010).

81. Sinnamon, H. M. Preoptic and hypothalamic neurons and the initiation of locomotion in the anesthetized rat. *Progress in Neurobiology* **41,** 323–344. doi:10.1016/0301-0082(93)90003-B (1993).

82. Zhao, S. *et al.* Cell type–specific channelrhodopsin-2 transgenic mice for optogenetic dissection of neural circuitry function. *Nature Methods* **8,** 745–752. doi:10.1038/nmeth.1668 (2011).

83. Caggiano, V. *et al.* Midbrain circuits that set locomotor speed and gait selection. *Nature* **553,** 455–460. doi:10.1038/nature25448 (2018).

84. Josset, N. *et al.* Distinct Contributions of Mesencephalic Locomotor Region Nuclei to Locomotor Control in the Freely Behaving Mouse. *Current Biology* **28,** 884–901.e3. doi:10.1016/j.cub.2018.02.007 (2018).

85. Stecina, K. Midbrain stimulation-evoked lumbar spinal activity in the adult decerebrate mouse. *Journal of Neuroscience Methods* **288,** 99–105. doi:10.1016/j.jneumeth.2017.06.015 (2017).

86. Capelli, P., Pivetta, C., Soledad Esposito, M. & Arber, S. Locomotor speed control circuits in the caudal brainstem. *Nature.* doi:10.1038/nature24064 (2017).

87. Goñi-Erro, H., Selvan, R., Caggiano, V., Leiras, R. & Kiehn, O. Pedunculopontine Chx10+ neurons control global motor arrest in mice. *Nature Neuroscience.* doi:10.1038/s41593-023-01396-3 (2023).

88. Takakusaki, K., Chiba, R., Nozu, T. & Okumura, T. Brainstem control of locomotion and muscle tone with special reference to the role of the mesopontine tegmentum and medullary reticulospinal systems. *Journal of Neural Transmission* **123,** 695–729. doi:10.1007/s00702-015-1475-4 (2016).

89. Fadok, J. P., Markovic, M., Tovote, P. & Lüthi, A. New perspectives on central amygdala function. *Current Opinion in Neurobiology* **49,** 141–147. doi:10.1016/j.conb.2018.02.009 (2018).

90. Fanselow, M. S. Neural organization of the defensive behavior system responsible for fear. *Psychonomic Bulletin & Review* **1,** 429–438. doi:10.3758/BF03210947 (1994).

91. Tovote, P. *et al.* Midbrain circuits for defensive behaviour. *Nature* **534,** 206–212. doi:10.1038/nature17996 (2016).

92. Mangold, S. A. & M Das, J. in *Neuroanatomy, Reticular Formation* (StatPearls Publishing, Treasure Island (FL), 2024).

93. Brownstone, R. M. & Chopek, J. W. Reticulospinal Systems for Tuning Motor Commands. *Frontiers in Neural Circuits* **12,** 30. doi:10.3389/fncir.2018.00030 (2018).

94. Greene, R. W. & Carpenter, D. O. Actions of neurotransmitters on pontine medical reticular formation neurons of the cat. *Journal of Neurophysiology* **54,** 520–531. doi:10.1152/jn.1985.54.3.520 (1985).

95. Peterson, B. W. in *Brainstem Control of Spinal Cord Function* (ed Barnes, C. D.) 27–86 (Academic Press, New York, NY, 1984).

96. Noga, B. R., Kriellaars, D. J., Brownstone, R. M. & Jordan, L. M. Mechanism for Activation of Locomotor Centers in the Spinal Cord by Stimulation of the Mesencephalic Locomotor Region. *Journal of Neurophysiology* **90,** 1464–1478. doi:10.1152/jn.00034.2003 (2003).

97. Du Beau, A. *et al.* Neurotransmitter phenotypes of descending systems in the rat lumbar spinal cord. *Neuroscience* **227,** 67–79. doi:10.1016/j.neuroscience.2012.09.037 (2012).

98. Mitchell, E. J., McCallum, S., Dewar, D. & Maxwell, D. J. Corticospinal and Reticulospinal Contacts on Cervical Commissural and Long Descending Propriospinal Neurons in the Adult Rat Spinal Cord; Evidence for Powerful Reticulospinal Connections. *PLOS ONE* **11** (ed Sugihara, I.) e0152094. doi:10.1371/journal.pone.0152094 (2016).

99. Shapovalov, A. I. Evolution of neuronal systems of suprasegmental motor control. *Neurophysiology* **4,** 346–359. doi:10.1007/BF01063005 (1973).

100. Kupfermann, I. & Weiss, K. R. The command neuron concept. *Behavioral and Brain Sciences* **1,** 3–10. doi:10.1017/S0140525X00059057 (1978).

101. Kimmel, C. B., Powell, S. L. & Metcalfe, W. K. Brain neurons which project to the spinal cord in young larvae of the zebrafish. *Journal of Comparative Neurology* **205,** 112–127. doi:10.1002/cne.902050203 (1982).

102. Sillar, K., Picton, L. & Heitler, W. *The Neuroethology of Predation and Escape.* 1st ed. (Wiley-Blackwell, Oxford, 2016).

103. Hildebrand, D. G. C. *et al.* Whole-brain serial-section electron microscopy in larval zebrafish. *Nature* **545,** 345–349. doi:10.1038/nature22356 (2017).

104. Fetcho, J. & Faber, D. Identification of motoneurons and interneurons in the spinal network for escapes initiated by the mauthner cell in goldfish. *The Journal of Neuroscience* **8,** 4192–4213. doi:10.1523/JNEUROSCI.08-11-04192.1988 (1988).

105. Faber, D. S., Fetcho, J. R. & Korn, H. Neuronal Networks Underlying the Escape Response in Goldfish: General Implications for Motor Control[a]. *Annals of the New York Academy of Sciences* **563,** 11–33. doi:10.1111/j.1749-6632.1989.tb42187.x (1989).

106. Fetcho, J. R. Spinal Network of the Mauthner Cell (Part 2 of 2). *Brain, Behavior and Evolution* **37,** 307–316. doi:10.1159/000316094 (1991).

107. Yasargil, G. M. & Sandri, C. Topography and ultrastructure of commissural interneurons that may establish reciprocal inhibitory connections of the Mauthner axons in the spinal cord of the tench,Tinca tinca L. *Journal of Neurocytology* **19,** 111–126. doi:10.1007/BF01188443 (1990).

108. Nissanov, J., Eaton, R. C. & DiDomenico, R. The motor output of the Mauthner cell, a reticulospinal command neuron. *Brain Research* **517,** 88–98. doi:10.1016/0006-8993(90)91012-6 (1990).

109. O'Malley, D. M., Kao, Y.-H. & Fetcho, J. R. Imaging the Functional Organization of Zebrafish Hindbrain Segments during Escape Behaviors. *Neuron* **17,** 1145–1155. doi:10.1016/S0896-6273(00)80246-9 (1996).

110. Eaton, R., Lee, R. & Foreman, M. The Mauthner cell and other identified neurons of the brainstem escape network of fish. *Progress in Neurobiology* **63,** 467–485. doi:10.1016/S0301-0082(00)00047-2 (2001).

111. Brocard, F. & Dubuc, R. Differential Contribution of Reticulospinal Cells to the Control of Locomotion Induced By the Mesencephalic Locomotor Region. *Journal of Neurophysiology* **90,** 1714–1727. doi:10.1152/jn.00202.2003 (2003).

112. Deliagina, T., Beloozerova, I., Zelenin, P. & Orlovsky, G. Spinal and supraspinal postural networks. *Brain Research Reviews* **57,** 212–221. doi:10.1016/j.brainresrev.2007.06.017 (2008).

113. Juvin, L. *et al.* A Specific Population of Reticulospinal Neurons Controls the Termination of Locomotion. *Cell Reports* **15,** 2377–2386. doi:10.1016/j.celrep.2016.05.029 (2016).

114. Bouvier, J. *et al.* Descending Command Neurons in the Brainstem that Halt Locomotion. *Cell* **163,** 1191–1203. doi:10.1016/j.cell.2015.10.074 (2015).

115. Ruder, L. *et al.* A functional map for diverse forelimb actions within brainstem circuitry. *Nature* **590,** 445–450. doi:10.1038/s41586-020-03080-z (2021).

116. Braun, J., Hurtak, F., Wang-Chen, S. & Ramdya, P. Descending networks transform command signals into population motor control. *Nature* **630,** 686–694. doi:10.1038/s41586-024-07523-9 (2024).

117. Engeszer, R. E., Patterson, L. B., Rao, A. A. & Parichy, D. M. Zebrafish in The Wild: A Review of Natural History And New Notes from The Field. *Zebrafish* **4,** 21–40. doi:10.1089/zeb.2006.9997 (2007).

118. Roosen-Runge, E. C. ON THE EARLY DEVELOPMENT—BIPOLAR DIFFERENTIATION AND CLEAVAGE—OF THE ZEBRA FISH, BRACHYDANIO RERIO. *The Biological Bulletin* **75,** 119–133. doi:10.2307/1537678 (1938).

119. Ahrens, M. B. *et al.* Brain-wide neuronal dynamics during motor adaptation in zebrafish. *Nature* **485,** 471–477. doi:10.1038/nature11057 (2012).

120. Orger, M. B. The Cellular Organization of Zebrafish Visuomotor Circuits. *Current Biology* **26,** R377–R385. doi:10.1016/j.cub.2016.03.054 (2016).

121. Budick, S. A. & O'Malley, D. M. Locomotor Repertoire of The Larval Zebrafish: Swimming, Turning and Prey Capture. *Journal of Experimental Biology* **203,** 2565–2579. doi:10.1242/jeb.203.17.2565 (2000).

122. Marques, J. C., Lackner, S., Félix, R. & Orger, M. B. Structure of the Zebrafish Locomotor Repertoire Revealed with Unsupervised Behavioral Clustering. *Current Biology* **28,** 181–195.e5. doi:10.1016/j.cub.2017.12.002 (2018).

123. Mearns, D. S., Donovan, J. C., Fernandes, A. M., Semmelhack, J. L. & Baier, H. Deconstructing Hunting Behavior Reveals a Tightly Coupled Stimulus-Response Loop. *Current Biology* **30,** 54–69.e9. doi:10.1016/j.cub.2019.11.022 (2020).

124. Zelenin, P. V. Activity of individual reticulospinal neurons during different forms of locomotion in the lamprey. *The European Journal of Neuroscience* **22,** 2271–2282. doi:10.1111/j.1460-9568.2005.04395.x (2005).

125. Korn, H. & Faber, D. S. The Mauthner Cell Half a Century Later: A Neurobiological Model for Decision-Making? *Neuron* **47,** 13–28. doi:10.1016/j.neuron.2005.05.019 (2005).

126. Deliagina, T. G., Zelenin, P. V. & Orlovsky, G. N. Encoding and decoding of reticulospinal commands. *Brain Research. Brain Research Reviews* **40,** 166–177. doi:10.1016/s0165-0173(02)00199-6 (2002).

127. Higashijima, S.-I., Mandel, G. & Fetcho, J. R. Distribution of prospective glutamatergic, glycinergic, and GABAergic neurons in embryonic and larval zebrafish. *Journal of Comparative Neurology* **480,** 1–18. doi:10.1002/cne.20278 (2004).

128. Kinkhabwala, A. *et al.* A structural and functional ground plan for neurons in the hindbrain of zebrafish. *Proceedings of the National Academy of Sciences* **108,** 1164–1169. doi:10.1073/pnas.1012185108 (2011).

129. Kimura, Y. *et al.* Hindbrain V2a Neurons in the Excitation of Spinal Locomotor Circuits during Zebrafish Swimming. *Current Biology* **23,** 843–849. doi:10.1016/j.cub.2013.03.066 (2013).

130. Severi, K. E., Böhm, U. L. & Wyart, C. Investigation of hindbrain activity during active locomotion reveals inhibitory neurons involved in sensorimotor processing. *Scientific Reports* **8.** doi:10.1038/s41598-018-31968-4 (2018).

131. Rajan, G. *et al.* Evolutionary divergence of locomotion in two related vertebrate species. *Cell Reports* **38,** 110585. doi:10.1016/j.celrep.2022.110585 (2022).

132. Ritson, E. J. & Li, W.-C. The neuronal mechanisms underlying locomotion termination. *Current Opinion in Physiology* **8,** 109–115. doi:10.1016/j.cophys.2019.01.009 (2019).

133. Eaton, R. C., Bombardieri, R. A. & Meyer, D. L. The mauthner-initiated startle response in teleost fish. *Journal of Experimental Biology* **66,** 65–81. doi:10.1242/jeb.66.1.65 (1977).

134. Hecker, A., Schulze, W., Oster, J., Richter, D. O. & Schuster, S. Removing a single neuron in a vertebrate brain forever abolishes an essential behavior. *Proceedings of the National Academy of Sciences* **117,** 3254–3260. doi:10.1073/pnas.1918578117 (2020).

135. Liu, Y.-C. & Hale, M. E. Local Spinal Cord Circuits and Bilateral Mauthner Cell Activity Function Together to Drive Alternative Startle Behaviors. *Current Biology* **27,** 697–704. doi:10.1016/j.cub.2017.01.019 (2017).

136. Nakayama, H. & Oda, Y. Common sensory inputs and differential excitability of segmentally homologous reticulospinal neurons in the hindbrain. *The Journal of Neuroscience: The Official Journal of the Society for Neuroscience* **24,** 3199–3209. doi:10.1523/JNEUROSCI.4419-03.2004 (2004).

137. Eaton, R. C., Lavender, W. A. & Wieland, C. M. Alternative neural pathways initiate fast-start responses following lesions of the mauthner neuron in goldfish. *Journal of Comparative Physiology ? A* **145,** 485–496. doi:10.1007/BF00612814 (1982).

138. DiDomenico, R., Nissanov, J. & Eaton, R. C. Lateralization and adaptation of a continuously variable behavior following lesions of a reticulospinal command neuron. *Brain Research* **473,** 15–28. doi:10.1016/0006-8993(88)90310-1 (1988).

139. Foreman, M. & Eaton, R. The direction change concept for reticulospinal control of goldfish escape. *The Journal of Neuroscience* **13,** 4101–4113. doi:10.1523/JNEUROSCI.13-10-04101.1993 (1993).

140. Fetcho, J. R. & O'Malley, D. M. Visualization of active neural circuitry in the spinal cord of intact zebrafish. *Journal of Neurophysiology* **73,** 399–406. doi:10.1152/jn.1995.73.1.399 (1995).

141. Liu, K. S. & Fetcho, J. R. Laser Ablations Reveal Functional Relationships of Segmental Hindbrain Neurons in Zebrafish. *Neuron* **23,** 325–335. doi:10.1016/S0896-6273(00)80783-7 (1999).

142. Orger, M. B., Kampff, A. R., Severi, K. E., Bollmann, J. H. & Engert, F. Control of visually guided behavior by distinct populations of spinal projection neurons. *Nature Neuroscience* **11,** 327–333. doi:10.1038/nn2048 (2008).

143. Huang, K.-H., Ahrens, M. B., Dunn, T. W. & Engert, F. Spinal Projection Neurons Control Turning Behaviors in Zebrafish. *Current Biology* **23,** 1566–1573. doi:10.1016/j.cub.2013.06.044 (2013).

144. Bouchard, M. B. *et al.* Swept confocally-aligned planar excitation (SCAPE) microscopy for high-speed volumetric imaging of behaving organisms. *Nature Photonics* **9,** 113–119. doi:10.1038/nphoton.2014.323 (2015).

145. Voleti, V. *et al.* Real-time volumetric microscopy of in vivo dynamics and large-scale samples with SCAPE 2.0. *Nature Methods* **16,** 1054–1062. doi:10.1038/s41592-019-0579-4 (2019).

146. Dunn, T. W. *et al.* Brain-wide mapping of neural activity controlling zebrafish exploratory locomotion. *eLife* **5.** doi:10.7554/eLife.12741 (2016).

147. Severi, K. E. *et al.* Neural Control and Modulation of Swimming Speed in the Larval Zebrafish. *Neuron* **83,** 692–707. doi:10.1016/j.neuron.2014.06.032 (2014).

148. Thiele, T. R., Donovan, J. C. & Baier, H. Descending Control of Swim Posture by a Midbrain Nucleus in Zebrafish. *Neuron* **83,** 679–691. doi:10.1016/j.neuron.2014.04.018 (2014).

149. Berg, E. M. *et al.* Brainstem circuits encoding start, speed, and duration of swimming in adult zebrafish. *Neuron* **111,** 372–386.e4. doi:10.1016/j.neuron.2022.10.034 (2023).

150. Sankrithi, N. & O'Malley, D. Activation of a multisensory, multifunctional nucleus in the zebrafish midbrain during diverse locomotor behaviors. *Neuroscience* **166,** 970–993. doi:10.1016/j.neuroscience.2010.01.003 (2010).

151. Pujala, A. & Koyama, M. Chronology-based architecture of descending circuits that underlie the development of locomotor repertoire after birth. *eLife* **8,** e42135. doi:10.7554/eLife.42135 (2019).

152. Gahtan, E., Sankrithi, N., Campos, J. B. & O'Malley, D. M. Evidence for a Widespread Brain Stem Escape Network in Larval Zebrafish. *Journal of Neurophysiology* **87,** 608–614. doi:10.1152/jn.00596.2001 (2002).

153. Sugioka, T., Tanimoto, M. & Higashijima, S.-i. Biomechanics and neural circuits for vestibular-induced fine postural control in larval zebrafish. *Nature Communications* **14,** 1217. doi:10.1038/s41467-023-36682-y (2023).

154. Zhu, Y. *et al. A brainstem circuit for gravity-guided vertical navigation* 2024. doi:10.1101/2024.03.12.584680.

155. Siegel, J. M. Behavioral functions of the reticular formation. *Brain Research Reviews* **1,** 69–105. doi:10.1016/0165-0173(79)90017-1 (1979).

156. Gahtan, E. Visual Prey Capture in Larval Zebrafish Is Controlled by Identified Reticulospinal Neurons Downstream of the Tectum. *Journal of Neuroscience* **25,** 9294–9303. doi:10.1523/JNEUROSCI.2678-05.2005 (2005).

157. Koyama, M. *et al.* A circuit motif in the zebrafish hindbrain for a two alternative behavioral choice to turn left or right. *eLife* **5,** e16808. doi:10.7554/eLife.16808 (2016).

158. Dunn, T. W. *et al.* Neural Circuits Underlying Visually Evoked Escapes in Larval Zebrafish. *Neuron* **89,** 613–628. doi:10.1016/j.neuron.2015.12.021 (2016).

Chapter 2

Gait switching behaviour during the optomotor response in larval zebrafish

*Animals deploy a variety of gaits to navigate their environment. Larval zebrafish move in distinct episodes of locomotion called bouts. A recent study identified that larval zebrafish perform 13 different bout types across different behavioural contexts, such as escapes, exploration or hunting. In the context of forward swimming, larval zebrafish perform slow and fast/burst swims, which occur spontaneously during exploration and can be elicited by visual stimuli. In the optomotor response (**OMR**), moving gratings from the tail to head cause the fish to orient in the direction of the grating and match its speed. In accordance with previous studies [1] and utilising novel bout classification algorithms [2], I confirmed that slow gratings elicit Slow1 and Slow2 bouts, whereas fast gratings drive Slow2 and an increasing number of fast/burst swims. Even during fast grating speeds, fish are more likely to commence with a Slow2 swim before switching to sustained trains of fast/burst swims. In preparation for subsequent imaging experiments, I adapted this assay to a head-restrained, tail-free preparation. Utilising a closed-loop system and high-resolution online tracking, it was revealed that head-restrained fish are still able to perform slow and fast swims in the OMR. Head-restrained fish show differences in bouts kinematics to freely-swimming fish, with longer movements that included switches in frequency within a single bout. I contributed to developing and testing a toolbox that includes a novel bout decomposition method, Megabouts [3], to decompose bouts into smaller locomotor motifs, matching slow swims, fast swims, struggles/escapes and turns. In summary, this chapter demonstrates the usefulness of detailed locomotor analyses to describe gait switching behaviour in both freely-swimming and head-restrained fish.*

2.1 Introduction

Animals use a variety of locomotor gaits and different speeds to navigate their environment. They achieve this by dynamically generating appropriate motor commands, based on sensory information and past experience. To accurately describe and quantify behaviour, it is useful to decompose behaviours into smaller movement motifs. Larval zebrafish are ideally suited to study movement composition within behavioural sequences. At one week old, larval zebrafish move in distinct, temporally segregated swim events called bouts. Swimming occurs in a 'burst-and-glide' fashion, where fish propel themselves forward in short bursts of tail movement followed by passive periods of gliding [4]. One recent study identified 13 different bout types, which contribute to behaviours such as prey capture, escapes and forward-swimming and occur naturally or can be elicited by a variety of visual and auditory stimuli [2].

For instance, in the optomotor response (**OMR**), fish turn and swim in the direction of perceived motion when presented with whole-field moving gratings [5, 6]. A study by Severi *et al.* [1] investigating the neural control of speed in larval zebrafish found that OMR gratings could elicit slow and fast bouts in response to slow and fast gratings, respectively. The two bout types can be distinguished based on several kinematic parameters, most significantly maximum tail-beat frequency, head yaw (angular displacement of head during successive side-to-side bends of a swim bout) and rostral tail bend amplitude. Except for tail-beat frequency within fast bouts, which increases as a function of grating speed, these kinematic parameters remain stable across different grating speeds [1]. Fish gradually switch from predominantly utilising slow swims to fast swims as grating speed increases (around 10 mm/s). In addition, larval zebrafish utilise their pectoral fins in different manners depending on the bout type involved. During slow swims, the pectoral fins undulate in a symmetric fashion, whereas during fast swims, they are tucked against the body [7, 8]. Together, these results argue for distinct locomotor gaits employed flexibly to adapt to changes in the environment.

However, are different swim bouts truly stereotyped or do they merely reflect extremes along a behavioural continuum [9–13]? One recent study explored these

questions by deconstructing the hunting sequence of larval zebrafish [13]. Using unsupervised methods, Mearns *et al.* argued that swim bouts of larval zebrafish lie on a low dimensional behavioural continuum. The behavioural space could be clustered to reveal broad bout types matching previous reports [2, 4, 14]. For instance, stereotyped hunting sequences were achieved by chaining together flexible movement motifs and maintained through tight stimulus-response loops [13]. One approach to answering the question of whether different types of swims are distinct gaits or merely extremes along a continuum involves the delineation of their neural correlates. Are slow and fast swims controlled by distinct brainstem circuits, as is the case for turns [15] vs escapes [16], or by a modulation of the same supraspinal structures [1]? What is lacking to address these questions in an awake, behaving animal is a suitable head-fixed paradigm for gait-switching behaviour in forward swimming, which would open up possibilities for imaging studies.

Here, I first set out to recapitulate forward swimming and gait transition experiments in larval zebrafish in freely-swimming conditions. To elicit different types of forward swims, fish were placed in a circular arena and presented with moving gratings at a range of speeds. Using a recently published unsupervised bout classification method [2], revealed a transition from Slow1 to Slow2 to fast/burst swims as a function of grating speed, matching previous reports [1].

To reliably record neuronal activity in behaving animals at high spatial and temporal resolution, fish are often placed in a head-embedded, tail-free preparation. However, it has been challenging to elicit fast/burst swims in head-fixed fish [1]. I adapted the behavioural assay from freely-swimming fish to a head-embedded, tail-free preparation that can be combined with calcium imaging. To simulate natural visual feedback, I introduced a 'virtual reality' closed-loop system. Head-fixed fish showed differences in bout kinematics from freely swimming fish, with longer movements that included switches in frequency within a single bout. Given that information on the trajectory of the animal is not available in head-restrained conditions, I utilised two methods to analyse head-fixed swimming kinematics. In the first, bouts were decomposed into half-beats, which were labelled as slow, fast or struggle according to known kinematic parameters from

freely-swimming data. In the second one, named *Megabouts*, a dictionary of different locomotor motifs (slow swims, fast swims, struggles and turns) was created using convolutional sparse coding [3]. In contrast to ballistic movements during freely-swimming conditions, multiple behavioural motifs can be active within a given bout. Moving gratings at different speeds elicited different types of forward swimming in head-fixed fish, including slow, fast, mixed swims and occasional struggles. Slow gratings predominantly elicited slow swimming, with increasing periods of fast swimming at fast grating speeds, matching freely-swimming conditions. Combined with calcium imaging, the head-restrained assay and novel behavioural analysis enable future experiments to identify the neural correlates of different swim bouts.

2.2 Materials and Methods

2.2.1 Fish husbandry

Adult fish were raised and bred at 28°C on a 14h light / 10h dark cycle following standard husbandry methods as detailed in [17]. All fish colonies were maintained by importing wild types every 1-3 years and line-specific breeding schemes designed to reduce inbreeding depression [17]. Embryos were collected and larvae were raised at 28°C in E3 embryo medium (5 mM NaCl, 0.17 mM KCl, 0.33 mM CaCl2 and 0.33 mM MgSO4, changed daily) at a density of 60 larvae per 200mL until behavioural testing at 6-8 dpf. From 5 dpf onwards, approximately 10mL of a live L-type rotifer *Brachionus plicatilis* polyculture (containing 1000-2000 rotifers per mL) were added to each dish twice a day and larvae were allowed to feed freely. Behavioural experiments were conducted using the wild-type line Tübingen (**Tu**) between 6 and 7 days post fertilisation (**dpf**). Zebrafish do not sexually differentiate until approximately 3 months of age, therefore the sex of the animals cannot be reported. All experimental procedures were approved by the Champalimaud Foundation Ethics Committee and the Portuguese Direcção Geral Veterinária, and were performed according to the European Directive 2010/63/EU.

2.2.2 Freely-swimming behavioural assay

Setup Experiments were conducted on a custom-built behavioural set up [3]. Arenas were milled from acrylic and polished using a CNC machine (Núcleo de Oficinas, Instituto Superior Técnico). Each circular arena had a diameter of 50 mm with a graded slope towards a maximum depth of 4 mm, produced by a progressive bevel with a radius of curvature of 11 mm. Each larva was recorded for 45 minutes using a high-speed camera (EoSens® CL 1362, Mikrotron) fitted with a fixed focal length lens (86-207, f = 16 mm, Edmund Optics) and an infrared long-pass filter (#LP780-37, 780 nm, VisionLightTech) that blocked visible light. Camera images were acquired using a frame grabber (PCIe-1433, National Instruments). The camera was positioned above the arena, which was illuminated from below using a custom-built 100 x 100 mm LED-based diffusive backlight (64 LEDs at 850nm, TSHG6400, Vishay Semiconductor) controlled by a T-Cube LED Driver (LEDD1B, Thorlabs). Visual stimuli were projected onto a diffusive screen (Rosco Cinegel White Diffuser 3000) placed 5 mm below the arena via a cold mirror (64-452, Edmunds Optics) using a portable LED projector (ML750e, Optoma). Behaviour was recorded at 700 frames per second (**fps**) with a frame size of 948 x 948 pixels and a shutter time of 1.423 ms covering an area just larger than the arena, resulting in a resolution of 0.055 mm per pixel.

Behavioural tracking Acquisition was controlled using a custom software suite (SARDINE, Martins, Laborde and Orger, in prep.) written in C# and built using .NET 8 (.NET Foundation). The software tracks, in real-time, both eyes, the centre of mass and the tail curvature using 10 segments, starting at the swim bladder. The background of each image was subtracted before further processing. To calculate the background, the mode of each pixel was computed from 100 frames across several seconds while the fish was swimming. Contamination by the fish image can be prevented by using the mode rather than the mean, assuming that the fish is not present in most frames collected during that period. The background-subtracted image is smoothed by a large Gaussian kernel, revealing the fish location at the maximum value. From there, a flood-fill algorithm creates

a binarized image of the fish trunk. The moments of the binarized region are used to compute the principal axis. The relative position of the eye to the fish centroid is used to identify the fish heading direction. The mid-eye position is computed by finding the point on the principal axis with the maximal intensity summed along the orthogonal direction. An iterative arc-search algorithm is used to identify the tail. It tracks the fish skeleton by identifying subsequent key points along an arc of +/- 60°. Key points are localised by computing the weighted mean along the arc. The weight is assigned zero if it is below a given threshold or equal to the pixel value of the background-subtracted image. To track the fish in real-time, the algorithm leverages the fast frame rate by limiting the search to a region of interest around the fish position in the previous frame. In addition, full-frame operations are avoided. Rather, computations are performed locally, for instance by performing thresholding only on pixels along the arc rather than on the entire image.

Visual stimuli Before the start of the experiment, larvae were allowed to acclimatise in the arena for 15 minutes. During the experiment, black and white forward gratings moving at a range of speeds (15 speeds, 0 - 32.8 mm/s) were displayed below the arena for 20 seconds in a randomised order, with 5 repetitions each. The width of the stripes was adjusted to a 10 mm width at 5 mm distance to match previous studies [1, 3, 15]. Gratings were stationary for 10 seconds in-between trials, and forward direction was maintained by reorienting according to fish heading direction. Visual stimuli were displayed at 60 fps using a custom-written rendering engine using OpenTK and generated using OpenGL Shaders (A. Lucas Martins and Alexandre Laborde, unpublished).

2.2.3 Kinematic analysis of freely-swimming data

Bouts were detected and classified following an established method [2]. Together with colleagues, I refactored the code to build a modular toolbox for use in the lab.

Bout detection Briefly, to reliably detect bouts the change in tail curvature is computed. The raw tail angles are smoothed using a boxcar filter (3 segments, 10 frames), which minimises noise from individual tail segments during interbout intervals. The cumulative sum along the tail segments at each moment in time is computed. To minimise slow drifts in tail position, the minimum curvature measure from the previous 400 ms window is subtracted. To smooth out fluctuations owing to the periodic beating of the tail, a maximum filter with a 20 ms window is applied. To standardise across fish, for each fish the 80th percentile of this tail measure was used as a threshold to segment individual bouts. To segment true bouts, a minimum bout duration of 57 ms and a minimum interbout interval of 14 ms was set. The precise time points of the bout start and end are subsequently determined from the raw tail position data, ignoring the gliding period of the bout.

Bout classification From the tail curvature, different kinematic parameters such as minimum, maximum and mean tail-beat frequency, mean, maximum, and mean rostral and total tail-bend amplitude, number of half-beats and others were calculated. Paired with parameters such as bout duration, displacement, eye position, head yaw, and movement trajectory, this yielded a total of 240 kinematic parameters per bout. In the study by Marques *et al.* a 'bout map' was created containing a large (4 million) dataset of bouts [2]. Using density-valley clustering different bout classes were extracted. Bout types in this study were assigned using the k-nearest neighbour algorithm on the previously labelled data set 'bout map'.

2.2.4 Head-restrained behavioural assay

Setup Experiments were conducted on a custom-built behavioural set up using acrylic arenas, carved and polished using a CNC machine (Núcleo de Oficinas, Instituto Superior Técnico). Arenas were cylindrical with an inserted flattened cone made from Sylgard (SYLGARD 184 Silicone Elastomer Kit, The Dow Chemical Company), on which the larvae were mounted. Each larva was recorded for 45 minutes using a high-speed camera (EoSens® CL 1362, Mikrotron) fitted with an infrared long-pass filter (LP780-37, 780 nm, VisionLightTech) to block visi-

ble light and a lens (M30.5mm Edmund Optics) to optimally focus on the larva. The camera was positioned above the arena, which was illuminated from below using a mounted high-power infrared LED (M780L2, Thorlabs) and controlled by a T-Cube LED Driver (LEDD1B, Thorlabs). Using a portable LED projector (ML500, Optoma), visual stimuli were projected onto a diffusive screen (Rosco Cinegel White Diffuser 3000) placed below the arena via three cold mirrors (64-452, Edmunds Optics). The mirrors (one below, two laterally) were placed around the arena for 270°visual stimulation. Behaviour was recorded at 700 fps with a frame size of 500 x 400 pixels and a shutter time of 1.423 ms covering an area just larger than the fish, resulting in a resolution of 0.013 mm per pixel.

Mounting Larvae were embedded dorsally in low-melting point agarose (UltraPure LMP Agarose, Cat#16520100, Invitrogen by Life Technologies) the evening before, at least 1 hour after feeding, and their tails were freed by removing agarose in a square caudal to the swim bladder, allowing for maximum tail movement. The arena was filled with E3 embryo medium and larvae were allowed to recover and habituate overnight at 28°C.

Tracking Acquisition was controlled using a custom-built script in C# [18, 19]. Similarly to freely-swimming conditions, fish tracking is performed on background-subtracted images. The shape of each eye was found by performing a flood-fill of a thresholded area surrounding the eye, starting from a manually defined eye centre. The orientation of each eye in the horizontal plane was defined as the angle to the mid-axis of the fish. The tail was tracked in 16 segments in real-time using the iterative arc-search algorithm described in section 2.2.2.

Visual stimuli During the experiment, forward gratings moving at a range of speeds (15 speeds, 0 - 32.8 mm/s) were displayed for 20 seconds in a randomised order, with 5 repetitions each. Gratings were stationary for 10 seconds in-between trials. The width of the stripes was adjusted to 26 mm width at 13 mm distance, matching the ratio used in the freely-swimming assay (10 mm width at 5 mm distance). Grating speed was updated continuously in closed-loop. Velocity was

estimated by tracking 16 points along the tail and taking the cumulative sum of angular changes along the tail, convolved with an exponential filter, which empirically is proportional to forward velocity in freely swimming fish. This velocity was added to the grating with a fixed gain adjusted to a level that allows head-fixed larvae to match grating speed over a normal range (personal communication with Dr R. Félix, Champalimaud Foundation).

2.2.5 Kinematic analysis of head-embedded data using half-beat labelling

Pre-processing and bout detection The tail angle was smoothed using the Savitzky-Golay filter by applying the *savgol_filter* function from scipy. Then, I adapted the method described above and in [2] for 16 segments along the tail to create a hyper-smoothed tail trace. Using a box car filter, periods of tail activity were maximised while noise in interbout intervals was minimised. Using a threshold of minimum activity (5 a.u.), minimum inter-bout interval (28 ms) and bout duration (71 ms), allowed segmentation of bouts and yielded precise timings of bout start, bout end and interbout duration.

Half-beat detection To decompose bouts into half-beats, I utilised the Python package scipy *find_peaks* function on tail segments 6 and 10. The following parameters were chosen after careful evaluation: a minimum distance of 5 frames (7.1 ms) and a prominence threshold of 0.03 and 0.2 for tail segments 6 and 10, respectively. Calculating kinematic parameters, such as tail-bend amplitude, in a caudal and rostral segment for the same half-beat is challenging due to the peaks occurring shifted in time. While a time shift is not an issue *per se* in the middle of the bout, in the rostral part of the tail the first and last peaks are much smaller and thus may not be picked up by the peak finding algorithm. To overcome this, splines of the half-beat peaks of the rostral and most caudal tail angle traces were computed using the scipy function *pchip_interpolate*. This allowed the corresponding rostral tail-bend amplitude for a caudal peak to be computed. Tail-beat frequency was calculated as peak-peak distance.

Half-beat labelling To label individual half-beats, histograms of all half-beat peak-to-peak durations and amplitudes were computed. Individual distributions across fish were consistent, allowing the selection of thresholds to label half-beats as slow, fast or struggle. To subsequently compute bout selection as a function of grating speed, two approaches were taken. As a first approach, bouts were labelled as slow when they contained only slow half-beats, fast when they contained more than one fast half-beat and struggle when they contained more than one struggle half-beat. As a second approach, bouts were labelled as 'pure' if they were composed of over 75% of one half-beat type, else they were labelled as 'mixed'.

2.2.6 Kinematic analysis of head-embedded data using sparse coding (Megabouts)

The head-restrained sparse coding pipeline was established in collaboration with A. Jouary and has been published on bioRxiv [3].

Preprocessing and detrending First, the tail angles were smoothed using the Savitzky-Golay filter and interpolated from 16 to 10 segments to match freely-swimming conditions. Next, the baseline was de-trended by subtracting a low-frequency component, utilising the *Whittaker* algorithm from the python library *pybaselines*.

Sparse coding Convolutional sparse coding is an unsupervised method that decomposes a continuous image or multidimensional time series into the sparse contributions of motifs. The ensemble of motifs forms a dictionary that is learned from the data to reconstruct the original signal from a convolution of motifs with a sparse code. The specific algorithm used here was designed to recover the individual keystrokes from piano auditory recordings [20, 21]. Data from the tail angle of head-restrained zebrafish was collected and used for the algorithm to learn a dictionary of 4 locomotor motifs that could be associated with slow forward movements, fast forward movements, turns, and escape/struggle-like movements. Although the duration of tail movements could exceed 1 s in head-fixed conditions, the duration of motifs did not exceed 200 ms, suggesting that the basic time scale is similar to

freely swimming bouts. From the sparse code, the tail angle time series can be decomposed into the contributions of the four motifs. Convolution of the sparse code over a 40 ms window computes a 'regressor' for each movement motif. This was used to assign the dominant movement motif active at any time.

Sparse coding dictionary learning The sparse deconvolution was computed using the *ConvBPDN* algorithm from SPORCO. The dictionary learning used the *ConvBPDNDictLearnConsensus* method. To have dictionary motifs with matching first half beat locations a learning schedule was employed. For each iteration, the sparsity was increased and the learned motif was shifted so that their first half beat would be localized at the beginning. After 10 iterations the algorithm converged.

2.3 Results

The first objective of the project was to study forward swimming in the optomotor response in freely-swimming larval zebrafish, with a particular focus on gait switching behaviour. Wild-type larval zebrafish at 6-7 days post-fertilisation (Tu n = 35) were placed in a custom-made circular arena, allowing continuous swimming (Figure 2.1A). To elicit the optomotor response (**OMR**), forward gratings moving from tail-to-head at a range of speeds (15 speeds, 0 - 32.8 mm/s) were displayed by a projector below the fish for 20 seconds in a randomised order, with 5 repetitions each. Gratings were stationary for 10 seconds in-between trials. A pilot experiment had indicated that without an inter-trial-interval, behaviour at the beginning of a trial was influenced by the previous trial. Forward direction was maintained by reorienting the grating according to fish heading direction using a closed-loop system. Using high-resolution online tracking, bout detection and classification established previously in the lab [2], different bout types were observed in response to varying grating speeds in each animal.

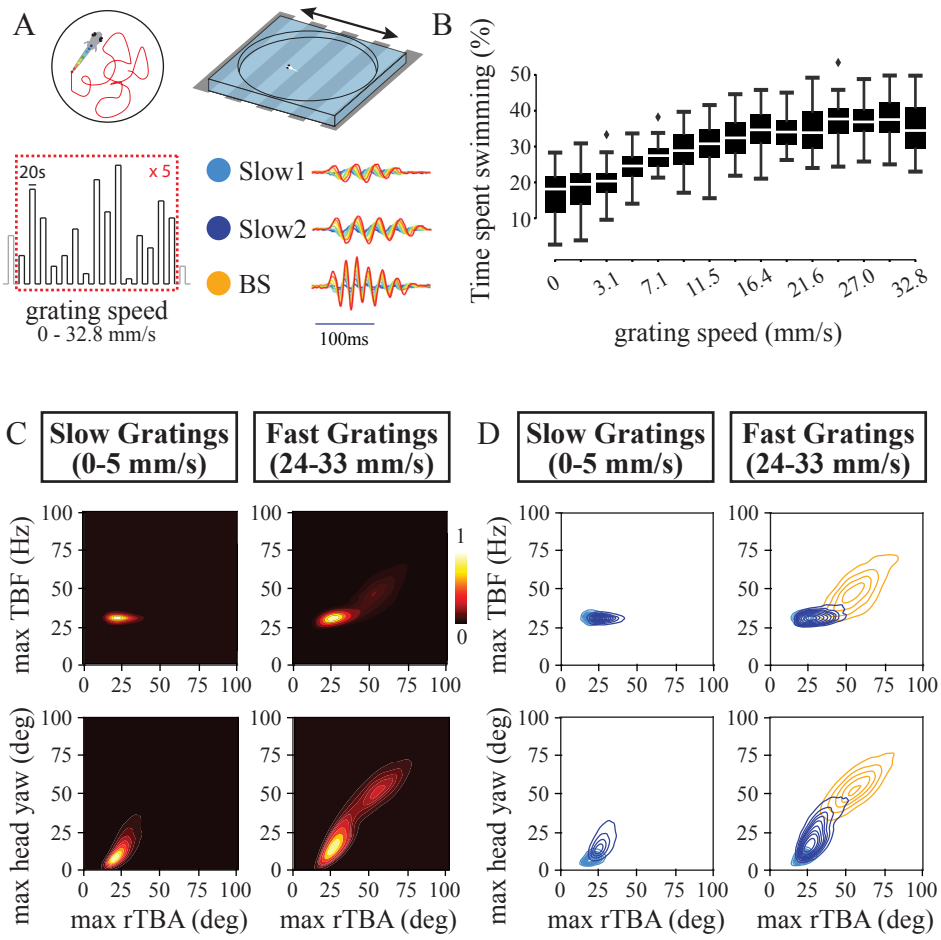

Figure 2.1: Moving gratings elicit different types of forward swims in freely-swimming conditions.
A) Freely-swimming experimental set up and paradigm with key bout types visualised.
B) Time spent swimming across grating speeds.
C) Heatmap of kinematic parameter kernel-density estimates across slow (left, 9064 bouts) and fast (right, 23004 bouts) grating speeds, each normalised to peak.
D) Same as D but with bout types overlaid.
For A and D: light blue, Slow1 swim; dark blue, Slow2 swim; orange, burst swim (BS). All data from 35 fish, Tu, 6-7 dpf.

2.3.1 Moving gratings elicit different types of forward swims in freely-swimming conditions

Fish spend more time swimming as grating speed increases (Figure 2.1B). To distinguish between the animal simply swimming more or employing different types of swims to successfully track the grating, kinematic parameters of swims across different grating speeds were computed. During slow gratings (0 - 5 mm/s), fish predominantly performed swims characterised by low maximum tail-beat frequency (**TBF**; 25 - 35 Hz), low maximum rostral tail bend amplitude (**rTBA**, 20 - 30 deg) and low maximum head yaw (5 - 25 deg; Figure 2.1C left). During fast gratings (24 - 32.8 mm/s), a second cluster emerged, characterized by high maximum TBF (30 - 75 Hz), high maximum rTBA (30 - 75 deg) and high maximum head yaw (35 - 75 deg; Figure 2.1C right). This modulation of kinematic parameters as a function of grating speed had been reported before, using a long rectangular arena and manually labelled slow and fast swims [22]. Using an unsupervised bout classification method [2] revealed a subdivision into slow (Slow1, Slow2) swims and slow as well as fast (burst; **BS**) swims during slow and fast gratings, respectively (Figure 2.1D). Despite using different experimental set-ups and bout classification methods, the kinematic parameters distinguishing slow and fast swims reported by Severi *et al.* match the ones observed in this study almost exactly, which argues for conserved locomotor mechanisms across the different OMR assays.

2.3.2 Modulation of kinematic parameters with grating speed

An array of kinematic parameters can be used to classify swim bouts, with TBF, rTBA and head yaw being the most prominent for distinguishing different types of forward swims [2]. Among others, Slow1 and Slow2 swims were characterized by low TBF (∼30 Hz), low rTBA (∼20 deg and ∼30 deg, respectively) and low head yaw (∼10 deg and ∼20 deg, respectively), whereas burst swims were characterized by high TBF (∼33 - 48 Hz), high rTBA (∼50 deg) and high head yaw (∼50 deg; Figure 2.2A-C left). Looking at all kinematic parameters independent of bout type suggested a modulation by grating speed (Figure 2.2A-C middle). However, separating into bout types revealed that most kinematic parameters remained

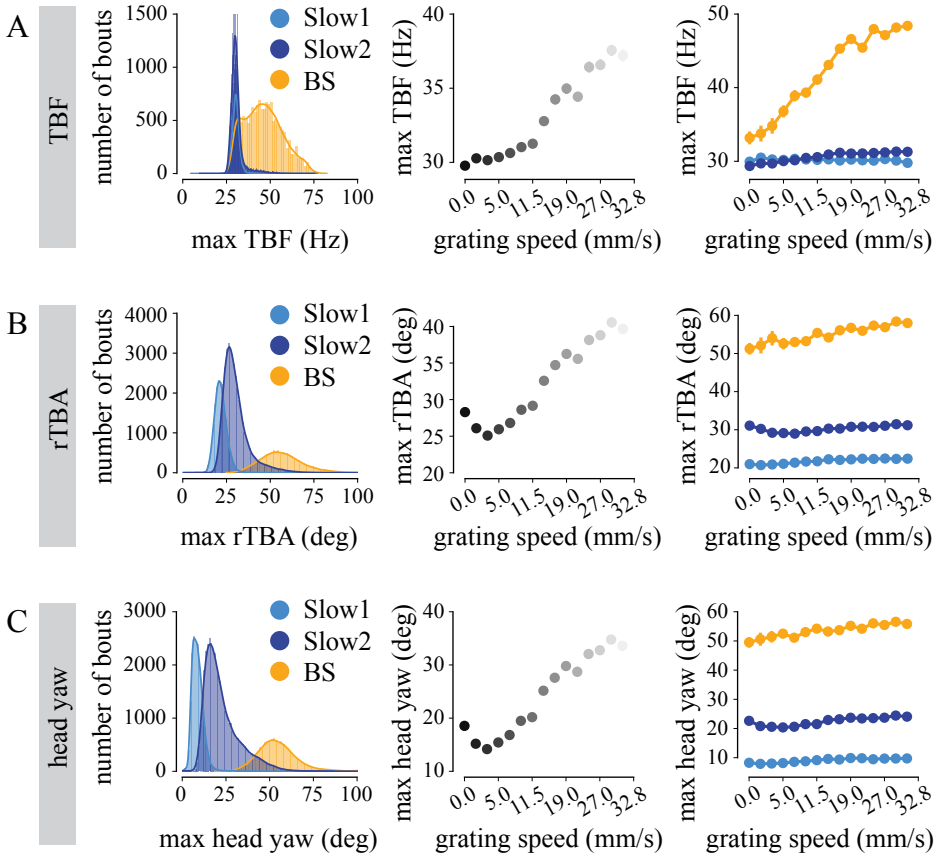

Figure 2.2: Modulation of kinematic parameters across grating speeds. Left panels show histogram of A) maximum TBF B) maximum rTBA and C) head yaw across different forward swims. Middle panels show modulation of kinematic parameters across grating speeds independent of bout type. Right panels show modulation of kinematic parameters across grating speeds when split into different forward swims. TBF; tail-bend frequency, rTBA; rostral tail-bend amplitude, light blue; Slow1 swim, dark blue; Slow2 swim, orange; burst swim. All data from 91 458 total bouts from 35 fish, Tu, 6-7dpf.

stable across grating speeds, except for TBF in burst swims, which increased as a function of grating speed (Figure 2.2A-C right).

Other kinematic parameters that varied as a function of grating speed included bout duration, inter-bout interval and latency to first bout after trial onset. Bout duration increased from ∼150 to ∼200 ms. Separating by bout type revealed that the different types of forward swims generally differed by their average bout duration, which gradually increased as a function of grating speed (Figure 2.3A). Inter-bout interval decreased as a function of grating speed, and did so in a similar fashion for all types of forward swims (Figure 2.3B). Latency of the first bout after trial onset was more variable, and decreased from 5 mm/s onwards with increasing grating speeds (Figure 2.3C). The initial shorter latency in the 0 mm/s and 1.5 mm/s conditions was likely due to the stimulus not being sufficiently different to inter-trial periods, where the grating was stationary. The trends of increasing bout duration, decreasing inter-bout interval and decreasing latency as a function of grating speed are consistent with previous findings [1, 2].

To extract and classify different bout types, Marques *et al.* placed a dataset of clustered swim bouts, collected from a battery of visuomotor assays, in a principal component analysis (**PCA**) space (referred to as bout map) [2]. To assess the stereotypy of different bout types the distance to the centroid of each bout cluster on the bout map can be computed [2].[1] Interestingly, the distance to the centroid was more variable at slow grating speeds for burst swims than during fast gratings (Figure 2.3D). This indicated greater variability of burst swim kinematics as a function of grating speed and further underscored the modulation of TBF shown above (Figure 2.2A).

[1]Note that different clusters have different spreads, for instance the cluster of burst swims is wider than for Slow1 and Slow2 swims. Therefore the absolute distance value for each bout is relative to the size of each cluster.

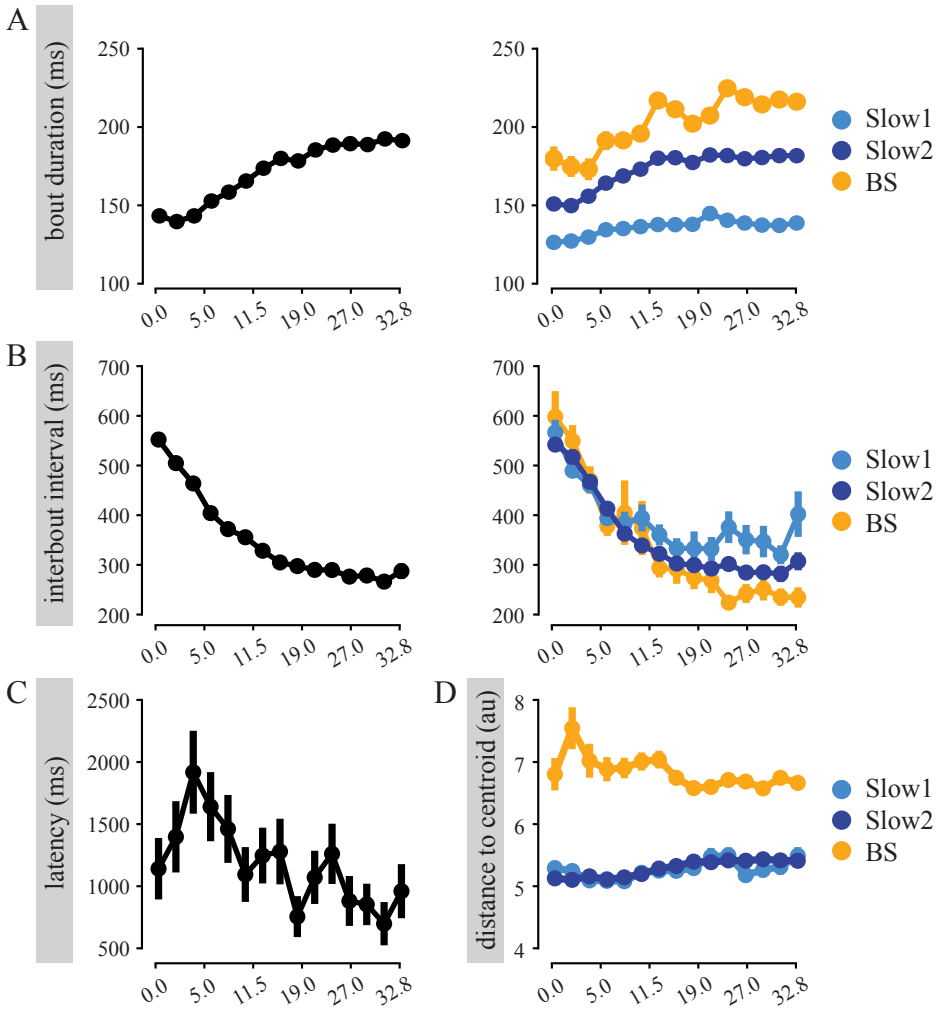

Figure 2.3: Bout duration, inter-bout interval and latency vary as a function of grating speed. A) Bout duration increases with grating speed for all bout types (left) and for each type of forward swim (right). B) Inter-bout interval decreases with grating speed for all bout types (left) and for each type of forward swim (right). C) Latency to first bout after trial onset decreases as a function of grating speed. D) Distance to centroid of PCA bout map per forward swim type is constant but more variable for burst swims at lower grating speeds. TBF; tail-bend frequency, rTBA; rostral tail-bend amplitude, light blue; Slow1 swim, dark blue; Slow2 swim, orange; burst swim. All data from 91 458 total bouts from 35 fish, Tu, 6-7 dpf.

2.3.3 Transition from slow to fast bouts with increasing grating speed

Considering all bout types and grating speeds confirmed that indeed forward swims were the predominant bout types employed when fish were presented with forward moving gratings (Figure 2.4A). There was a transition from Slow1 to Slow2 to BS as grating speed increased, with peaks at 3.1 mm/s, 13.9 mm/s and 29.9 mm/s, respectively. Bout choice appeared more stochastic at slower grating speeds, as seen in the slightly higher probability of routine turns (**RT**) and approach swims (**AS**) during gratings of 0 - 5 mm/s. One explanation could be that slow gratings were less engaging following a stationary inter-trial period than a salient, fast grating. More generally, the higher proportion of routine turns (compared to [1]), particularly at slow speeds and during inter-trial intervals when gratings were stationary, may be explained by the novel circular arena used here as opposed to the previously used rectangular arena [1, 2]. One benefit of using a circular arena was that it permitted continuous swimming, allowing the investigation of bout transitions over longer periods of time.

Single trials from an example fish illustrate behavioural transitions at a bout-to-bout level following trial onset (Figure 2.4B). While Slow1, Slow2, and RT were abundant at lower grating speeds in this fish, there was no immediately apparent pattern on the order of bouts. From 13.9 mm/s onwards, the occasional BS evolved to sustained trains of BS that were often preceded, and sometimes interrupted, by Slow2 swims. A possible explanation for the interruption of these 'BS trains' is the physical demands that burst swims require [23]. A large proportion of animals followed a trend similar to the one shown here, where slow swims dominated at slower grating speeds and BS were increasingly and repeatedly used at higher grating speeds. The behavioural transition from Slow1 to Slow2 to BS following trial onset at faster grating speeds was a common occurrence. At grating speeds >13.9 mm/s, Slow1 swims were unlikely to happen, however, when they did, they occurred as the first or second bout following trial onset. Slow2 swims dominated at all grating speeds, and at grating speeds >19.0 mm/s particularly in the first few bouts after the trial began. At fast grating speeds, fish were very likely to

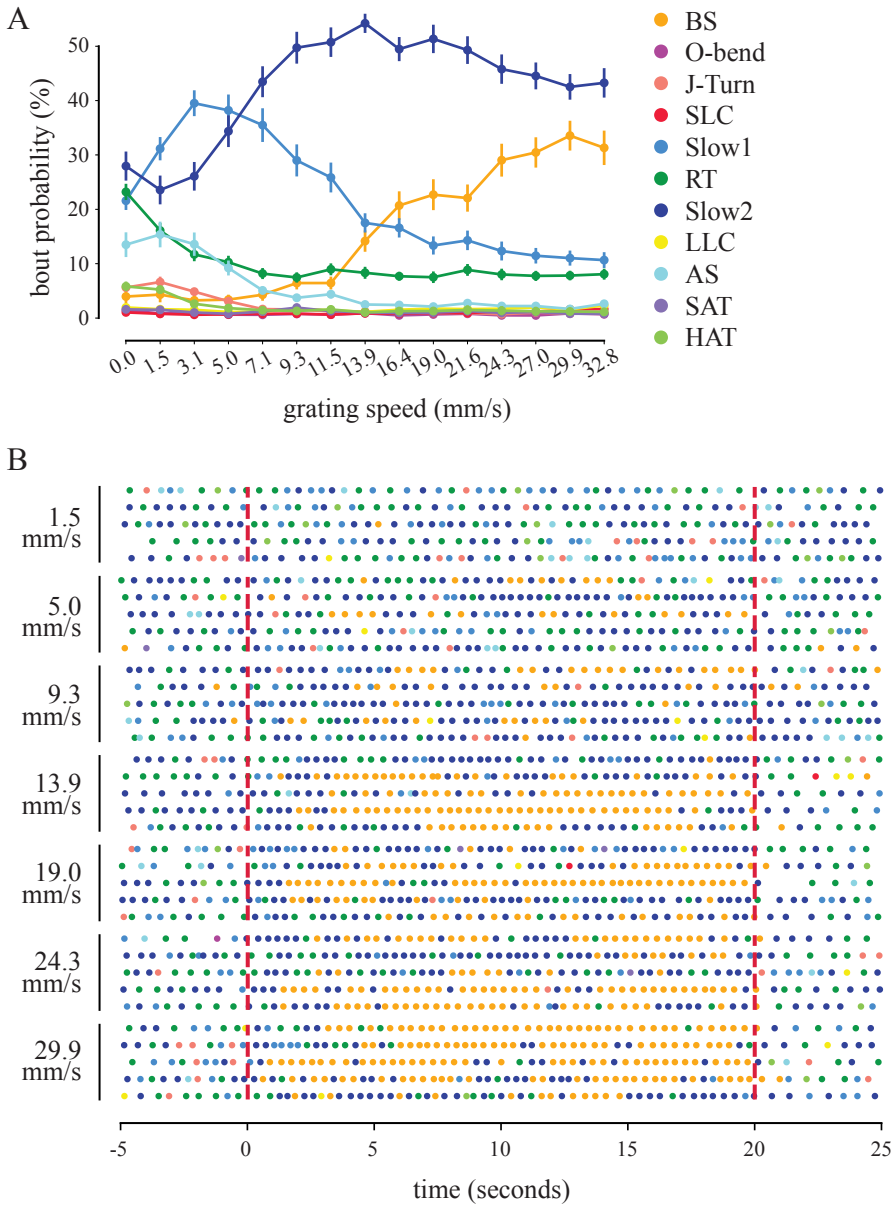

Figure 2.4: Transition from slow to fast swims across grating speed.
A) Probability of bout types across grating speeds. Data from ∼151 000 total bouts from 35 fish, Tu, 6-7 dpf.
B) Exemplary fish showing bouts across single trials at different grating speeds. Red dotted lines indicate start and end of trials. Same legend for bout types as in A.
BS, burst swim; SLC, slow-latency C-start; RT, routine turn; LLC, long-latency C-start; AS, approach swim; SAT, shadow avoidance turn; HAT, high-angle turn.

commence with Slow1 swims, followed by Slow2 swims and then transitioned to BS around the 4th to 5th bout after trial onset (Figure 2.5). This data is consistent with previous findings showing that slow swims are the first to occur in response to fast gratings, followed by fast swims [1, 2]. It should be noted, however, that in these studies trials were triggered by the fish performing slow swims following the direction of the grating.

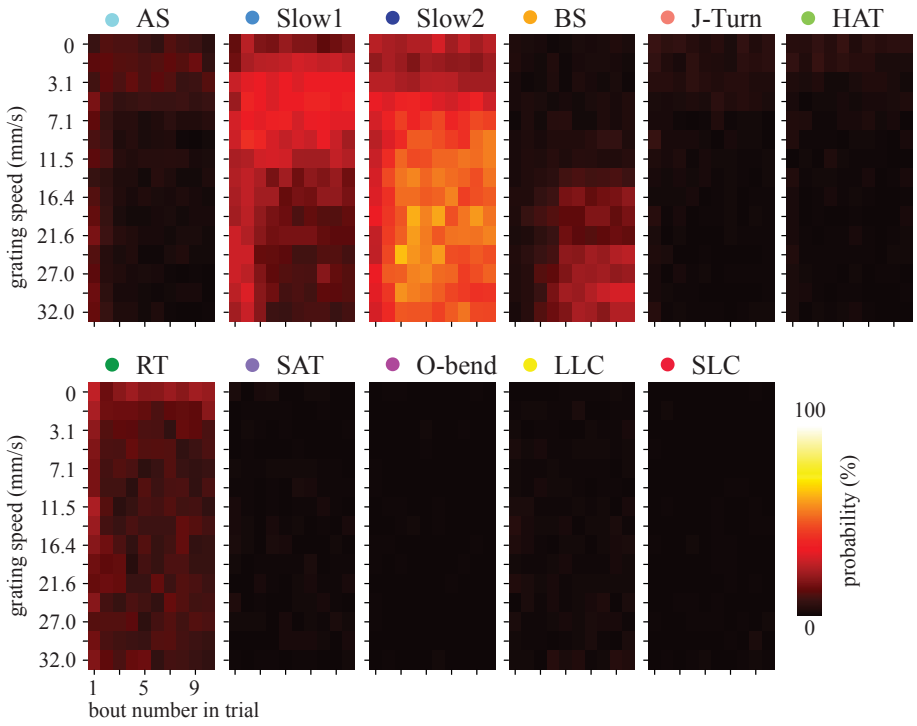

Figure 2.5: Probability of bout types within first ten bouts of each trial across grating speed. Data from ∼151 000 total bouts from 35 fish, Tu, 6-7dpf. BS, burst swim; SLC, slow-latency C-start; RT, routine turn; LLC, long-latency C-start; AS, approach swim; SAT, shadow avoidance turn; HAT, high-angle turn.

Utilising the circular arena allowed trials of longer duration. As already seen in the individual trials from an example fish (Figure 2.4), burst swims often occurred in sequences. Looking at the first 30 bout types following trial onset revealed this is common across the entire dataset (Figure 2.6). At higher grating speeds, particularly from bout 15 onwards, fish were likely to perform BS, interrupted at times by Slow2 swims. The data was represented in bout sequences rather than

time due to the decreasing bout latency and inter-bout interval with increasing grating speeds. These findings recapitulate the trends observed in the example fish.

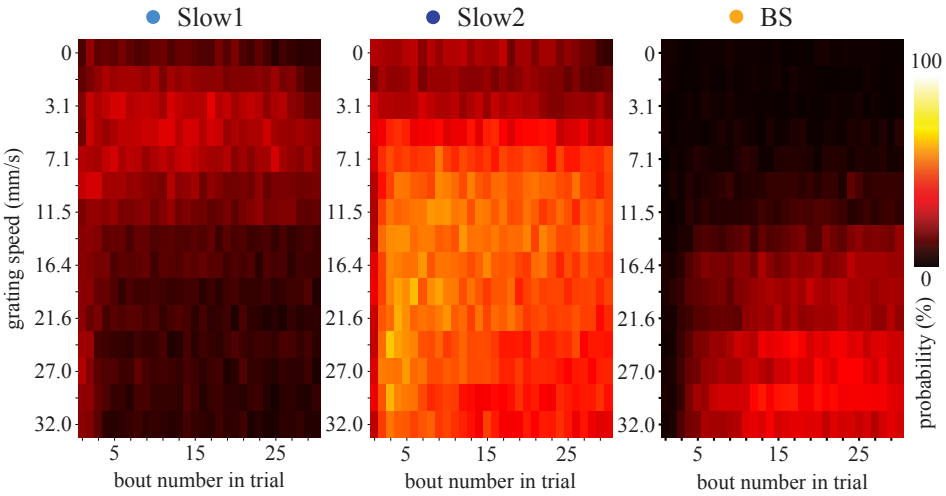

Figure 2.6: Transition of Slow1 to Slow2 to BS swims at longer timescales. Probability of bout types across the first 30 bouts following trial onset for different grating speeds. Data from 91 458 forward bouts from 35 fish, Tu, 6-7 dpf. Slow1, Slow1 swim; Slow2, Slow2 swim; BS, burst swim.

2.3.4 A closed-loop optomotor assay drives different forward swimming modes in head-restrained fish

Many preparations that seek to study the neural basis of behaviour require the animal to be restrained [15, 19, 24–26]. However, it has previously been difficult to elicit burst swims in head-restrained preparations [1], making it difficult to identify their neural correlates. Considering this, I set out to examine gait switching behaviour in the forward optomotor response in a head-embedded preparation. Larval zebrafish at 6-9 days post-fertilisation (Tu n = 40) were embedded in low-melting point agarose on a sylgard cone and their tails were freed. OMR gratings moving at a range of speeds (15 speeds, 0 - 32.8 mm/s) were displayed from below and on a 270° surround screen (Figure 2.7A). During the experiment, moving gratings were shown in closed-loop for 20 seconds in a randomised order with 10 second inter-trial intervals, and 5 repetitions each. Providing visual feedback

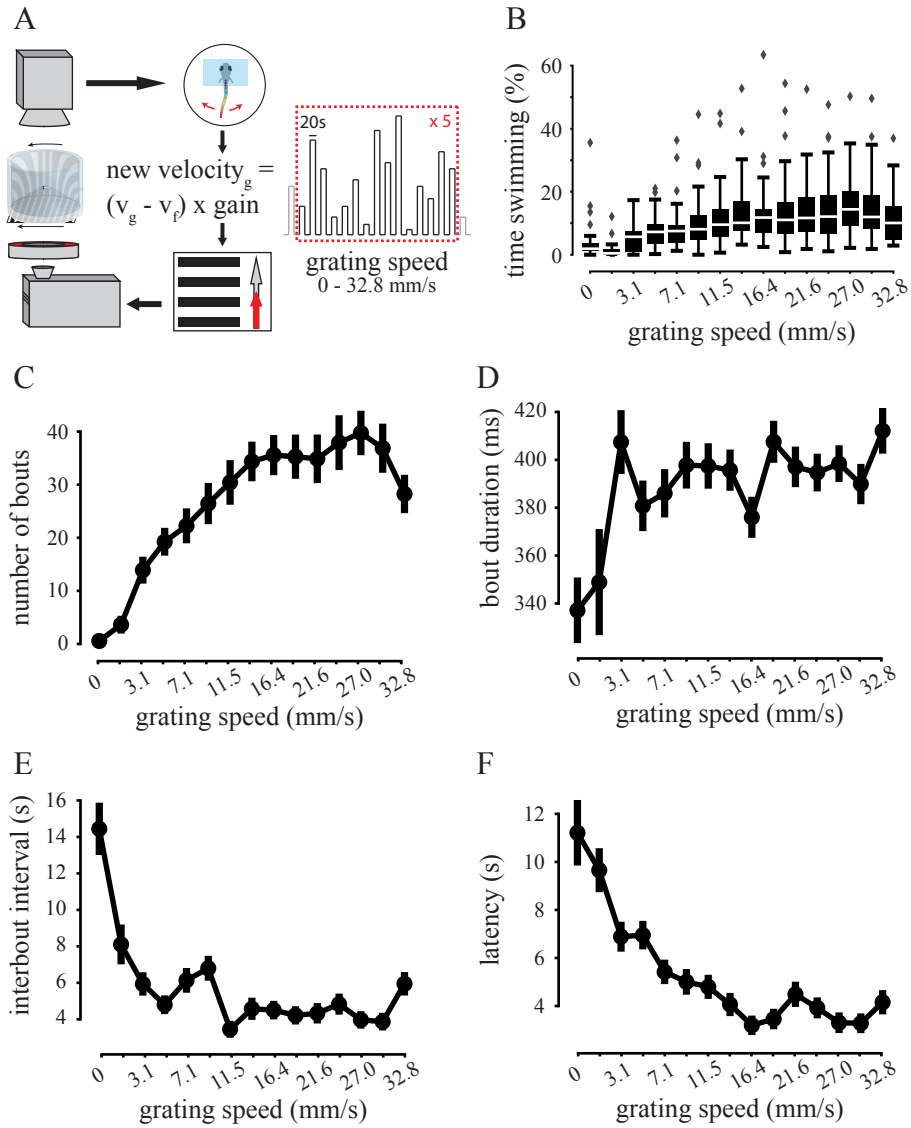

Figure 2.7: A closed-loop optomotor assay drives different forward swimming modes in head-restrained fish.
A) Experimental design including closed-loop set up. Fish embedded in circular arena with visual stimulus displayed below and around with camera above. Online tail tracking allows fish velocity-dependent update of visual stimulus. v grating, velocity of grating; v fish, velocity of fish.
B) Time spent swimming across different grating speeds.
All data from 40 fish, Tu, 6-9dpf.

from the fish' own motor output resembles freely-swimming conditions and stimulates swimming in head-restrained preparations [27, 28]. Reproducing behaviour exactly as previously seen in freely-swimming conditions is challenging. In head-restrained conditions, fish generally swim less and perform movements not seen in freely-swimming fish, such as struggles. In addition, the previously used method for bout classification [2] heavily relies on motion cues from the animal and can therefore not be applied directly to restrained animals. This chapter explores different approaches to utilising tail kinematic data only to detect and separate swims into different movement categories.

Similar to freely-swimming conditions, time spent swimming increased with grating speed in head-restrained conditions (Figure 2.7B). However, as a whole, fish spent less time swimming than during freely-swimming conditions. The average number of bouts per trial and bout duration both increased as a function of grating speed (Figure 2.7C-D). For bout duration, the increase was more pronounced during grating speeds under 10 mm/s. The inter-bout interval and latency to the first bout after trial onset both decreased as a function of grating speed (Figure 2.7E-F). Again, inter-bout interval and latency, as a whole, were both longer than in freely-swimming fish.

To determine whether the animals simply swam more to keep up with the grating or performed different movements, the same kinematic parameters were used to describe putative slow and fast bouts in head-restrained fish: maximum tail-beat frequency (**TBF**) and maximum rostral tail-bend amplitude (**rTBA**) [2]. Slow gratings (0 - 5mm/s) elicited swims of low maximum TBF (15 - 35 Hz) and low maximum rTBA (10 - 40 deg) (Figure 2.8A). Based on this kinematics, many of those swims likely constitute slow swims. Fast gratings (24 - 33mm/s) elicited both slow-like swims as well as putative fast swims, characterised by high TBF (40 - 75 Hz) and high rTBA (25 - 50 deg, Figure 2.8B). The range of TBF observed in head-restrained fish resembled the kinematics of freely-swimming slow and fast swims. However, rTBA was slightly lower, possibly due to the rostral part of the tail being restrained and head-restraint by itself likely affecting whole body kinematics.

[2]Note that since animals are head-embedded, head yaw is not instructive in this assay.

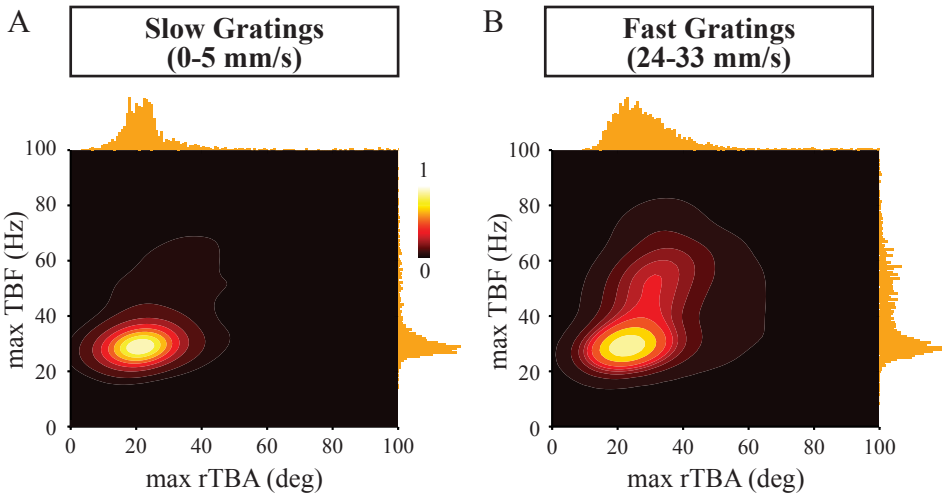

Figure 2.8: Kinematic parameters of head-restrained bouts across grating speeds.
A) Heatmap of kinematic parameter kernel-density estimates during slow gratings, n=1471 bouts, normalised to peak.
B) Heatmap of kinematic parameter kernel-density estimates during fast gratings, n = 4195 bouts, normalised to peak. Data from 40 fish, Tu, 6-9 dpf.

2.3.5 Head-fixed bouts include intra-bout modulation of kinematics

Figure 2.9 shows the tail angle of one example fish (Tu, 7 dpf) for each trial and grating speed. In this fish, swimming activity was almost exclusively restricted to trial periods. This is strikingly different to freely-swimming fish, which moved throughout the experiment but adapted their behaviour in line with the gratings displayed. In freely-swimming fish, each bout consists of one bout type [2]. In head-restrained fish, however, I observed intra-bout modulation of tail-beat frequency in some swims, particularly at higher grating speeds. This could be due to unnatural feedback from the animal being restrained and has been reported previously [27]. Therefore, instead of classifying bouts as whole, I established and contributed to devising two methods to decompose bouts into movement motifs.

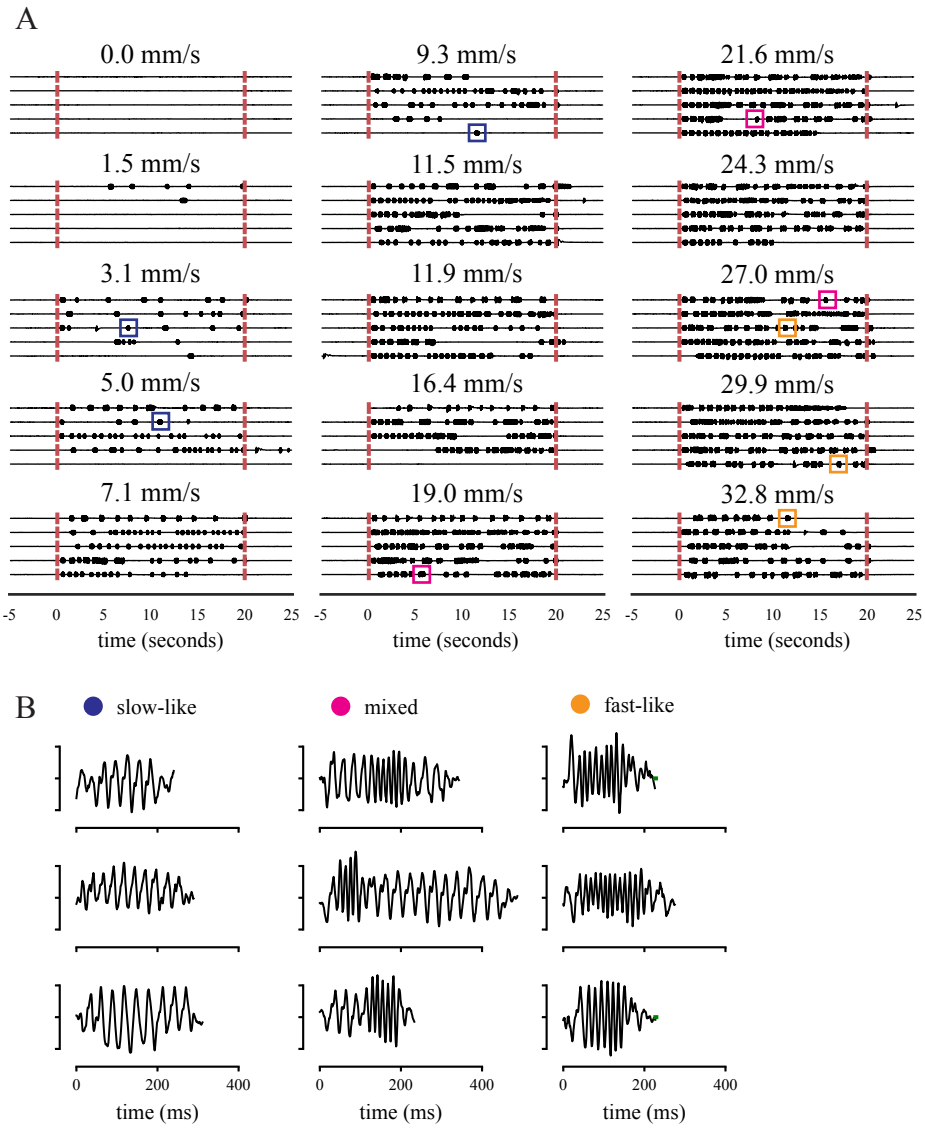

Figure 2.9: Head-fixed example fish shows intra-bout modulation of tail kinematics. A) Tail angle of one example fish (Tu, 7 dpf) for each trial across grating speeds. Red dashed line; trial start and end, coloured boxed; inset for bout examples in B.
B) Bout examples from different trials to illustrate intra-bout modulation of tail kinematics. Can be qualitatively grouped into slow- and fast-resembling swims as well as mixed swims.

2.3.6 Approach 1: Decomposing bouts into half-beats

Since there were clearly visible periods of different swimming activity visible within single bouts, as a first approach, I decomposed bouts into half-beats. Individual half-beats were labelled as slow, fast or struggle depending on their inter-beat timings and amplitude (Figure 2.10A):

- Slow beat: long interval (15 - 30 Hz), low amplitude (10 - 40 deg)
- Fast beat: short interval (30 - 70 Hz), low amplitude (25 - 50 deg)
- Struggle: any interval, high amplitude (>40 deg)

To understand if these different half-beats were following a similar pattern of slow to fast transitions as a function of grating speed, each bout was labelled according to its composition of half-beat types. First, any bout containing a fast half-beat was labelled as a fast bout (essentially grouping mixed and 'pure' fast bouts), any bout containing a struggle beat was labelled as a struggle, and any bouts containing only slow beats were labelled as slow bouts. Across the entire cohort (16 389 bouts from 40 fish) the number of slow bouts dominated at slow grating speeds, the number of mixed and fast bouts increased as grating speed increased, and there were very few struggles (Figure 2.10B). In the second approach, any bout containing >75% of one half-beat type was labelled as a 'pure' slow-like swim, fast-like swim or struggle, depending on the predominant half-beat type. Bouts containing several half-beat types were labelled as mixed bouts. Again, slow-like swims were the predominantly used bout type at any grating speed, whereas the proportion of fast and mixed bouts increased as a function of grating speed (Figure 2.10C).

While these two approaches were more supervised attempts at classifying bouts with thresholds tuned specifically to this dataset, it did provide an indication that a transition in swimming modes occurs in a head-restrained assay.

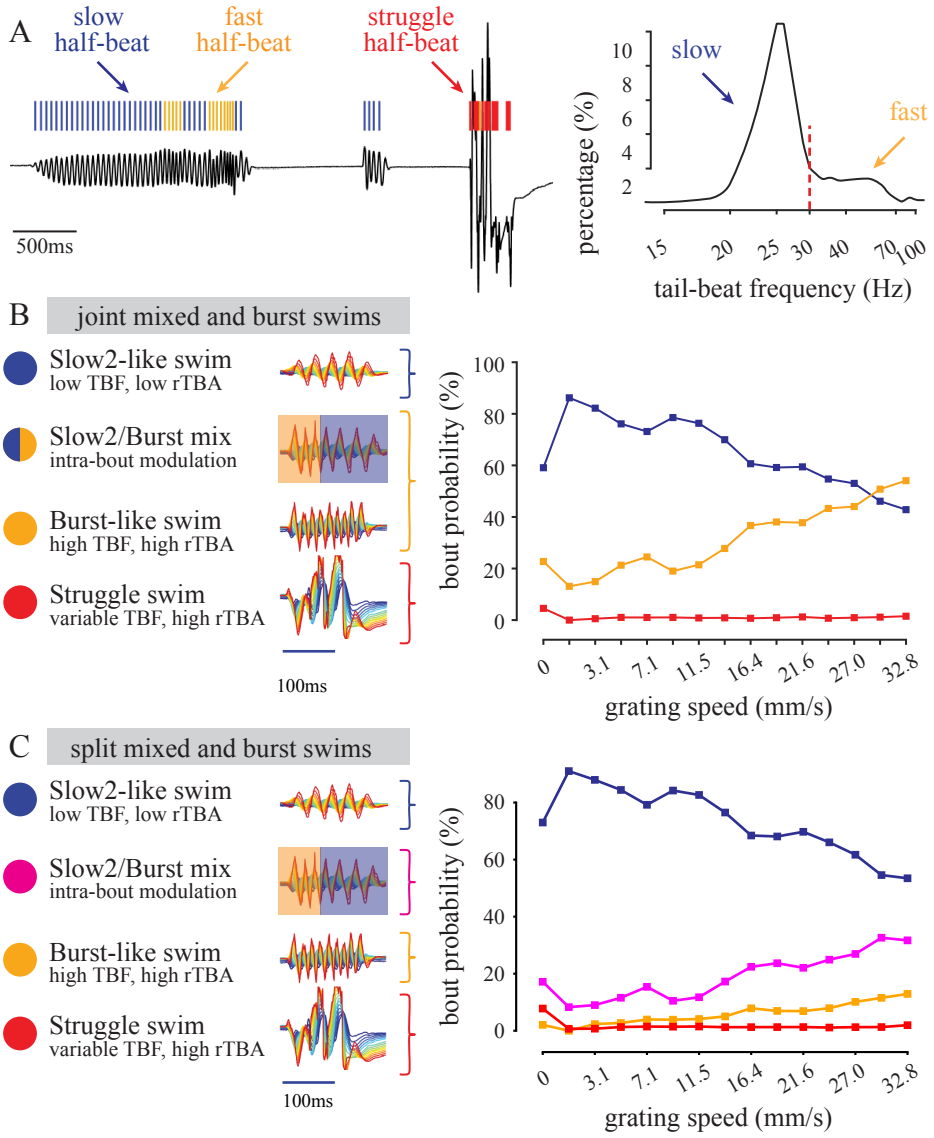

Figure 2.10: Intra-bout modulation and decomposing bouts into half-beats in head-restrained conditions.
A) Bouts in head-restrained condition reveal intrabout modulation. Decomposition into half-beats allows labelling as slow, fast or struggle based on TBF and rTBA. Left show an exemplary tail trace with half-beats labelled, right shows bimodal distribution of peak-to-peak intervals of half-beats. Dashed red line indicates threshold.
B-C) Left shows four bout types observed in head-restrained conditions: slow, mixed, fast and struggles. Right shows probability of those bouts as a function of grating speed. In B) mixed and BS were combined, ie any bout that contained a fast-half beat was labelled as mixed. In C) bouts were assigned a bout type if 75% of one half-beat label were present.

2.3.7 Approach 2: Megabouts, a novel method using sparse coding to decompose bouts in head-restrained fish.

As part of a collaboration, the dataset on head-restrained fish performing the forward OMR (among others) was used to build a pipeline for unsupervised bout decomposition [3]. Termed Megabouts, the project includes a specific pipeline for analysing head-restrained tail data (Figure 2.11A). To quantify the less stereotyped, variable-length tail movements, we developed a new approach based on convolutional sparse coding [20, 21]. This method is grounded in the hypothesis that complex tail movements are generated by sparse control signals driving different tail oscillation motifs [29]. Convolutional sparse coding represents the tail angle as a combination of these basic motifs, learned from the data through an optimization process that enforces sparsity so that only a few motifs are active at any time. The unsupervised learning revealed the following motifs: slow, fast, turn, and escape/struggle (Figure 2.11B).

Figure 2.11: Novel method using convolutional sparse coding to decompose tail activity into motifs in head-restrained conditions.
A) Schematic of *Megabouts* suite. Left shows classification pipeline flow from tail + trajectory data. Starting with tracking data at variable resolution, tail traces are denoised, segmented and classified to build an ethogram. Right shows decomposition pipeline flow from tail only data. Tail trace is denoised, decomposed into a sparse code based on the motif dictionary and the vigour for each motif is computed.
B) Illustration of the four motifs learnt from the data: slow, fast, turn, struggle. Left shows heat map of each motif showing tail beat propagation along rostral-caudal segments and time, with accompanying time series for each motif. Right shows illustration of sparse coding and motif vigour. Top panel shows the original (black) and reconstructed (red) tail angle. Middle panels: each component is computed by the convolution of a sparse code and the motif. Bottom. The contribution of each motif can be computed as the rolling variance of each component (over a 40ms window).

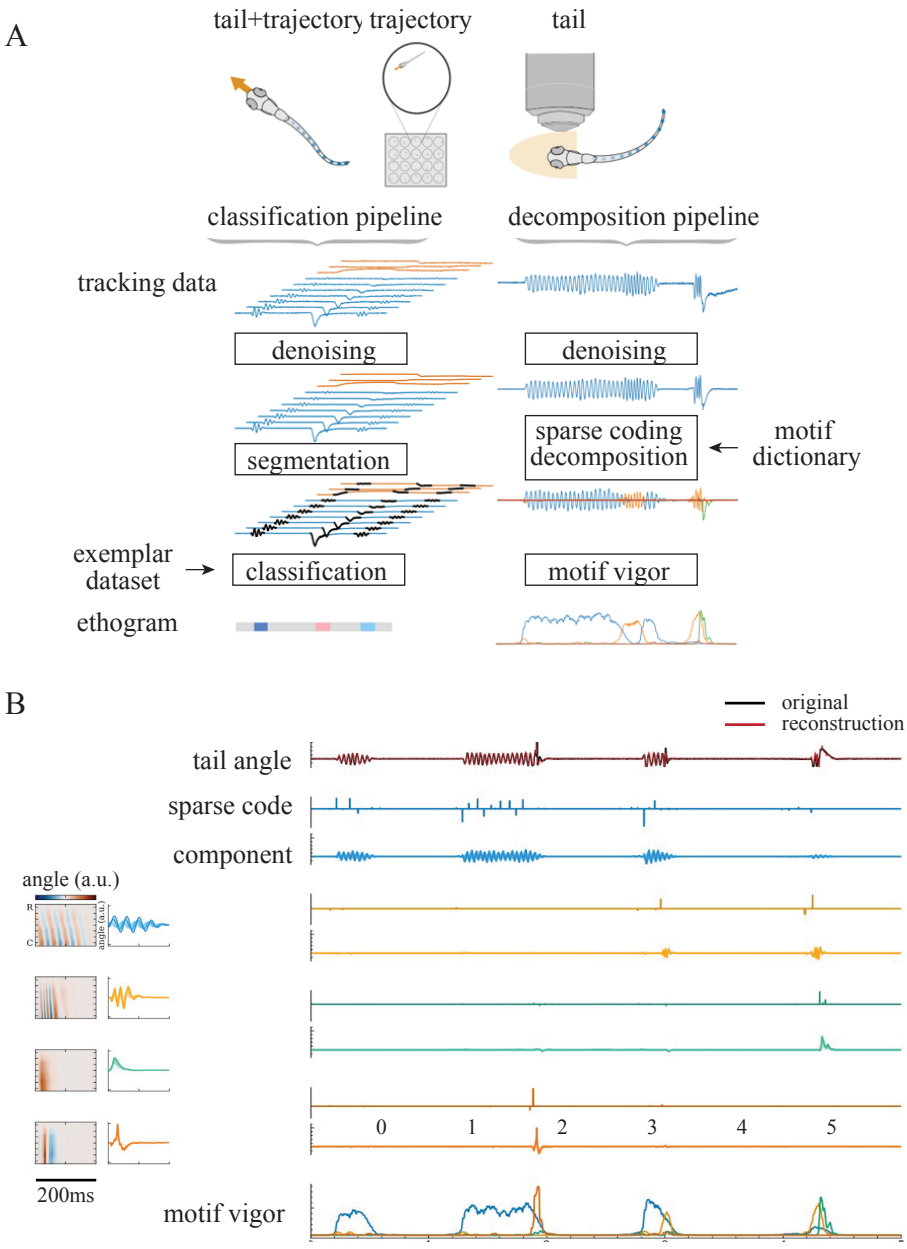

(Caption on previous page.)

Considering again our 9 example bouts, Figure 2.12 illustrates the activity of different movement motifs derived from the Megabouts sparse coding decomposition. The 'pure' slow-like and fast-like bouts are indeed marked as such by the sparse code regressors, with the respective motif being active over the entire duration of the bout. For mixed swims, several configurations occur: different motifs can alternate, or the bout starts with one motif and then switches to another.

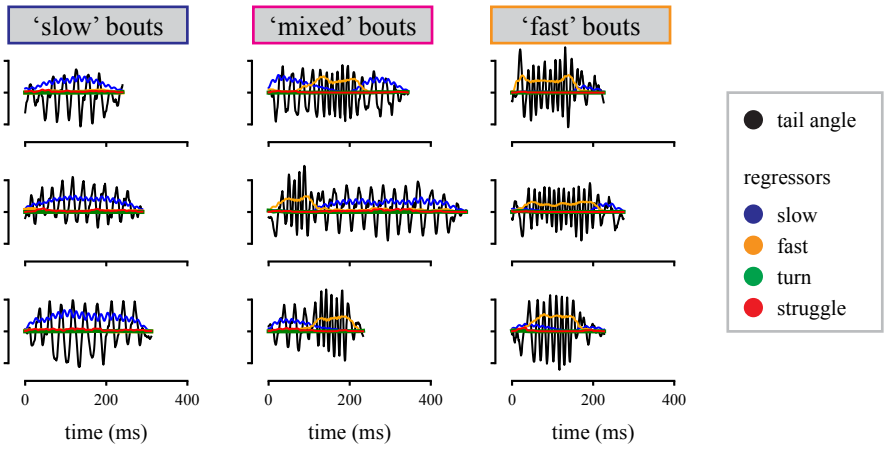

Figure 2.12: Head-fixed example bouts with active movement motifs from the Megabouts suite. Blue, slow; orange, fast; green, turn; red, struggle.

Looking at the dominant movement motif at each time point across the entire experiment for this example fish illustrates a general increase in movement, as well as increasing use of the fast motif as a function of grating speed (Figure 2.13A). To understand whether this trend applied to the whole dataset, I computed the time each movement motif was active as a proportion to total time spent swimming per trial for each fish. Matching the results derived from the half-beat labelling, this shows that fish pre-dominantly used the slow movement motif but increasingly used the fast movement motif at faster grating speeds (Figure 2.13B).

In conclusion, both the half-beat labelling approach and the sparse coding pipeline both decomposed bouts into smaller movement motifs. Both revealed a general trend of the slow movement motif being predominantly used by head-fixed fish, with the fast movement motif being increasingly used during fast grating speeds, either in 'pure' fast bouts, or within mixed swims.

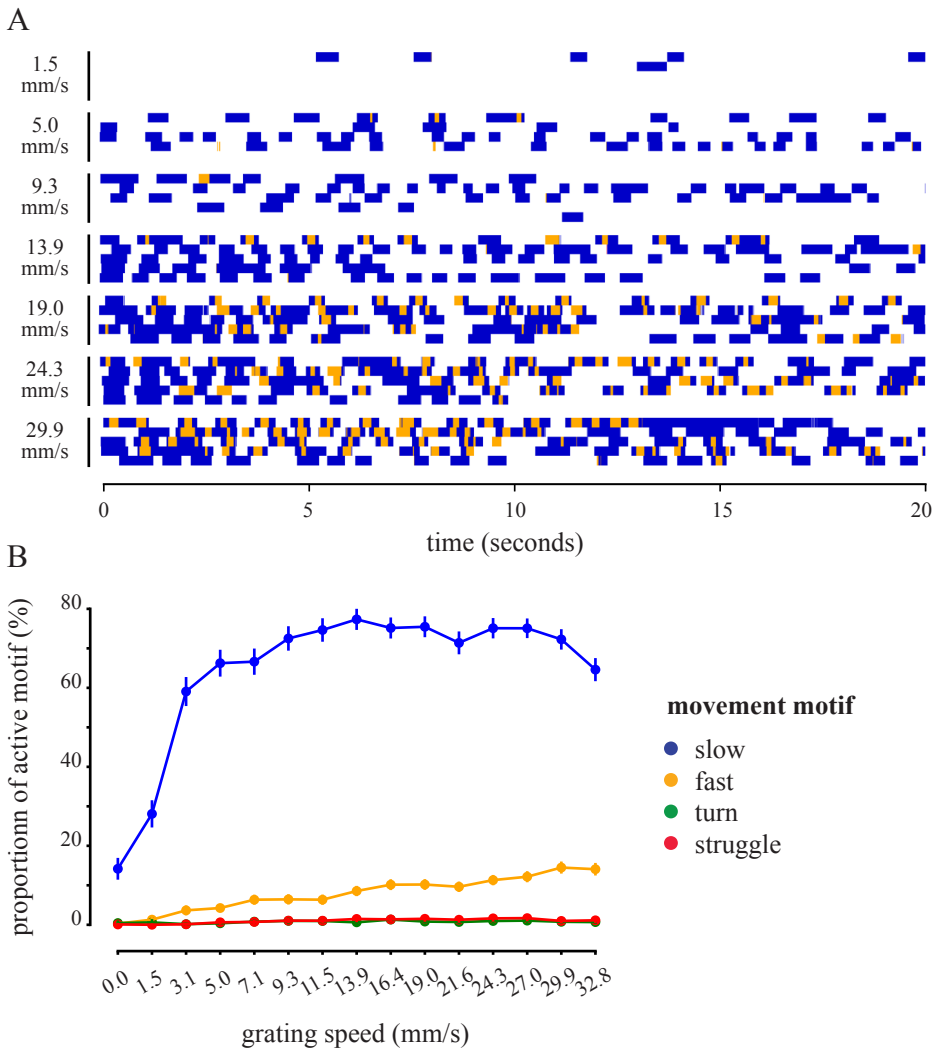

Figure 2.13: Movement motifs per trial across select grating speeds in head-fixed fish. A) Example fish (Tu, 7 dpf) showing the dominant movement motif across time for each trial at select grating speeds.
B) Proportion of active movement motif across grating speeds for all fish (Tu, 6-9 dpf, n = 40). Blue, slow; orange, fast; green, turn; red, struggle.

2.3.8 Summary of behavioural results

This chapter characterised different types of forward swimming in response to optomotor gratings in both a freely-swimming and a head-restrained assay (Figure 2.14). Slow gratings predominantly elicited slow swims: in freely-swimming conditions these could be classified as Slow1 and Slow2 swims using unsupervised clustering [2], in head-restrained conditions Slow2-like swims were characterised by low tail-beat frequency and low rostral tail-bend amplitude. Fast gratings elicited Slow2 as well as burst swims in freely-swimming conditions. In head-restrained conditions, there are burst-like swims characterised by high TBF and high rTBA, as well as mixed bouts with different periods of TBF. Additionally, fish performed a small number of struggles in head-restrained conditions, characterised by usually large tail-bend amplitude and variable TBF.

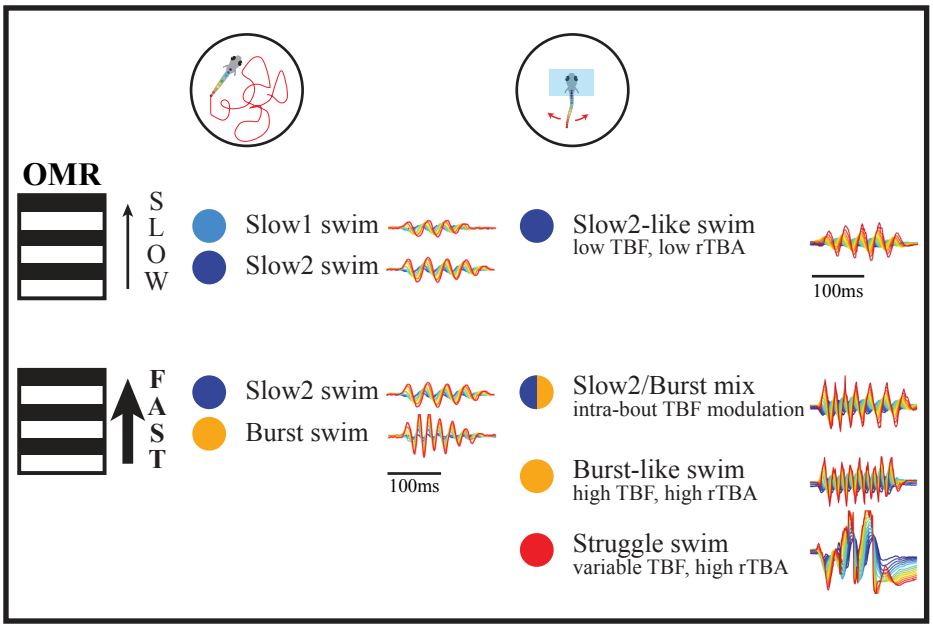

Figure 2.14: Summary of forward swim types used at slow and fast grating speeds in freely-swimming and head-restrained conditions.

2.4 Discussion

The first aim of the study was to recapitulate slow and fast forward swimming behaviour of larval zebrafish in freely-swimming conditions. As reported previously [2, 22] larval zebrafish exhibited slow swims in response to slow forward moving gratings, and a mixture of slow and fast swims in response to fast forward moving gratings. I expanded these findings by applying a recently published bout classification method [2] and using a circular arena, which allowed for longer continuous sequences of fast swimming. This revealed a transition from Slow1 to Slow2 to burst swims as grating speed increases. Looking at the transition between movements after trial onset revealed that even at fast grating speeds, the animal is likely to commence with several Slow2 swims before transitioning to sustained trains of burst swims. As a whole, despite using different shapes of experimental chambers, analysis methods and fish strains, my assay in freely-swimming fish corroborates previous findings from Severi *et al.* [1], suggesting the basic mechanisms of forward swimming and movement transitions are stable across different experimental set-ups.

Forward swims can best be distinguished using several kinematic parameters, such as tail-beat frequency, rostral-bend amplitude and head yaw. These parameters remained stable across grating speeds within each bout category, with the notable exception of maximum tail-beat frequency of burst swims, which increased as a function of grating speed. This exception for burst swims was also reflected in their increased variability of distance to the cluster centroid during slow grating speeds. Even though swims can be grouped into different bout types, and stereotypic movements exist, these results provide further evidence that a degree of variability within bout classes is present [2, 13]. This leads to the question at what point different movements should be considered as distinct vs part of a continuum without clear boundaries [12].

Studies on the organisation of spinal circuits in larval zebrafish point towards a more continuous behavioural space, particularly in relation to speed changes. McLean *et al.* were able to identify a topographic map of ventral to dorsal interneurons, that are recruited sequentially and inhibit more ventral populations as

a function of swimming speed [30]. However, while fine axial control is needed to produce flexible and adaptive swims, strong evidence for bout types representing different swimming gaits comes from considering whole-body coordination of the animal.

Although I have focused primarily on the gross movement of the body/trunk to define swimming and swim bouts, animals also make varied use of their limbs during locomotion [7, 31–34]. For instance, different pectoral fin movements have been described for slow vs fast swimming in larval zebrafish. During slow swimming, larval zebrafish synchronise their pectoral fin movements with the body axis, matching both the frequency and phase of tail beats. The alternating undulation of left and right pectoral fins during slow swimming (mediated by abduction and adduction) is in stark contrast to the tucked fins observed during burst swims (mediated by adduction alone) following escape movements [7, 33].

Movement of the pectoral fins does not necessarily occur to generate additional propulsive force [8]. Initially, it had been suggested that synchronous pectoral fin movement may aid in offsetting head yaw by stabilising the propulsive effect of the tail movement [31]. The tucking of fins during fast swims is actively controlled and could possibly streamline the hydrodynamic forces encountered by larvae to reduce drag [7, 33]. More recently, pectoral fin movement in larval zebrafish has been linked to fluid exchange near the body for cutaneous respiration [8, 35]. Across development, body-fin coordination in the pitch axis is necessary for climbing swims up the water column [34]. It has been proposed that the neural control of fins and body axis are similarly organised. Considering the spatial separation of reticulospinal circuits driving exploratory swimming vs escapes [1, 15, 16, 36, 37], a joint study of brainstem circuits controlling pectoral fin and axial movements would underline the distinction of swimming gaits. Given their small size and optical accessibility, larval zebrafish present an excellent model to address these questions in a whole-brain imaging preparation.

Recording neural activity in larval zebrafish often require the animal to be restrained. However, burst swims in head-fixed fish have been challenging to elicit in OMR assays [1]. To accomplish this, I introduced a closed-loop feedback system,

in which the grating speed is updated in response to the fish's own scaled motor output. Scaling the motor output proved vital. Fish were consistently able to stop the grating by beating the tail, which corresponds to a stabilisation of the visual field following a swim upstream in a body of flowing water. Closed-loop feedback systems offer the advantage of creating more naturalistic swimming conditions. In fact, a previous study showed that the lack of perceived effect on their visual environment leads to head-fixed fish 'giving up' [28]. Of course, this only updates the visual feedback while sensorimotor feedback from water flow and movement along the water column are unaffected. For instance, fish perform rheotaxis, where they utilise their lateral line to align swimming to water currents [38, 39]. During embedding, removing the agarose around the tail damages the hair cells of the lateral line. To mitigate this, fish were embedded the day before in order to allow regeneration of the neuromasts of the lateral line [40]. Last but not least, larval zebrafish movement occurs in 3-dimensions and body torque, specifically, has been reported to change with swimming speed [41–44]. Taken together, it is not surprising that head-fixation induces changes in bout kinematics compared to freely-swimming assays.

Here, head-fixed fish showed differences in tail kinematics, such as more variable and sometimes longer bout duration, longer inter-bout intervals, as well as intra-bout modulation of tail-beat frequency. One apparent difference to freely-swimming bouts was the incorrect termination of swims. Whereas freely-swimming burst swims had a relatively stable TBF throughout [2], head-fixed bouts that commenced as burst swims often transitioned into slow swims before termination. Often, this occurred half-way throughout the swim or only affected the last few half-beats. Furthermore, large head yaw is an important feature of burst swims [1, 2], which was restricted by the agarose. Incorrect termination of burst swims in particular is most likely due to the unnatural mechanosensory feedback experienced in a head-fixed preparation.

Nonetheless, I observed bouts and periods of bouts where the key kinematic parameters, particularly TBF, matched those reported in freely-swimming fish. Rostral tail bend amplitude was lower than in freely-swimming fish, most likely

due to the rostral part of the tail being restrained. This parameter also differed for freely-swimming bouts from the values reported by Severi *et al.* [1], most likely due to measuring slightly different parts along the tail. I validated my findings using two different approaches to label movement motifs within bouts: labelling half-beats based on tail kinematics, and decomposing bouts into movement motifs using convolutional sparse coding [3]. In both cases, bouts containing burst-swim-like movement motifs, either partially or completely, increased as a function of grating speed.

An alternative to head-fixation would have been a fictive preparation, where the fish is completely paralysed and recordings are made from motor neurons [45]. This approach has been successfully used in a number of studies to simultaneously record neural activity and fictive behaviour [30, 46, 47]. It is a particularly useful method when combined with whole-brain imaging [48, 49], which is sensitive to even the smallest of motion artifacts. However, since burst swims had not been reported in either fictive or head-restrained preparations, and pilot data from the lab had indicated that swims of higher TBF may be achieved by using closed-loop feedback, I opted for a head-fixed preparation for this study. One recent study has begun to characterise speed changes during fictive swims in response to a variety of visual stimuli [50]. They were able to elicit swims up to 30 Hz, consistent with a switch of using the more dorsal musculature, as opposed to the ventral muscles used during slow swimming [30, 51, 52]. It remains to be seen whether burst swims of higher TBF can be elicited in a fictive preparation. However, this presents an exciting new avenue of research. If possible, it would be intriguing to combine a fictive preparation recording axial as well as pectoral fin motor neurons and whole-brain imaging during the forward OMR to dissect the joint neural circuits driving slow vs burst swims.

2.5 Acknowledgements

Part of the work of this chapter has been published in a research article on the pre-print server bioRxiv and has been submitted for peer-review in a journal in November 2024.

Jouary, A., Silva, P.T., Laborde, A., Mata, M.J., Marques, J.C., **Collins, E.M.D.**, Peterson, R.T., Machens, C.K and Orger, M.B. (2024) Megabouts: a flexible pipeline for zebrafish locomotion analysis.
doi: https://doi.org/10.1101/2024.09.14.613078v2

E.M.D. Collins designed and performed all experiments and analysis discussed in this chapter. A. Jouary built the freely-swimming behaviour set-up. S. Renninger and M.B. Orger built the head-restrained set-up. A. Laborde and A.L. Martins wrote the SARDINE software and OpenGL Shader software to acquire experiments on the freely-swimming behaviour-set up (Martins, Laborde and Orger, in prep.). J. Marques established the bout classification method [2] and E.M.D. Collins, A. Jouary and A. Laborde refactored the code into a toolbox for the laboratory to use. The Megabouts toolbox was built by A. Jouary and A. Laborde with user feedback by P.T. Tomas and E.M.D. Collins (see www.megabouts.ai [3]). E.M.D. Collins wrote the chapter with helpful input from A. Jouary in the sections regarding Megabouts, and A. Ostrovsky and M.B. Orger for the whole chapter.

2.6 References

1. Severi, K. E. *et al.* Neural Control and Modulation of Swimming Speed in the Larval Zebrafish. *Neuron* **83,** 692–707. doi:10.1016/j.neuron.2014.06.032 (2014).
2. Marques, J. C., Lackner, S., Félix, R. & Orger, M. B. Structure of the Zebrafish Locomotor Repertoire Revealed with Unsupervised Behavioral Clustering. *Current Biology* **28,** 181–195.e5. doi:10.1016/j.cub.2017.12.002 (2018).
3. Jouary, A. *et al. Megabouts: a flexible pipeline for zebrafish locomotion analysis* 2024. doi:10.1101/2024.09.14.613078.
4. Budick, S. A. & O'Malley, D. M. Locomotor Repertoire of The Larval Zebrafish: Swimming, Turning and Prey Capture. *Journal of Experimental Biology* **203,** 2565–2579. doi:10.1242/jeb.203.17.2565 (2000).
5. Neuhauss, S. C. *et al.* Genetic disorders of vision revealed by a behavioral screen of 400 essential loci in zebrafish. *The Journal of Neuroscience: The Official Journal of the Society for Neuroscience* **19,** 8603–8615 (1999).
6. Orger, M. B., Smear, M. C., Anstis, S. M. & Baier, H. Perception of Fourier and non-Fourier motion by larval zebrafish. *Nature Neuroscience* **3,** 1128–1133. doi:10.1038/80649 (2000).
7. Thorsen, D. H., Cassidy, J. J. & Hale, M. E. Swimming of larval zebrafish: fin–axis coordination and implications for function and neural control. *Journal of Experimental Biology* **207,** 4175–4183. doi:10.1242/jeb.01285 (2004).
8. Green, M. H., Ho, R. K. & Hale, M. E. Movement and function of the pectoral fins of the larval zebrafish (Danio rerio) during slow swimming. *Journal of Experimental Biology* **214,** 3111–3123. doi:10.1242/jeb.057497 (2011).
9. Patterson, B. W., Abraham, A. O., MacIver, M. A. & McLean, D. L. Visually guided gradation of prey capture movements in larval zebrafish. *Journal of Experimental Biology,* jeb.087742. doi:10.1242/jeb.087742 (2013).
10. Katsov, A. Y., Freifeld, L., Horowitz, M., Kuehn, S. & Clandinin, T. R. Dynamic structure of locomotor behavior in walking fruit flies. *eLife* **6,** e26410. doi:10.7554/eLife.26410 (2017).
11. Berman, G. J., Choi, D. M., Bialek, W. & Shaevitz, J. W. Mapping the stereotyped behaviour of freely moving fruit flies. *Journal of The Royal Society Interface* **11,** 20140672. doi:10.1098/rsif.2014.0672 (2014).
12. Szigeti, B., Deogade, A. & Webb, B. Searching for motifs in the behaviour of larval *Drosophila melanogaster* and *Caenorhabditis elegans* reveals continuity between behavioural states. *Journal of The Royal Society Interface* **12,** 20150899. doi:10.1098/rsif.2015.0899 (2015).

13. Mearns, D. S., Donovan, J. C., Fernandes, A. M., Semmelhack, J. L. & Baier, H. Deconstructing Hunting Behavior Reveals a Tightly Coupled Stimulus-Response Loop. *Current Biology* **30,** 54–69.e9. doi:10.1016/j.cub.2019.11.022 (2020).

14. Mirat, O., Sternberg, J. R., Severi, K. E. & Wyart, C. ZebraZoom: an automated program for high-throughput behavioral analysis and categorization. *Frontiers in Neural Circuits* **7.** doi:10.3389/fncir.2013.00107 (2013).

15. Orger, M. B., Kampff, A. R., Severi, K. E., Bollmann, J. H. & Engert, F. Control of visually guided behavior by distinct populations of spinal projection neurons. *Nature Neuroscience* **11,** 327–333. doi:10.1038/nn2048 (2008).

16. Fetcho, J. & Faber, D. Identification of motoneurons and interneurons in the spinal network for escapes initiated by the mauthner cell in goldfish. *The Journal of Neuroscience* **8,** 4192–4213. doi:10.1523/JNEUROSCI.08-11-04192.1988 (1988).

17. Martins, S. *et al.* Toward an Integrated Zebrafish Health Management Program Supporting Cancer and Neuroscience Research. *Zebrafish* **13,** S–47–S–55. doi:10.1089/zeb.2015.1198 (S1 2016).

18. Félix, R. *et al.* Structural and functional organization of visual responses in the inferior olive of larval zebrafish. *The Journal of Neuroscience,* e2352212023. doi:10.1523/JNEUROSCI.2352-21.2023 (2024).

19. Feierstein, C. E. *et al.* Dimensionality reduction reveals separate translation and rotation populations in the zebrafish hindbrain. *Current Biology* **33,** 3911–3925.e6. doi:10.1016/j.cub.2023.08.037 (2023).

20. Wohlberg, B. *SPORCO: A Python package for standard and convolutional sparse representations* in *Proceedings of the 16th Python in Science Conference* Python in Science Conference (SciPy, Austin, Texas, 2017), 1–8. doi:10.25080/shinma-7f4c6e7-001.

21. Cogliati, A., Duan, Z. & Wohlberg, B. Piano Transcription With Convolutional Sparse Lateral Inhibition. *IEEE Signal Processing Letters* **24,** 392–396. doi:10.1109/LSP.2017.2666183 (2017).

22. Severi, K. E., Böhm, U. L. & Wyart, C. Investigation of hindbrain activity during active locomotion reveals inhibitory neurons involved in sensorimotor processing. *Scientific Reports* **8.** doi:10.1038/s41598-018-31968-4 (2018).

23. Müller, U. K. & Van Leeuwen, J. L. Swimming of larval zebrafish: ontogeny of body waves and implications for locomotory development. *Journal of Experimental Biology* **207,** 853–868. doi:10.1242/jeb.00821 (2004).

24. Ahrens, M. B., Orger, M. B., Robson, D. N., Li, J. M. & Keller, P. J. Whole-brain functional imaging at cellular resolution using light-sheet microscopy. *Nature Methods* **10,** 413–420. doi:10.1038/nmeth.2434 (2013).

25. Vladimirov, N. *et al.* Light-sheet functional imaging in fictively behaving zebrafish. *Nature Methods* **11,** 883–884. doi:10.1038/nmeth.3040 (2014).

26. Bouchard, M. B. *et al.* Swept confocally-aligned planar excitation (SCAPE) microscopy for high-speed volumetric imaging of behaving organisms. *Nature Photonics* **9,** 113–119. doi:10.1038/nphoton.2014.323 (2015).

27. Portugues, R. & Engert, F. Adaptive Locomotor Behavior in Larval Zebrafish. *Frontiers in Systems Neuroscience* **5.** doi:10.3389/fnsys.2011.00072 (2011).

28. Mu, Y. *et al.* Glia Accumulate Evidence that Actions Are Futile and Suppress Unsuccessful Behavior. *Cell* **178,** 27–43.e19. doi:10.1016/j.cell.2019.05.050 (2019).

29. Mullen, T. *et al. Learning interpretable control inputs and dynamics underlying animal locomotion* in. 3rd International Conference on Learning Representations (ICLR) (Vienna, Austria, 2024).

30. McLean, D. L., Masino, M. A., Koh, I. Y. Y., Lindquist, W. B. & Fetcho, J. R. Continuous shifts in the active set of spinal interneurons during changes in locomotor speed. *Nature Neuroscience* **11,** 1419–1429. doi:10.1038/nn.2225 (2008).

31. Batty, R. Locomotion of plaice larvae. *Symp. Zool. Soc. Zool.,* 53–69 (1981).

32. Hale, M. E. Pectoral fin coordination and gait transitions in steadily swimming juvenile reef fishes. *Journal of Experimental Biology* **209,** 3708–3718. doi:10.1242/jeb.02449 (2006).

33. Green, M. H. & Hale, M. E. Activity of pectoral fin motoneurons during two swimming gaits in the larval zebrafish (*Danio rerio*) and localization of upstream circuit elements. *Journal of Neurophysiology* **108,** 3393–3402. doi:10.1152/jn.00623.2012 (2012).

34. Ehrlich, D. E. & Schoppik, D. A primal role for the vestibular sense in the development of coordinated locomotion. *eLife* **8,** e45839. doi:10.7554/eLife.45839 (2019).

35. Hale, M. E. Developmental Change in the Function of Movement Systems: Transition of the Pectoral Fins between Respiratory and Locomotor Roles in Zebrafish. *Integrative and Comparative Biology* **54,** 238–249. doi:10.1093/icb/icu014 (2014).

36. Dunn, T. W. *et al.* Brain-wide mapping of neural activity controlling zebrafish exploratory locomotion. *eLife* **5.** doi:10.7554/eLife.12741 (2016).

37. Dunn, T. W. *et al.* Neural Circuits Underlying Visually Evoked Escapes in Larval Zebrafish. *Neuron* **89,** 613–628. doi:10.1016/j.neuron.2015.12.021 (2016).

38. Montgomery, J. C., Baker, C. F. & Carton, A. G. The lateral line can mediate rheotaxis in fish. *Nature* **389,** 960–963. doi:10.1038/40135 (1997).

39. Valera, G. *et al.* A neuronal blueprint for directional mechanosensation in larval zebrafish. *Current Biology* **31,** 1463–1475.e6. doi:10.1016/j.cub.2021.01.045 (2021).

40. Harris, J. A. *et al.* Neomycin-Induced Hair Cell Death and Rapid Regeneration in the Lateral Line of Zebrafish (Danio rerio). *JARO - Journal of the Association for Research in Otolaryngology* **4,** 219–234. doi:10.1007/s10162-002-3022-x (2003).

41. Voesenek, C. J., Pieters, R. P. M. & Van Leeuwen, J. L. Automated Reconstruction of Three-Dimensional Fish Motion, Forces, and Torques. *PLOS ONE* **11** (ed Borazjani, I.) e0146682. doi:10.1371/journal.pone.0146682 (2016).

42. Nair, A., Azatian, G. & McHenry, M. J. The kinematics of directional control in the fast start of zebrafish larvae. *Journal of Experimental Biology,* jeb.126292. doi:10.1242/jeb.126292 (2015).

43. Van Leeuwen, J. L., Voesenek, C. J. & Müller, U. K. How body torque and Strouhal number change with swimming speed and developmental stage in larval zebrafish. *Journal of The Royal Society Interface* **12,** 20150479. doi:10.1098/rsif.2015.0479 (2015).

44. Horstick, E. J., Bayleyen, Y., Sinclair, J. L. & Burgess, H. A. Search strategy is regulated by somatostatin signaling and deep brain photoreceptors in zebrafish. *BMC Biology* **15,** 4. doi:10.1186/s12915-016-0346-2 (2017).

45. Fetcho, J. R. & Svoboda, K. R. Fictive swimming elicited by electrical stimulation of the midbrain in goldfish. *Journal of Neurophysiology* **70,** 765–780. doi:10.1152/jn.1993.70.2.765 (1993).

46. Buss, R. R. & Drapeau, P. Synaptic Drive to Motoneurons During Fictive Swimming in the Developing Zebrafish. *Journal of Neurophysiology* **86,** 197–210. doi:10.1152/jn.2001.86.1.197 (2001).

47. Buss, R. R. & Drapeau, P. Activation of Embryonic Red and White Muscle Fibers During Fictive Swimming in the Developing Zebrafish. *Journal of Neurophysiology* **87,** 1244–1251. doi:10.1152/jn.00659.2001 (2002).

48. Ahrens, M. B., Huang, K. H., Narayan, S., Mensh, B. D. & Engert, F. Two-photon calcium imaging during fictive navigation in virtual environments. *Frontiers in Neural Circuits* **7.** doi:10.3389/fncir.2013.00104 (2013).

49. Kist, A. M. & Portugues, R. Optomotor Swimming in Larval Zebrafish Is Driven by Global Whole-Field Visual Motion and Local Light-Dark Transitions. *Cell Reports* **29,** 659–670.e3. doi:10.1016/j.celrep.2019.09.024 (2019).

50. Koning, H. K., Ahemaiti, A. & Boije, H. A deep-dive into fictive locomotion - a strategy to probe cellular activity during speed transitions in fictively swimming zebrafish larvae. *Biology Open* **11,** bio059167. doi:10.1242/bio.059167 (2022).

51. Bhatt, D. H., McLean, D. L., Hale, M. E. & Fetcho, J. R. Grading movement strength by changes in firing intensity versus recruitment of spinal interneurons. *Neuron* **53,** 91–102. doi:10.1016/j.neuron.2006.11.011 (2007).

52. McLean, D. L., Fan, J., Higashijima, S.-i., Hale, M. E. & Fetcho, J. R. A topographic map of recruitment in spinal cord. *Nature* **446,** 71–75. doi:10.1038/nature05588 (2007).

Chapter 3

Characterisation of transgenic lines labelling reticulospinal neurons

*From lamprey to monkeys, the organisation of the descending control of locomotion is conserved across vertebrates. Reticulospinal neurons (**RSNs**) form a bottleneck for descending commands, receiving innervation from diencephalic and mesencephalic locomotor centres and providing locomotor drive to spinal motor circuits. Given their optical accessibility in early development, larval zebrafish offer a unique opportunity to study reticulospinal circuitry. In fish, RSNs are a small, highly stereotyped, uniquely identifiable group of large neurons spanning from the midbrain to the medulla. Classically labelled by tracer dye injections into the spinal cord, recent advances in genetic tools have facilitated the targeted expression of transgenes in diverse brainstem neurons of larval zebrafish. Here, I provide a comparative characterization of four existing and three newly established transgenic lines in larval zebrafish. I determine which identified neurons are consistently labelled and offer projection-specific genetic access to subpopulations of RSNs. I showcase transgenic lines that label most or all RSNs (nefma, adcyap1b^{ccu96Et}) or subsets of RSNs, including ipsilateral (vsx2, calca^{ccu75Et}), contralateral (pcp4a^{ccu97Tg}) or all (tiam2a^{y264Et}) components of the Mauthner array, or midbrain-only RSNs (s1171tEt). In addition to RSNs, selected transgenic lines (nefma, s1171tEt, calca^{ccu75Et}) labelled other potential neurons of interest in the brainstem. For those, I performed in situ hybridisation to show expression patterns of several excitatory and inhibitory neurotransmitters at larval stages as well as glutamatergic expression patterns in juvenile fish. I provide an overview of transgene expression in the brainstem of larval zebrafish that serves to lay a foundation for future studies in the supraspinal control of locomotion.*

3.1 Introduction

Animals are constantly faced with the need to produce flexible behaviour in response to a rapidly changing environment. From foraging for food, finding a mate, to escaping from predators – movement is central to survival. As such, many regions of the central nervous system are dedicated to its production [1]. A key processing site for descending locomotor commands is the reticular formation (**RF**), situated in the brainstem and comprised of several nuclei. The RF contains cholinergic [2, 3], monoaminergic [4], GABA/glycinergic and glutamatergic neurons [5], with glutamatergic reticulospinal neurons (**RSNs**) forming the key excitatory descending output [6]. RSNs receive descending input from the mesencephalic and diencephalic locomotor regions (**MLR, DLR**) and the cerebellum, as well as ascending signals from the spinal cord allowing for sensorimotor integration. Their main output is to central pattern generators comprised of spinal inter- and motor neurons, responsible for movement production (for a comprehensive review on the descending control of locomotion see [7]). A central question in neuroscience has long been whether different behaviours are generated by distinct or overlapping populations of RSNs [8], and if so, whether activity is localised or distributed across the brainstem. The ability to label, activate and manipulate subsets of RSNs is critical in addressing these questions.

Larval zebrafish are ideally suited to studying brainstem circuitry due to their small size, high fecundity, array of available genetic tools, optical accessibility and well-characterised behavioural repertoire [9]. For decades, researchers have labelled reticulospinal neurons by spinal injections of tracer compounds, such as horseradish peroxidase or dextran-conjugated dyes [10–14]. While these have been instrumental in disentangling reticulospinal circuity, labelling can be variable depending on the skill of the experimenter, and it is challenging to consistently label descending neurons of small axon calibre. In addition, spinal injections are necessarily damaging to spinal axon tracts and carry the risk of affecting subsequent behavioural studies. A solution comes from several recently established transgenic lines with expression in the brainstem [15–18]. Given the sometimes stochastic expression patterns in Gal4 lines [19], it would be useful to understand precisely

which RSNs are labelled by each transgenic line across a number of animals. Additionally, gaining genetic access to all as well as to selected subpopulations of RSNs, for instance ipsi- vs contralaterally-projecting RSNs, would offer an excellent opportunity when combined with optogenetic tools to decipher cell-specific functions in the control of locomotion.

Here, I characterised seven transgenic lines driving gene expression in the brainstem in larval zebrafish at 6 days-post-fertilisation: four existing transgenic lines *(nefma, vsx2, s1171tEt, tiam2a*^{y264Et}) and three newly established transgenic lines *(calca*^{ccu75Et}*, pcp4a*^{ccu97Tg}*, adcyap1b*^{ccu96Et}*).* For each transgenic line, I performed retrograde labelling of reticulospinal neurons followed by immunohistochemistry and quantified overlap across fish at the single-cell level. I showcase transgenic lines that label most or all RSNs (*nefma, adcyap1b*^{ccu96Et}), midbrain-only RSNs (*s1171tEt*), or subsets of RSNs, including ipsilateral (*vsx2, calca*^{ccu75Et}), contralateral (*pcp4a*^{ccu97Tg}) or all (*tiam2a*^{y264Et}) components of the Mauthner array.

For select transgenic lines *(nefma, s1171tEt, calca*^{ccu75Et}*)* I performed *in situ* hybridisation to show expression patterns of genes associated with several neurotransmitter phenotypes *(vglut1, vglut2a, vglut2b, chata, gad1b, gad2, glyt1, glyt2)* at larval stages as well as glutamatergic expression in juvenile fish demonstrating consistency across development. By providing a comprehensive overview of transgene expression in the brainstem of larval zebrafish I set a foundation for future studies in the supraspinal control of locomotion.

3.2 Materials and Methods

3.2.1 Fish husbandry

Adult fish were raised and bred at 28°C on a 14h light / 10h dark cycle following standard husbandry methods as detailed in [20]. All fish colonies were maintained under meticulous plans involving importation of wild types every 1-3 years and line-specific breeding schemes designed to reduce inbreeding depression [20]. Embryos were collected and larvae were raised at 28°C in E3 embryo medium (5 mM NaCl, 0.17 mM KCl, 0.33 mM CaCl2 and 0.33 mM MgSO4, changed daily) at

a density of 100 larvae per 200 mL until euthanasia at 6 days-post-fertilisation (**dpf**). From 5 dpf onwards, approximately 10 mL of a live L-type rotifer polyculture (containing 1000-2000 rotifers per mL) were added to each dish twice a day and larvae were allowed to feed freely. Zebrafish do not sexually differentiate until approximately 3 months of age, therefore the sex of the animals cannot be reported. All experimental procedures were approved by the Champalimaud Foundation Ethics Committee and the Portuguese Direcção Geral Veterinária, and were performed according to the European Directive 2010/63/EU.

3.2.2 Transgenic lines

The following transgenic lines were used in a nacre (mitfa -/-) background (see Table 3.1). With the exception of *vsx2*, which the lab received as an mRFP line, and *s1171tEt*, which was crossed with Tg[10xUAS:GCaMP6f^{ccu1Tg}] [21], the lines used in the experiments were created by crossing with Tg[10x UAS:GCaMP6fEF05^{ccu2Tg}] [22].

Short name	**Transgenic line**	**Source**
nefma	Tg[nefma:KalTa4]	[15]
tiam2a^{y264Et}	Tg[tiam2a$^{y264Et(B)}$]	[18]
s1171tEt	Tg[-0.6hsp70l:Gal4-VP16$^{s1171tEt+}$]	[16, 23]
vsx2	TgBAC[vsx2:Gal4FF^{nns18Tg}]	[24]
calca^{ccu75Et}	Tg[-5.0calca:Gal4FF^{ccu75Et}]	this paper
adcyap1b^{ccu96Et}	Tg[-1.7adcyap1b:Gal4FF^{ccu96Et}]	this paper
pcp4a^{ccu97Tg}	TgBAC[pcp4a:Gal4FF^{ccu97Tg}]	this paper
	Tg[10xUAS:GCaMP6f^{ccu1Tg}]	[21]
	Tg[10xUAS:GCaMP6fEF05^{ccu2Tg}]	[22]
	Tg[UAS:mRFP]	[25]

Table 3.1: Transgenic fish lines used for immunohistochemistry and *in situ* hybridisation experiments.

3.2.3 Cloning

adcyap1b:Gal4FF A 1679bp promoter region upstream of adcyap1b start codon was cloned into pCR™8/GW/ TOPO™ (Invitrogen™) using the following primers:

- 5'-GAACTGGAACACTTGGTGGCAGTATTG-3'
- 5'-GATCTGGCCAGGCTGTAAAGATACAAGAAAG-3'.

The adcyap1b promoter (Entry Clone) was then recombined into an Gal4FF destination vector (Gateway™ LR recombination, Invitrogen™), derived from the Tol2Kit [26], so that the construct was bracketed by two Tol2 [27] inverted terminal repeats.

calca:Gal4FF A 5023bp promoter region upstream of calca start codon was cloned into pCR™8/GW/TOPO™ (Invitrogen™) using the following primers:

- 5'-GTGCCTGCTGAGGAGCATAAC-3'
- 5'-GGTCCCCTGTAGTAAAACATC-3'

The calca promoter (Entry Clone) was then recombined into the Tol2 Gal4FF destination vector (Gateway™ LR recombination, Invitrogen™).

pcp4a:Gal4FF The Tg[pcp4a:Gal4FF^{ccu97Tg} line was generated using bacterial artificial chromosome (BAC) recombineering following [28]. In short, the iTol2-amp cassette was introduced into BAC CH211-231M12. Positive clones were selected to further introduce the Gal4FF-pA-FRT-kan-FRT at the ATG site of *pcp4a*. To do so, homology arms, short DNA sequences of about 300bp that flanked the ATG site and with sequence overlap to the Gal4FF-pA-FRT-kan-FRT, were amplified from the BAC:

- *pcp4a-HI-for* CACACACCAATGCATACATCAAAGCG
- *pcp4a-HI-rev* ACAGTAGCTTCATGGTGGCGCTGGATGAAGAGTATGAA-GATGAAGGAA GAAG
- *pcp4a-HII-for* CCAGCCTACACGCGGGTGAGCTTTCCTCCATACACATTG-CACA
- *pcp4a-HII-rev* GCGCACATACAATATCCTCCATCCCT

Similarly, the Gal4FF-pA-FRT-kan-FRT cassette was amplified using primers overlapping with the homology arms:

- *pcp4a-GFF-for* CATCTTCATACTCTTCATCCAGCGCCACCATGAAGCTACTGTCTTCTATCGAAC
- *pcp4a-GFF-rev* TGTGTATGGAGGAAAGCTCACCCGCGTGTAGGCTGGAGCTGCTTC

The 3 DNA fragments were fused using the Gibson Assembly Cloning kit (New England Biolabs) and subcloned into the pCR2.1-TOPO vector (Invitrogen). The pcp4a-HI-for and pcp4a-HII-rev primer were used for further amplification of the cassette. 500ng of it was used for recombination with the CH211-231M12/iTol2-amp BAC.

Line establishment DNA constructs were injected together with Tol2 transposase mRNA and non-integrating UAS:GFP plasmid into 1-2 cell stage mitfa-/- eggs. Embryos with GFP expression were raised and screened as adults for germ line transmission. Progeny of positive animals with stable expression pattern were selected as founders for the respective Gal4FF driver line.

3.2.4 Screening

Larvae were pre-screened at 3-4 dpf to select fish with positive expression of GCaMP or RFP. While this is standard practice, I note that some lines appear to have less than Mendelian numbers of offspring with expression presumably due to silencing [19]. For instance, the $pcp4a^{ccu97Tg}$ line seems to be particularly prone to silencing, which can be remedied by setting multiple crosses and rigorous pre-screening.

3.2.5 Immunohistochemistry

The staining was performed in all seven transgenic lines (Table 3.1) according to a modified protocol [29].

Dye injections Larvae were raised in standard conditions (see above) until 5 dpf, fed with rotifers in the morning and injected in the afternoon. Larvae were injected while mounted sideways on a small petri dish containing a layer of agarose

gel (SeaKem LE Agarose, #50004, Lonza), following previously described methods [30]. The dye (10,000MW at 50mg/mL of Dextran, Alexa Fluor 647, Invitrogen by Life Technologies) was pressure-injected into the spinal cord near myomere 8 using a pulled capillary glass needle (GC100F-10, Harvard Apparatus) positioned with a micro-manipulator (MN-153, Narishige) and a stereo-microscope (Stereo Discovery V8, Zeiss). Pressure was applied using a pneumatic picopump (WPI, PV820). Following injection, larvae were allowed to recover overnight and checked for normal swimming behaviour before euthanasia.

Immunohistochemistry At 6 dpf, larvae were anaesthetized in 15mM tricaine (E10521, Sigma-Aldrich) for 10 min and fixed with 4% paraformaldehyde (**PFA**) for 2 hours at room temperature while covered and with agitation. From this step onwards, larvae were kept in darkness. To stop fixation, larvae were rinsed and washed 2 x 5 min in phosphate-buffered saline with 0.25% Triton (**PBT**) with agitation. For epitope retrieval, larvae were rinsed twice, washed 1 x 5 min, and finally incubated in 150mM Tris-HCl with pH 9.0 at 70°C in a water bath. Following incubation, samples were cooled on ice and washed 3 x 5 min in PBT. To permeabilise, larvae were incubated in 0.05% Trypsin-EDTA in phosphate-buffered saline (**PBS**) for 5 min on ice, followed by a rinse and 2 x 5 min washes in PBT. Next, larvae were incubated in blocking solution (PBS, bovine serum albumin, normal goat serum, dimethyl sulfoxide, Triton, azide, sterilised H_2O) at 4°C overnight. A primary antibody solution was prepared by diluting primary antibodies for anti-tERK and anti-GFP or anti-mCherry (Table 3.2) in blocking solution at 1:500. Blocking solution was replaced by the primary antibody solution and larvae were allowed to incubate for at least three over-nights at 4°C under cover with agitation. To remove primary antibodies, larvae were rinsed three times and washed 3 x 30 min in PBT. A secondary antibody solution was prepared by diluting secondary antibodies in blocking solution at 1:500. Larvae were incubated in secondary antibody solution for at least three over-nights at 4°C with agitation. To remove secondary antibodies (Table 3.2), larvae were rinsed three times and washed 3 x 30 min in PBT. Samples were stored in PBT at 4°C in the dark until imaging.

Reagents	Source	Identifier
Dye for Backfills		
Dextran, Alexa Fluor™ 647	Life Technologies	D22914
Primary Antibodies		
Chicken anti-GFP	Abcam Limited	ABCAM-13970
Mouse anti-tERK	Cell Signaling Tech.	#4696
Rabbit anti-mCherry	Abcam Limited	ABCAM-167453
Secondary Antibodies		
Goat anti-Chicken IgY Alexa Fluor™ 488	Life Technologies	A-11039
Goat anti-Mouse IgG Alexa Fluor™ 568	Life Technologies	A-11004
Goat anti-Mouse IgG Alexa Fluor™ 488	Life Technologies	A-11001
Goat anti-Rabbit IgG Alexa Fluor™ 568	Life Technologies	A-11011

Table 3.2: Reagents used for immunohistochemistry experiments in this study.

3.2.6 *In situ* hybridisation chain reaction in larval zebrafish

In situ hybridisation chain reaction (**isHCR**) reagents, including probes, hairpins, and buffers, were purchased from Molecular Instruments (Los Angeles, CA, USA) for detection of mRNAs. The staining was performed according to the "HCR v3.0 protocol for whole-mount zebrafish embryos and larvae" protocol provided by Molecular Instruments [31]. The following transgenic lines were used in a nacre (mitfa -/-) background: Tg[nefma:KalTa4, 10xUAS:GCaMP6fEF05], Tg[-5.0calca:Gal4FF^{ccu75Et}, 10xUAS:GCaMP6fEF05] and Tg[-0.6hsp70l:Gal4-VP16$^{s1171tEt+}$, 10xUAS:GCaMP6f].

Tissue fixation At 6 dpf, larvae were anaesthetised in 15mM tricaine (E10521, Sigma-Aldrich) and fixed with 4% PFA overnight at 4°C while covered and gently agitated. From this step onwards, larvae were continuously kept in darkness.

Tissue preparation On the following day, larvae were washed 3 x 5 min in PBS to stop fixation, dehydrated and permeabilised with a series of 100% methanol (**MeOH**) washes and stored at -20°C for up to 6 months before use. MeOH-fixed

larvae were re-hydrated progressively with a series of graded MeOH in PBS with Tween 0.1% (**PBST**) washes at room temperature with agitation for 5 min each. Next, larvae were treated with proteinase K (30μg/mL) for 45 minutes at room temperature, rinsed twice with PBST, post-fixed with 4% PFA for 20 minutes at room temperature and finally washed thoroughly 5 x 5 min with PBST with agitation.

Detection Larvae were pre-hybridised with 500μL of probe hybridisation buffer for 30 minutes at 37°C. Probe solutions were prepared by adding 2pmols of each probe set (Table 3.3) to 500μL of probe hybridisation buffer at 37°C. The pre-hybridisation solution was replaced with the probe solution mix and larvae were incubated overnight at 37°C. The following day, excess probes were removed by washing larvae 4 x 15 min with 500μL of probe wash buffer at 37°C, followed by 2 x 5 min washes with 5x sodium chloride sodium citrate buffered with 0.1% Tween (**5xSSCT**) at room temperate with agitation. Note that in the isHCR 3.0 method, detection of an mRNA requires a mixture of primers, each of them including a part that is complementary to the target RNA and another part that is used for amplification of the signal (named B1 to B5). Table 3.3 summarises the probes indicating their target and the amplification reagent used.

Amplification Pre-amplification was performed by incubating with 500μL of amplification buffer for 30 min at room temperature. Next, 30pmol of hairpin h1 and 30pmol of hairpin h2 were prepared by snap-cooling 10μL of 3μM stock: hairpins were heated separately at 95°C for 90 seconds and allowed to cool down to room temperature in a dark drawer for 30 min. After cooling down, the hairpin solution was prepared by adding snap-cooled h1 and h2 hairpins to 500μL of amplification buffer at room temperature. The pre-amplification solution was replaced with the hairpin solution and larvae were incubated overnight in the dark at room temperature. On the next day, excess hairpins were removed by washing the samples with 500μL of 5xSSCT at room temperature with agitation for 2 x 5min, 2 x 30min and 1 x 5min. Samples were stored at 4°C in 5xSSCT in the dark until imaging.

3.2.7 *In situ* hybridisation chain reaction in juvenile zebrafish

To perform *in situ* hybridisation chain reaction in juvenile fish, the aforementioned *isHCR* 3.0 protocol for larval zebrafish from Molecular Instruments (Los Angeles, CA) was adapted using methods from [32] as well as considering advice from Molecular Instruments on adapting the protocol for adult zebrafish (Dr. Chanpreet Singh, personal communication).

Tissue fixation Juvenile zebrafish Tg[-0.6hsp70l:Gal4-VP16$^{s1171tEt+}$] at 4 weeks post-fertilisation were anaesthetised in 15 mM tricaine tricaine (E10521, Sigma-Aldrich) for 5 minutes and immersed in ice-cold fish facility water for 20 minutes. Absence of reflexes were assessed before fish were dissected caudal to cloaca using a razor blade and heads were placed in ice-cold PBS for 10 minutes to let blood drain. Samples were fixed in 4% PFA overnight at 4°C with gentle agitation.

Tissue preparation The next day, samples were washed 2x for 5min in cold PBS, followed by careful dissection of brains into cold, sterile PBS and stored at 4°C until further processing. Following dissection, samples were split into groups of 4 and washed 3x for 5min in PBS at room temperature with gentle agitation. Then, samples were dehydrated using a series of MeOH/PBS mixtures (1h each in 20%, 40%, 60%, 80% and 2x 100% MeOH). Samples were washed 2x for 5min in 100% MeOH and incubated in 5% hydrogen peroxide in MeOH overnight at 4°C. The next day, samples were rehydrated using a series of MeOH/PBS mixtures (1h each in 80%, 60%, 40% and 20% MeOH). Samples were washed 2x for 5min in PBS and then 2x for 1h in PBS with 0.2% TritonX-100 (**PTx.2**). Samples were then washed overnight at 37°C in permeabilisation solution (PTx.2, 0.3M glycine, 20% DMSO).

Detection and amplification The next day, samples were washed 2x for 5min in PTx.2. From here on, RNA detection was performed following the Detection and Amplification sections described above, with the following modifications: In the detection stage, probe solutions were prepared by adding 10pmols of each

probe set to 500μL of probe hybridisation buffer at 37°C. In the Amplification stage, 45pmol of hairpin h1 and 30pmol of hairpin h2 were used by snap-cooling 15μL of 3μM stock.

Clearing Samples were washed 2x for 5min in 50%SSC/50%PBS, dehydrated using a series of MeOH/PBS mixtures (1h each in 20%, 40%, 60%, 80% and 2x 100% MeOH) and incubated in 100% MeOH overnight at 4°C. The following day, samples were incubated in 66% dichloromethane in MeOH for 3h at room temperature. Samples were washed 2x for 15min dichloromethane and then stored in dibenzyl ether until imaging.

Reagents	**Source**	**Identifier**
HCR probes		
gad1b-B1: PRA299	Molecular Instruments	NM194419.1
gad2-B1: PRH743	Molecular Instruments	NM001017708.2
vglut2.1-B2: PRB128	Molecular Instruments	NM001128821.1
vglut2.2-B2: PRG620	Molecular Instruments	NM001009982.1
chATa-B3: RTA359	Molecular Instruments	NM001130719
glyt1-B4 (slc6a9): RTM844	Molecular Instruments	NM001030073
glyt2-B4 (slc6a5): B4RTO773	Molecular Instruments	NM001009557.1
vglut1-B5 (slc17a7a): RTM843	Molecular Instruments	NM001098755

Table 3.3: Reagents used for *in situ* hybridisation experiments in this study.

3.2.8 Imaging and Image Processing

Imaging conditions for larval zebrafish Samples were cut to remove most of the spinal cord for easier handling and mounted dorsal-side up in 1% low-melting point agarose (UltraPure LMP Agarose, Cat#16520100, Invitrogen by Life Technologies) prepared in PBS or SSC. Imaging of samples was performed on an upright confocal laser-scanning microscope (Zeiss, LSM 980) with a 25x multi-immersion objective (Zeiss, NA 0.8, Plan-Apochromat), using laser wavelengths 488, 594 and 650 nm. Images were acquired with a pixel size of 0.79μm in x

and y and sampled with a 1μm interval in the z axis. Pinhole size was 35μm, corresponding to 1.9μm confocal section.

Imaging conditions for juvenile zebrafish Samples were mounted dorsal-side up by attaching to a small petri dish lid using UV-cured glue (Bondic, UV Liquid Plastic Welder Starter Kit) and filling the lid with immersion oil (Gelest, PHENYLMETHYLSILOXANE OLIGOMER #PDM-7040) matching the refractive index of dibenzyl ether. Imaging of samples was performed on an upright confocal laser-scanning microscope (Zeiss, LSM 980) with a 25x multi-immersion objective (Zeiss, NA 0.8, Plan-Apochromat), using laser wavelengths 594 and 650 nm. Images were acquired with a pixel size of 0.79μm in x and y and sampled with a 2μm interval in the z axis. Pinhole size was 35μm, corresponding to 1.9μm confocal section.

Image processing Image analysis was performed using custom-written scripts in ImageJ processing package (Fiji). Briefly, where applicable, tiles were stitched and converted to a resolution that matches an in-house reference image. Using ANTs [33], each fish was registered to an in-house reference image of total extracellular signal-related kinase (**tERK**), which labels all neurons, or a transgenic line-specific reference image. All image processing was performed on a computer with 64.0 GB RAM and a Intel(R) Core(TM) i7-5820K CPU @ 3.30 GHz 3.30 GHz processor.

3.3 Results

In this study I characterised four existing (*nefma*, Tg[nefma:KalTa4]; *tiam2a*^{y264Et}, Tg[tiam2a$^{y264Et(B)}$]; *s1171tEt*, Tg[-0.6hsp70l:Gal4-VP16$^{s1171tEt+}$]; *vsx2*, TgBAC[vsx2: Gal4FF^{nns18Tg}]) and three new (*calca*^{ccu75Et}, Tg[-5.0calca: Gal4FF^{ccu75Et}]; *pcp4a*^{ccu97Tg}, TgBAC[pcp4a:Gal4FF^{ccu97Tg}]; *adcyap1b*^{ccu96Et}, Tg[-1.7adcyap1b:Gal4FF^{ccu96Et}]) transgenic lines. Each line was crossed with Tg[10xUAS:GCaMP6fEF05] unless reported otherwise. I note that transgenic lines based on small promoter regions will have expression patterns that may reflect the locus of insertion in the genome.

I have therefore denoted these lines as enhancer traps, indicating that they are not expected to be faithful reporters of the natural expression pattern of the genes from which the construct was derived. Here I aim to characterise these transgenic lines as tools in themselves, to lay a basis for dissecting the role of premotor brainstem neurons in movement production. I chose these transgenic lines as they label reticulospinal (**RSNs**) and other potential neurons of interest in the brainstem of larval zebrafish at 6 days-post-fertilisation (**dpf**) (Figure 3.1A). Briefly, *nefma*, *adcyap1b*^{ccu96Et} and *tiam2a*^{y264Et} label cells across the brainstem, *s1171tEt* in the tegmentum, and *pcp4a*^{ccu97Tg}, *calca*^{ccu75Et} and *vsx2* in the hindbrain. Larval zebrafish of each transgenic line were injected with dextran-conjugated tracer dye to retrogradely label RSNs and compared to their transgene expression profiles following immunohistochemistry and confocal imaging.

For transgenic lines (*nefma, calca*^{ccu75Et}*, s1171tEt*) that labelled cells beyond the classical RSNs I performed *in situ* hybridisation chain reaction (**isHCR**) to study the mRNA expression of different excitatory and inhibitory neurotransmitters: glutamate *(vglut1, vglut2a, vglut2b)*, acetyl choline transferase *(chata)*, gamma-aminobutyric acid *(GABA; gad1b, gad2)* and glycine *(glyt1, glyt2)* (Figure 3.1B). The vesicular glutamate transporter *vglut2* has two orthologs in zebrafish, *vglut2a* and *vglut2b*, which had largely overlapping brain-wide expression with two exceptions (Figure 3.2A). Two pairs of bilateral clusters were found in the medial hindbrain close to rhombomere 4 that strongly and exclusively expressed *vglut2b*, whereas *vglut2a* was more prominent in selected cells in the nucleus of the

---

Figure 3.1: Overview of transgenic lines and neurotransmitter-associated gene expression patterns.
A) Graphical summary of methods for reticulospinal backfills paired with immunohistochemistry (left) or *in situ* hybridisation (right), followed by confocal imaging, image registration to an average reference brain and analysis.
B) GCaMP expression in transgenic lines used in this study as indicated in each panel.
C) Expression of genes associated with neurotransmitter phenotypes as indicated in each panel.
For B) and C) each panel shows a maximum intensity projection from the dorsal and sagittal view, taken from average stack following image registration. Number of fish: *nefma* n=7, *calca*^{ccu75Et} n=12, *vsx2* n=11, *s1171tEt* n=5, *pcp4a*^{ccu97Tg} n=6, *adcyap1b*^{ccu96Et} n=8, *tiam2a*^{y264Et} n=6, *vglut1* n=16, *vglut2* n=13, *chata* n=8, *gad1b/2* n=4, *glyt1* n=16, *glyt2* n=15. Scale bar 100μm.

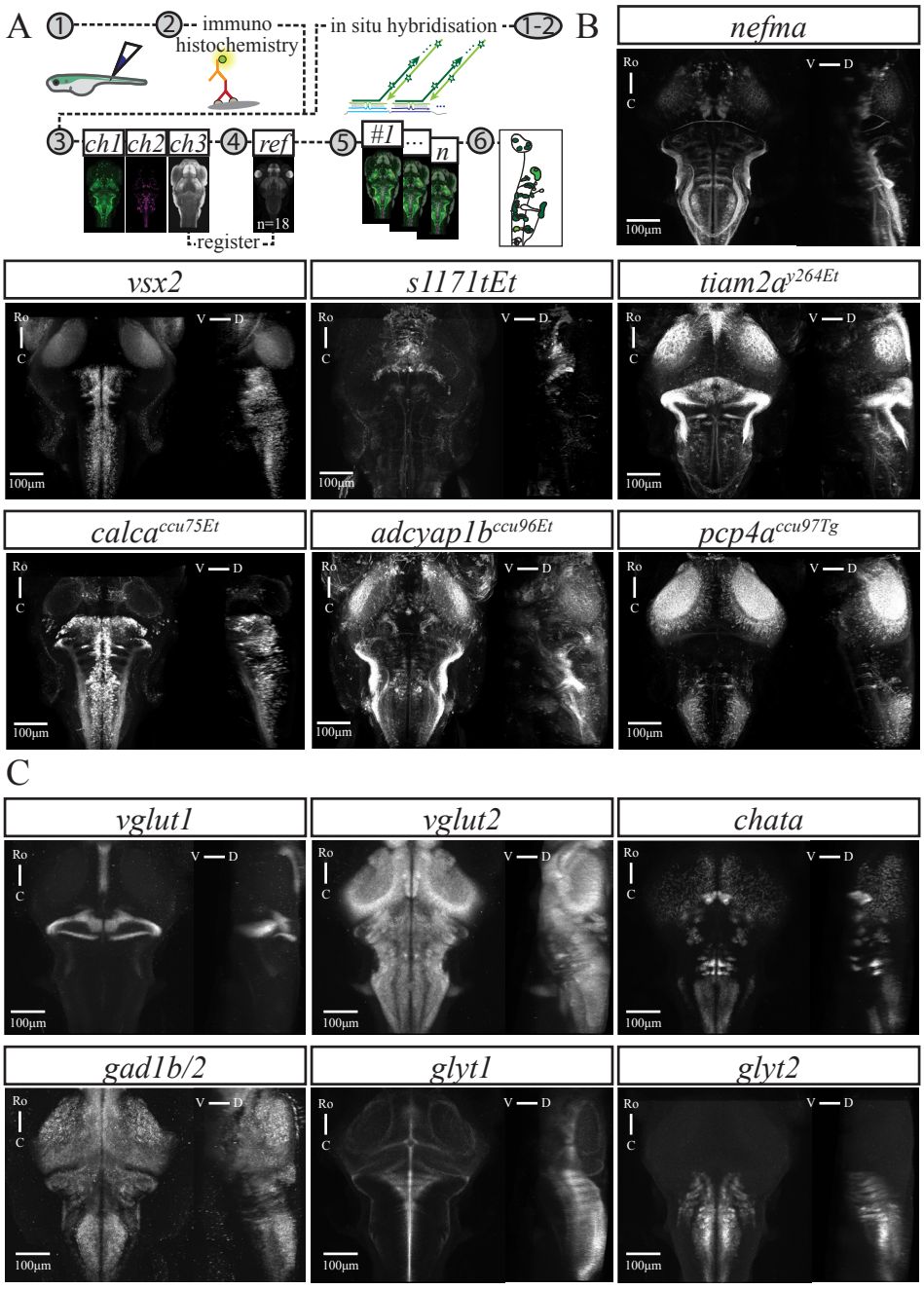

(Caption on previous page.)

medial longitudinal fasciculus (**nMLF**; Figure 3.2B). Overall the mRNA expression profiles are consistent with those found in the zebrafish brain atlas *mapzebrain* [34]. Except where explicitly stated, I refer to *vglut2* as a combination of *vglut2a* and *vglut2b*.

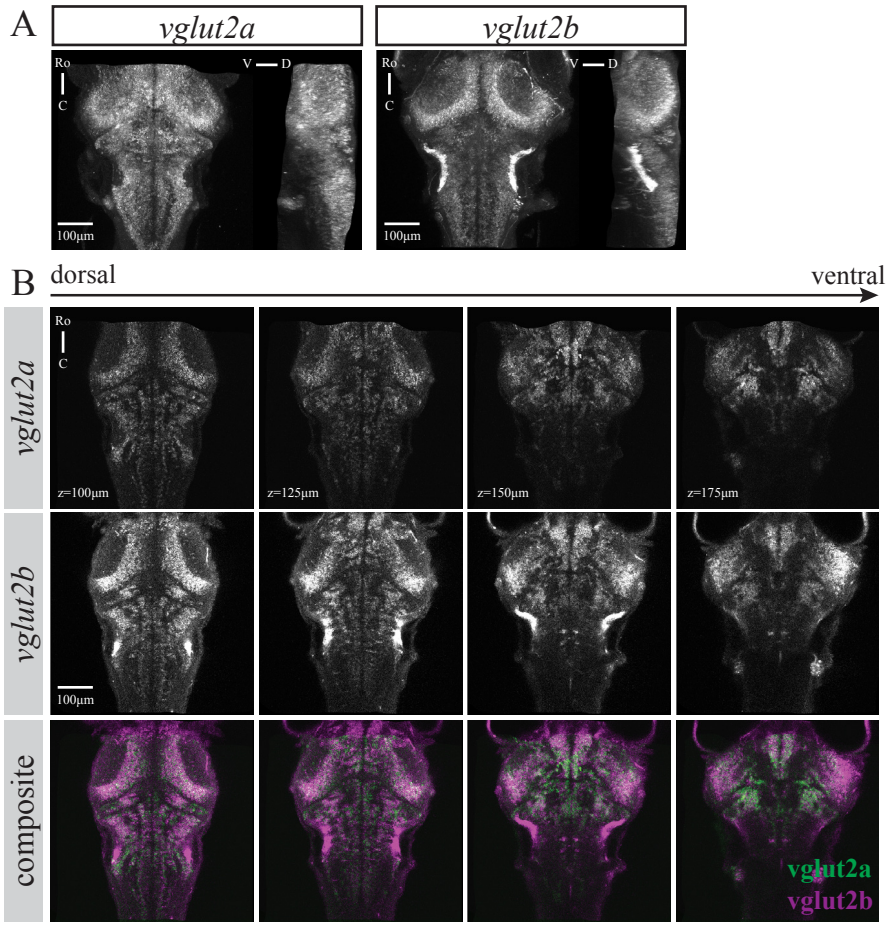

Figure 3.2: Difference in expression pattern between *vglut2a* and *vglut2b* in larval zebrafish at 6dpf.
A) Maximum intensity projections from dorsal and sagittal views of *vglut2a* and *vglut2b* mRNA expression following in situ hybridisation.
B) Single planes from dorsal (100μm) to ventral (175μm) at 50μm intervals in *vglut2a*, *vglut2b* and composite.
For both A and B, images are from two different single fish that were registered to a common average reference brain. Representative examples of *nefma* fish with either *vglut2a* (n=8) or *vglut2b* (n=7) expression. Scale bar is 100μm.

3.3.1 The *nefma* line labels all RSNs and cranial nerves

I examined the organisation of RSNs in a knock-in reporter line in the *nefma* gene [15] using dextran-conjugated retrograde labelling in larval zebrafish at 6 dpf (n=10). The *nefma* line has expression in the tectum, pre-tectum, tegmentum and hindbrain, as well as labelling the anterior and posterior lateral line ganglia, the trigeminal ganglion and neuromasts. In this line, the Mauthner cell is not present at this age because it degenerates between 3-5 dpf (data not shown; Dr J. Bin and Dr D. Lyons, The University of Edinburgh, personal communication). The back-labelled cells closely match the organisation previously described [11], which I term the 'classical' RSNs. All other classical RSNs that were back-labelled were present and expressing GCaMP (Figure 3.3A-B). This includes the four large canonical cells (MeM1, MeLm, MeLr, MeLc) in the nucleus of the medial longitudinal fasciculus (**nMLF**), also referred to as the interstitial nucleus of Cajal [35], and RSNs in the hindbrain, including the rostral RoL1 and RoM1-3 cells, various medial cell groups (MiV1, MiV2, MiM1, MiR1, MiR2), and the caudal MiD2, MiD3 and MiT cells (Table 3.4). Note that the rostro-lateral RoL2-RoL3 and the caudal CaD and CaV cells were not successfully back-labelled, most likely requiring a different injection strategy. However, it is highly likely these cells are still present in the *nefma* line. I see numerous small GCaMP-positive cells lateral to the RoM3 cells, which could be the RoL2-3, and there are large GCaMP-positive cells situated caudally to the MiD3 cells most likely constituting the CaD/CaV cells [11, 13].

Figure 3.3: The *nefma* line labels all RSNs as well as cranial nerve nuclei.
A) Maximum intensity projections (MIPs) from dorsal and sagittal view of an exemplary *nefma* fish (n=10) at 6 dpf with RSNs labelled via retrograde dye injection.
B) Close ups at several planes to illustrate overlap between *nefma* line and backfill, indicated by red triangles. Putative CaD and CaV cells indicated by blue triangle.
C) MIPs from dorsal and sagittal view of a *nefma* fish (n=24) at 6 dpf with *vglut2* mRNA expression.
D) Close ups at several planes to illustrate considerable overlap between *nefma* line and *vglut2*.
E) MIPs from dorsal and sagittal view of a *nefma* fish (n=16) at 6 dpf with *chata* mRNA expression.
F) Close ups at several planes to illustrate cranial nerves III-VII, IX-X and octavolateralis efferent nucleus (OLe) are labelled in the *nefma* line. For A,C,E scale bar 100μm, for B,D,F scale bar is 25μm.

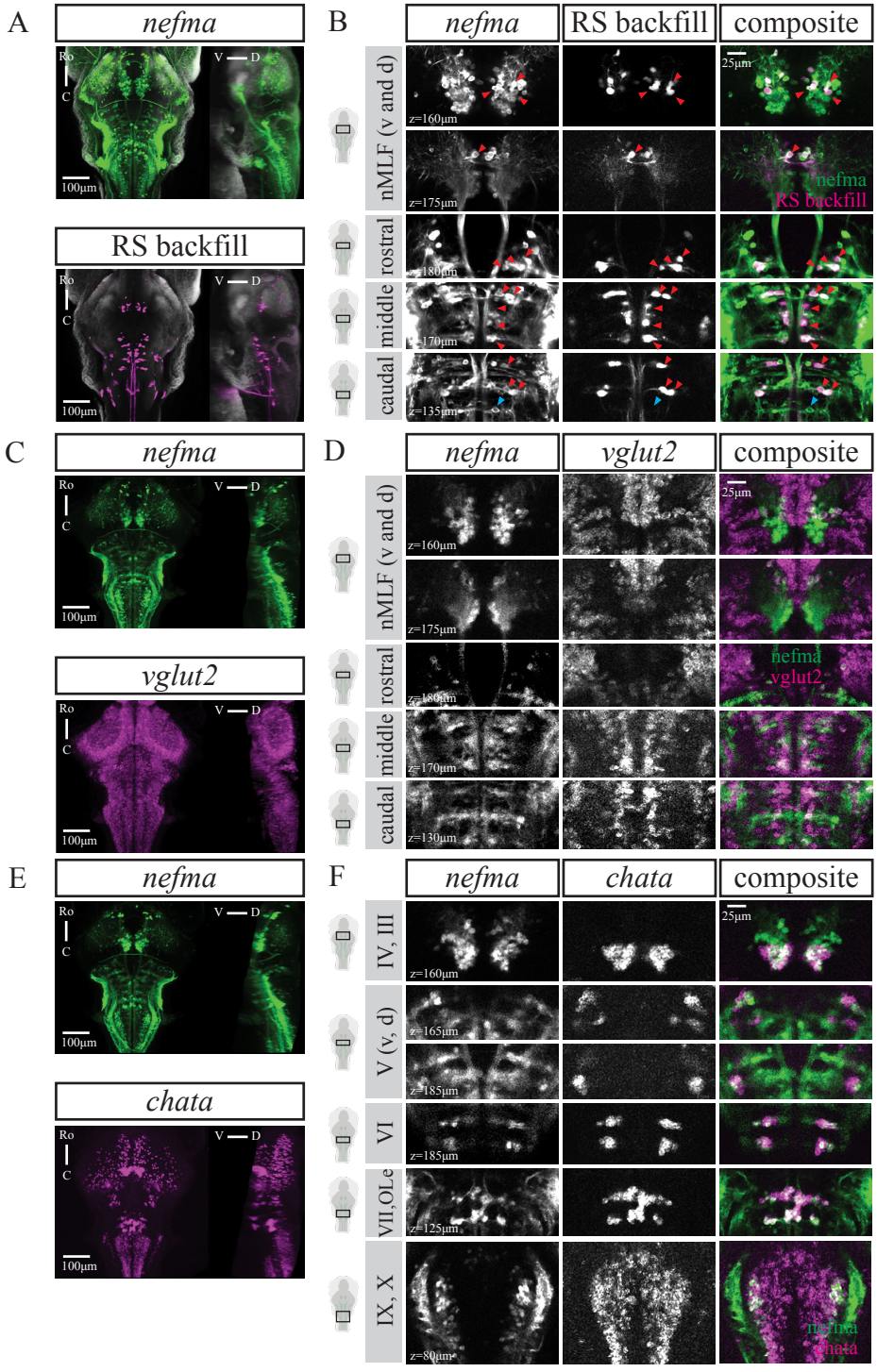

(Caption on previous page.)

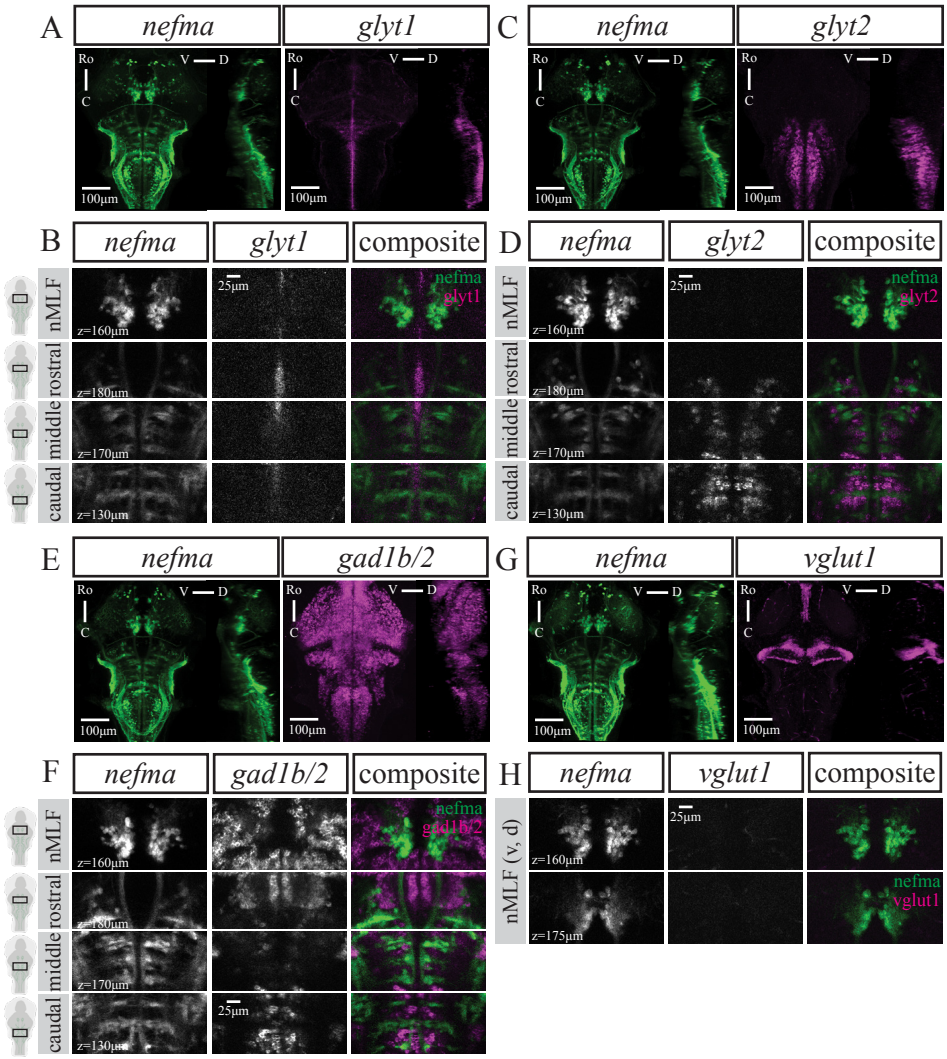

Figure 3.4: No GABAergic (*gad1b/2*), glycinergic (*glyt1, glyt2*) or glutamatergic (*vglut1*) expression in neurons labelled by the *nefma* line.
A,C,E,G) Maximum intensity projections from dorsal and sagittal view of an exemplary *nefma* fish at 6dpf with A) *gad1b/2* (n=8), C) *glyt1* (n=16), E) *glyt2* (n=15) or G) *vglut1* (n=14) mRNA expression. Scale bar is 100μm.
Close ups at several planes to better illustrate no overlap between *nefma* line and B) *gad1b/2*, D) *glyt1*, F) *glyt2* or H) *vglut1* mRNA-expressing neurons. Scale bar is 25μm.

The majority of cells labelled by the *nefma* line, including the classical RSNs, are glutamatergic (*vglut2*; Figure 3.3C-D) as confirmed by isHCR (n=24). In addition, the *nefma* line (n=16) labels cholinergic cells, which could be identified as the cranial nuclei (CNIII, oculomotor; CNIV, trochlear; CNV, trigeminal; CNVI, abducens; CNVII, facial; CNIX, glossopharyngeal; CNX, vagus) and octavolateralis efferent neurons (OLe; Figure 3.3E-F), with locations consistent with anatomical annotations in zebrafish atlases [34]. There was no *vglut1*, GABAergic *(gad1b/2)* or glycinergic *(glyt1, glyt2)* mRNA expression in cells labelled by the *nefma* line (Figure 3.4).

3.3.2 Transgenic lines offer access to subpopulations of RSNs

calca^{ccu75Et} A new Gal4 transgenic line was established using a 5kb fragment of the *calca* promoter. cRNA expression of calcitonin gene-related peptide alpha (**CALCA**) is brain-wide [**wang˙novel˙2016**] and a large genetic screen in our laboratory seeking to identify potentially interesting new transgenic lines showed promising expression in the hindbrain. Indeed, the *calca^{ccu75Et}* line mostly labels cells in the hindbrain, as well as a small number of cells in the mid- and forebrain, and outer retina. The organisation of RSNs in the *calca^{ccu75Et}* line was examined using dextran-conjugated retrograde labelling at 6dpf (n=12). Many of the classical RSNs that were visualised by the dye injection into the rostral spinal cord were

---

Figure 3.5: The *calca^{ccu75Et}* line labels only IL-RSNs and closely matches the *vsx2* line.
A) Maximum intensity projections from dorsal and sagittal view of an exemplary *calca^{ccu75Et}* fish (of n=12) at 6 dpf with reticulospinal neurons labelled via retrograde dye injection.
B) Close ups at several planes to illustrate overlap between *calca^{ccu75Et}* line and backfill. Note that only IL-RSNs are present in *calca^{ccu75Et}* as indicated by red triangles.
C) Maximum intensity projections from dorsal and sagittal view of an exemplary *calca^{ccu75Et}* fish (of n=8) at 6dpf with *vglut2* mRNA expression.
D) Close ups at several planes to illustrate overlap between *calca^{ccu75Et}* line and *vglut2*, particularly of the RSNs as well as a rostro-caudal glutamatergic (*vglut2*) stripe in the dorsal hindbrain.
E) Single planes from dorsal (105μm) to ventral (180μm) at 15μm intervals in *calca^{ccu75Et}*, *vsx2* and composite. For both top and middle panel, images are from two single fish (of n=12 each) that were registered to a common reference brain (tERK). For A,C,E scale bar 100μm, for B,D scale bar 25μm.

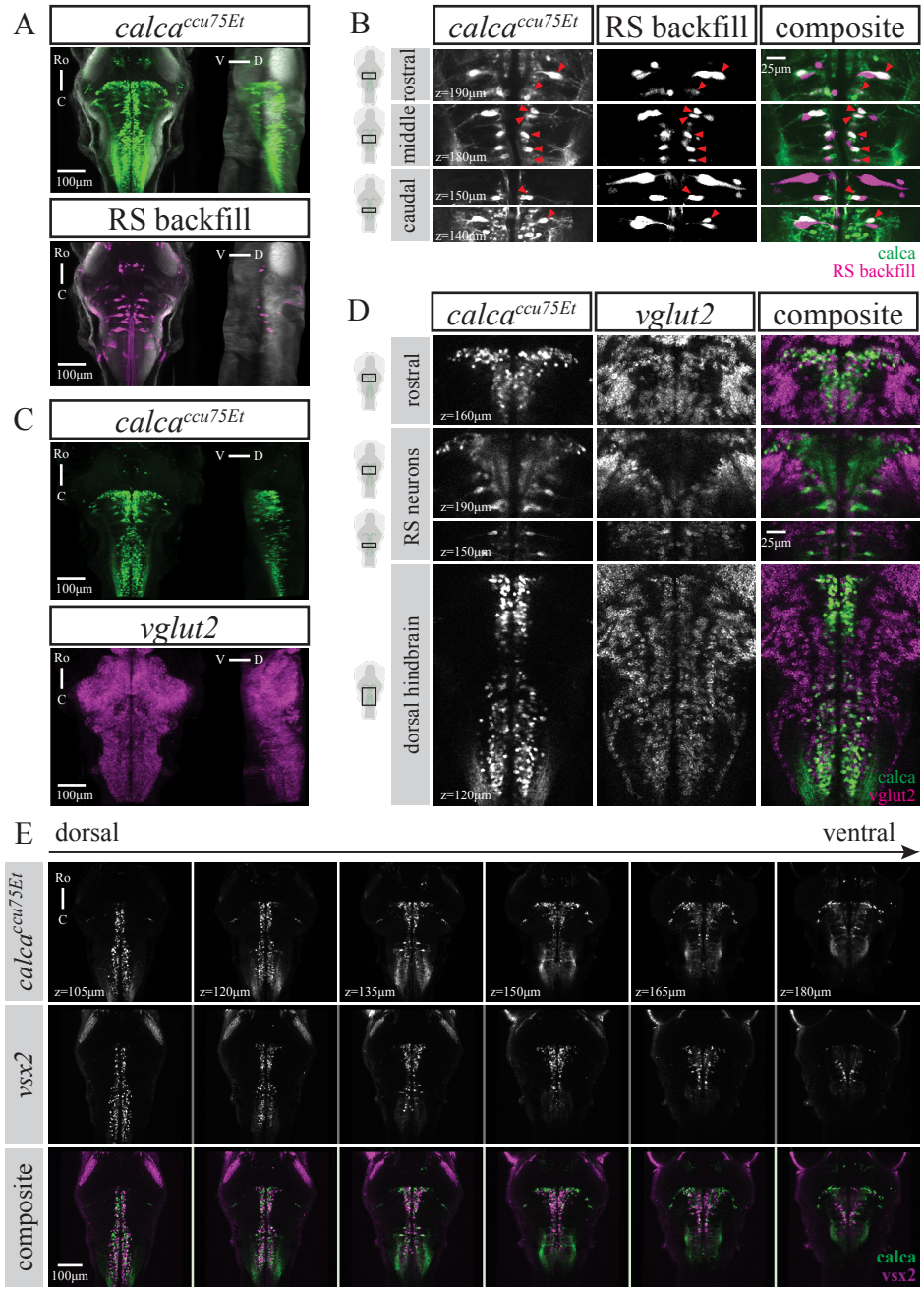

(Caption on previous page.)

also labelled by the *calca*^{ccu75Et} line (Figure 3.5A-B). This includes the rostral RoM2, RoM3 and RoV3 cells, the ventromedial cells (MiV1, MiV2, MiM1, MiR1, MiR2), and notably the caudal ipsilaterally-projecting (**IL**) MiD2i and MiD3i cells, but not their contralaterally-projecting (**CL**) counterparts. Following the projections of MiD2i and MiD3i at higher spatial resolution confirmed their identity as no decussation at the midline occurred (data not shown). In this line, the Mauthner cell is present but not labelled. For detailed RSN labelling across multiple fish see Table 3.6.

There was no cholinergic (*chata*), GABAergic (*gad1b/2*) or glycinergic (*glyt1, glyt2*) mRNA expression in cells labelled by the *calca*^{ccu75Et} line (Figure 3.6). In fact, most cells labelled in the *calca*^{ccu75Et} line were glutamatergic (*vglut2*), with a particularly prominent glutamatergic stripe spanning the whole medial dorsal hindbrain (Figure 3.5C-D). This strongly resembled the well-characterised *vsx2* line that has a characteristic medial stripe of glutamatergic V2a neurons in the hindbrain [17].

vsx2 I therefore compared the expression profiles of two *calca*^{ccu75Et} and *vsx2* fish registered to a shared reference brain. This revealed a high degree of overlap between the two transgenic lines, with the exception of additional dorso-lateral transgene expression close to the midbrain boundary in the *calca*^{ccu75Et} line (Figure 3.5E-F).

To illustrate the similarity between the *calca*^{ccu75Et} and *vsx2* lines at a cellular level, I also performed back-labelling of RSNs in *vsx2* fish at 6 dpf (n=12). Again, only ipsilaterally-projecting RSNs in the hindbrain were present in *vsx2* (Figure 3.7A-B). This includes the rostral RoM2, RoM3 and RoV3 cells, the ventromedial cells (MiV1, MiV2, MiM1, MiR1, MiR2), and the caudal ipsilaterally-projecting MiD2i and MiD3i cells. Following the projections of MiD2i and MiD3i at higher spatial resolution confirmed their identity with no decussation at the midline present (data not shown). Similarly to the *calca*^{ccu75Et} line, the Mauthner cell was present but not labelled in *vsx2*. For detailed RSN labelling across multiple fish see Table 3.7.

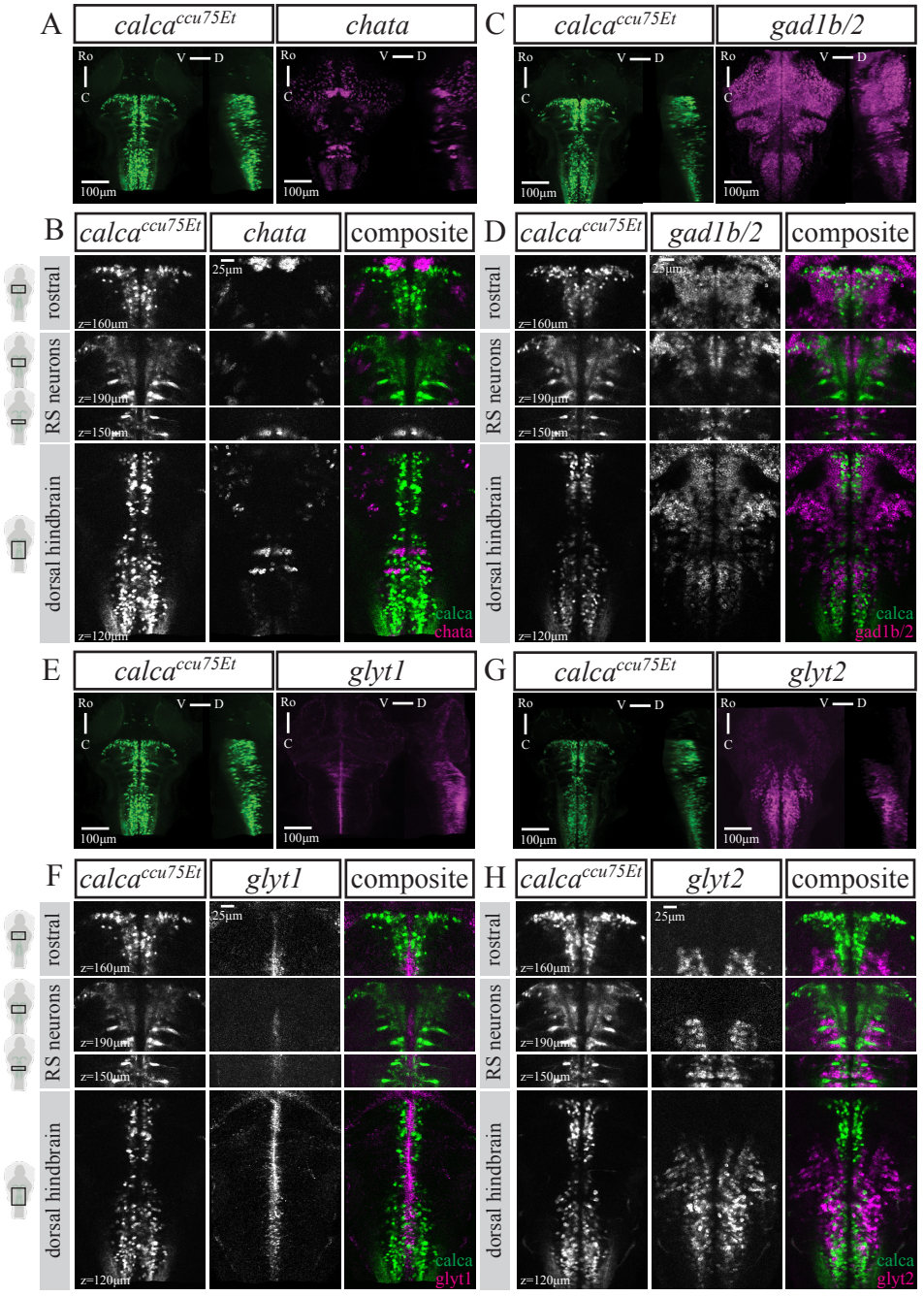

(Caption on next page).

Figure 3.6: No cholinergic (*chata*), GABAergic (*gad1b/2*) or glycinergic (*glyt1, glyt2*) expression in neurons labelled by the *calca*^{ccu75Et} line.
A,C,E,G) Maximum intensity projections from dorsal and sagittal view of an exemplary *calca*^{ccu75Et} fish at 6 dpf with A) *chata* (n=15), C) *gad1b/2* (n=7), E) *glyt1* (n=16), G) *glyt2* (n=16) mRNA expression. Scale bar is 100μm.
B,D,F,H) Close ups at several planes to better illustrate no overlap between *calca*^{ccu75Et} line and B) *chata*, D) *gad1b/2*, F) *glyt1* or H) *glyt2* or mRNA-expressing neurons. Scale bar is 25μm.

***pcp4a*^{ccu97Tg}** A new transgenic line was established driving GAL4FF expression under the *pcp4a* promoter using a recombineered BAC. *Pcp4a* had been shown to be expressed in the telencephalon, habenula, pretectum, pre-glomerular complex, mammillary bodies, optic tectum and a subset of reticulospinal neurons [36]. The *pcp4a*^{ccu97Tg} line has sparse labelling of cells in the forebrain and tectum, expression in the habenula, hindbrain, and the anterior and posterior lateral line ganglia. The reticulospinal back-labelling (n=12) specifically and reliably includes the dorso-caudal contralaterally-projecting MiD2cm, MiD2cl, MiD3cm and MiD3cl but not their ipsilateral counterparts (Figure 3.7C-D). Labelling of other RSNs in this line was more variable, with different combinations of the ventromedial cells (MiV1, MiV2, MiM1, MiR1, MiR2) being labelled in 50% of fish (Table 3.9). To my knowledge, this is the first transgenic line specifically labelling the contralaterally-projecting MiD cells of the Mauthner array.

***adcyap1b*^{ccu96Et}** A new transgenic line was established in which GAL4FF expression is driven by a 1.7kb upstream promoter region of the adenylate cyclase activating polypeptide 1b (*adcyap1b*) gene. The *adcyap1b* gene encodes pituitary adenylate cyclase-activating polypeptide 2 (**PACAP2**), is evolutionarily conserved

Figure 3.7: Reticulospinal cell labelling in four different transgenic lines.
A,C,E,G) Maximum intensity projections from dorsal and sagittal view of an exemplary fish from A) *vsx2* (n=12), C) *pcp4a*^{ccu97Tg} (n=12), E) *adcyap1b*^{ccu96Et} (n=11) and G) *tiam2a*^{y264Et} (n=12) at 6 dpf with RSNs labelled via retrograde dye injection. Scale bar is 100μm.
B,D,F,H) Close ups at several planes to illustrate overlap between B) *vsx2*, D) *pcp4a*^{ccu97Tg}, F) *adcyap1b*^{ccu96Et} or H) *tiam2a*^{y264Et} and RS backfill. Blue triangle in F, rostral panel indicates putative RoL1. Blue triangle in F and H, caudal panel indicates putative CaD and CaV cells. Scale bar is 25μm.

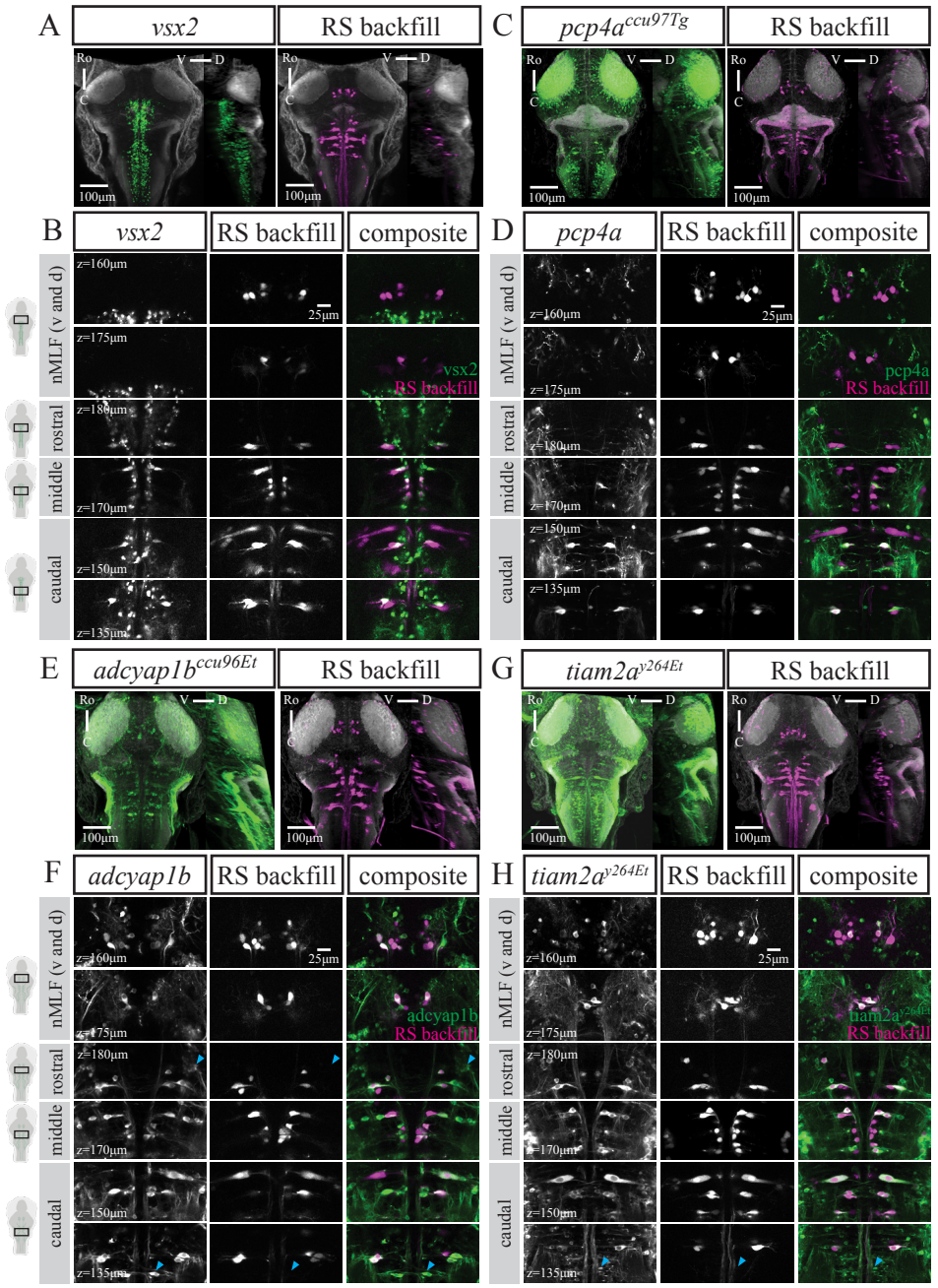

(Caption on previous page).

and expressed in the telencephalon, diencephalon, rhombencephalon, and dorsal spinal cord [37]. PACAP2 plays a role in brain development [38] and the neuropeptide *adcyap1b* has been shown to enhance sensory responsiveness in larval zebrafish [39]. Due to gene expression in the rhombencephalon, *adcyap1b* was included in the aforementioned genetic screen to identify novel transgenic lines with expression in the hindbrain. In addition to labelling cells in the tegmentum and hindbrain, our *adcyap1b*^{ccu96Et} line has expression in the olfactory epithelium, olfactory bulb, anterior and posterior lateral line ganglia, as well as sparse labelling in the tectum. Following back-filling with dextran-conjugated tracer dye (n=11), I report overlap with GCaMP-expression in the four identified cells of the nMLF (MeM1, MeLm, MeLr, MeLc), the Mauthner cell and most other RSNs including the vestibular cells (Figure 3.7E-F). I observed labelling of most of the caudal contralaterally-projecting MiD cells (MiD2cm, MiD2cl, MiD2i, MiD3cm and MiD3cl) but not the MiD3i and MiT cells. For detailed RSN labelling across multiple fish see Table 3.8. As mentioned previously, the CaD, CaV, RoL1 and RoL2 cells were not retrogradely labelled in this preparation. However, it is likely that the *adcyap1b*^{ccu96Et} line labels those cells well, as there are large cell bodies visible in their respective putative locations [11, 13].

***tiam2a*^{y264Et}** Finally, the previously established *tiam2a*^{y264Et} line [18] was of interest due to labelling the Mauthner cell and homologues. It has brain-wide expression, including the olfactory epithelium, optic chiasm, tectum, interpeduncular nucleus, tegmentum, hindbrain and cerebellum. Backfills (n=12) revealed that this line labelled MeM1 more reliably than the other identified nMLF neurons (MeLm, MeLr, MeLc), as well as consistently labelling the rostral RoM2l, RoM3m and RoM3l, the Mauthner cell, and both the CL- and IL-projecting MiD2 and MiD3 cells in the hindbrain (Figure 3.7G-H). Labelling of other RSNs was more variable across fish (Table 3.10). Similarly to above, it is likely the CaD and CaV cells are also labelled in the *tiam2a*^{y264Et} line [11, 13].

3.3.3 The *s1171tEt* line labels *vglut2*-expressing neurons in the tegmentum

The organisation of midbrain RSNs in the *s1171tEt* line was examined using dextran-conjugated retrograde labelling in larval zebrafish at 6dpf (n=12). The *s1171tEt* has a triangular expression profile centred around the nMLF in the tegmentum, rostral to the cholinergic oculomotor nucleus [23]. It includes the four canonical large nMLF cells (MeM1, MeLm, MeLr, MeLc), as well as small mesencephalic cells (**MeS**; Figure 3.8A-B). For detailed RSN labelling across multiple fish see Table 3.5.

The majority of cells in the *s1171tEt* line were glutamatergic, specific for the vesicular glutamate transporter 2 (*vglut2*; Figure 3.8B). I did not detect *vglut1*-expressing cells near the nMLF, as well as no cholinergic (*chata*), GABAergic (*gad1b/2*) or glycinergic (*glyt1, glyt2*) mRNA expression in cells labelled by the *s1171tEt* line (Figure 3.8C). A previous study distinguished lateral and medial regions of the nMLF in juvenile zebrafish at 4-weeks post-fertilisation based on different levels of expression observed in *vglut1* and *vglut2a* transgenic lines [40]. This difference with the isHCR results could reflect a change in the expression pattern over development, or alternatively could be due to a feature of these transgenic lines that is not reflected in the natural gene expression patterns.

To understand this, I asked whether glutamatergic expression profiles change across development. I performed a modified *in situ* hybridisation chain reaction protocol on brains dissected from juvenile zebrafish (n=4; 4-weeks post-fertilisation). Using landmarks identified with the adult zebrafish brain atlas (**AZBA** [32]) —such as the torus longitudinalis (**TL**), valvula cerebelli, and the diencephalic ventricle —allowed us to identify several brain regions. Glutamatergic expression appears stable across development, with *vglut1* expression being restricted to the TL and the cerebellum, in contrast to brain-wide *vglut2* expression, including the putative nMLF (Figure 3.9). To identify the nMLF in the juvenile brain, I again utilised the AZBA. Matching the triangular shape of the nMLF on AZBA in the transverse view, situated between the diencephalic ventricle and a cluster of *vglut2* cells most likely belonging to the red nucleus, is a cluster of large

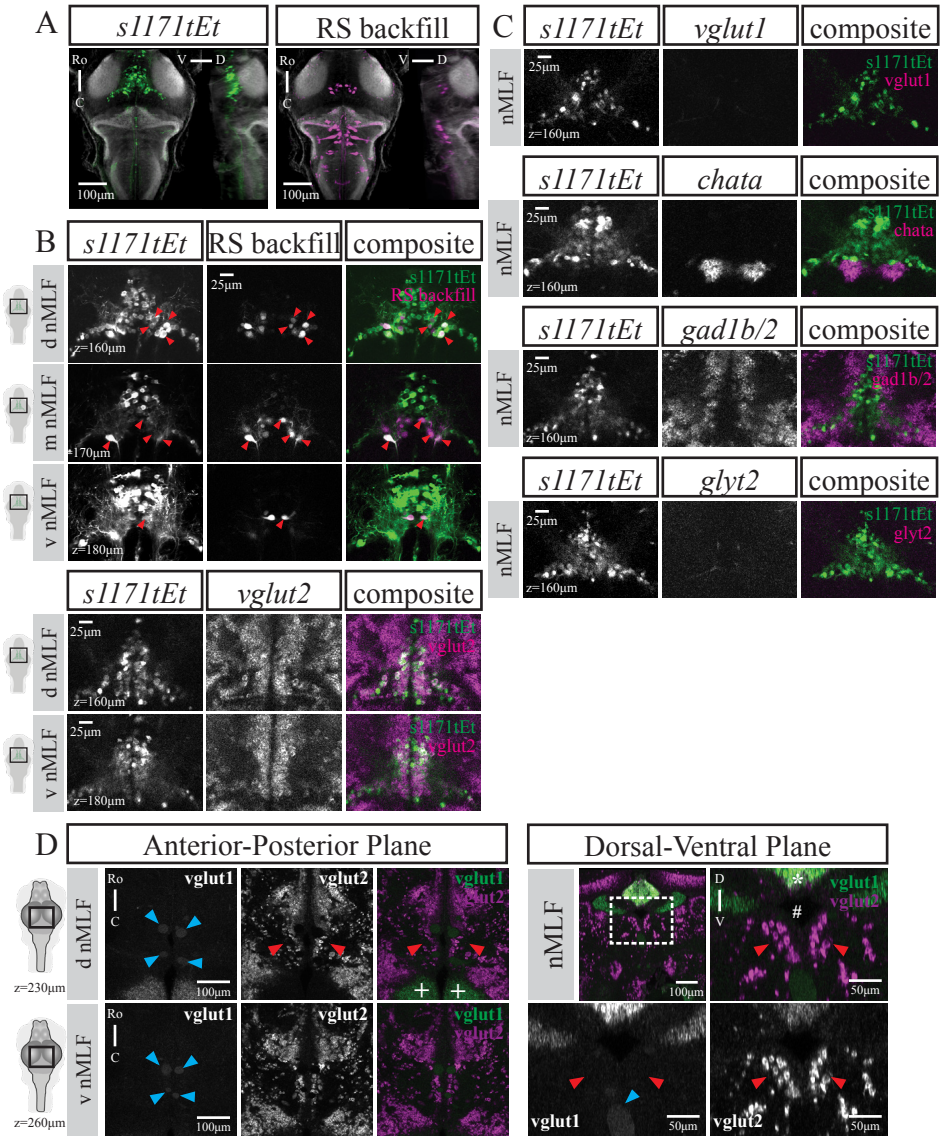

Figure 3.8: The *s1171tEt* line labels RSNs in the nMLF and is glutamatergic (*vglut2*) across development.
A) Dorsal and sagittal maximum intensity projections from an example *s1171tEt* fish (of n=12) at 6 dpf with RSNs labelled via retrograde dye injection. Scale bar 100μm.
B) Close ups at several planes to illustrate overlap between *s1171tEt* line and backfill, note the four main RSNs as indicated by red triangles. Scale bar 25μm.
C) Close ups at several planes of exemplary fish to show considerable overlap between *s1171tEt* and *vglut2* (n=8), particularly in RSNs. No overlap between *s1171tEt* and *vglut1* (n=7), *chata* (n=8), *gad1b/2* (n=8) or *glyt2* (n=7). Scale bar 25μm.
D) *vglut1* and *vglut2* expression in exemplary 4 week-old juvenile fish (n=4). Left) two planes in dorsal view, scale bar 100μm. Right) matching transverse view, scale bar 50μm. Blue triangles indicate blood vessels, red triangles point towards region of nMLF.

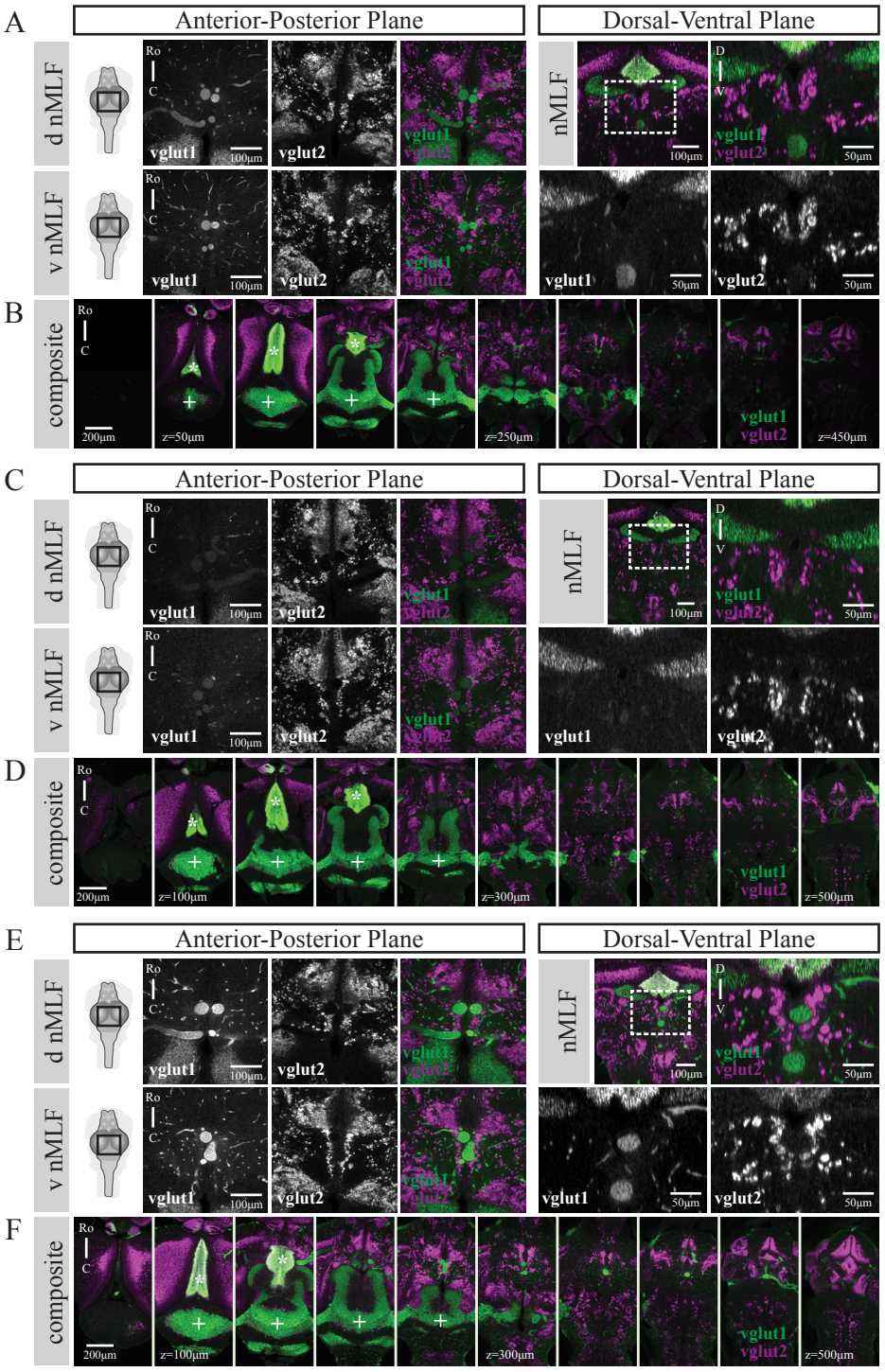

(Caption on next page.)

Figure 3.9: Glutamatergic expression patterns in three 4 week-old juvenile fish (of n=4). A,C,E) Left panels show *vglut1*, *vglut2*, composite in two planes from the dorsal view, scale bar is 100μm. Right panels show *vglut1*, *vglut2*, composite from the transverse view, scale bar is 50μm.
B,D,F) Composite images of several planes from dorsal to ventral. Note the presence of torus longitudinalis (*) and cerebellum (+) in *vglut1* (green), with brain wide expression in *vglut2* (magenta). Auto-fluorescence of blood vessels is seen in the *vglut1* channel, as indicated by blue triangles. Scale bar 200μm.

vglut2 cells characteristic of the nMLF (Figure 3.8D). I did not observe *vglut1* expression near this cluster of cells, only auto-fluorescent blood vessels.

3.3.4 Summary of RSN labelling across transgenic lines

The transgenic lines characterised in this study can be utilised in a complementary fashion to study reticulospinal circuits at larval stages (Figure 3.10). The *nefma* line (n=10) reliably labels all RSNs. However, it cannot be used to study the Mauthner cell since it degenerates early in development, which could also have compensatory effects by other RSNs. This is not the case in *adcyap1b*^{ccu96Et} (n=11), which labels most RSNs including the Mauthner cell. However, the MiD3i and MiT cells are absent, and I emphasise the need for rigorous pre-screening due to silencing. The most suitable line to study Mauthner and homologue activity is the *tiam2a*^{y264Et} line (n=12), with labelling of other RSNs being more variable. The *calca*^{ccu75Et}/*vsx2* and *pcp4a*^{ccu97Tg} lines offer an interesting opportunity by giving genetic access to complementary projection patterns in the Mauthner array, with the *calca*^{ccu75Et} line (n=12) only labelling the ipsilaterally-projecting MiD cells (as well as other rostral and ventromedial RSNs) and the *pcp4a*^{ccu97Tg} line (n=12) specifically labelling contralaterally-projecting MiD cells, while labelling of ventromedial RSNS is rare. In addition, I have demonstrated that the *calca*^{ccu75Et} line closely matches the existing *vsx2* line (n=12), both in broad expression pattern and at the single-RSN-level – though it labels additional cells in the rostro-lateral hindbrain. For exact numbers across fish for all transgenic lines, see Extended Data 3.4 until 3.10). Finally, for wider nMLF-related studies the *s1171tEt* line (n=12) offers broad labelling in the tegmentum, including the four canonical nMLF-RSNs (MeM1, MeLr, MeLc, MeLm). I further demonstrate that

cells labelled in these transgenic lines are glutamatergic (*vglut2*), with the *nefma* line additionally labelling the cholinergic cranial neurons.

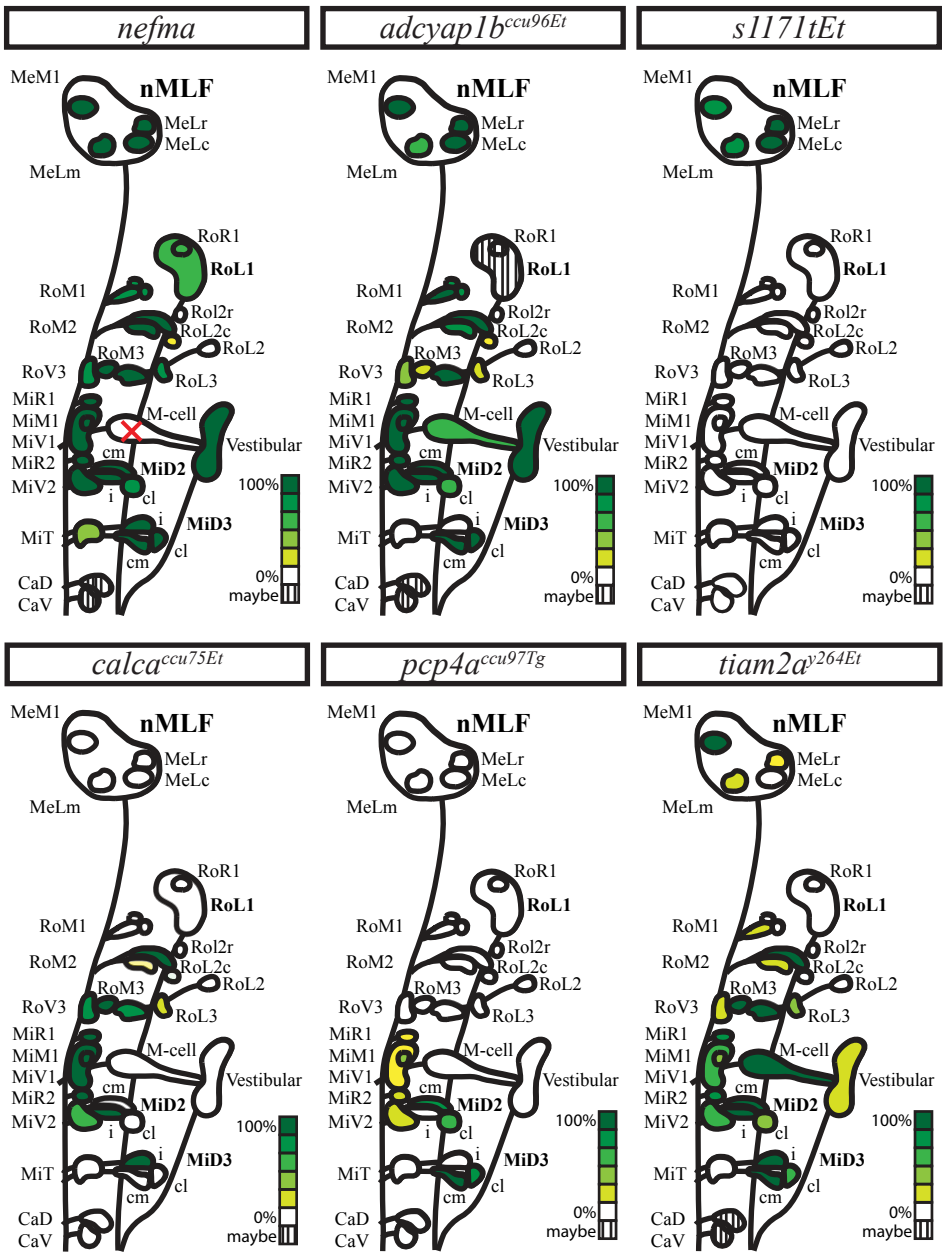

Figure 3.10: Graphical summary of the number of RSNs labelled in each transgenic line across multiple fish. *nefma* n=10, *calca*^{ccu75Et} n=12, *vsx2* n=12, *s1171tEt* n=12, *pcp4a*^{ccu97Tg} n=12, *adcyap1b*^{ccu96Et} n=11, *tiam2a*^{y264Et} n=12

3.4 Discussion

The aim of this study was to provide a detailed account of seven transgenic lines with gene expression in the brainstem of larval zebrafish. I characterized four existing transgenic lines *(nefma, vsx2, s1171tEt, tiam2a*^{y264Et}) and presented three newly established transgenic lines *(calca*^{ccu75Et}*, pcp4a*^{ccu97Tg}*, adcyap1b*^{ccu96Et}*)*. For each transgenic line, I performed retrograde labelling of reticulospinal neurons (**RSNs**) followed by immunostaining against GCaMP/RFP and the whole-brain activity marker total ERK for subsequent registration purposes.

As previously reported [23] the *s1171tEt* line reliably labels the four large cells (MeLr, MeLc, MeLm, MeM1) in the nucleus of the medial longitudinal fasciculus (**nMLF**) as well as many other neurons in the surrounding area. I observed occasional overlap with other backfilled RSNs, most likely constituting the small mesencephalic cells (**MeS**), first identified by [23].

Two transgenic lines labelled almost all RSNs, with notable exceptions: the *nefma* line reliably labels all RSNs except for the Mauthner cell, which degenerates earlier in development. I was also not able to confirm labelling of the rostral RoL2-3 and caudal CaD and CaV neurons, as these were not successfully labelled by backfilling in this preparation and may require a different injection strategy. However, there are GCaMP-expressing cells in the *nefma* line where I would expect the RoL2-3 and CaD and CaV cells to be based on previous studies [11, 13]. I thus conclude that the *nefma* line labels all RSNs except the Mauthner cell. As aforementioned, the Mauthner cell degenerates early in development in the *nefma* line from Eschstruth *et al.* [15]. Another transgenic line under the *nefma* promoter exists: Tg[nefma:Gal4; UAS:GFP] [41], in which the Mauthner cell does not degenerate. While to my knowledge, no systematic characterisation of the line exists, it likely also labels most or all other RSNs. The newly generated *adcyap1b*^{ccu96Et} line reliably labels most RSNs including the Mauthner cells and most homologues and the putative CaD and CaV cells, with a specific exception: I did not observe labelling of the MiT and ipsilaterally-projecting MiD3i cells in the *adcyap1b*^{ccu96Et} line.

To study the Mauthner array, three complementary transgenic lines can be

used. The *tiam2a*^{y264Et} line reliably labels the Mauthner cells and homologues (including the MiD2i and MiD3i), however, labelling of other RSNs is stochastic, as previously reported by [42]. I presented two new lines that offer complementary genetic access to different projection patterns within the Mauthner array. The *calca*^{ccu75Et} line largely overlaps with the well-known line *vsx2*, with the addition of gene expression in the rostral lateral hindbrain. The *calca*^{ccu75Et} line reliably labels the RoM2, RoM3 and ventromedial RSNs as well as the ipsilaterally-projecting Mauthner homologues MiD2i and MiD3i. Conversely, the *pcp4a*^{ccu97Tg} line reliably labels the contralaterally-projecting medial and lateral MiD2cm, MiD2cl, MiD3cm, MiD3cl as well as more rarely the ventromedial cells. To my knowledge, this is the first description of a transgenic line in zebrafish providing specific genetic access to the contralaterally-projecting Mauthner homologues.

There is ample evidence for the usefulness of transgenic lines labelling different subpopulations in the hindbrain to dissect premotor circuitry and function. For instance, using a Gal4-transgenic line under the *nefma* promoter allowed experimenters to reliably record convergent afferent signals in vestibulospinal neurons in vivo [41]. It was later shown in the same line that vestibulospinal neuron activity increases as a function of ipsilateral tilt amplitude using tilt-in-place microscopy [43].

Another transgenic line identified in a Gal4 enhancer trap screen, *s1171tEt*, with expression in the thalamus, cerebellum and trunk musculature [16] was instrumental in showing that the four large (MeLr, MeLc, MeLm, MeM1) as well as smaller (MeS) nMLF neurons are involved in steering movements [23], tail bending [44] and relay commands from the pretectal AF7 to the hindbrain, potentially involved in hunting behaviour [45]. In addition to their terminal arbours in the spinal cord, it was also demonstrated that nMLF cells labelled in the *s1171tEt* line have extensive axon collaterals in the hindbrain, suggesting they may be in involved in coordination of different premotor regions [23].

Information on RSNs involved in steering behaviours also comes from another study using a transgenic line that labels V2a neurons, showing they receive inner-

vation from the mesencephalic locomotor region (**MLR**) and are also involved in forward swimming [35]. Initially generated as a BAC line named chx10 after the mammalian homologue, it has been named *alx* and *vsx2* in fish. It labels medial ipsilaterally-projecting cells in the hindbrain and spinal cord, shown to be glutamatergic descending interneurons providing excitatory drive to motoneurons in the spinal cord [17]. It was subsequently confirmed that they overlap with the most medial V2a glutamatergic stripe in the hindbrain [46]. Optogenetic activation of *chx10*-expressing neurons in the hindbrain using channelrhodopsin evoked swimming, while forced inactivation using Archearhodopsin3 or Halorhodopsin reliably stopped ongoing swimming [24].

Finally, the $tiam2a^{y264Et}$ line labels the Mauthner array reliably, and other RSNs more stochastically, as well as the anterior lateral line ganglia amongst others. Studies using the $tiam2a^{y264Et}$ line showed that direct activation of the Mauthner cell by electric field pulses could drive ultrarapid escape responses [42], and that it receives pre-pulse inhibition from gsx2-glutamatergic neurons [47].

In addition to reticulospinal backfills, I also confirmed that cells labelled by the *nefma*, $calca^{ccu75Et}$ and *s1171tEt* transgenic lines are glutamatergic (*vglut2*). In addition, the *nefma* line also labels the cholinergic cranial motor neurons III-VII and IX-X. A previous study had reported medial *vglut2*-positive and lateral *vglut1*-positive cells in the nMLF in zebrafish at 4-6 weeks-post-fertilisation based on expression patterns of transgenic lines [40]. I did not observe *vglut1*-positive cells in the nMLF in my study on larval zebrafish, instead, *vglut1*-expression was restricted to the torus longitudinalis (**TL**) and cerebellum. This finding is corroborated by isHCR data available in the larval zebrafish atlas *mapzebrain* [34].

I thus wanted to understand whether glutamatergic expression profiles change over development. I performed isHCR against *vglut1* and *vglut2* in brains dissected from 4 week old zebrafish, an age consistent with the study by Berg et al. [40]. Similarly to the larvae, I only observed *vglut1*-expression in the TL and cerebellum, identified using the adult zebrafish brain atlas *AZBA* [32]. *Vglut2*-expression was more widespread, including expression in a region likely constituting the nMLF –

identified using landmarks, such as the diencephalic ventricle, from AZBA. Again, I wondered whether glutamatergic expression profiles in the nMLF would change at later stages of development. However, this does not seem to be the case: a study in adult zebrafish (older than 90 days) using *in situ* hybridisation reports *vglut1*-expression in the TL and cerebellum only [48]. I therefore think that the distinction between nMLF subregions in Berg *et al.* (2023) reflects variation in transgenic expression patterns, rather than the natural expression of these genes. However, this hypothesis needs to be tested by directly comparing *in situ* hybridisation data with expression in those transgenic lines.

In conclusion, I have provided a detailed account of the degree of RSN labelling in seven transgenic lines with glutamatergic (*vglut2*) expression in the brainstem in larval zebrafish, offering projection-specific genetic access to subpopulations of RSNs. This resource provides a useful basis for future research, including the possibility to combine with genetically-encoded Calcium reporters and optogenetic tools, in the hope to uncover fundamental principles in the descending control of locomotion.

3.5 Acknowledgements

This chapter has been published as a research article on the pre-print server *bioRxiv* in December 2024. It has since been accepted for publication (pending minor revisions) in the open-access journal *eNeuro*.

> **Collins, E.M.D.**, Silva, P.T., Ostrovsky, A., Renninger, S., Tomas, R., Diez del Corral, R. and Orger, M.B. (2024) Characterisation of transgenic lines labelling reticulospinal neurons in larval zebrafish. doi: https://doi.org/10.1101/2024.12.20.629714

E.M.D. Collins and M.B. Orger designed experiments. E.M.D. Collins analysed all experiments, performed all *in situ* hybridisation experiments and confocal imaging on larval and juvenile zebrafish, and performed immunohistochemistry experiments and confocal imaging on larval zebrafish from backgrounds *nefma, calca*^{ccu75Et}*, vsx2, s1171tEt.* P.T. Silva performed dye injections for all immuno-

histochemistry experiments and performed immunohistochemistry experiments on larval zebrafish from backgrounds *pcp4a*^{ccu97Tg}, *adcyap1b*^{ccu96Et}, *tiam2a*^{y264Et}. For the latter, confocal imaging was shared between P.T. Silva, A. Ostrovsky and E.M.D. Collins. A. Ostrovsky and R. Diez del Corral assisted with registration pipeline and experimental design. S. Renninger provided in-house reference brains and performed cloning, injection, screening and stable line establishment for TgBAC[pcp4a:Gal4FF^{ccu97Tg}, 10xUAS:GCaMP6fEF05]. A.R. Tomas performed cloning, injection, screening and stable line establishment for Tg[-1.7adcyap1b: Gal4FF^{ccu96Et}, 10xUAS: GCaMP6fEF05]. S. Lackner performed cloning and A.R. Tomas performed injection, screening and stable line establishment for Tg[-5.0calca: Gal4FF^{ccu75Et}, 10xUAS:GCaMP6fEF05]. R. Diez del Corral provided protocols, reagents and invaluable assistance learning techniques. E.M.D. Collins wrote the manuscript with helpful input from all authors.

I would like to thank R. Tomas and S. Renninger for generating the UAS: GCaMP6fef05 construct. I would like to thank the Champalimaud Foundation Advanced Bio-imaging and Bio-optics Experimental platform (ABBE) for technical support with confocal imaging and the Champalimaud Foundation Fish Platform for meticulous fish care. I would like to thank Dr Chanpreet Singh (Molecular Instruments) for technical advice on adapting the *in situ* hybridisation protocol to juvenile fish. I would like to thank J. Bin and D. Lyons (University of Edinburgh, UK) for sharing unpublished data on the Mauthner cell degeneration in Tg[nefma:KalTa4]. I would like to thank the Giudicelli lab (Sorbonne University, France) for generating and sharing embryos from Tg[nefma:KalTa4], the Schuster lab (University of Bayreuth, Germany) for sending embryos from Tg[tiam2a$^{y264Et(B)}$] and the Wyart lab (Paris Brain Institute, France) for sending embryos from TgBAC[vsx2:Gal4FF^{nns18Tg}, UAS:mRFP].

3.6 Appendix

	RSN overlap in individual *nefma* fish										
	#1	#2	#3	#4	#5	#6	#7	#8	#9	#10	Total
MeM1	1	1	1	1	1	1	1	1	1	1	100 %
MeLm	1	1	1	1	1	1	1	1	1	1	100 %
MeLr	1	1	1	1	1	1	1	1	1	1	100 %
MeLc	1	1	1	1	1	1	1	1	1	1	100 %
RoL1	1	0	0	1	1	0	1	1	0	1	60 %
RoR1	0	0	0	0	0	0	0	0	0	0	0 %
RoM1c	1	1	1	1	1	0	1	1	1	1	90 %
RoM1r	1	1	1	1	0	1	0	1	1	1	80 %
RoM2m	1	1	1	1	1	1	1	1	1	1	100 %
RoM2l	1	1	1	1	1	1	1	1	1	1	100 %
RoLr	0	0	0	0	0	0	0	0	0	0	0 %
RoLc	0	0	0	0	1	0	0	0	0	0	10 %
RoL2	0	0	0	0	0	0	0	0	0	0	0 %
RoV3	1	1	0	1	1	1	1	1	1	0	80 %
RoM3m	1	1	1	1	1	1	1	1	1	1	100 %
RoM3l	1	1	1	1	1	1	1	1	1	1	100 %
RoL3	1	1	1	1	1	1	0	1	1	0	80 %
MiR1	1	1	1	1	1	1	1	1	1	1	100 %
MiM1	1	1	1	1	1	1	1	1	1	1	100 %
MiV1	1	1	1	1	1	1	1	1	1	1	100 %
MiR2	1	1	1	1	1	1	1	1	1	1	100 %
Mauthner	0	0	0	0	0	0	0	0	0	0	0 %
Vestibular	1	1	1	1	1	1	1	1	1	1	100 %
MiV2	1	1	1	1	1	1	1	1	1	1	100 %
MiD2cm	1	1	1	1	1	1	0	1	1	1	90 %
MiD2cl	1	1	1	1	1	0	1	1	1	0	80 %
MiD2i	1	1	1	1	1	1	1	1	1	1	100 %
MiT	0	1	0	1	1	0	0	0	0	1	40 %
MiD3cm	1	1	1	1	1	1	1	1	1	1	100 %
MiD3cl	1	1	1	1	1	0	1	1	1	1	100 %
MiD3i	1	1	1	1	1	1	1	1	1	1	100 %
CaD	0	0	0	0	0	0	0	0	0	0	0 %
CaV	0	0	0	0	0	0	0	0	0	0	0 %

Table 3.4: Reticulospinal cells labelled in each *nefma* fish

	RSN overlap in individual *s1171tEt* fish												
	#1	#2	#3	#4	#5	#6	#7	#8	#9	#10	#11	#12	Total
MeM1	0	1	0	1	1	1	1	1	1	1	1	1	83%
MeLm	0	1	1	1	1	1	1	1	1	0	1	1	83%
MeLr	1	1	1	1	1	1	1	1	1	1	1	1	100%
MeLc	1	1	1	1	1	1	1	1	1	1	1	1	100%
RoL1	0	0	0	0	0	0	0	0	0	0	0	0	0%
RoR1	0	0	0	0	0	0	0	0	0	0	0	0	0%
RoM1c	0	0	0	0	0	0	0	0	0	0	0	0	0%
RoM1r	0	0	0	0	0	0	0	0	0	0	0	0	0%
RoM2m	0	0	0	0	0	0	0	0	0	0	0	0	0%
RoM2l	0	0	0	0	0	0	0	0	0	0	0	0	0%
RoL2r	0	0	0	0	0	0	0	0	0	0	0	0	0%
RoL2c	0	0	0	0	0	0	0	0	0	0	0	0	0%
RoL2	0	0	0	0	0	0	0	0	0	0	0	0	0%
RoV3	0	0	0	0	0	0	0	0	0	0	0	0	0%
RoM3m	0	0	0	0	0	0	0	0	0	0	0	0	0%
RoM3l	0	0	0	0	0	0	0	0	0	0	0	0	0%
RoL3	0	0	0	0	0	0	0	0	0	0	0	0	0%
MiR1	0	0	0	0	0	0	0	0	0	0	0	0	0%
MiM1	0	0	0	0	0	0	0	0	0	0	0	0	0%
MiV1	0	0	0	0	0	0	0	0	0	0	0	0	0%
MiR2	0	0	0	0	0	0	0	0	0	0	0	0	0%
Mauthner	0	0	0	0	0	0	0	0	0	0	0	0	0%
Vestibular	0	0	0	0	0	0	0	0	0	0	0	0	0%
MiV2	0	0	0	0	0	0	0	0	0	0	0	0	0%
MiD2cm	0	0	0	0	0	0	0	0	0	0	0	0	0%
MiD2cl	0	0	0	0	0	0	0	0	0	0	0	0	0%
MiD2i	0	0	0	0	0	0	0	0	0	0	0	0	0%
MiT	0	0	0	0	0	0	0	0	0	0	0	0	0%
MiD3cm	0	0	0	0	0	0	0	0	0	0	0	0	0%
MiD3cl	0	0	0	0	0	0	0	0	0	0	0	0	0%
MiD3i	0	0	0	0	0	0	0	0	0	0	0	0	0%
CaD	0	0	0	0	0	0	0	0	0	0	0	0	0%
CaV	0	0	0	0	0	0	0	0	0	0	0	0	0%

Table 3.5: Reticulospinal cells labelled in each *s1171tEt* fish

	RSN overlap in individual *calca*^{ccu75Et} fish												
	#1	#2	#3	#4	#5	#6	#7	#8	#9	#10	#11	#12	Total
MeM1	0	0	0	0	0	0	0	0	0	0	0	0	0%
MeLm	0	0	0	0	0	0	0	0	0	0	0	0	0%
MeLr	0	0	0	0	0	0	0	0	0	0	0	0	0%
MeLc	0	0	0	0	0	0	0	0	0	0	0	0	0%
RoL1	0	0	0	0	0	0	0	0	0	0	0	0	0%
RoR1	0	0	0	0	0	0	0	0	0	0	0	0	0%
RoM1c	0	0	0	0	0	0	0	0	0	0	0	0	0%
RoM1r	0	0	0	0	0	0	0	0	0	0	0	0	0%
RoM2m	0	0	0	0	0	0	0	1	0	0	0	0	8%
RoM2l	1	1	1	1	1	1	1	1	1	1	1	1	100%
RoL2r	0	0	0	0	0	0	0	0	0	0	0	0	0%
RoL2c	0	0	0	0	0	0	0	0	0	0	0	0	0%
RoL2	0	0	0	0	0	0	0	0	0	0	0	0	0%
RoV3	0	0	1	1	1	1	1	1	1	1	1	1	83%
RoM3m	1	1	1	1	1	1	1	1	1	1	1	1	100%
RoM3l	1	1	1	1	0	0	1	1	1	0	1	1	75%
RoL3	0	1	1	0	0	0	0	0	0	0	0	0	17%
MiR1	1	1	1	1	1	1	1	1	1	1	1	1	100%
MiM1	1	1	1	1	1	1	1	1	1	1	1	1	100%
MiV1	1	1	1	1	1	1	1	1	1	1	1	1	100%
MiR2	1	1	1	1	1	1	1	1	1	1	1	1	100%
Mauthner	0	0	0	0	0	0	0	0	0	0	0	0	0%
Vestibular	0	0	0	0	0	0	0	0	0	0	0	0	0%
MiV2	1	1	1	1	0	0	1	1	0	1	0	0	58%
MiD2cm	0	0	0	0	0	0	0	0	0	0	0	0	0%
MiD2cl	0	0	0	0	0	0	0	0	0	0	0	0	0%
MiD2i	1	1	1	0	1	1	1	1	1	1	1	1	92%
MiT	0	0	0	0	0	0	0	0	0	0	0	0	0%
MiD3cm	0	0	0	0	0	0	0	0	0	0	0	0	0%
MiD3cl	0	0	0	0	0	0	0	0	0	0	0	0	0%
MiD3i	1	1	1	1	1	1	1	1	1	1	1	1	100%
CaD	0	0	0	0	0	0	0	0	0	0	0	0	0%
CaV	0	0	0	0	0	0	0	0	0	0	0	0	0%

Table 3.6: Reticulospinal cells labelled in each *calca*^{ccu75Et} fish

	RSN overlap in individual *vsx2* fish												
	#1	#2	#3	#4	#5	#6	#7	#8	#9	#10	#11	#12	Total
MeM1	0	0	0	0	0	0	0	0	0	0	0	0	0%
MeLm	0	0	0	0	0	0	0	0	0	0	0	0	0%
MeLr	0	0	0	0	0	0	0	0	0	0	0	0	0%
MeLc	0	0	0	0	0	0	0	0	0	0	0	0	0%
RoL1	0	0	0	0	0	0	0	0	0	0	0	0	0%
RoR1	0	0	0	0	0	0	0	0	0	0	0	0	0%
RoM1c	0	0	0	0	0	0	0	0	0	0	0	0	0%
RoM1r	0	0	0	0	0	0	0	0	0	0	0	0	0%
RoM2m	1	0	1	1	0	0	0	1	0	1	1	0	50%
RoM2l	1	0	1	1	1	1	0	1	0	1	1	1	75%
RoL2r	0	0	0	0	0	0	0	0	0	0	0	0	0%
RoL2c	0	0	0	0	0	0	0	0	0	0	0	0	0%
RoL2	0	0	0	0	0	0	0	0	0	0	0	0	0%
RoV3	0	0	0	0	0	0	0	0	0	0	1	0	8%
RoM3m	1	0	1	1	1	0	0	1	0	1	1	1	67%
RoM3l	1	1	0	0	1	1	1	1	0	0	1	1	67%
RoL3	0	0	0	0	0	0	0	0	0	0	0	0	0%
MiR1	1	1	1	1	1	1	1	1	0	1	1	1	92%
MiM1	1	1	1	1	1	0	1	1	0	1	1	1	83%
MiV1	1	1	1	1	1	1	1	1	0	1	1	1	92%
MiR2	1	1	1	1	1	1	1	1	0	1	1	1	92%
Mauthner	0	0	0	0	0	0	0	0	0	0	0	0	0%
Vestibular	0	0	0	0	0	0	0	0	0	0	0	0	0%
MiV2	1	1	1	1	0	0	1	1	0	0	1	0	58%
MiD2cm	0	0	0	0	0	0	0	0	0	0	0	0	0%
MiD2cl	0	0	0	0	0	0	0	0	0	0	0	0	0%
MiD2i	1	1	1	1	1	1	0	1	0	1	1	0	75%
MiT	0	0	0	0	0	0	0	0	0	0	0	0	0%
MiD3cm	0	0	0	0	0	0	0	0	0	0	0	0	0%
MiD3cl	0	0	0	0	0	0	0	0	0	0	0	0	0%
MiD3i	1	1	1	1	1	0	1	0	0	1	1	1	75%
CaD	0	0	0	0	0	0	0	0	0	0	0	0	0%
CaV	0	0	0	0	0	0	0	0	0	0	0	0	0%

Table 3.7: Reticulospinal cells labelled in each *vsx2* fish

	RSN overlap in individual *adcyap1b*^{ccu96Et} fish											
	#1	#2	#3	#4	#5	#6	#7	#8	#9	#10	#11	Total
MeM1	1	1	1	1	1	1	1	1	1	1	1	100%
MeLm	1	1	0	1	0	1	1	1	0	0	1	64%
MeLr	1	1	1	1	0	1	1	1	1	1	1	91%
MeLc	1	1	1	1	1	1	1	1	1	1	1	100%
RoL1	0	0	0	0	0	0	0	0	0	0	0	0%
RoR1	0	0	0	0	0	0	0	0	0	0	0	0%
RoM1c	1	1	1	1	1	1	1	1	1	1	1	100%
RoM1r	1	1	1	1	1	1	1	1	0	0	0	73%
RoM2m	1	1	1	1	0	1	1	1	1	0	1	82%
RoM2l	1	1	1	1	1	1	1	1	1	1	1	100%
RoL2r	0	0	0	0	0	0	0	0	0	0	0	0%
RoL2c	0	0	0	0	0	0	0	0	0	0	1	9%
RoL2	0	0	0	0	0	0	0	0	0	0	0	0%
RoV3	0	0	1	1	0	0	0	1	1	0	0	36%
RoM3m	0	0	0	0	1	0	0	0	1	0	0	18%
RoM3l	1	1	1	1	1	1	1	1	1	1	1	100%
RoL3	0	0	0	0	0	0	0	0	1	0	1	18%
MiR1	1	1	1	1	1	1	1	1	1	1	1	100%
MiM1	1	1	1	1	1	1	1	1	1	1	1	100%
MiV1	1	1	1	1	1	1	1	1	1	1	1	100%
MiR2	1	1	1	1	1	1	1	1	1	1	1	100%
Mauthner	0	1	1	1	0	0	1	1	1	0	0	55%
Vestibular	1	1	1	1	1	1	1	1	1	0	1	91%
MiV2	1	1	0	1	1	1	1	1	1	1	1	91%
MiD2cm	1	1	1	1	1	1	1	1	1	1	1	100%
MiD2cl	1	1	0	1	0	1	0	1	0	1	0	55%
MiD2i	1	1	1	1	1	1	1	0	1	1	1	91%
MiT	0	0	0	0	0	0	0	0	0	0	0	0%
MiD3cm	1	1	1	1	1	1	1	1	1	1	1	100%
MiD3cl	1	1	1	1	1	1	1	1	1	1	1	100%
MiD3i	0	0	0	0	0	0	0	0	0	0	0	0%
CaD	0	0	0	0	0	0	0	0	0	0	0	0%
CaV	0	0	0	0	0	0	0	0	0	0	0	0%

Table 3.8: Reticulospinal cells labelled in each *adcyap1b*^{ccu96Et} fish

	RSN overlap in individual *pcp4a*^{ccu97Tg} fish												
	#1	#2	#3	#4	#5	#6	#7	#8	#9	#10	#11	#12	Total
MeM1	0	0	0	0	0	0	0	0	0	0	0	0	0%
MeLm	0	0	0	0	0	0	0	0	0	0	0	0	0%
MeLr	0	0	0	0	0	0	0	0	0	0	0	0	0%
MeLc	0	0	0	0	0	0	0	0	0	0	0	0	0%
RoL1	0	0	0	0	0	0	0	0	0	0	0	0	0%
RoR1	0	0	0	0	0	0	0	0	0	0	0	0	0%
RoM1c	0	0	0	0	0	0	0	0	0	0	0	0	0%
RoM1r	0	0	0	0	0	0	0	0	0	0	0	0	0%
RoM2m	0	0	0	0	0	0	0	0	0	0	0	0	0%
RoM2l	0	0	0	0	0	0	0	0	0	0	0	0	0%
RoL2r	0	0	0	0	0	0	0	0	0	0	0	0	0%
RoL2c	0	0	0	0	0	0	0	0	0	0	0	0	0%
RoL2	0	0	0	0	0	0	0	0	0	0	0	0	0%
RoV3	0	0	0	0	0	0	0	0	0	0	0	0	0%
RoM3m	0	0	0	0	0	0	0	0	0	0	0	0	0%
RoM3l	0	0	0	0	0	0	0	0	0	0	0	0	0%
RoL3	0	0	0	0	0	0	0	0	0	0	0	0	0%
MiR1	0	1	0	0	0	0	0	0	0	0	0	0	8%
MiM1	0	0	1	0	0	0	0	1	1	0	1	1	42%
MiV1	0	1	0	0	0	0	0	0	0	0	0	0	8%
MiR2	0	1	0	0	0	0	1	0	0	0	0	0	17%
Mauthner	0	0	0	0	0	0	0	0	0	0	0	0	0%
Vestibular	0	0	0	0	0	0	0	0	0	0	0	0	0%
MiV2	0	1	0	0	0	0	0	0	1	0	1	1	33%
MiD2cm	1	1	1	1	0	1	0	1	1	1	1	1	83%
MiD2cl	1	1	1	1	0	1	0	0	1	0	0	1	58%
MiD2i	0	0	0	0	0	0	0	0	0	0	0	0	0%
MiT	0	0	0	0	0	0	0	0	0	0	0	0	0%
MiD3cm	1	1	1	1	1	1	1	1	1	1	1	1	100%
MiD3cl	1	1	1	0	0	1	1	1	1	1	1	1	83%
MiD3i	0	0	0	0	0	0	0	0	0	0	0	0	0%
CaD	0	0	0	0	0	0	0	0	0	0	0	0	0%
CaV	0	0	0	0	0	0	0	0	0	0	0	0	0%

Table 3.9: Reticulospinal cells labelled in each *pcp4a*^{ccu97Tg} fish

	RSN overlap in individual *tiam2a*^{y264Et} fish												
	#1	#2	#3	#4	#5	#6	#7	#8	#9	#10	#11	#12	Total
MeM1	0	1	1	1	1	1	1	1	1	1	1	1	92%
MeLm	0	0	0	0	1	0	0	0	0	0	0	1	17%
MeLr	0	0	0	0	1	0	0	0	0	0	0	0	8%
MeLc	0	0	0	0	0	0	0	0	0	0	0	0	0%
RoL1	0	0	0	0	0	0	0	0	0	0	0	0	0%
RoR1	0	0	0	0	0	0	0	0	0	0	0	0	0%
RoM1c	0	0	0	0	1	0	0	0	1	0	0	0	17%
RoM1r	0	0	0	0	0	0	0	0	0	0	0	0	0%
RoM2m	0	0	0	0	0	1	0	0	0	0	1	0	17%
RoM2l	1	1	1	1	1	1	1	1	1	1	1	1	100%
RoL2r	0	0	0	0	0	0	0	0	0	0	0	0	0%
RoL2c	0	0	0	0	0	0	0	0	0	0	0	0	0%
RoL2	0	0	0	0	0	0	0	0	0	0	0	0	0%
RoV3	0	0	0	0	0	0	0	0	1	1	0	0	17%
RoM3m	1	1	1	1	1	1	1	1	1	1	1	1	100%
RoM3l	1	1	1	1	1	1	1	1	1	1	1	1	100%
RoL3	0	0	0	0	0	0	1	0	1	1	1	1	42%
MiR1	1	0	0	1	1	1	0	1	1	1	1	1	75%
MiM1	0	0	0	0	1	1	0	0	1	1	1	0	42%
MiV1	0	0	0	0	1	1	0	1	1	1	1	0	50%
MiR2	1	0	0	1	1	1	0	1	1	1	1	1	75%
Mauthner	1	1	1	1	1	1	1	1	1	1	1	1	100%
Vestibular	0	0	0	0	0	0	0	0	1	0	1	1	25%
MiV2	0	1	0	1	1	1	0	0	1	1	1	1	67%
MiD2cm	1	1	1	1	1	1	1	1	1	1	1	1	100%
MiD2cl	1	0	1	1	1	0	0	0	0	0	0	0	33%
MiD2i	1	1	1	1	1	1	1	1	1	1	1	1	100%
MiT	0	0	0	0	0	0	0	0	0	0	0	0	0%
MiD3cm	1	1	1	1	1	1	1	1	1	1	1	1	100%
MiD3cl	1	0	1	1	1	0	0	1	0	1	0	0	50%
MiD3i	1	1	1	1	1	1	1	1	1	1	1	1	100%
CaD	0	0	0	0	0	0	0	0	0	0	0	0	0%
CaV	0	0	0	0	0	0	0	0	0	0	0	0	0%

Table 3.10: Reticulospinal cells labelled in each *tiam2a*^{y264Et} fish

3.7 References

1. Brownstone, R. M. & Chopek, J. W. Reticulospinal Systems for Tuning Motor Commands. *Frontiers in Neural Circuits* **12,** 30. doi:10.3389/fncir.2018.00030 (2018).
2. Le Ray, D., Bertrand, S. S. & Dubuc, R. Cholinergic Modulation of Locomotor Circuits in Vertebrates. *International Journal of Molecular Sciences* **23,** 10738. doi:10.3390/ijms231810738 (2022).
3. Josset, N. *et al.* Distinct Contributions of Mesencephalic Locomotor Region Nuclei to Locomotor Control in the Freely Behaving Mouse. *Current Biology* **28,** 884–901.e3. doi:10.1016/j.cub.2018.02.007 (2018).
4. McLean, D. L. & Fetcho, J. R. Relationship of tyrosine hydroxylase and serotonin immunoreactivity to sensorimotor circuitry in larval zebrafish. *Journal of Comparative Neurology* **480,** 57–71. doi:10.1002/cne.20281 (2004).
5. Higashijima, S.-I., Mandel, G. & Fetcho, J. R. Distribution of prospective glutamatergic, glycinergic, and GABAergic neurons in embryonic and larval zebrafish. *Journal of Comparative Neurology* **480,** 1–18. doi:10.1002/cne.20278 (2004).
6. Perreault, M.-C. & Giorgi, A. Diversity of reticulospinal systems in mammals. *Current Opinion in Physiology* **8,** 161–169. doi:10.1016/j.cophys.2019.03.001 (2019).
7. Grillner, S. & El Manira, A. Current Principles of Motor Control, with Special Reference to Vertebrate Locomotion. *Physiological Reviews* **100,** 271–320. doi:10.1152/physrev.00015.2019 (2020).
8. Siegel, J. M. Behavioral functions of the reticular formation. *Brain Research Reviews* **1,** 69–105. doi:10.1016/0165-0173(79)90017-1 (1979).
9. Fetcho, J. R. & Liu, K. S. Zebrafish as a Model System for Studying Neuronal Circuits and Behavior. *Annals of the New York Academy of Sciences* **860,** 333–345. doi:10.1111/j.1749-6632.1998.tb09060.x (1998).
10. Metcalfe, W. K., Mendelson, B. & Kimmel, C. B. Segmental homologies among reticulospinal neurons in the hindbrain of the zebrafish larva. *Journal of Comparative Neurology* **251,** 147–159. doi:10.1002/cne.902510202 (1986).
11. Kimmel, C. B., Powell, S. L. & Metcalfe, W. K. Brain neurons which project to the spinal cord in young larvae of the zebrafish. *Journal of Comparative Neurology* **205,** 112–127. doi:10.1002/cne.902050203 (1982).
12. Severi, K. E. *et al.* Neural Control and Modulation of Swimming Speed in the Larval Zebrafish. *Neuron* **83,** 692–707. doi:10.1016/j.neuron.2014.06.032 (2014).
13. Orger, M. B., Kampff, A. R., Severi, K. E., Bollmann, J. H. & Engert, F. Control of visually guided behavior by distinct populations of spinal projection neurons. *Nature Neuroscience* **11,** 327–333. doi:10.1038/nn2048 (2008).

14. Kimmel, C. B., Hatta, K. & Metcalfe, W. K. Early axonal contacts during development of an identified dendrite in the brain of the zebrafish. *Neuron* **4,** 535–545. doi:10.1016/0896-6273(90)90111-R (1990).

15. Eschstruth, A., Schneider-Maunoury, S. & Giudicelli, F. Creation of zebrafish knock-in reporter lines in the *nefma* gene by Cas9-mediated homologous recombination. *genesis* **58.** doi:10.1002/dvg.23340 (2020).

16. Scott, E. K. & Baier, H. The cellular architecture of the larval zebrafish tectum, as revealed by gal4 enhancer trap lines. *Frontiers in Neural Circuits* **3,** 13. doi:10.3389/neuro.04.013.2009 (2009).

17. Kimura, Y., Okamura, Y. & Higashijima, S.-i. *alx* , a Zebrafish Homolog of *Chx10* , Marks Ipsilateral Descending Excitatory Interneurons That Participate in the Regulation of Spinal Locomotor Circuits. *The Journal of Neuroscience* **26,** 5684–5697. doi:10.1523/JNEUROSCI.4993-05.2006 (2006).

18. Marquart, G. D. *et al.* A 3D Searchable Database of Transgenic Zebrafish Gal4 and Cre Lines for Functional Neuroanatomy Studies. *Frontiers in Neural Circuits* **9.** doi:10.3389/fncir.2015.00078 (2015).

19. Akitake, C. M., Macurak, M., Halpern, M. E. & Goll, M. G. Transgenerational analysis of transcriptional silencing in zebrafish. *Developmental Biology* **352,** 191–201. doi:10.1016/j.ydbio.2011.01.002 (2011).

20. Martins, S. *et al.* Toward an Integrated Zebrafish Health Management Program Supporting Cancer and Neuroscience Research. *Zebrafish* **13,** S–47–S–55. doi:10.1089/zeb.2015.1198 (S1 2016).

21. Van Opbergen, C. J. *et al.* Optogenetic sensors in the zebrafish heart: a novel in vivo electrophysiological tool to study cardiac arrhythmogenesis. *Theranostics* **8,** 4750–4764. doi:10.7150/thno.26108 (2018).

22. Félix, R. *et al.* Structural and functional organization of visual responses in the inferior olive of larval zebrafish. *The Journal of Neuroscience,* e2352212023. doi:10.1523/JNEUROSCI.2352-21.2023 (2024).

23. Thiele, T. R., Donovan, J. C. & Baier, H. Descending Control of Swim Posture by a Midbrain Nucleus in Zebrafish. *Neuron* **83,** 679–691. doi:10.1016/j.neuron.2014.04.018 (2014).

24. Kimura, Y. *et al.* Hindbrain V2a Neurons in the Excitation of Spinal Locomotor Circuits during Zebrafish Swimming. *Current Biology* **23,** 843–849. doi:10.1016/j.cub.2013.03.066 (2013).

25. Asakawa, K. *et al.* Genetic dissection of neural circuits by *Tol2* transposon-mediated Gal4 gene and enhancer trapping in zebrafish. *Proceedings of the National Academy of Sciences* **105,** 1255–1260. doi:10.1073/pnas.0704963105 (2008).

26. Kwan, K. M. *et al.* The Tol2kit: A multisite gateway-based construction kit for *Tol2* transposon transgenesis constructs. *Developmental Dynamics* **236,** 3088–3099. doi:10.1002/dvdy.21343 (2007).

27. Kawakami, K., Shima, A. & Kawakami, N. Identification of a functional transposase of the *Tol2* element, an *Ac* -like element from the Japanese medaka fish, and its transposition in the zebrafish germ lineage. *Proceedings of the National Academy of Sciences* **97,** 11403–11408. doi:10.1073/pnas.97.21.11403 (2000).

28. Suster, M. L., Abe, G., Schouw, A. & Kawakami, K. Transposon-mediated BAC transgenesis in zebrafish. *Nature Protocols* **6,** 1998–2021. doi:10.1038/nprot.2011.416 (2011).

29. Randlett, O. *et al.* Whole-brain activity mapping onto a zebrafish brain atlas. *Nature Methods* **12,** 1039–1046. doi:10.1038/nmeth.3581 (2015).

30. O'Malley, D. M., Kao, Y.-H. & Fetcho, J. R. Imaging the Functional Organization of Zebrafish Hindbrain Segments during Escape Behaviors. *Neuron* **17,** 1145–1155. doi:10.1016/S0896-6273(00)80246-9 (1996).

31. Choi, H. M. T. *et al.* Third-generation *in situ* hybridization chain reaction: multiplexed, quantitative, sensitive, versatile, robust. *Development* **145,** dev165753. doi:10.1242/dev.165753 (2018).

32. Kenney, J. W. *et al.* A 3D adult zebrafish brain atlas (AZBA) for the digital age. *eLife* **10,** e69988. doi:10.7554/eLife.69988 (2021).

33. Avants, B., Tustison, N. & Song, G. *Advanced normalization tools (ANTS).* 2009.

34. Kunst, M. *et al.* A Cellular-Resolution Atlas of the Larval Zebrafish Brain. *Neuron* **103,** 21–38.e5. doi:10.1016/j.neuron.2019.04.034 (2019).

35. Carbo-Tano, M. *et al.* The mesencephalic locomotor region recruits V2a reticulospinal neurons to drive forward locomotion in larval zebrafish. *Nature Neuroscience.* doi:10.1038/s41593-023-01418-0 (2023).

36. Mione, M., Lele, Z., Kwong, C. T., Concha, M. L. & Clarke, J. D. Expression of *pcp4a* in subpopulations of CNS neurons in zebrafish. *Journal of Comparative Neurology* **495,** 769–787. doi:10.1002/cne.20907 (2006).

37. Alexandre, D., Alonzeau, J., Bill, B. R., Ekker, S. C. & Waschek, J. A. Expression Analysis of PAC1-R and PACAP Genes in Zebrafish Embryos. *Journal of Molecular Neuroscience* **43,** 94–100. doi:10.1007/s12031-010-9397-y (2011).

38. Wu, S., Adams, B. A., Fradinger, E. A. & Sherwood, N. M. Role of Two Genes Encoding PACAP in Early Brain Development in Zebrafish. *Annals of the New York Academy of Sciences* **1070,** 602–621. doi:10.1196/annals.1317.091 (2006).

39. Woods, I. G. *et al.* Neuropeptidergic Signaling Partitions Arousal Behaviors in Zebrafish. *The Journal of Neuroscience* **34,** 3142–3160. doi:10.1523/JNEUROSCI.3529-13.2014 (2014).

40. Berg, E. M. *et al.* Brainstem circuits encoding start, speed, and duration of swimming in adult zebrafish. *Neuron* **111,** 372–386.e4. doi:10.1016/j.neuron.2022.10.034 (2023).

41. Liu, Z. *et al.* Central Vestibular Tuning Arises from Patterned Convergence of Otolith Afferents. *Neuron* **108,** 748–762.e4. doi:10.1016/j.neuron.2020.08.019 (2020).

42. Tabor, K. M. *et al.* Direct activation of the Mauthner cell by electric field pulses drives ultrarapid escape responses. *Journal of Neurophysiology* **112,** 834–844. doi:10.1152/jn.00228.2014 (2014).

43. Hamling, K. R., Zhu, Y., Auer, F. & Schoppik, D. Tilt in Place Microscopy: a Simple, Low-Cost Solution to Image Neural Responses to Body Rotations. *The Journal of Neuroscience* **43,** 936–948. doi:10.1523/JNEUROSCI.1736-22.2022 (2023).

44. Dal Maschio, M., Donovan, J. C., Helmbrecht, T. O. & Baier, H. Linking Neurons to Network Function and Behavior by Two-Photon Holographic Optogenetics and Volumetric Imaging. *Neuron* **94,** 774–789.e5. doi:10.1016/j.neuron.2017.04.034 (2017).

45. Semmelhack, J. L. *et al.* A dedicated visual pathway for prey detection in larval zebrafish. *eLife* **3,** e04878. doi:10.7554/eLife.04878 (2014).

46. Kinkhabwala, A. *et al.* A structural and functional ground plan for neurons in the hindbrain of zebrafish. *Proceedings of the National Academy of Sciences* **108,** 1164–1169. doi:10.1073/pnas.1012185108 (2011).

47. Tabor, K. M. *et al.* Presynaptic Inhibition Selectively Gates Auditory Transmission to the Brainstem Startle Circuit. *Current Biology* **28,** 2527–2535.e8. doi:10.1016/j.cub.2018.06.020 (2018).

48. Bae, Y.-K. *et al.* Anatomy of zebrafish cerebellum and screen for mutations affecting its development. *Developmental Biology* **330,** 406–426. doi:10.1016/j.ydbio.2009.04.013 (2009).

Chapter 4

Imaging neural population dynamics during gait switching behaviour in larval zebrafish

*The organisation of descending locomotor pathways is remarkably conserved across vertebrates, with reticulospinal neurons (**RSNs**) in the brainstem forming a key bottleneck between higher centres mediating action selection and movement production in the spinal cord. A long-standing question in the field of locomotion has been whether different movements are controlled by distinct or overlapping supraspinal circuits [1]. Owing to their small size, optical accessibility, complex behavioural repertoire and wide array of genetic tools available, larval zebrafish make an excellent model system to study conserved mechanisms of supra-spinal circuitry and locomotor control. To uncover the neural correlates of slow and fast swims and elucidate the population dynamics underlying gait transitions, I recorded activity from genetically labelled neural populations in the brainstem of head-fixed larval zebrafish while they performed the optomotor response in a closed-loop configuration, utilising a light-sheet microscope. Images were corrected for motion artefacts and segmented into cell-sized regions-of-interest, while swims were decomposed into slow, fast, turn and struggle movement motifs. Given the sparse labelling of RSNs and thus their uniquely identifiable nature across animals, revealed a modulation of RSN activity with different movement motifs. Forward swimming-associated RSNs included the nMLF, RoL, MiV2 and MiD cells, with an increase in excitation from slow to fast swims. Turns were associated with ventromedial cells, and most RSNs were active during struggles. By showing how the brain dynamically selects and switches between two distinct but related movement patterns, I strive to understand fundamental principles in the supra-spinal control of locomotion.*

4.1 Introduction

Animals use a variety of locomotor gaits to navigate their environment. To do this, they need to dynamically generate appropriate motor commands, based on sensory information and past experience. A central question in the control of locomotion has long been whether different behaviours are controlled by distinct or overlapping neural circuits in supraspinal structures [1]. Larval zebrafish, *Danio rerio*, are small teleost fish with homologies to other vertebrates in key genetic, physiological and behavioural features [2, 3]. This, paired with their transparent brain early in development offering optical accessibility, makes them a good model to investigate general, conserved mechanisms of supraspinal circuitry and locomotor control.

Descending locomotor pathways are conserved across vertebrate species, with the basal ganglia mediating action selection [4]. Locomotor centres in the mesencephalon and diencephalon (**MLR, DLR**) provide graded control, where locomotion output scales with stimulation strength [5–7]. From the MLR and DLR, motor commands are relayed to the spinal cord via reticulospinal neurons (**RSNs**) in the brainstem [8]. RSNs are a relatively small, bilateral set of neurons, uniquely identifiable across animals due to their large soma size and large axon calibre, with both ipsilateral and contralateral projections [9]. These excitatory descending neurons form a bottleneck, passing motor commands to central pattern generators (**CPG**) in the spinal cord. CPGs consist of excitatory interneurons and motoneurons that innervate musculature to produce movement patterns [10, 11]. A detailed body of work from the El Manira lab has shown that at the level of the spinal cord, three different types of excitatory V2a interneurons project to three classes of motor neurons, which in turn innervate three layers of muscle, to drive slow, intermediate and fast swimming, respectively [12–15]. Could a similar organization of descending neurons, specialized to produce different movements, exist in the brainstem?

There are arguments and experimental evidence for and against separate pathways. Within the reticulospinal system, it is likely that spatially distributed populations of neurons work together to produce finely-tuned behaviours [16]. The small size and transparency of the larval zebrafish brain yields the advantage of being able to investigate the population dynamics on a brain-wide scale that is not

possible in higher organisms[17]. Studies from lamprey and zebrafish show that the Mauthner network is responsible for eliciting different kinds of escape swims [18–23], whereas ventromedial RSNs drive turning behaviour [24, 25]. Forward swimming has been linked to caudal V2a neurons as well as nMLF neurons and rostral RSNs [24, 26–32]. This supports a view of spatially distinct sets of RSNs driving different types of swims. If such a direct mapping between individual behaviours and corresponding circuitry exists for all motor patterns, the question arises how the brain accomplishes the challenge of switching its activity from one population of neurons to the next. Focusing on the stimulus driven transitions between two distinct, but similar bout types may facilitate to uncover the mechanism by which an animal abruptly switches from one motor pattern to another.

An alternative view would be that different sub-components of swims can be assembled to produce whole movements. For instance, swims can be decomposed into a turn and forward component, which have shown to be mediated by distinct sets of RSNs [31]. In this case, it was proposed that turning neurons add an asymmetrical component to convert symmetrical forward swims into turns [25]. Another study showed that within forward swimming, nMLF neurons were active 100% of the time but that their activity scaled with swimming speed [27]. This supports a framework of overlapping neural populations with graded modulation producing different movements. In light of these findings, three hypotheses arise:

1. Distinct sets of RSNs encode commands for distinct behavioural motifs, with a graded or abrupt switch between those different populations.
2. Distinct behavioural motifs arise from the combinatorial population activity of all RSNs, for instance by changes in excitation.
3. Movement motifs can be grouped into larger sets of behaviours, for instance escapes vs exploration vs hunting, that are also distinctly organised in the RS system. Within those sets there can be modulation, for instance progressive recruitment.

Here, I attempted to address these questions by recording activity from genetically labelled neural populations in the brainstem of head-fixed larval zebrafish while they performed the optomotor response (**OMR**) in a closed-loop configu-

ration, utilising a light-sheet microscope. This light sheet microscope has been adapted to include an electrically tunable lens, enabling whole-brain volumetric imaging at 5 volumes per second – a critical point considering swims of larval zebrafish often last only ∼200 ms [33]. Head-fixed fish showed differences in bout kinematics from freely swimming fish, with longer movements that included switches in frequency within a single bout. I therefore utilised a novel method based on convolutional sparse coding, *Megabouts* [34], to decompose bouts into slow, fast, turn and struggle movement motifs. Given the sparse labelling of RSNs and thus their uniquely identifiable nature across animals, revealed a modulation of RSN activity with different movement motifs. Forward swimming-associated RSNs included the nMLF, RoL, MiV2 and MiD cells, with an increase in excitation from slow to fast swims. Turns were associated with ventromedial cells, and most RSNs were active during struggles. My findings demonstrate how the brain of a small vertebrate selects dynamically between two distinct motor outputs, providing insight into fundamental principles in the supra-spinal control of locomotion in animals.

4.2 Materials and Methods

4.2.1 Fish husbandry

Adult fish were raised and bred at 28°C on a 14h light / 10h dark cycle following standard husbandry methods as detailed in [35]. All fish colonies were maintained by importing wild types every 1-3 years and line-specific breeding schemes designed to reduce inbreeding depression [35]. Embryos were collected and larvae were raised at 28°C in E3 embryo medium (5 mM NaCl, 0.17 mM KCl, 0.33 mM CaCl2 and 0.33 mM MgSO4, changed daily) at a density of 60 larvae per 200 mL until behavioural testing at 6-8 dpf. From 5 dpf onwards, approximately 10 mL of a live L-type rotifer polyculture (containing 1000-2000 rotifers per mL) were added to each dish twice a day and larvae were allowed to feed freely. Zebrafish do not sexually differentiate until approximately 3 months of age, therefore the sex of the animals cannot be reported. All experimental procedures were approved by the

Champalimaud Foundation Ethics Committee and the Portuguese Direcção Geral Veterinária, and were performed according to the European Directive 2010/63/EU.

4.2.2 Transgenic lines

The following transgenic lines were used in a nacre (*mitfa -/-*) background (see Table 4.1). With the exception of *s1171tEt*, which was crossed with Tg[10xUAS:GCaMP6f^{ccu1Tg}] [36], the lines used in the experiments were created by crossing them with Tg[10xUAS:GCaMP6fEF05^{ccu2Tg}] [37].

Short name	**Transgenic line**	**Source**
nefma	Tg[nefma:KalTa4]	[38]
s1171tEt	Tg[-0.6hsp70l:Gal4-VP16$^{s1171tEt+}$]	[28, 39]
calca^{ccu75Et}	Tg[-5.0calca:Gal4FF^{ccu75Et}]	this thesis and [40]
	Tg[10xUAS:GCaMP6f^{ccu1Tg}]	[36]
	Tg[10xUAS:GCaMP6fEF05^{ccu2Tg}]	[37]

Table 4.1: Transgenic fish lines used in functional imaging experiments.

4.2.3 Cloning

calca:Gal4FF A 5023bp promoter region upstream of the calca start codon was cloned into pCR™8/GW/TOPO™ (Invitrogen™) using the following primers:

- 5'-GTGCCTGCTGAGGAGCATAAC-3'
- 5'-GGTCCCCTGTAGTAAAACATC-3'

The calca promoter (Entry Clone) was then recombined into an Gal4FF destination vector (Gateway™ LR recombination, Invitrogen™), derived from the Tol2Kit [41], so that the construct was bracketed by two Tol2 [42] inverted terminal repeats.

Line establishment DNA constructs were injected together with Tol2 transposase mRNA and non-integrating UAS:GFP plasmid into 1-2 cell stage mitfa-/- eggs. Embryos with GFP expression were raised and screened as adults for germ line transmission. Progeny of positive animals with stable expression pattern were selected as founders for the respective Gal4FF driver line.

Screening Larvae were pre-screened at 3-4 dpf to select fish with positive expression of GCaMP.

4.2.4 Light-sheet imaging

The custom-built light-sheet microscope enabled the simultaneous acquisition of behavioural and functional data and the delivery of precisely timed visual stimulation. Briefly, a 473 nm excitation laser (Cobolt Skyra, HÜBNER Photonics) is shaped into a thin sheet by focusing it in one axis using a plano-convex cylindrical lens (LJ1212L1-A, Thorlabs) to illuminate and record a planar section of the brain. The illuminated section was scanned throughout the brain volume using a galvanometer (GVS001, Thorlabs) at a rate of 5 volumes per second (17-19 planes, 85-95 Hz), spanning a total volume of approximately 100 µm in the dorso-ventral axis. The laser power was set to 250 µW. Fluorophore emission was collected using a water immersion objective with a focal distance of 9 mm and a numerical aperture of 0.5 (UMPLFLN20XW, Olympus) paired with a tube lens with a focal distance of 200 mm (TTL200-A, Thorlabs) for a total optical magnification of 22.22x. The collected light was filtered using a short-pass frequency filter with a cut-off wavelength of 600 nm (FESH0600, Thorlabs) to discard infrared emission from the behavioural tracking system and a band-pass filter with a central wavelength of 525 nm and a bandwidth of 39 nm (MF525-39, Thorlabs) to select GFP emission. An electrically tunable lens (EL-16-40-TC-VIS-5D-C, Optotune), controlled by an industrial lens controller (TR-CL180, Gardasoft), was used to refocus the acquired light, which was then detected by a sCMOS camera (ORCA-Flash4.0 V3, Hamamatsu Photonics) with a spatial resolution of 0.3 μm/pixel. A data acquisition system (PCIe-6343, National Instruments) was used to generate and collect control signals for all equipment.

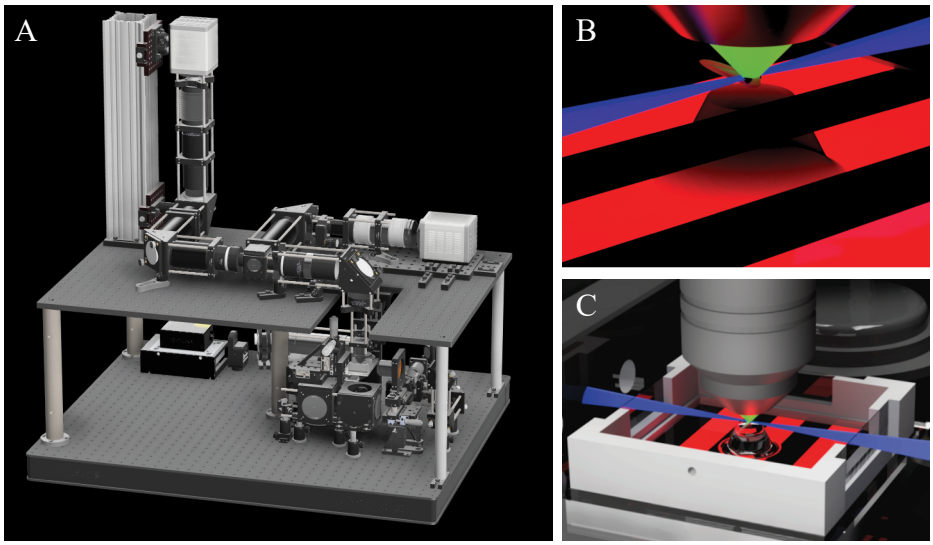

Figure 4.1: Light-sheet microscope set-up built by A.L. Martins.
A) Overview of set-up.
B) Close-up of fish positioned in arena with gratings displayed below and light-sheet passing from right-side.
C) Close up of arena with excitation and detection paths outlined.

4.2.5 Head-restrained behavioural assay

I used a custom-built microscopy system that enables simultaneous light-sheet functional imaging and head-restrained behavioural assays.

Mounting For fish preparation, larvae aged 6-7 days post fertilization (**dpf**) were placed in 2% low melting point agarose (UltraPure LMP Agarose, Cat#16520100, Invitrogen by Life Technologies, USA), which was heated to 35°C. The fish were drawn into a glass capillary (P/N: 701904, BRAND, Fisher Scientific) using a matching stainless steel piston rod (P/N: 701932, BRAND, Fisher Scientific). The glass capillary was inserted into a custom-made imaging chamber with the fish head resting on top of a silicone dome (SYLGARD 184 Silicone Elastomer Kit, The Dow Chemical Company, Germany) located at the centre of the chamber. The arenas were square-shaped: one side had an opening for capillary insertion, while the other three sides were fitted with glass windows allowing the light sheet to pass through. After aligning the fish, a droplet of agarose was positioned to

secure the fish preparation to the dome. The tail was freed by cutting the agarose around it and gently removing the capillary. Finally, the chamber was filled with E3 and larvae were allowed to habituate for a minimum of 15 minutes.

Behaviour set-up within light-sheet microscope Two 850 nm LEDs (TSHG 6400, Vishay) were positioned near the imaging objective to illuminate the tail, capturing images from below at a rate of 700 Hz using a USB camera (Mako U-029B, Allied Vision Technologies) fitted with a machine vision lens with a focal distance of 50 mm (HF50SA-1, Edmund Optics) and a long-pass frequency filter with a cut-on wavelength of 780 nm (P/N:10CGA-780, Newport). An LED projector (ML750e, Optoma), equipped with a long-pass filter with a cutoff wavelength of 610 nm (FGL610, Thorlabs), was used so that only red light could pass through, projecting visual stimuli onto a diffuser screen placed below the fish. A small opening was cut into the screen to allow for tail recordings. A hot mirror with a cut-off wavelength of 700 nm (P/N: 64471, Edmund Optics) enabled emitted visible light from the projector to reach the screen while diverting collected infrared light to the tail tracking camera. The entire system was controlled by a custom-written software suite developed in C# and built on .NET 8 (Martins, Laborde and Orger, in prep.).

Experimental paradigm Each larva was recorded for 30-45 minutes. During the experiment, forward gratings moving at a range of speeds (15 speeds, 0 - 32.8 mm/s) were displayed for 10 seconds in a randomised order, with 5 repetitions each. Gratings were stationary for 10 seconds in-between trials. The width of the stripes was adjusted to a 1 cm width at 5 mm distance to match previous studies [24, 27, 34]. Grating speed was updated continuously in closed-loop. Velocity was estimated by tracking 16 points along the tail and taking the cumulative sum of angular changes along the tail, convolved with an exponential filter, which empirically is proportional to forward velocity in freely swimming fish. This velocity was added to the grating with a fixed gain adjusted to a level that allows head-fixed larvae to match grating speed over a normal range.

4.2.6 Imaging and behaviour data processing

All behaviour data were pre-processed offline using MATLAB r2018a (Mathworks, RRID:SCR-001622) and Python 3.7 on a computer with 64.0GB RAM and a Intel(R) Core(TM) i7-5820K CPU @ 3.30GHz 3.30 GHz processor.

Synchronising with acquisition Controlling the entire experiment with one software suite allowed for precise post-hoc synchronisation of visual/auditory stimulation, imaging camera frames and behaviour camera frames. Briefly, a log of stimulus frame rates was passed to the behaviour-suite in real-time in steps of 10 stimulus-fps, allowing for precise matching of behaviour frames and their corresponding visual stimulation. To synchronise neural activity recordings with behavioural output, a log of imaging frames with matching behaviour frames was saved.

Processing of tail data 16 points along the tail were tracked in x and y in real-time and used to calculate displacement and swimming speed for closed-loop visual stimulation. For detailed offline behavioural analysis, tail positions were smoothed using a Savitzky-Golay polynomial filter, angles between segments were calculated and summed. Subsequent processing (baseline removal, bout segmentation, sparse coding) was done using the Megabouts suite [34]. Briefly, to counteract any drift over the course of the experiment due to water evaporation or fish displacement, tail angle traces were detrended utilising the *Whittaker* algorithm from the python library *pybaselines*. To detect bouts, a threshold of 20 was used as this reliably segmented bouts while disregarding noise. The tail angle was decomposed into four motifs (slow, fast, turn, struggle) using convolutional sparse coding. For more detail see subsection 2.2.6 and www.megabouts.ai [34].

4.2.7 Light-sheet imaging data preprocessing

All imaging data were preprocessed offline using MATLAB r2018a (Mathworks, RRID:SCR-001622) on an in-house high-performance computing cluster running CentOS Linux 7.7.

Data saving and storage

Bitmaps recorded from the microscope camera were organised into volumes and losslessly compressed into an HDF5 file. This file was passed through an analysis pipeline to correct motion artefacts during imaging and segment regions of interest (**ROIs**). A camera offset value of 400 was subtracted from each camera frame. The five ventral-most planes were discarded from the analysis due to blurring caused by the turn-around of the tunable lens.

Motion correction

Template generation To correct motion artefacts, a series of templates was built to serve as reference volumes for the motion correction algorithm. Due to drift over the duration of the experiment, templates spanning 5 minute windows were created for each imaging plane. First, for each plane and subset, 10 random volumes during which no bouts were detected were selected. Volumes in each subset and plane were averaged to form the initial averages and serve as templates for the subsequent step. Second, another 10 random volumes during which no bouts were detected were selected for each subset and plane, and registered to their corresponding 'average template' using the *imregtform* and *imwarp* functions in Matlab. For *imregtform*, the parameters *translation* and $pyramid\_levels = 2$ were selected. For *imwarp*, the *interpolate_nearest_neighbour* parameter was chosen. Third, for each plane, each 'registered template' was aligned to the first 'registered template' using the same functions and parameters as above.

Lateral displacements First, the displacement of a central subregion of each image frame to the subregion of its corresponding 'registered template' was computed using the *imregtform* function with parameters *translation* and $pyramid\_levels = 2$. Then, the calculated displacement value was applied to the whole frame using the *imwarp* function with the *interpolate_nearest_neighbour* parameter. An alignment of subregions was chosen for computing efficiency. The lateral registration was performed separately for each plane, as drift and axial displacement were corrected for in the next step.

Axial displacements To calculate observed drift, a hierarchical motion estimation algorithm using a rigid body model was applied, as described in [43]. Briefly, a Laplacian pyramid with four levels is built. For each level, a motion vector is computed that minimises the mean squared error of the difference between the reference image and the moving image, and this process is repeated iteratively four times. The drift estimation calculation is done over the central 50% of the image to avoid edge effects and to ensure the algorithm is applied to a highly structured region, and the values of the input images are first normalised and centred around zero.

Due to the significant difference in lateral and axial resolutions, lateral and axial displacements were corrected separately using 2D images. All sub-pixel translations were estimated using linear interpolation. A 3D volume was corrected in the following sequence of operations: first, the previous estimate of axial drift was applied to the entire volume; then, for each image plane, lateral drift was computed and applied to that plane; finally, a new estimate of axial drift was computed and applied to the whole volume. A coronal mean projection was used as input to the motion estimation algorithm to estimate axial drift, and the result was filtered through an exponential smoother with alpha = 0.075.

ROI Segmentation

ROI segmentation was performed independently for each plane. A correlation map was computed using a technique described in [44], where the following intermediate operations were performed on the fluorescence vectors: detrending over time using a ridge filter with a window of 150 frames and convolution with a Gaussian-shaped kernel of radius of 1. Next, a greedy selection algorithm to iteratively grow the ROIs was applied. The pixel with the highest value in the correlation map that had not yet been used was selected, which served as the seed for the new putative ROI. Then, the following process was repeated iteratively: First, the region was grown by dilation with a diamond-shaped structuring element of size 3x3. Second, the Pearson correlation coefficient between the detrended fluorescence trace of each new pixel and the detrended average fluorescence of the putative ROI was

computed. Third, the top 25% of new pixels were kept as part of the ROI if their correlation coefficient was at least 0.5. This process continued until no new pixels were added or the total size of the ROI exceeded 200 pixels. The ROI selection process ended when a pre-defined transgenic line-dependent maximum number of ROIs was found, or the new seed pixel had a correlation map value below 0.06. Finally, a binary closure operation was performed on the resulting ROIs and any ROIs smaller than 25 pixels were discarded.

4.2.8 Data Analysis

Following pre-processing of imaging and behaviour data, all analysis was performed in Python (Anaconda3) and ImageJ (Fiji). Having access to individual fluorescence traces for each ROI, paired with tail angle and grating speed, allowed me to analyse the data with multiple different approaches. First, change in fluorescence over baseline () was computed for each ROI by subtracting and dividing by a moving baseline (60s windows) of that ROI, taking into account background subtraction and adding a constant to prevent division by 0. Next, ROIs were clustered hierarchically based on similar activity using optimal LEAF ordering [45], revealing potential groups of RSNs with similar activity.

4.3 Results

4.3.1 Fast volumetric imaging paired with high-speed behavioural recordings in an OMR assay

To elucidate the neural basis of different types of forward swimming and the population activity of gait transitions, I recorded the activity of genetically labelled neurons in the brain stem of larval zebrafish, while simultaneously recording tail movements using high-speed tracking (n=76). Larval zebrafish from backgrounds Tg[nefma:KalTa4, UAS:GCaMP6fEF05], Tg[-5.0calca:Gal4FF^{ccu75Et}] and Tg[-0.6hsp70l:Gal4-VP16$^{s1171tEt+}$, 10xUAS:GCaMP6f] at 6-9 days post-fertilization were embedded in low-melting point agarose on a sylgard cone using a glass capillary and their tails were freed. Gratings moving at a range of speeds (15 speeds, 0

- 32.8 mm/s) were displayed from below. During the experiment, moving gratings were shown in closed-loop for 10 seconds in a randomised order with 10 second inter-trial intervals, and 5 repetitions each (Figure 4.2A).

The variable and rapid timescale of behaviour, with bouts lasting from 100 ms to several seconds and including intra-bout modulation, paired with the stereotyped, yet distributed neural population of interest spanning from the midbrain to the caudal hindbrain, imposed several restrictions on suitable imaging methods. To achieve sufficient temporal resolution, I utilised a light-sheet microscope that can scan through the whole-brain volume at 5 volumes per second using an electrically tunable lens. To label different reticulospinal populations of interest, several transgenic lines with sparse expression in the mid- and hindbrain were selected (for characterisation of these lines see Chapter 3).

4.3.2 The forward optomotor response is conserved but more variable under imaging conditions

It has previously been reported that blue light from the excitation laser can interfere with fish behaviour [46]. To avoid this, a thin needle was placed in the microscopy set up in a plane conjugate to the fish to physically block light from reaching the eyes of the fish. To confirm that head-restrained fish still performed

---

Figure 4.2: Simultaneous light-sheet imaging of genetically labelled brainstem neurons paired with high-speed behaviour recordings.
A) Top panel shows fish schematic in microscope (left) and image-preprocessing pipeline (right). Plane-wise rigid motion correction of imaging frames to a rolling template (60s window), followed by computation of a correlation map and ROI segmentation, yielding raw activity traces for each ROI. Bottom panel shows experimental design (left) and behaviour pre-processing pipeline (right). Tail is tracked along 16 positions on tail from which tail angle is computed and segmented into bouts, followed by decomposition into slow, fast, turn or struggle movement motifs utilising convolutional sparse coding.
B) Average number of bouts per trial as a function of grating speed.
C) Bout duration (ms) as a function of grating speed.
D) Interbout interval (s) as a function of grating speed.
E) Latency to first bout (s) as a function of grating speed.
For B-E) black trace, 9541 bouts from transgenic fish (n=76) in head-restrained (HR) OMR assay in light-sheet microscope (LSM); gray trace, 15974 bouts from wildtype fish (n=40) in head-restrained (HR) OMR assay and 3D visual stimulation without microscope. Errors bars are standard error of the mean.

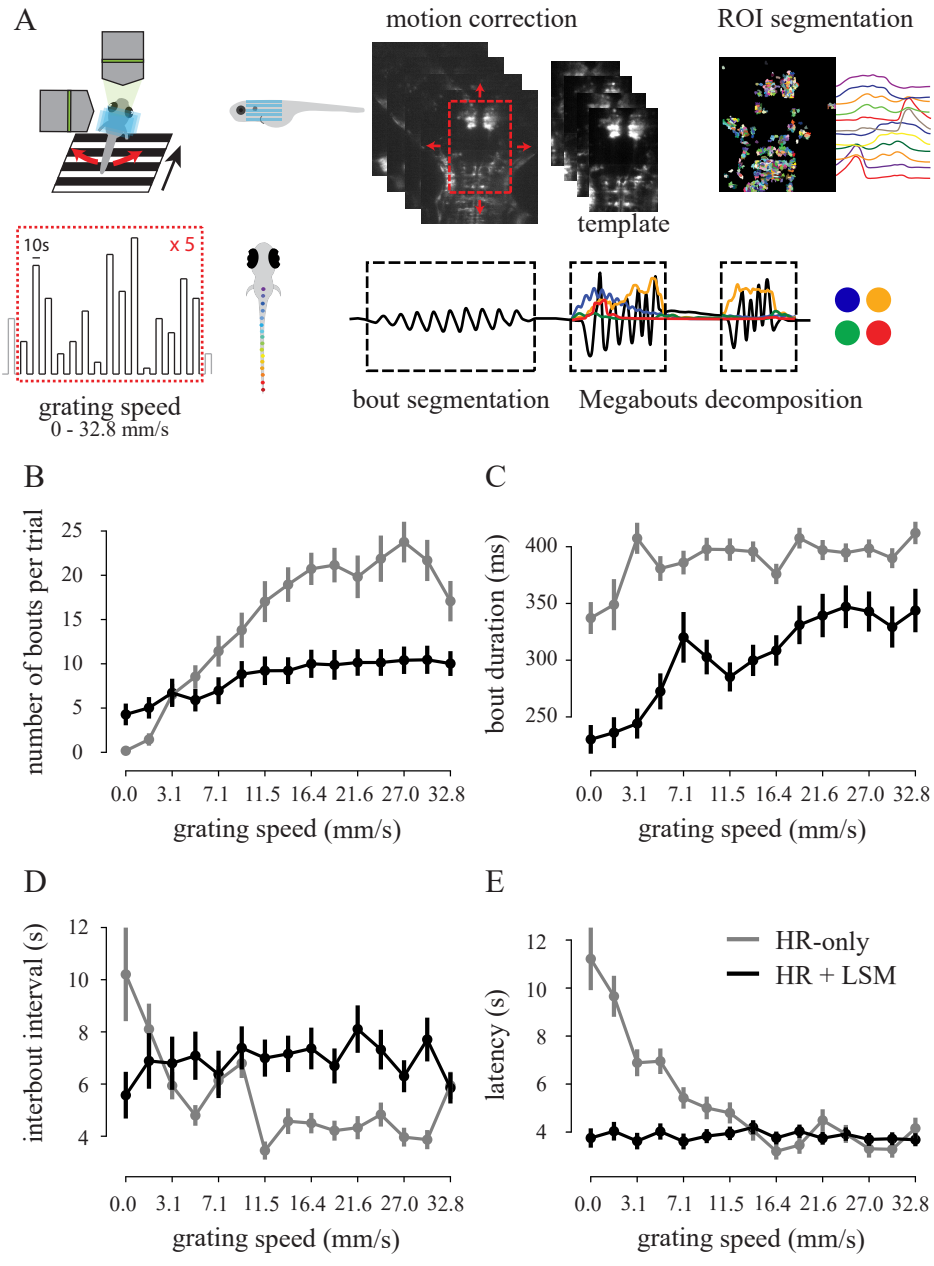

(Caption on previous page)

the OMR when presented with forward moving gratings under the microscope (referred to as HR+LSM), several kinematic variables were computed and compared to data from head-fixed fish (referred to as HR-only) presented in Chapter 2.

Behaviour of head-fixed fish under the light-sheet was generally a bit more variable. The average number of bouts per trial was computed for both cohorts. HR+LSM fish (n=76) still showed a slight increase as a function of grating speed, increasing from 4 to 10 bouts per trial. However, this was much less pronounced than for HR-only fish, which over a similar 10s window increased from 0 to 15-25 bouts per trial (Figure 4.2B). Average bout duration increased for both cohorts as a function of grating speed, with bouts from HR+LSM fish increasing from 200 to 350 ms in duration, compared to an increase from 340 to 400 ms in HR-only fish (Figure 4.2C). HR-only fish showed a marked decrease in interbout interval and latency to first bout after trial onset as a function of grating speed. These parameters did not change in HR+LSM fish (Figure 4.2D-E). From individual fish responses, it was clear that behaviour from head-fixed fish under the microscope was more variable. For instance, it was often not locked to trial periods, as had been observed in HR-only fish. It is impossible to pinpoint a sole reason for the differences observed here, but it is likely due to a combination of different genetic backgrounds, differences in visual stimulation (3D for HR-only fish, only from below for HR+LSM fish), methods of embedding and scattered light from the light-sheet.

Even though responses were more variable under imaging conditions, fish still performed a variety of swims in response to optomotor gratings. Computing tail-beat frequency (**TBF**) revealed a near-bimodal distribution, possibly indicating slow-like and burst-like swims (Figure 4.3A, left). Similarly to HR-only fish, rostral tail-bend amplitude (**rTBA**) did not fall into two clusters, likely due to the rostral part of the tail being restrained (Figure 4.3A, right). Separating kinematic parameters by grating speed revealed a cluster of low rTBA (20-60 deg), low TBF (40-70 Hz) swims during slow gratings (Figure 4.3B, left). This cluster was also present during fast gratings, with a second cluster of higher TBF (100 Hz) emerging (Figure 4.3B, right).

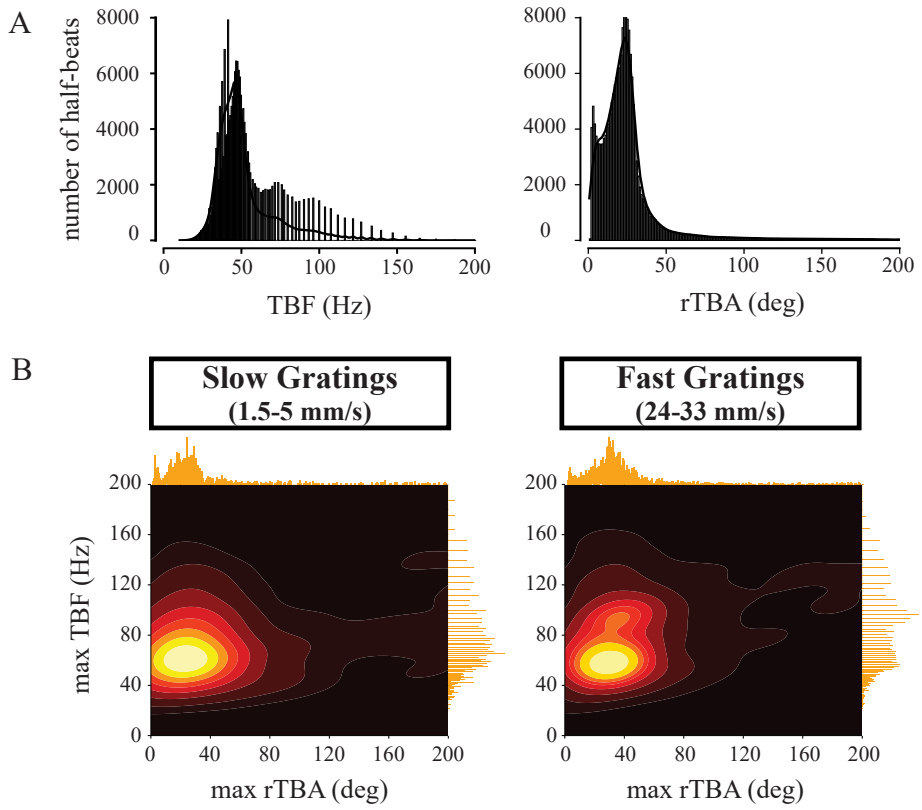

Figure 4.3: B) Histogram of tail-beat frequency (TBF) and rostral tail-bend amplitude (rTBA) of half-beats across all trials and fish, n=76.
C) Heatmap showing tail kinematics of (left) 1181 bouts during slow gratings (1.5-5 mm/s) and (right) 2922 bouts during fast gratings (24-33 mm/s) from 76 fish.

Reproducing behaviour exactly as previously seen in freely-swimming conditions is challenging, as in head-restrained conditions bouts tend to be longer, sparser, and occasionally the animal struggles. In addition, the previously used method for bout classification [33] relies on motion cues from the animal and can therefore not be applied directly to restrained animals. Using convolutional sparse coding as part of the Megabouts suite [34], bouts were decomposed into slow, fast, turn and struggle movement motifs. The dominant movement motif at any time point was computed and visualised for each trial across several grating speeds in an example fish (Figure 4.4)

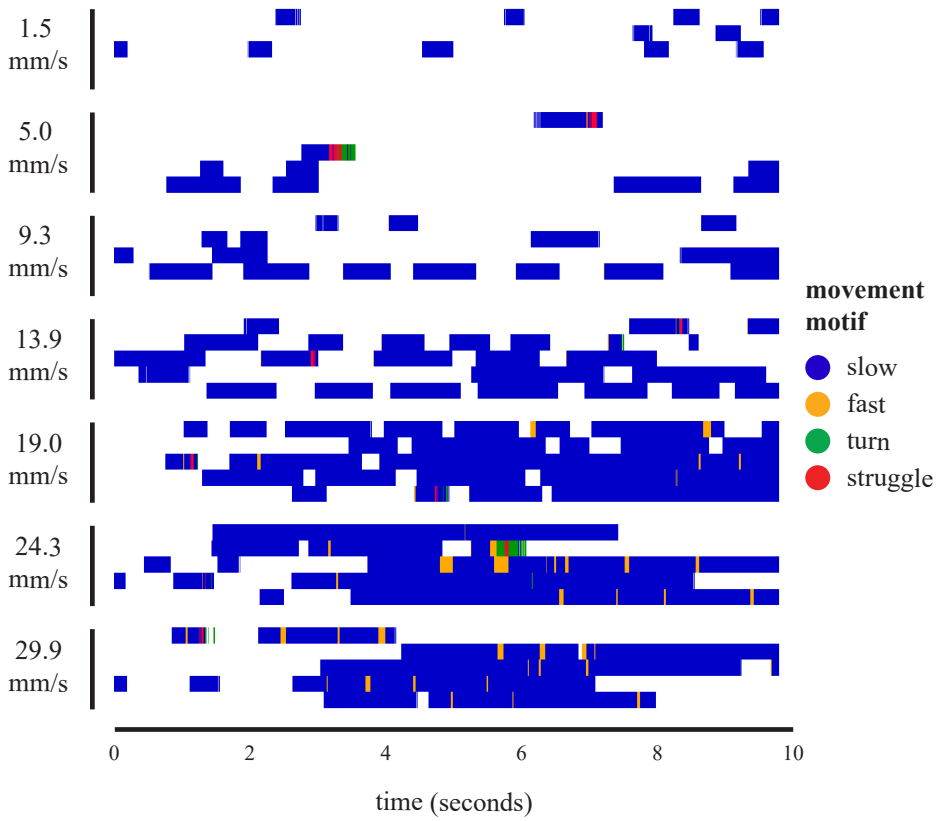

Figure 4.4: Active movement motif across grating speeds in an example fish (*calca*^{ccu75Et}, 6 dpf) performing the OMR under imaging conditions. In each speed block, each line represent a trial lasting 10 seconds. Colours represent movement motifs where blue, slow; orange, fast; green, turn; red, struggle.

4.3.3 Activity of RSNs correlates with swimming

To extract activity traces from single neurons, my colleagues and I developed a modular imaging data processing pipeline. First, plane-wise rigid registration corrected for motion artifacts introduced by fish motion and drift over time, by aligning a subsection of each image frame with that of a rolling template. Next, a correlation map of long-scale activity over the course of the experiment was computed. This allowed the extraction of seeds, from which ROIs could be grown based on correlation with neighbouring pixels. Changes in fluorescence activity compared to baseline (dF/F) were computed from the raw extracted traces, and paired with tail recordings and stimulus speed.

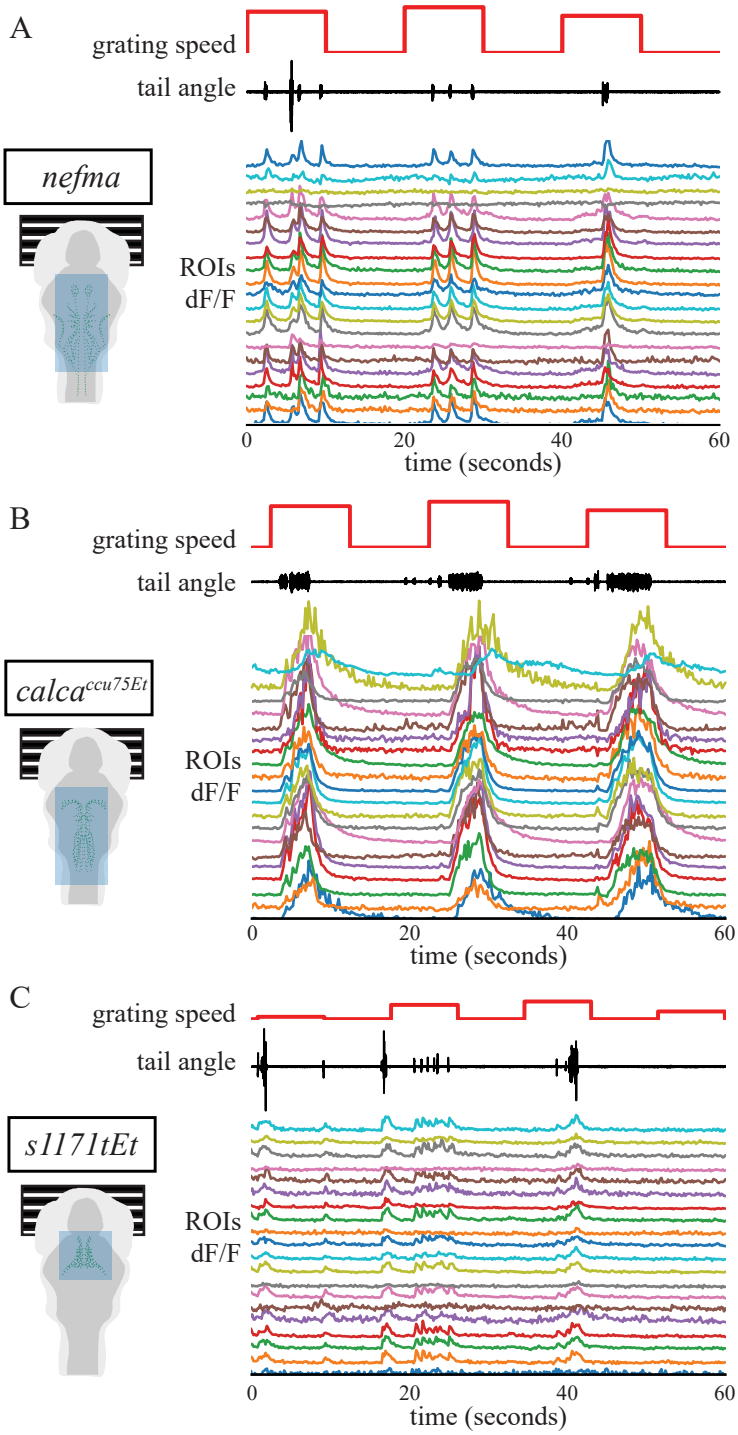

Figure 4.5: Exemplary ROI dF/F activity traces from individual A) *nefma*, B) *calca*^{ccu75Et} and C) *s1171tEt* fish paired with tail angle and grating speed. ROIs are 20 randomly chosen examples from several thousand extracted per fish. F, fluorescence; ROI, region of interest.

Based on findings from previous literature, three transgenic lines (*nefma*, Tg[nefma:KalTa4]; *s1171tEt*, Tg[-0.6hsp70l:Gal4-VP16$^{s1171tEt+}$]; *calca*^{ccu75Et}, Tg[-5.0calca:Gal4FF^{ccu75Et}]) labelling different subpopulations of reticulospinal neurons in the mid- and hindbrain were selected.[1] The transgenic line *nefma* [38] labels all 'classical' glutamatergic (*vglut2*) RSNs, as well as cholinergic (*chata*) cranial neurons [40]. The transgenic line *s1171tEt* [28] labels glutamatergic (*vglut2*) cells near the nMLF in the midbrain [40]. The newly generated transgenic line *calca*^{ccu75Et} has a high degree of similarity to the well-characterised Tg[vsx2:mRFP] line – *vsx2* was previously also referred to as *alx* and is the homologue to the mammalian *Chx10* [47] – and labels glutamatergic, ipsilaterally-projecting V2a-RSNs in the hindbrain [40].

Data from three representative example fish (one for each transgenic line) show that the activity of many ROIs was synchronized with swimming (Figure 4.5). Upon closer inspection, there appeared to be subtle differences between ROIs. Given that the transgenic lines used in these experiments predominantly label neurons in the brainstem related to motor control, this a reassuring finding validating my method.

4.3.4 Distributed, scaled activity of RS populations during different swims

A central question in locomotion control has long been whether distinct sets of RSNs produce different behaviours, or whether there is modulation of the same population of RSNs. To date, only turns [16, 24, 25] and escape swims [18–20, 22, 23, 48, 49] have been successfully mapped to distinct descending pre-motor pathways. Other studies have argued for a modulation of the same neurons, for instance by an increase in excitation, to increase swimming speed [27]. In light of these findings, I postulated three hypotheses: 1) Distinct sets of RSNs encode commands for distinct behavioural motifs, with a graded or abrupt switch between those different populations, 2) Distinct behavioural motifs arise from the combinatorial population activity of all RSNs, for instance by changes in exci-

[1] For a more detailed characterisation of these transgenic lines, see Chapter 3 and [40].

tation or 3) Movement motifs can be grouped into larger sets of behaviours, for instance escapes vs exploration vs hunting, that are also distinctly organised in the RS system. Within those sets there can be modulation, for instance progressive recruitment.

As a first pass, to assess whether neural activity differs between swim types, I computed depth colour-coded maps of individual randomly chosen bouts for example fish from each transgenic line. Due to the stereotyped, sparse labelling of large RSNs in the *nefma* line, individual RSNs could be identified by eye by comparison with previous maps of RSNs [9, 24, 40]. In an exemplary *nefma* fish, slow swims were associated with low activity in the nMLF and oculomotor nucleus, (situated just caudally to the nMLF), low activity in the RoL cells and

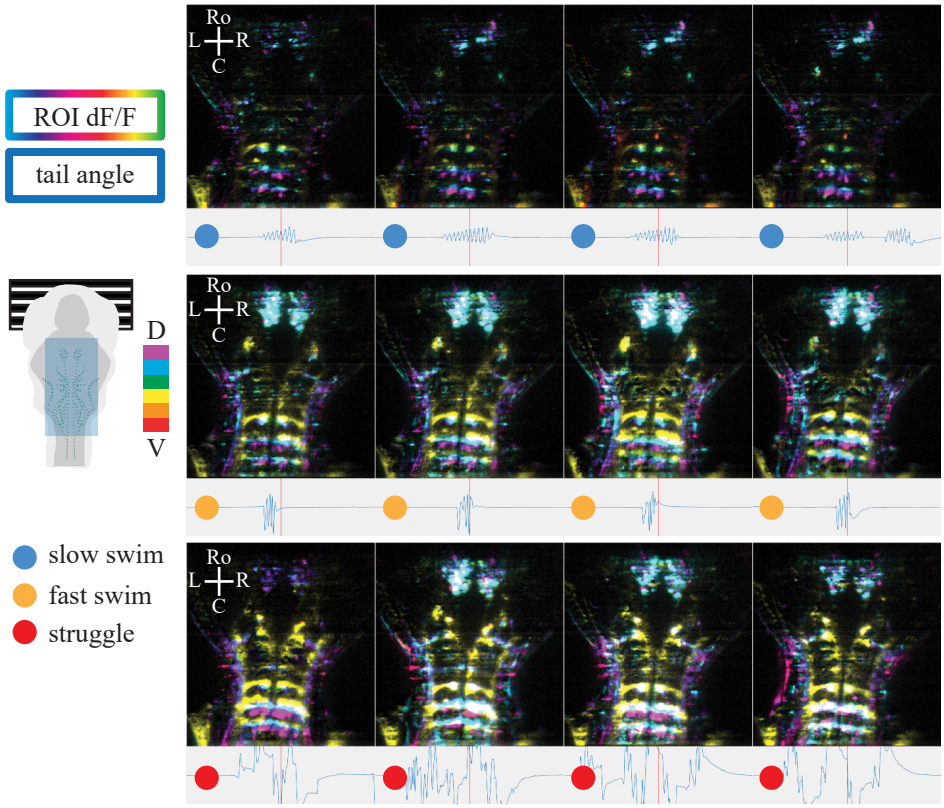

Figure 4.6: Neural activity maps across slow (top row), fast (middle row) and struggle swims (bottom row) in an exemplary *nefma* fish. Colours in brain maps indicate depth of ROI. Blue trace, tail angle; red line, time point of imaging frame, D, dorsal; V, ventral.

strong bilateral activity in the medial hindbrain (MiV2, MiD2, MiD3). During fast swims, there appeared to be a general increase in excitation, particularly in the nMLF, oculomotor nucleus, RoL cells, MiV2, MiD2, MiD3 and possibly the CaD/CaV cells. During struggles, most cells labelled by *nefma* appeared to be active. In comparison to fast swims, these included the RoM2, RoM3 and MiV1 cells (Figure 4.6). These preliminary observations were consistent across 15 fish from this line and match reports from previous studies [24, 27]. For instance, in the study by Severi *et al.*, cells in the nMLF were correlated with tail-beat frequency and duration, with an increase in excitation as opposed to additional cells being recruited [27]. Orger *et al.* also reported calcium activity in the RoL and MiV2 cells in response to moving gratings that elicit slow swimming [24].

Activity in an example $calca^{ccu75Et}$ fish was more distributed across the hindbrain (Figure 4.7). A general increase in excitation in struggle swims was evident, compared to slow and fast swims. There was strong sustained bilateral activation of caudal and medial hindbrain neurons, with higher activity during fast swims than slow swims. In some fish, I also observed strong, selective activation of cells situated in the rostral, lateral horns. The study by Carbo-Tano and Lapoix *et al.* also reported distributed calcium activity across the hindbrain in V2a-RSNs labelled under the *vsx2* promoter during spontaneous slow swims [31]. Considering the high degree of overlap between the two transgenic lines [40], I hope to build on the findings in [31] by also including fast swims in my analysis. Given the large number of cells labelled in this line and the distributed activity I observed, future work will focus on regression analysis to identify populations of cells associated with different modes of swimming.

Considering activity maps in an exemplary *s1171tEt* fish tells a slightly different story. The transgenic line *s1171tEt* labels glutamatergic (*vglut2*) neurons in the tegmentum, including the four large nMLF cells (MeM1, MeLm, MeLc, MeLr) and the small mesencephalic (**MeS**) cells [28, 40]. I observed a general increase in excitation from slow to fast to struggle swims, with a tendency to extend in a medial to lateral direction (Figure 4.8). These observations are in line with findings from Berg *et al.*, who reported a recruitment of medial nMLF neurons

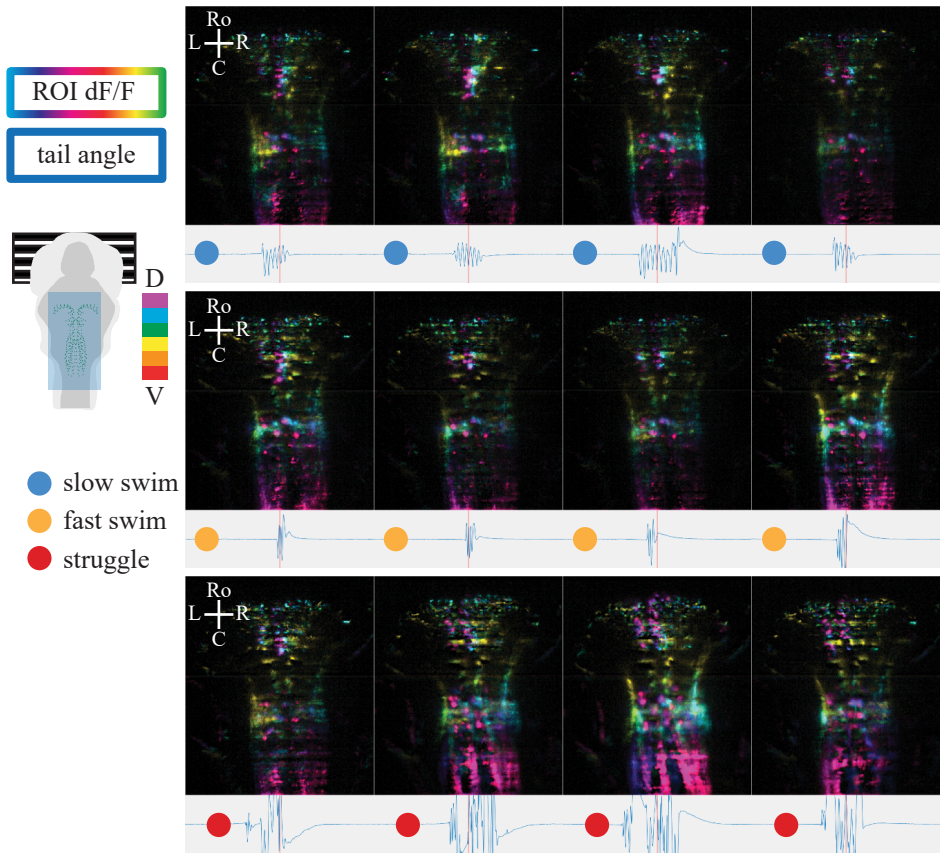

Figure 4.7: Neural activity maps across slow (top row), fast (middle row) and struggle (bottom row) swims in an exemplary *calca*^{ccu75Et} fish. Colours in brain maps indicate depth of ROI. Blue trace, tail angle; red line, timepoint of imaging frame, D, dorsal; V, ventral.

during slow swims and lateral nMLF neurons during fast swims in adult zebrafish [30]. However, due to the dense neuropil and large blood vessels in the region, it was challenging to record from individual neurons in this transgenic line. Future work will focus on a more refined approach to proceed with analysis of this dataset.

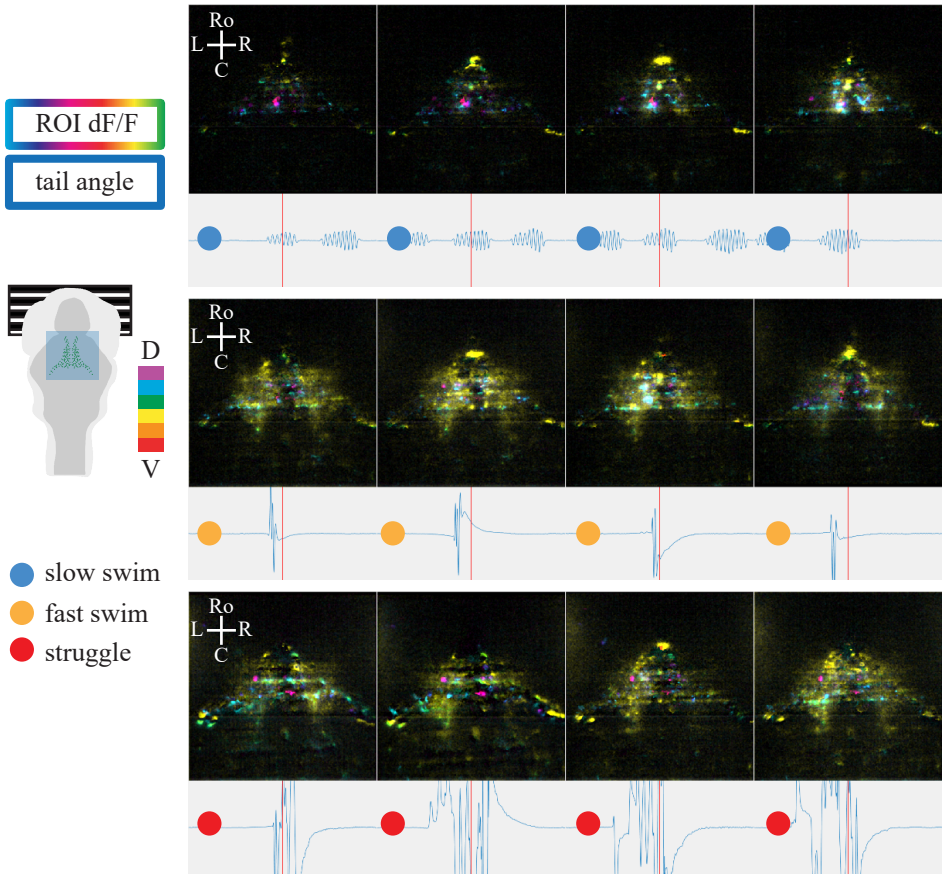

Figure 4.8: Neural activity maps across slow (top row), fast (middle row) and struggle swims (bottom row) in an exemplary *s1171tEt* fish. Colours in brain maps indicate depth of ROI. Blue trace, tail angle; red line, timepoint of imaging frame, D, dorsal; V, ventral.

4.3.5 Modulation of RSN activity in forward swims

Due to its sparse labelling, the *nefma* line lends itself perfectly to distinguish individual RSNs based on their stereotyped, uniquely identifiable location across animals. To extract the activity of single RSNs, the change in fluorescence compared to baseline (**dF/F**) of several regions-of-interest (**ROIs**) was averaged. This was done because ROIs were extracted by plane-wise segmentation but due to the dense sampling of the light-sheet, cells could span multiple planes.

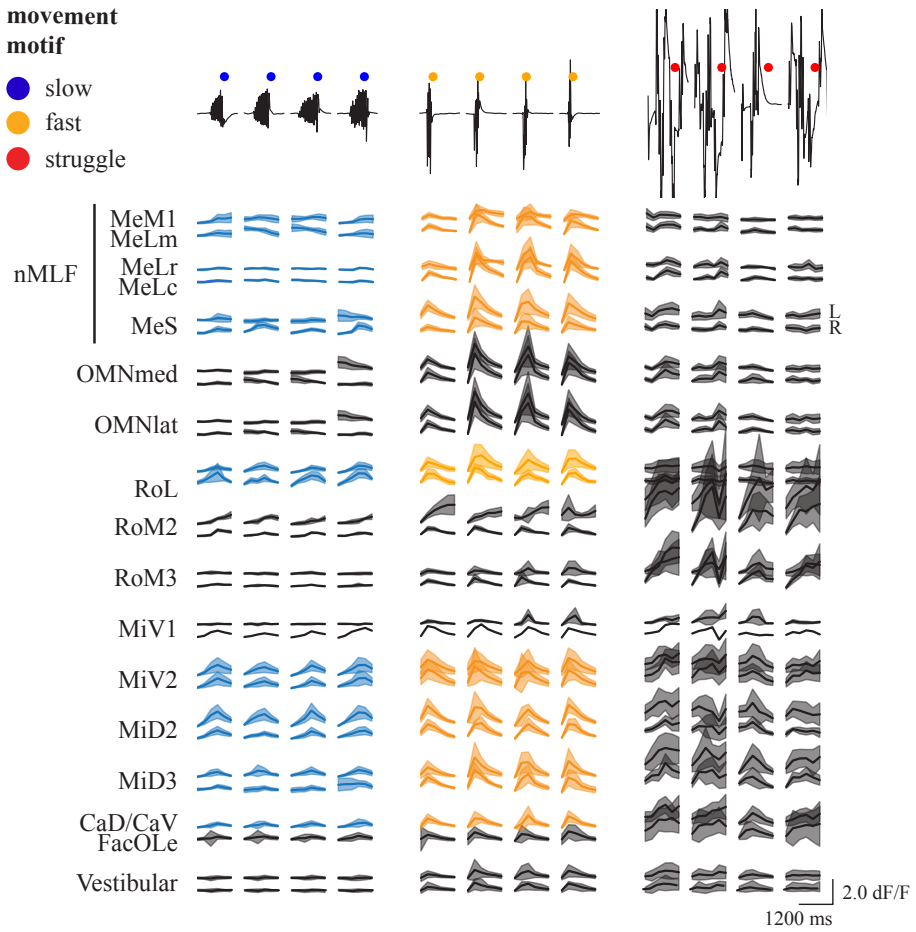

Figure 4.9: Responses in named RSNs across bout types in an exemplary *nefma* fish. Top shows tail angle trace in black, with dots representing bout type. Bottom shows dF/F responses of averaged ROIs in named RSNs for individual bouts. Top of each RSN group is left, bottom is right. Selected group coloured for emphasis. nMLF, nucleus of the medial longitudinal fasciculus; MeS, mesencephalic small cells in the nMLF; OMNmed and OMNlat, medial and lateral oculomotor nucleus; FacOLe, facial nucleus and octavolateralis efferent nucleus. Shaded area indicates the standard deviation.

Considering the change in fluorescence compared to baseline of ROIs across individual bouts revealed consistent bout-type specific responses in selected RSNs across individual swims (Figure 4.9). Bouts were labelled by their active movement motif, obtained from the Megabouts sparse code, and for subsequent analysis only bouts consisting of one dominant movement motif were considered. As alluded to in the depth-colour-coded map of an example *nefma* fish (Figure 4.6), there was

an increase in excitation in several identified RSNs when comparing slow to fast bouts. In particular, calcium activity in the nMLF, medial and lateral oculomotor nucleus (**OMN**), RoL and to a degree in the MiV1 and CaD/CaV cells increased from slow to fast bouts. The MiV2, MiD2 and MiD3 cells were active for both swim types. The MiD2 and MiD3 can be further subdivided into ipsilaterally-, medial contralaterally- and lateral contralaterally-projecting cells [9]. However, they are situated in close proximity and it was not possible to follow the projections to verify their individual identity, therefore I did not subdivide by projection pattern in my analysis. Many RSNs were active during struggles, however, due to the large non-rigid motion artefacts present during struggles that could not be corrected by rigid registration, it is not instructive to consider single cell responses during those movements.

The nMLF is a collection of reticulospinal cells in the tegmentum that extends dendrites towards tectal and pre-tectal areas and descends down the medial longitudinal fasciculus to the spinal cord [9, 20, 50]. It consists of four large identified cells (MeM1, MeLm, MeLr, MeLc) and smaller mesencephalic cells (**MeS**), all of which have glutamatergic (*vglut2*) neurotransmitter expression [28, 40]. Previous studies had reported a modulation of the individual large nMLF cells with changes in tail-beat frequency [27]. This was also observed here, where there was strong activation of all four cells during burst swims (Figure 4.9).

RS cells were active for the entire duration each bout, however, bout duration did not dictate scaling of activity. For instance, the slow swims illustrated below were of longer bout duration than the fast swims, and yet RS activity was much higher during fast swims compared to slow swims.

To illustrate the variability within cell groups, the activity of individual ROIs (3 from left side, 2 from right side) for relevant cell groups (nMLF, OMN, RoL, MiV2, MiD2, MiD3) were plotted for different bout types (Figure 4.10). There were slight differences between ROIs within bouts, which could be due to noise, small movement artifacts or the fact that imaging planes were acquired in sequence and thus slightly shifted in time ($\sim$12 ms). Overall, responses across ROIs within a cell group followed a similar pattern of activation.

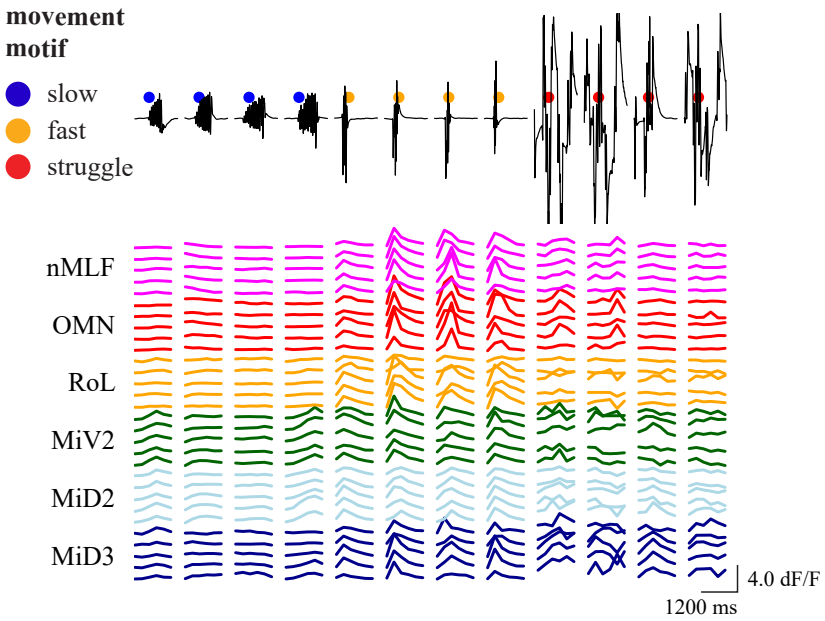

Figure 4.10: Single ROI responses in selected RSNs across bout types in an exemplary *nefma* fish. Top shows tail angle trace in black, with dots representing bout type. Bottom shows dF/F responses of individual ROIs in selected RSNs.

To compare across multiple fish, the bout-triggered dF/F response for each RSN was computed for an average of all bouts within a bout type for each fish (Figure 4.11). Only bouts consisting of one dominant movement motif were considered. A window of 1200 ms (6 volumes in total; 2 before bout onset and 4 after bout onset) was chosen to encompass the decay kinetics of the calcium reporter, as such the duration of individual bouts was ignored. Small differences in amplitude existed between fish, but as whole a similar profile of increases in excitation from slow to fast swims could be observed in the nMLF, OMN, RoL, MiD3 and CaD/CaV as well as consistent activity in the MiV2 for both slow and fast swims.

4.3.6 Switches in movement pattern within bouts reveal a ramping up of activity within rostral RSNs

As shown in Chapter 2 (Figure 2.12), head-fixed fish exhibit intra-bout modulation of tail-beat frequency. Utilising the *Megabouts* suite [34] reveals a transition in active movement motifs even within bouts. While changes in movement motifs

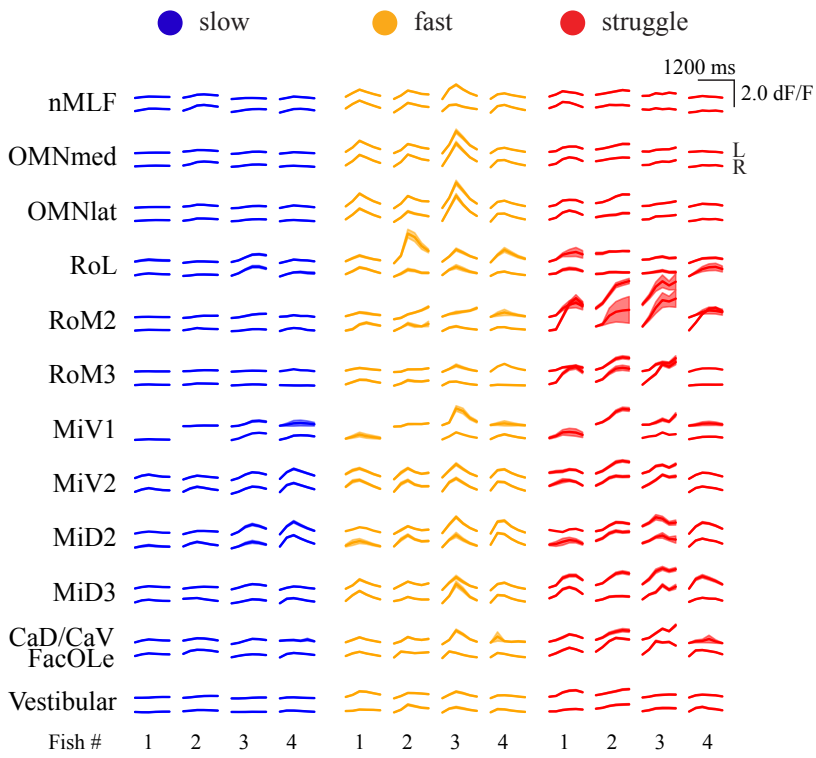

Figure 4.11: Bout averages across selected RSNs for four *nefma* fish. Each column is the bout-triggered average dF/F response for a given bout type for one of four example fish. Shaded area indicates the standard error of the mean.

does not occur in freely-swimming conditions [33, 34], this specific case can be leveraged to investigate changes in neural activity during gait transitions. Focusing on the switch from slow to fast swims in an example *nefma* fish (7 dpf) reveals a ramping up of activity in the nMLF, OMN and RoL, with peak activity coinciding with onset of the fast movement motif. Activity in the MiV2, MiD2 and MiD3 cells starts with the slow motif onset, equivalent to bout onset.

4.3.7 Ventromedial, but also Mauthner homologues, are active during turns

So far, my findings indicate a bilateral increase in excitation in select cell groups from slow to fast bouts, with a recruitment of most RSNs during struggles. To demonstrate that activity was specific to forward swims and struggles but not all

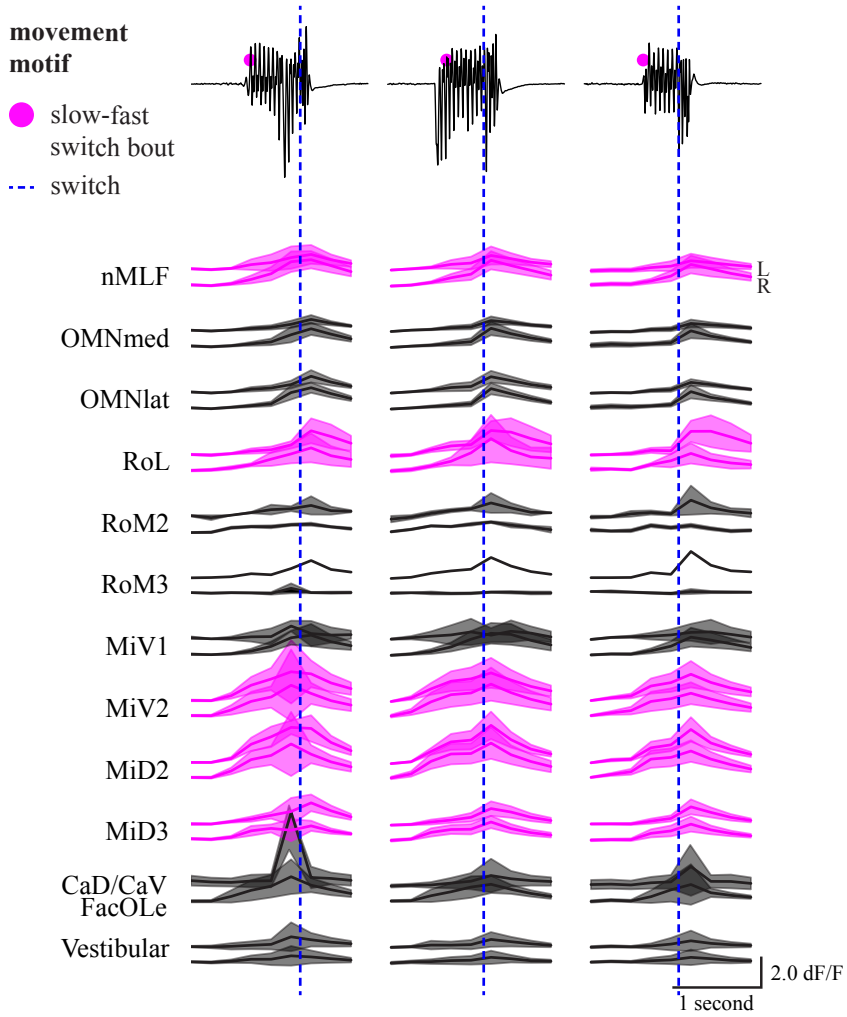

Figure 4.12: Activity of rostral RSNs ramps up with changes from slow to fast swimming. Each column is the bout-triggered average dF/F response for a given swim characterised by a slow to fast movement motif switch. Dotted blue line indicates switch in movement motif as identified by convolutional sparse coding. Selected group coloured for emphasis. Shaded area indicates the standard deviation.

movements, bout-triggered dF/F responses of RS cells were computed for turns.

In support of previous studies [24, 25], ventromedial cells (MiV1, MiV2) were active unilaterally depending on turn direction (Figure 4.13). Ventromedial cells on the left side of the brain (top row) were active during left turns, and vice versa. I also observed unilateral activity in the MiD3 cells, which had not been

previously reported. In addition, the MiD2 cells on the left side of the brain were active during turns in either direction. Activation of the Mauthner homologues (MiD2, MiD3) during turns elicited by the OMR has not been reported previously. There was also a slight increase in activity in cells in the OMN, which controls eye movements and is responsible for gaze stabilisation during swimming [51].

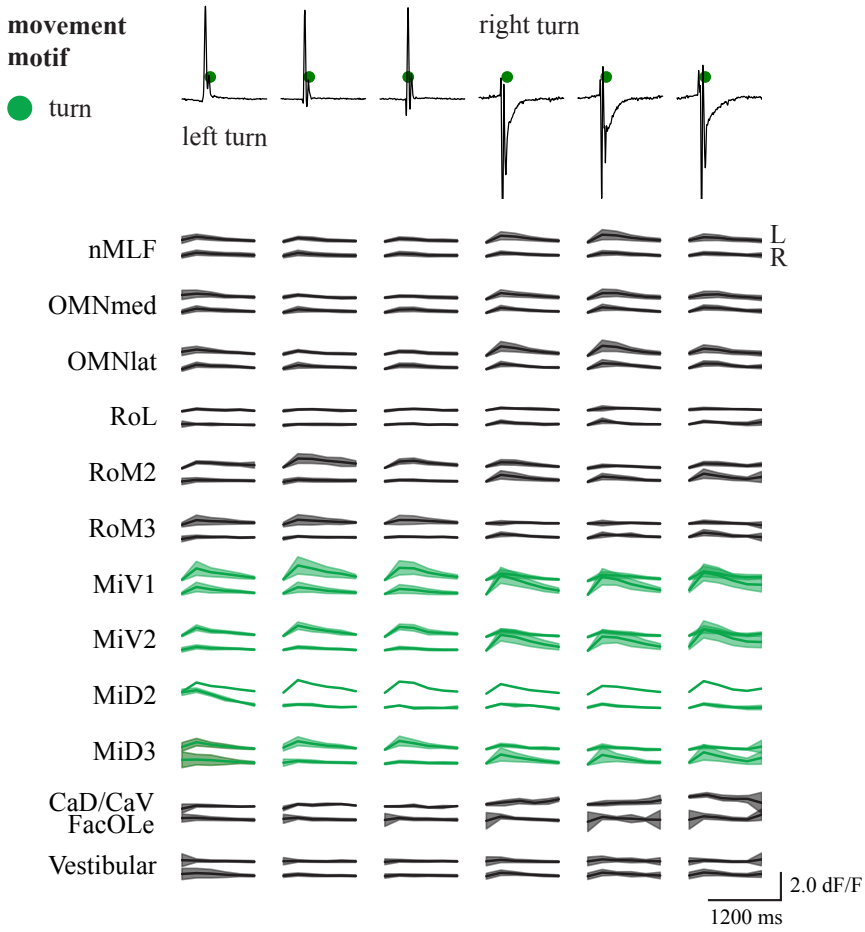

Figure 4.13: Activity in RSNs during turns in an exemplary *nefma* fish. Top shows tail angle trace in black, with dots representing bout type. Bottom shows dF/F responses of averaged ROIs in identified RSNs for individual turns. Top of each RSN group is left, bottom is right. Selected group coloured for emphasis. nMLF, nucleus of the medial longitudinal fasciculus; OMNmed and OMNlat, medial and lateral oculomotor nucleus; FacOLe, facial nucleus and octavolateralis efferent nucleus. Shaded area indicates the standard deviation.

4.3.8 Preliminary summary of RSNs associated with different bout types

In summary, a careful examination of the different reticulospinal neurons in an optomotor assay in head-fixed fish has revealed modulation of reticulospinal activity to produce different types of forward swimming. MiV2 cells were consistently active during both slow and fast swims, whereas cells in the nMLF, the RoL, MiD2 and MiD3, CaD/CaV were active during slow swims but dramatically increased in excitation during fast swims. During struggles, most named RSNs were active, though the non-rigid motion artifacts made it challenging to assess single neuron responses. During turns, ventromedial cells (MiV1, MiV2) and MiD2 and Mid3 were active, corroborating previous studies [24, 25].

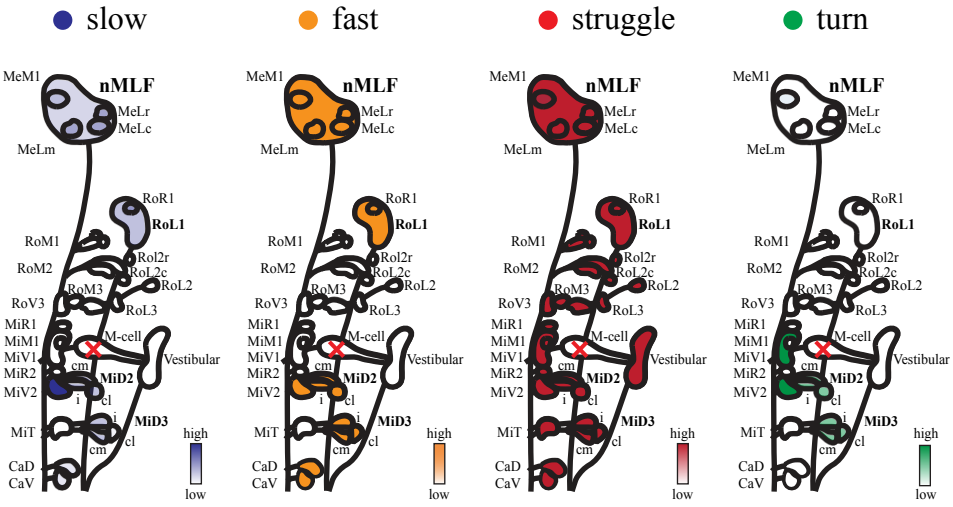

Figure 4.14: Preliminary summary schematic of RSNs associated with different bout types in the *nefma* line. Shading indicates level of activity. The Mauthner cell is crossed out as it degenerates in the *nefma* line after 3 dpf.

4.4 Discussion

In this chapter, I aimed to identify the neural correlates of different types of forward swims in the brainstem and their mechanism of transition. It has been a long-standing question in the field of locomotor control whether different behaviours are

driven by distinct or overlapping neural circuits [1], with experimental evidence having been put forward for both possibilities. Visually driven selection of swim bouts is thought to be mediated by brainstem reticulospinal neurons, which provide the predominant excitatory connection between the brain and spinal cord. Within the reticulospinal system, it is likely that spatially distributed populations of neurons work together to produce finely tuned behaviours [16]. Owing to their diverse behavioural repertoire and optical accessibility in early development, larval zebrafish are ideally suited to study mechanisms of supra-spinal control.

Here, I first set out by confirming that head-fixed larval zebrafish performed the forward optomotor response under imaging conditions. Behaviour was more variable compared to fish in a head-embedded, no microscope conditions. Several potential explanations for this difference in behaviour exist. First, as aforementioned, the eyes of the fish were masked to block visible light from the excitation laser. However, it has previously been shown that deep brain photoreceptors near the pre-optic area, as well as light-sensitive cells in the hindbrain, respond to light and can influence behaviour, even in the absence of eyes and pineal [52, 53]. Second, the head-restrained assay described in Chapter 2 offered visual stimulation from below as well as from around the fish, whereas the preparation in the light-sheet microscope only projected moving gratings from below the fish due to space constraints. Third, different illumination and tracking algorithms were employed between the two setups, which led to slightly noisier tracking under microscope. While it was possible to remedy this by carefully adjusted smoothing functions in post-hoc analysis, it is possible that this affected the closed-loop feedback that the fish received. Finally, there could be an effect of wild-type vs transgenic fish, as it has been previously reported that behaviour can vary based on the genetic background [54]. To address this, appropriate control experiments should be performed, for instance by testing the transgenic fish in the HR-only set up. Nonetheless, head-fixed fish still performed slow, fast, mixed and struggle swims in response to moving gratings under imaging conditions. Ultimately, the focus of this Chapter was not to characterise OMR behaviour under imaging conditions *per se*, but to focus on identifying the neural correlates of different swims independent

of the stimulus that elicited them.

Several studies have linked various RSNs to forward swimming, with prime candidates being the nMLF in the tegmentum [27, 28, 30] and caudal V2a glutamatergic RSNs in the hindbrain [26, 29, 31]. While it is likely that the command neurons for forward swimming are distributed across the reticulospinal system, I posed the question whether there would be distinct sets of RSNs for slow and fast swims, or whether the same neurons could modify their activity to produce different locomotor patterns.

Here, I provide evidence supporting the latter. Several RSNs were active during forward swims: the four large (MeM1, MeLm, MeLr, MeLc) and mesencephalic small (MeS) cells in the nMLF, the RoL, MiV2, MiD2, MiD3 and CaD/CaV with all but the MiV2 increasing in excitation from slow to fast swims. From a functional perspective, this matches results seen in previous studies. Severi *et al.* had reported an increase in excitation in nMLF cells as a function of tail-beat frequency and duration rather than a recruitment of additional cells [27]. Orger *et al.* had reported activity in the RoL and MiV2 cells during optomotor gratings that are expected to elicit slow swims [24]. It was thus particularly interesting to observe a similar increase in activity in the RoL cells in fast swims compared to slow swims, as seen in the nMLF. Surprisingly, activity in the MiV2 cells was consistent across different modes of forward swimming.

A modulation of activity with increases in swimming speed instead of recruitment of additional cells contrasts with findings reported by Berg *et al.* in adult zebrafish, where medial nMLF neurons were active during slow and fast swims, but lateral nMLF were only recruited with sudden increases in swimming speed [30]. It is difficult to directly compare the larval and adult nMLF, so it is possible that these lateral nMLF neurons were not labelled under the *nefma* promoter in the larvae. Alternatively, it is possible that their function changes across development. To shed light on this, I had planned to investigate cells in and surrounding the nMLF in more detail using the transgenic *s1171tEt* line. Unfortunately, while the depth-colour-coded maps did indicate a medial to lateral increase in activity from slow to fast swims, I was unable to confirm this in single cell responses. A

different approach to denoising the cell traces in these data is needed to further investigate recruitment patterns during different modes of forward swimming in the tegmentum.

I also observed calcium activity in the Mauthner homologues MiD2 and MiD3 during fast swims. This had not been reported before, instead, the Mauthner homologues have been associated with escape swims. Specifically, stimuli to the head following ablation of the Mauthner cell drive Mauthner homologue-mediated escape responses [55], demonstrating sufficiency. In light of the activity in the Mauthner homologues during fast forward swimming observed here, poses the question whether the Mauthner homologues are truly sufficient to elicit escapes or whether their activity and participation in driving different swims is stimulus-dependent. Closely related to escapes, I also observed a general recruitment and strong activation of the entire reticulospinal population during struggles, matching reports from [32]. This was also evident in the *calca*^{ccu75Et} line, where many cells across the brainstem were active during struggles, particularly in the lateral medulla. This corroborates findings from Carbo-Tano and Lapoix *et al.*, who also observed activity in lateral medullary RSNs in the *vsx2* line during struggles in response to MLR stimulation [31]. Glutamatergic V2a-neurons in the brainstem labelled by *vsx2* are also active during spontaneous and MLR activation-evoked slow forward swimming [26, 31]. Next steps in analysing the *calca*^{ccu75Et} dataset will include regression-based analysis to identify whether different distributed V2a-populations can be associated with slow and fast swims.

To unify these observations, I lean on a concept recently postulated in *D. melanogaster* by Braun et al. [56]. They reported that command-descending neurons recruit additional descending neurons to drive complex and adaptable behaviours, whereas command neuron activation alone drives stereotyped movements. It would be interesting to test this framework by investigating the temporal pattern of recruitment following bout onset of different RSNs associated with forward swimming.

Ablating different RSNs involved in forward swims would help establish a causal link. For instance, one could hypothesise that due to their consistent activity with

both slow and fast swims, that MiV2 are the command cells responsible for driving forward swims and that ablating them would impair forward swimming. However, this was not the case [24, 25]. Instead, ablation of all four large nMLF cells impaired fast swimming [27]. Yet, considering no projections from the MLR to the nMLF exist [31] and the increasingly observed association of the nMLF in postural control [28, 57, 58], it is possible that forward swims were affected by nMLF ablation due to loss of postural control. As a result, it is unlikely that the nMLF neurons are the true command neurons for forward swimming. Could the RoL serve this role instead? To my knowledge, the RoL have not been ablated in relation to forward swimming, since this is the first study reporting their increased activation during fast swims. Concurrently, considering the scaling of activity it would be interesting to modulate RoL (and other RSN) activity using optogenetics to evaluate the effect on forward swimming vigour. Ideally, this would be done in a preparation combining holographic optogenetics with functional imaging and behavioural readout as demonstrated by [59]. Together, ablation and modulation of the RoL provide an ideal entry point for future experiments on identifying the command cells for forward swimming.

4.5 Acknowledgements

E.M.D. Collins designed and performed all experiments and analysis discussed in this chapter. S. Lackner performed cloning and A.R. Tomas performed injection, screening and stable line establishment for Tg[-5.0calca: Gal4FF^{ccu75Et}, 10xUAS:GCaMP6fEF05]. A.L. Martins built the hybrid light-sheet microscope. A. Laborde and A.L. Martins wrote the SARDINE software suite and OpenGL Shader software to acquire experiments on the microscope (Martins, Laborde and Orger, in prep.). E.M.D. Collins, A. Ostrovsky, A.L. Martins and A. Laborde established a modular microscope imaging data post-processing toolbox to share within the lab. E.M.D. Collins wrote the chapter with helpful input from A.L. Martins for the technical microscopy section and M.B. Orger and A. Ostrovsky for the entire chapter. Finally, I would like to thank the Giudicelli lab for sharing Tg[nefma:KalTa4] embryos.

4.6 References

1. Siegel, J. M. Behavioral functions of the reticular formation. *Brain Research Reviews* **1,** 69–105. doi:10.1016/0165-0173(79)90017-1 (1979).
2. Orger, M. B. The Cellular Organization of Zebrafish Visuomotor Circuits. *Current Biology* **26,** R377–R385. doi:10.1016/j.cub.2016.03.054 (2016).
3. Randlett, O. *et al.* Whole-brain activity mapping onto a zebrafish brain atlas. *Nature Methods* **12,** 1039–1046. doi:10.1038/nmeth.3581 (2015).
4. Stephenson-Jones, M., Samuelsson, E., Ericsson, J., Robertson, B. & Grillner, S. Evolutionary Conservation of the Basal Ganglia as a Common Vertebrate Mechanism for Action Selection. *Current Biology* **21,** 1081–1091. doi:10.1016/j.cub.2011.05.001 (2011).
5. Sirota, M. G., Di Prisco, G. V. & Dubuc, R. Stimulation of the mesencephalic locomotor region elicits controlled swimming in semi-intact lampreys: Brainstem-induced swimming. *European Journal of Neuroscience* **12,** 4081–4092. doi:10.1046/j.1460-9568.2000.00301.x (2000).
6. Dubuc, R. *et al.* Initiation of locomotion in lampreys. *Brain Research Reviews* **57,** 172–182. doi:10.1016/j.brainresrev.2007.07.016 (2008).
7. El Manira, A., Pombal, M. & Grillner, S. Diencephalic projection to reticulospinal neurons involved in the initiation of locomotion in adult lampreysLampetra fluviatilis. *The Journal of Comparative Neurology* **389,** 603–616. doi:10.1002/(SICI)1096-9861(19971229)389:4<603::AID-CNE5>3.0.CO;2-4 (1997).
8. Brownstone, R. M. & Chopek, J. W. Reticulospinal Systems for Tuning Motor Commands. *Frontiers in Neural Circuits* **12,** 30. doi:10.3389/fncir.2018.00030 (2018).
9. Kimmel, C. B., Powell, S. L. & Metcalfe, W. K. Brain neurons which project to the spinal cord in young larvae of the zebrafish. *Journal of Comparative Neurology* **205,** 112–127. doi:10.1002/cne.902050203 (1982).
10. Grillner, S. & Zangger, P. On the central generation of locomotion in the low spinal cat. *Experimental Brain Research* **34.** doi:10.1007/BF00235671 (1979).
11. Grillner, S. & Kozlov, A. The CPGs for Limbed Locomotion–Facts and Fiction. *International Journal of Molecular Sciences* **22,** 5882. doi:10.3390/ijms22115882 (2021).
12. Ampatzis, K., Song, J., Ausborn, J. & El Manira, A. Pattern of Innervation and Recruitment of Different Classes of Motoneurons in Adult Zebrafish. *Journal of Neuroscience* **33,** 10875–10886. doi:10.1523/JNEUROSCI.0896-13.2013 (2013).
13. Ampatzis, K., Song, J., Ausborn, J. & El Manira, A. Separate Microcircuit Modules of Distinct V2a Interneurons and Motoneurons Control the Speed of Locomotion. *Neuron* **83,** 934–943. doi:10.1016/j.neuron.2014.07.018 (2014).

14. Ausborn, J., Snyder, A. C., Shevtsova, N. A., Rybak, I. A. & Rubin, J. E. State-dependent rhythmogenesis and frequency control in a half-center locomotor CPG. *Journal of Neurophysiology* **119,** 96–117. doi:10.1152/jn.00550.2017 (2018).

15. Ausborn, J., Shevtsova, N. A., Caggiano, V., Danner, S. M. & Rybak, I. A. Computational modeling of brainstem circuits controlling locomotor frequency and gait. *eLife* **8,** e43587. doi:10.7554/eLife.43587 (2019).

16. Dunn, T. W. *et al.* Brain-wide mapping of neural activity controlling zebrafish exploratory locomotion. *eLife* **5.** doi:10.7554/eLife.12741 (2016).

17. Ahrens, M. B., Orger, M. B., Robson, D. N., Li, J. M. & Keller, P. J. Whole-brain functional imaging at cellular resolution using light-sheet microscopy. *Nature Methods* **10,** 413–420. doi:10.1038/nmeth.2434 (2013).

18. O'Malley, D. M., Kao, Y.-H. & Fetcho, J. R. Imaging the Functional Organization of Zebrafish Hindbrain Segments during Escape Behaviors. *Neuron* **17,** 1145–1155. doi:10.1016/S0896-6273(00)80246-9 (1996).

19. Eaton, R. C., Bombardieri, R. A. & Meyer, D. L. The mauthner-initiated startle response in teleost fish. *Journal of Experimental Biology* **66,** 65–81. doi:10.1242/jeb.66.1.65 (1977).

20. Gahtan, E. Visual Prey Capture in Larval Zebrafish Is Controlled by Identified Reticulospinal Neurons Downstream of the Tectum. *Journal of Neuroscience* **25,** 9294–9303. doi:10.1523/JNEUROSCI.2678-05.2005 (2005).

21. Koyama, M. *et al.* A circuit motif in the zebrafish hindbrain for a two alternative behavioral choice to turn left or right. *eLife* **5,** e16808. doi:10.7554/eLife.16808 (2016).

22. Hecker, A., Schulze, W., Oster, J., Richter, D. O. & Schuster, S. Removing a single neuron in a vertebrate brain forever abolishes an essential behavior. *Proceedings of the National Academy of Sciences* **117,** 3254–3260. doi:10.1073/pnas.1918578117 (2020).

23. Dunn, T. W. *et al.* Neural Circuits Underlying Visually Evoked Escapes in Larval Zebrafish. *Neuron* **89,** 613–628. doi:10.1016/j.neuron.2015.12.021 (2016).

24. Orger, M. B., Kampff, A. R., Severi, K. E., Bollmann, J. H. & Engert, F. Control of visually guided behavior by distinct populations of spinal projection neurons. *Nature Neuroscience* **11,** 327–333. doi:10.1038/nn2048 (2008).

25. Huang, K.-H., Ahrens, M. B., Dunn, T. W. & Engert, F. Spinal Projection Neurons Control Turning Behaviors in Zebrafish. *Current Biology* **23,** 1566–1573. doi:10.1016/j.cub.2013.06.044 (2013).

26. Kimura, Y. *et al.* Hindbrain V2a Neurons in the Excitation of Spinal Locomotor Circuits during Zebrafish Swimming. *Current Biology* **23,** 843–849. doi:10.1016/j.cub.2013.03.066 (2013).

27. Severi, K. E. *et al.* Neural Control and Modulation of Swimming Speed in the Larval Zebrafish. *Neuron* **83,** 692–707. doi:10.1016/j.neuron.2014.06.032 (2014).

28. Thiele, T. R., Donovan, J. C. & Baier, H. Descending Control of Swim Posture by a Midbrain Nucleus in Zebrafish. *Neuron* **83,** 679–691. doi:10.1016/j.neuron.2014.04.018 (2014).

29. Pujala, A. & Koyama, M. Chronology-based architecture of descending circuits that underlie the development of locomotor repertoire after birth. *eLife* **8,** e42135. doi:10.7554/eLife.42135 (2019).

30. Berg, E. M. *et al.* Brainstem circuits encoding start, speed, and duration of swimming in adult zebrafish. *Neuron* **111,** 372–386.e4. doi:10.1016/j.neuron.2022.10.034 (2023).

31. Carbo-Tano, M. *et al.* The mesencephalic locomotor region recruits V2a reticulospinal neurons to drive forward locomotion in larval zebrafish. *Nature Neuroscience.* doi:10.1038/s41593-023-01418-0 (2023).

32. Sankrithi, N. & O'Malley, D. Activation of a multisensory, multifunctional nucleus in the zebrafish midbrain during diverse locomotor behaviors. *Neuroscience* **166,** 970–993. doi:10.1016/j.neuroscience.2010.01.003 (2010).

33. Marques, J. C., Lackner, S., Félix, R. & Orger, M. B. Structure of the Zebrafish Locomotor Repertoire Revealed with Unsupervised Behavioral Clustering. *Current Biology* **28,** 181–195.e5. doi:10.1016/j.cub.2017.12.002 (2018).

34. Jouary, A. *et al. Megabouts: a flexible pipeline for zebrafish locomotion analysis* 2024. doi:10.1101/2024.09.14.613078.

35. Martins, S. *et al.* Toward an Integrated Zebrafish Health Management Program Supporting Cancer and Neuroscience Research. *Zebrafish* **13,** S–47–S–55. doi:10.1089/zeb.2015.1198 (S1 2016).

36. Van Opbergen, C. J. *et al.* Optogenetic sensors in the zebrafish heart: a novel in vivo electrophysiological tool to study cardiac arrhythmogenesis. *Theranostics* **8,** 4750–4764. doi:10.7150/thno.26108 (2018).

37. Félix, R. *et al.* Structural and functional organization of visual responses in the inferior olive of larval zebrafish. *The Journal of Neuroscience,* e2352212023. doi:10.1523/JNEUROSCI.2352-21.2023 (2024).

38. Eschstruth, A., Schneider-Maunoury, S. & Giudicelli, F. Creation of zebrafish knock-in reporter lines in the *nefma* gene by Cas9-mediated homologous recombination. *genesis* **58.** doi:10.1002/dvg.23340 (2020).

39. Scott, E. K. & Baier, H. The cellular architecture of the larval zebrafish tectum, as revealed by gal4 enhancer trap lines. *Frontiers in Neural Circuits* **3,** 13. doi:10.3389/neuro.04.013.2009 (2009).

40. Collins, E. M. *et al. Characterisation of transgenic lines labelling reticulospinal neurons in larval zebrafish* 2024. doi:10.1101/2024.12.20.629714.

41. Kwan, K. M. *et al.* The Tol2kit: A multisite gateway-based construction kit for *Tol2* transposon transgenesis constructs. *Developmental Dynamics* **236,** 3088–3099. doi:10.1002/dvdy.21343 (2007).

42. Kawakami, K., Shima, A. & Kawakami, N. Identification of a functional transposase of the *Tol2* element, an *Ac* -like element from the Japanese medaka fish, and its transposition in the zebrafish germ lineage. *Proceedings of the National Academy of Sciences* **97,** 11403–11408. doi:10.1073/pnas.97.21.11403 (2000).

43. Bergen, J. R., Anandan, P., Hanna, K. J. & Hingorani, R. in *Computer Vision — ECCV'92* (ed Sandini, G.) red. by Goos, G. & Hartmanis, J. Series Title: Lecture Notes in Computer Science, 237–252 (Springer Berlin Heidelberg, Berlin, Heidelberg, 1992). doi:10.1007/3-540-55426-2_27.

44. Pachitariu, M. *et al. Suite2p: beyond 10,000 neurons with standard two-photon microscopy* preprint (Neuroscience, 2016). doi:10.1101/061507.

45. Bar-Joseph, Z., Gifford, D. K. & Jaakkola, T. S. Fast optimal leaf ordering for hierarchical clustering. *Bioinformatics* **17,** S22–S29. doi:10.1093/bioinformatics/17.suppl_1.S22 (suppl_1 2001).

46. Vladimirov, N. *et al.* Light-sheet functional imaging in fictively behaving zebrafish. *Nature Methods* **11,** 883–884. doi:10.1038/nmeth.3040 (2014).

47. Kimura, Y., Okamura, Y. & Higashijima, S.-i. *alx* , a Zebrafish Homolog of *Chx10* , Marks Ipsilateral Descending Excitatory Interneurons That Participate in the Regulation of Spinal Locomotor Circuits. *The Journal of Neuroscience* **26,** 5684–5697. doi:10.1523/JNEUROSCI.4993-05.2006 (2006).

48. Fetcho, J. R. Spinal Network of the Mauthner Cell (Part 2 of 2). *Brain, Behavior and Evolution* **37,** 307–316. doi:10.1159/000316094 (1991).

49. Liu, Z. *et al.* Central Vestibular Tuning Arises from Patterned Convergence of Otolith Afferents. *Neuron* **108,** 748–762.e4. doi:10.1016/j.neuron.2020.08.019 (2020).

50. Semmelhack, J. L. *et al.* A dedicated visual pathway for prey detection in larval zebrafish. *eLife* **3,** e04878. doi:10.7554/eLife.04878 (2014).

51. Dowell, C. K., Lau, J. Y., Antinucci, P. & Bianco, I. H. Kinematically distinct saccades are used in a context-dependent manner by larval zebrafish. *Current Biology* **34,** 4382–4396.e5. doi:10.1016/j.cub.2024.08.008 (2024).

52. Fernandes, A. M. *et al.* Deep brain photoreceptors control light-seeking behavior in zebrafish larvae. *Current biology: CB* **22,** 2042–2047. doi:10.1016/j.cub.2012.08.016 (2012).

53. Kokel, D. *et al.* Identification of nonvisual photomotor response cells in the vertebrate hindbrain. *The Journal of Neuroscience: The Official Journal of the Society for Neuroscience* **33,** 3834–3843. doi:10.1523/JNEUROSCI.3689-12.2013 (2013).

54. Audira, G., Siregar, P., Strungaru, S.-A., Huang, J.-C. & Hsiao, C.-D. Which Zebrafish Strains Are More Suitable to Perform Behavioral Studies? A Comprehensive Comparison by Phenomic Approach. *Biology* **9,** 200. doi:10.3390/biology9080200 (2020).

55. Liu, K. S. & Fetcho, J. R. Laser Ablations Reveal Functional Relationships of Segmental Hindbrain Neurons in Zebrafish. *Neuron* **23,** 325–335. doi:10.1016/S0896-6273(00)80783-7 (1999).

56. Braun, J., Hurtak, F., Wang-Chen, S. & Ramdya, P. Descending networks transform command signals into population motor control. *Nature* **630,** 686–694. doi:10.1038/s41586-024-07523-9 (2024).

57. Sugioka, T., Tanimoto, M. & Higashijima, S.-i. Biomechanics and neural circuits for vestibular-induced fine postural control in larval zebrafish. *Nature Communications* **14,** 1217. doi:10.1038/s41467-023-36682-y (2023).

58. Zhu, Y. *et al. A brainstem circuit for gravity-guided vertical navigation* 2024. doi:10.1101/2024.03.12.584680.

59. Dal Maschio, M., Donovan, J. C., Helmbrecht, T. O. & Baier, H. Linking Neurons to Network Function and Behavior by Two-Photon Holographic Optogenetics and Volumetric Imaging. *Neuron* **94,** 774–789.e5. doi:10.1016/j.neuron.2017.04.034 (2017).

Chapter 5

General Discussion

5.1 Brief summary of the main findings

The overarching goal of this project was to investigate the neural control of gait switching in larval zebrafish. Specifically, I set out to identify the neural correlates of slow and fast bouts and elucidate the population dynamics underlying bout transitions during the optomotor response (**OMR**).

Gait switching behaviour during the optomotor response in larval zebrafish In this chapter, I characterised different types of forward swims in response to forward optomotor gratings in both a freely-swimming and a head-restrained assay. Slow gratings predominantly elicited slow swims: in freely-swimming conditions these could be classified as Slow1 and Slow2 swims using unsupervised clustering [1], in head-restrained conditions Slow2-like swims are characterised by low tail-beat frequency and low rostral tail-bend amplitude. Fast gratings elicited a transition from Slow1 to Slow2 to burst swims (**BS**) in freely-swimming conditions. Head-restrained fish performed a mixture of slow and fast swims, often within the same bout, during fast gratings. Additionally, head-fixed fish performed a small number of struggles, characterised by unusually large tail-bend amplitudes. These observations corroborate previous findings in freely-swimming OMR assays [1, 2]. The addition of a closed-loop feedback system to the head-restrained assay resulted in fish performing burst-like swims, which had not been reported previously. However, swims sometimes included switches in tail-beat frequency within the bout. This led me to develop a bout decomposition method based on half-beats labelled by their different kinematics, as well as a collaboration to establish a novel bout decomposition method based on convolutional sparse coding to characterise movement motifs in head-fixed fish. Together, the application of novel bout decomposition and classification algorithms revealed generalised, conserved mechanisms of gait transitions in larval zebrafish.

Characterisation of transgenic lines labelling reticulospinal neurons This project was instrumental in characterising and selecting appropriate transgenic lines that label different subsets of reticulospinal neurons (**RSNs**). I gave a

detailed account of the degree of RSN labelling in seven transgenic lines with glutamatergic (*vglut2*) expression in the brain stem of larval zebrafish, offering projection-specific genetic access to subpopulations of RSNs. I showcased transgenic lines that label most or all RSNs (*nefma, adcyap1b*^{ccu96Et}) or subsets of RSNs, including ipsilateral (*vsx2, calca*^{ccu75Et}), contralateral (*pcp4a*^{ccu97Tg}) or all (*tiam2a*^{y264Et}) components of the Mauthner array, or midbrain-only RSNs (*s1171tEt*). In addition to RSNs, selected transgenic lines *(nefma, s1171tEt, calca*^{ccu75Et}*)* labelled other potential neurons of interest in the brainstem. For those, I performed *in situ* hybridisation to show expression patterns of several excitatory and inhibitory neurotransmitters at larval stages as well as glutamatergic expression patterns in juvenile fish. This resource provides a useful basis for future research, including the possibility to combine these transgenic lines with genetically encoded calcium reporters and optogenetic tools, with the hope of uncovering fundamental principles in the descending control of locomotion.

Imaging neural population dynamics during gait switching behaviour in larval zebrafish The work in Chapter 4 laid a good foundation in deciphering the neural basis of different forward swims, taking into account previous hypotheses from the field and supporting seemingly contradictory results with a unifying hypothesis. To do so, I recorded the activity of genetically labelled populations of RSNs in the brainstem using light-sheet microscopy at single-cell resolution, combined with a head-restrained assay showing forward OMR gratings in closed-loop. Utilising the unique, sparse nature of the reticulospinal system, I showed that neuronal activity in a midbrain nucleus (**nMLF**) is higher during fast swims than slow swims in *nefma* fish, supporting the findings by [2]. I also observed a similar modulation of activity in rostral (RoL1) cells in slow vs fast swims. There was consistent activity of ventromedial (MiV2, MiD) cells with swims, corroborating evidence from [3] and [4], however, this activity did not scale with changes in bout type. Furthermore, I reported a general recruitment and strong activation of the entire reticulospinal population during struggles, matching reports from [5]. In accord with previous studies [3, 6], ventromedial cells were active during turns, some of which (MiV2) overlapped with forward swims. Taken together, I propose a

framework as seen in [7], where selected cells act as command neurons for distinct bout types and recruit additional RSNs for fine control of movements. To test this framework, I propose taking a closer look at the temporal recruitment patterns of potential command neurons vs other RSNs. This could be followed up by optogenetic activation and silencing of selected subpopulations of RSNs utilising the transgenic lines described in Chapter 3.

In summary, I hope to have provided a useful foundation of tools and frameworks to further dissect the supraspinal control of locomotion.

5.2 Future directions of this project

There are several interesting avenues that are yet to be explored within the pursuit of understanding the neural control of gait switching. I have structured this 'experimental wish list' as questions with the order of the chapters of this thesis in mind.

How naturalistic are moving gratings really? The use of moving stripes to represent a translation of the visual field has often been a subject of debate, particularly at Neuroethology meetings. Of course, moving stripes do not usually occur in the small pools, streams and rice paddies in Myanmar and India that zebrafish are native to [8]. These bodies of water are often cloudy with debris, meaning in the wild, zebrafish often rely on their other sensory modalities, such as the lateral line to sense vibrations and the olfactory system for chemical cues [9]. In fact, it has recently been shown that these sensory modalities can override visual cues in laboratory settings [10, 11]. In the optomotor response, moving gratings are intended to simulate changes in the visual field of the animal as a result of being carried downstream. Swimming upstream stabilises the visual field and the animal is back at its original position, which may be of significance if it is a particularly good feeding ground or sheltered from predators. When encountering a constant water current, fish swim against it, a process called positive rheotaxis that depends on the lateral line [12]. A recent study identified water current-responsive cells in the tectum [10]. It would be very interesting to see if the same

behavioural transitions observed in this project (Slow1 to Slow2 to BS) could be observed in freely-swimming zebrafish presented with currents at different speeds. Adapting this to a head-fixed assay would allow the investigation if bouts that are generated in response to a forward OMR are driven by the same brainstem circuits, and in a similar fashion, as the bouts exhibited during positive rheotaxis.

Do transgenic zebrafish behave differently to wildtypes? A limitation of the behavioural experiments presented in this study concern the lack of controls regarding transgenics. In the freely-swimming and head-restrained behaviour assays, fish from the wildtype Tübingen strain were used. Fish from this strain are naturally pigmented, which aids the tracking algorithm used in both set ups. They are unsuitable, however, for imaging studies as the pigmentation leads to light scattering [13]. For this reason, fish used for imaging experiments are either treated with 1-phenyl 2-thiourea (**PTU**) to remove pigmentation [14], or have a mutation in the *mitfa-/-* gene, which removes melanophores [15]. While the tracking algorithm used in the light-sheet microscopy set up can track the tail in transparent zebrafish, the tracking algorithm employed in the behavioural head-restrained set up, which features 3D visual stimulation, cannot. It should in theory be possible to adapt the experimental configuration and tracking algorithm in the behavioural set up, however, this was out with the scope of this project.

Could eye movements differ for slow and burst swims? The calcium imaging data of the cholinergic oculomotor nucleus from this project suggests differential activity between slow and fast forward swims. The oculomotor nucleus controls gaze by determining horizontal eye position [16–18]. Activity in the oculomotor cells ramps up until a saccade is executed [18]. On a behavioural level, eye convergence has to date been reported as a marker of the initiation of a hunting sequence [19]. Recent works from the Bianco lab have characterised different types of saccades and their neural correlates in the OMN [20, 21]. They reported that zebrafish use small conjugate saccades to compensate for body rotation. This maintains a stable visual perception of close objects during forward swimming [20]. The authors did not report the swimming speed or type of forward swim during

which these 'mini'-saccades occurred. However, it could be possible that due to the large changes in the visual field experienced during burst swims, that larger saccades occur during burst swims than the forward swims reported by Dowell *et al.* [20]. Alternatively, it is possible that the eyes need to be held steadily in position during burst swims due to the larger hydrodynamic forces encountered, which would explain the increased OMN activity. Tracking of the eyes is possible in our behavioural head-restrained assay, and in light of the changes in calcium activity in the oculomotor nucleus observed in slow vs fast swims, this would be an interesting avenue to explore further.

Could Megabouts-HR be expanded to other bout types? The freely-swimming dataset of the Megabouts pipeline includes ∼4 million bouts across a wide array of behavioural contexts and corresponding swim types [22]. This was possible in part due to the large dataset available from [1] and complemented with further experiments in a battery of visuomotor and acoustic assays. If a similar dataset across behavioural contexts existed for head-restrained assays, the dictionary could be relearned to include movement motifs that were not present in the current dataset specific to forward swimming. Due to the time constraints occurred with embedding thousands of fish, the sparser nature of their behaviour when head-fixed, and the difficulties in adapting certain assays to a head-fixed preparation (e.g. prey capture and social behaviour), this is not a trivial task. Once collected, however, this dataset could be used a reference point for refining the algorithm and comparing it to other methods.

Does a similar supraspinal circuit exist for pectoral fin control? Many adult fish species primarily swim by alternating their pectoral fins, with minimal contributions from axial movements. Other fish, including zebrafish, use a combination of axial and pectoral fin movements across a range of speeds [23]. The movements of larval zebrafish have been predominantly described in terms of their axial movements [24], with comparatively little focus on their pectoral fins. Seminal studies by Hale and colleagues showed that larval zebrafish synchronise their pectoral fin movements with axial undulations during slow swimming, matching

both phase and frequency [23, 25]. During fast swims, arrhythmic adductor activity leads to tucked fins against the body. Serial trans-sections revealed that for pectoral movements during slow swimming, a small region of the caudal hindbrain and rostral spinal cord near the motor neuron pool are sufficient to generate rhythmic alternating abductor and adductor motor neuron activity. To generate the adductor motor neuron activity necessary to elicit tucked fins during burst swims, the entire hindbrain was necessary - suggesting it is under the control of midbrain structures, such as the MLR [26]. More recently, it was revealed that axial trunk and pectoral fin motor neurons both receive inhibitory innervation from the same *dI6dmrt3a* neurons. The latter are commissural interneurons and their ablation impairs left-right alternation [27, 28]. Together, these studies suggest a similar organisation of supraspinal circuits involved in the drive of both axial and pectoral fin movements. Given the small size and optical accessibility of larval zebrafish, combined with recent developments in whole-brain imaging, it should be experimentally feasible to image both supraspinal circuits simultaneously while recording either axial or pectoral fin movement, or acquire fictive recordings of both.

How can novel imaging methods serve supraspinal studies? One aspect of zebrafish behaviour that requires consideration when choosing an imaging modality, is that swim bouts occur at extremely fast timescales. With bouts lasting around 200 ms, individual half-beats may only be several tens of milliseconds apart [1]. This poses a trade-off between using traditional methods that allow high-speed, detailed recordings of individual neurons, e.g. electrophysiology (can capture spike rates), versus recordings of populations of neurons or even entire brains at low speeds, e.g. 2-photon microscopy (can capture around 1-2 volumes per second) [29]. Recent advances in optical methods include light-sheet microscopy (traditionally 1-3 volumes per second, with modifications up to 5 volumes per second, cellular resolution) [30, 31], oblique plane light-sheet microscopy (e.g. SCAPE, up to 5 volumes per second or faster for smaller fields of view, near-cellular resolution) [32, 33], light-field microscopy (up to dozens or hundreds of volumes per second, cellular resolution) [34] and most recently tracking microscopes

for freely swimming fish (several volumes per second, near-cellular resolution) [35, 36] – in practice only limited by the camera frame rate and decay dynamics of the calcium reporter used. A new avenue has swapped out slow calcium indicators for voltage indicators [37–39], which combined with these ultra-fast microscopy techniques essentially enables whole-brain electrophysiology. All of these methods, and voltage imaging in particular, are highly sensitive to motion artefacts and benefit from or even require a fictive behaviour preparation. For the question of slow vs fast gait transitions specifically, recent advances in fictive recordings of swims of different tail-beat frequency [40] offer promising opportunities when combined with whole-brain voltage imaging.

Manipulations of brainstem circuits driving forward swimming Finally, while my work and other studies have demonstrated a link between the modulation of neuronal activity in different reticulospinal neurons and slow vs fast swims, it is essential to test these correlations. First, optogenetic stimulation of different RSNs should demonstrate sufficiency for some or all subpopulations of RSNs related to forward swimming revealed here. Had Hypothesis 1 of distinct populations of RSNs for slow vs fast swims been true, ablations of either cell group should impair the corresponding behaviour while leaving the other swim type intact. Systematic ablation of different combinations of RSNs involved in forward swimming would still be useful to determine whether a neuron/group of neurons is essential for either swim type (e.g. demonstrating command neuron features) or merely recruited in a complementary fashion. Severi *et al.* provide important insights for this framework, as ablation of all four large nMLF neurons led to deficits in achieving high swimming speeds, whereas ablation of RoM or Mauthner cells did not affect fast swimming [2]. These results are in line with the principle described in Braun *et al.* of command vs other descending RSNs in insects [7]. In this case, nMLF neurons were sufficient and necessary for eliciting fast swims, whereas RoM cells were involved but not necessary. It remains to be seen which RSNs are the command cells that drive slow swimming.

How could neuromodulators influence forward swimming? It has long been demonstrated that neuromodulators, and in particular dopamine, can affect locomotion [41–48]. While many of these studies focused on isolated spinal cord preparation, a seminal study by Jay *et al.* recently went straight to the source and managed to record from and manipulate supraspinal dopamine neurons. They showed that diencephalo-spinal neurons generate tonic spiking, associated with locomotor inactivity, and phasic bursting during locomotor activity. Targeted ablation of supraspinal dopaminergic neurons decreased locomotor output [44]. Interestingly, the phasic bursting did not correlated with duration of swim bouts, but supposedly increased excitability of the spinal networks instead. These findings are supported by Jha and Thirumalai, who showed that activation of D1-like receptors increased swimming speed during the OMR in freely-swimming fish by modulation tail bend amplitude. This modulation was achieved by increasing intrinsic excitability and excitatory synaptic drive in primary and secondary MNs, where normally only secondary MNs would be active [46]. Considering the tail kinematics reported would likely constitute variation within the cluster of slow swims, it would be interesting to repeat this experiment with a protocol that elicits burst swims. Would there be a linear scaling of more secondary motor neurons recruited (as expected without dopaminergic modulation), or would dopaminergic modulation change the spinal circuitry entirely?

Is gait switching driven by RSNs or further upstream? In Chapter 4, I illustrate that in swims where head-fixed fish switch from utilising a slow to a fast movement motif, the activity of various RSNs (nMLF, RoL) ramps up, peaking at the transition point between the two movement patterns. This is most likely not reflective of a 'switching signal', but rather simply the onset of the fast movement motif. 'Switching signals' have not been reported in the reticulospinal population before. In the MLR, however, an increase in electrical stimulation drives a switch from a walking to a swimming gait in salamander [49]. A recent study by Wyart and colleagues identified the MLR in zebrafish for the first time, demonstrating functional, anatomical and molecular characteristics consistent with MLRs identified in other vertebrates [4]. In the study, an increase in MLR stimulation evoked

V2a-RSNs mediated increases in swimming speed, however only within the slow swimming module. The authors explain that this is possibly due to a stimulation site restricted to a subpopulation of the MLR, and that future studies experimenting with a larger stimulation area could possibly elicit fast swimming [4].

It remains an open question in the field if there are differences in neural activity between MLR-evoked, visually induced and spontaneous swims and swim transitions. The nMLF has long been a considered an integration site of visual, vestibular and sensorimotor signals [50, 51]. Considering the surprising lack of projections from the MLR to the nMLF [4], there must be integration of MLR and nMLF commands in reticulospinal cells. As such, stimulation of the MLR (without visual or other sensory stimulation) would most likely lead to different RS population activity than that driving visually-evoked or spontaneous swims. Leveraging the small size of larval zebrafish, and now identified MLR, would make an excellent model system to combine different stimulation modalities and concurrently record whole-brain activity in behaving fish.

5.3 Future perspectives on the control of locomotion

This is a very exciting time in the field of locomotor control. The acquisition of whole-brain electron microscopy data sets from zebrafish larvae [52–54], paired with recent computational advances in automatic segmentation and tracing [53, 55–57], enable the dissection of entire neural circuits at the synaptic level. This has led to recent insights into the modular organisation and associated functional roles of the oculomotor nucleus [54, 57]. The authors were able to identify modules of strongly connected neurons in the hindbrain of larval zebrafish and use those to predict neural coding and dynamics from the wiring diagram. This revealed specialised behavioural functions in oculomotor control for different modules, and the findings were verified by calcium-imaging of of neural activity [57]. It remains to be seen whether this sort of approach can be applied to more complex networks such as the axial RSNs, where less is known about their functional roles. Nonethe-

less, it is exciting to see that connectome-based analysis can uncover organisational and functional principles in previously hidden anatomical structures.

5.4 Concluding remarks

This thesis discusses the behavioural and neural bases of forward swimming and gait transitions in larval zebrafish. Different types of forward swims were observed in response to moving gratings, in both freely-swimming and head-fixed assays. Leveraging the optical accessibility and amenability to genetic tools of larval zebrafish enabled high-speed, volumetric calcium recordings of neuronal activity within the reticulospinal system of behaving, head-fixed animals performing the optomotor response. RSNs associated with different types of forward swims could be identified, with an increase in excitation from slow to fast swims. Future studies will focus on manipulating the RSNs identified here to elicit different modes of swimming, and continue the search in areas upstream of the reticulospinal system to identify signal associated with transitions between movements. In conclusion, though many open questions remain, in light of recent technical advances, zebrafish continue to stand at the forefront of studying supraspinal circuitry and locomotor control.

5.5 References

1. Marques, J. C., Lackner, S., Félix, R. & Orger, M. B. Structure of the Zebrafish Locomotor Repertoire Revealed with Unsupervised Behavioral Clustering. *Current Biology* **28,** 181–195.e5. doi:10.1016/j.cub.2017.12.002 (2018).
2. Severi, K. E. *et al.* Neural Control and Modulation of Swimming Speed in the Larval Zebrafish. *Neuron* **83,** 692–707. doi:10.1016/j.neuron.2014.06.032 (2014).
3. Orger, M. B., Kampff, A. R., Severi, K. E., Bollmann, J. H. & Engert, F. Control of visually guided behavior by distinct populations of spinal projection neurons. *Nature Neuroscience* **11,** 327–333. doi:10.1038/nn2048 (2008).
4. Carbo-Tano, M. *et al.* The mesencephalic locomotor region recruits V2a reticulospinal neurons to drive forward locomotion in larval zebrafish. *Nature Neuroscience.* doi:10.1038/s41593-023-01418-0 (2023).
5. Sankrithi, N. & O'Malley, D. Activation of a multisensory, multifunctional nucleus in the zebrafish midbrain during diverse locomotor behaviors. *Neuroscience* **166,** 970–993. doi:10.1016/j.neuroscience.2010.01.003 (2010).
6. Huang, K.-H., Ahrens, M. B., Dunn, T. W. & Engert, F. Spinal Projection Neurons Control Turning Behaviors in Zebrafish. *Current Biology* **23,** 1566–1573. doi:10.1016/j.cub.2013.06.044 (2013).
7. Braun, J., Hurtak, F., Wang-Chen, S. & Ramdya, P. Descending networks transform command signals into population motor control. *Nature* **630,** 686–694. doi:10.1038/s41586-024-07523-9 (2024).
8. Engeszer, R. E., Patterson, L. B., Rao, A. A. & Parichy, D. M. Zebrafish in The Wild: A Review of Natural History And New Notes from The Field. *Zebrafish* **4,** 21–40. doi:10.1089/zeb.2006.9997 (2007).
9. Moorman, S. J. Development of Sensory Systems in Zebrafish (Donio rerio). *ILAR Journal* **42,** 292–298. doi:10.1093/ilar.42.4.292 (2001).
10. Thompson, A. W., Vanwalleghem, G. C., Heap, L. A. & Scott, E. K. Functional Profiles of Visual-, Auditory-, and Water Flow-Responsive Neurons in the Zebrafish Tectum. *Current Biology* **26,** 743–754. doi:10.1016/j.cub.2016.01.041 (2016).
11. Suriyampola, P. S., Lopez, M., Ellsworth, B. E. & Martins, E. P. Reversibility of Multimodal Shift: Zebrafish Shift to Olfactory Cues When the Visual Environment Changes. *Integrative and Comparative Biology* **60,** 33–42. doi:10.1093/icb/icaa036 (2020).
12. Suli, A., Watson, G. M., Rubel, E. W. & Raible, D. W. Rheotaxis in Larval Zebrafish Is Mediated by Lateral Line Mechanosensory Hair Cells. *PLoS ONE* **7** (ed Riley, B.) e29727. doi:10.1371/journal.pone.0029727 (2012).
13. Jacques, S. L. Optical properties of biological tissues: a review. *Physics in Medicine and Biology* **58,** R37–R61. doi:10.1088/0031-9155/58/11/R37 (2013).

14. Westerfield, M. *The Zebrafish Book; A guide for the laboratory use of zebrafish (Danio rerio)* (2007).

15. Lister, J. A., Robertson, C. P., Lepage, T., Johnson, S. L. & Raible, D. W. *nacre* encodes a zebrafish microphthalmia-related protein that regulates neural-crest-derived pigment cell fate. *Development* **126,** 3757–3767. doi:10.1242/dev.126.17.3757 (1999).

16. Aksay, E., Gamkrelidze, G., Seung, H. S., Baker, R. & Tank, D. W. In vivo intracellular recording and perturbation of persistent activity in a neural integrator. *Nature Neuroscience* **4,** 184–193. doi:10.1038/84023 (2001).

17. Miri, A. *et al.* Spatial gradients and multidimensional dynamics in a neural integrator circuit. *Nature Neuroscience* **14,** 1150–1159. doi:10.1038/nn.2888 (2011).

18. Ramirez, A. D. & Aksay, E. R. F. Ramp-to-threshold dynamics in a hindbrain population controls the timing of spontaneous saccades. *Nature Communications* **12,** 4145. doi:10.1038/s41467-021-24336-w (2021).

19. Bianco, I. H., Kampff, A. R. & Engert, F. Prey Capture Behavior Evoked by Simple Visual Stimuli in Larval Zebrafish. *Frontiers in Systems Neuroscience* **5.** doi:10.3389/fnsys.2011.00101 (2011).

20. Dowell, C. K., Lau, J. Y., Antinucci, P. & Bianco, I. H. Kinematically distinct saccades are used in a context-dependent manner by larval zebrafish. *Current Biology* **34,** 4382–4396.e5. doi:10.1016/j.cub.2024.08.008 (2024).

21. Dowell, C. K., Hawkins, T. & Bianco, I. H. Subsets of extraocular motoneurons produce kinematically distinct saccades during hunting and exploration. *Current Biology,* S0960982224016506. doi:10.1016/j.cub.2024.12.010 (2025).

22. Jouary, A. *et al. Megabouts: a flexible pipeline for zebrafish locomotion analysis* 2024. doi:10.1101/2024.09.14.613078.

23. Thorsen, D. H., Cassidy, J. J. & Hale, M. E. Swimming of larval zebrafish: fin–axis coordination and implications for function and neural control. *Journal of Experimental Biology* **207,** 4175–4183. doi:10.1242/jeb.01285 (2004).

24. Budick, S. A. & O'Malley, D. M. Locomotor Repertoire of The Larval Zebrafish: Swimming, Turning and Prey Capture. *Journal of Experimental Biology* **203,** 2565–2579. doi:10.1242/jeb.203.17.2565 (2000).

25. Green, M. H., Ho, R. K. & Hale, M. E. Movement and function of the pectoral fins of the larval zebrafish (Danio rerio) during slow swimming. *Journal of Experimental Biology* **214,** 3111–3123. doi:10.1242/jeb.057497 (2011).

26. Green, M. H. & Hale, M. E. Activity of pectoral fin motoneurons during two swimming gaits in the larval zebrafish (*Danio rerio*) and localization of upstream circuit elements. *Journal of Neurophysiology* **108,** 3393–3402. doi:10.1152/jn.00623.2012 (2012).

27. Satou, C. *et al.* Functional Diversity of Glycinergic Commissural Inhibitory Neurons in Larval Zebrafish. *Cell Reports* **30,** 3036–3050.e4. doi:10.1016/j.celrep.2020.02.015 (2020).

28. Uemura, Y. *et al.* Neuronal Circuits That Control Rhythmic Pectoral Fin Movements in Zebrafish. *The Journal of Neuroscience* **40,** 6678–6690. doi:10.1523/JNEUROSCI.1484-20.2020 (2020).

29. Ahrens, M. B., Huang, K. H., Narayan, S., Mensh, B. D. & Engert, F. Two-photon calcium imaging during fictive navigation in virtual environments. *Frontiers in Neural Circuits* **7.** doi:10.3389/fncir.2013.00104 (2013).

30. Ahrens, M. B., Orger, M. B., Robson, D. N., Li, J. M. & Keller, P. J. Whole-brain functional imaging at cellular resolution using light-sheet microscopy. *Nature Methods* **10,** 413–420. doi:10.1038/nmeth.2434 (2013).

31. Keller, P. J., Ahrens, M. B. & Freeman, J. Light-sheet imaging for systems neuroscience. *Nature Methods* **12,** 27–29. doi:10.1038/nmeth.3214 (2014).

32. Bouchard, M. B. *et al.* Swept confocally-aligned planar excitation (SCAPE) microscopy for high-speed volumetric imaging of behaving organisms. *Nature Photonics* **9,** 113–119. doi:10.1038/nphoton.2014.323 (2015).

33. Voleti, V. *et al.* Real-time volumetric microscopy of in vivo dynamics and large-scale samples with SCAPE 2.0. *Nature Methods* **16,** 1054–1062. doi:10.1038/s41592-019-0579-4 (2019).

34. Zhang, Z. *et al.* Imaging volumetric dynamics at high speed in mouse and zebrafish brain with confocal light field microscopy. *Nature Biotechnology* **39,** 74–83. doi:10.1038/s41587-020-0628-7 (2021).

35. Kim, D. H. *et al.* Pan-neuronal calcium imaging with cellular resolution in freely swimming zebrafish. *Nature Methods.* doi:10.1038/nmeth.4429 (2017).

36. Cong, L. *et al.* Rapid whole brain imaging of neural activity in freely behaving larval zebrafish. *eLife* **6,** 20 (2017).

37. Hiyoshi, K., Shiraishi, A., Fukuda, N. & Tsuda, S. In vivo wide-field voltage imaging in zebrafish with voltage-sensitive dye and genetically encoded voltage indicator. *Development, Growth & Differentiation* **63,** 417–428. doi:10.1111/dgd.12744 (2021).

38. Wang, Z. *et al. Imaging the voltage of neurons distributed across entire brains of larval zebrafish* 2023. doi:10.1101/2023.12.15.571964.

39. Böhm, U. L. *et al.* Voltage imaging identifies spinal circuits that modulate locomotor adaptation in zebrafish. *Neuron* **110,** 1211–1222.e4. doi:10.1016/j.neuron.2022.01.001 (2022).

40. Koning, H. K., Ahemaiti, A. & Boije, H. A deep-dive into fictive locomotion - a strategy to probe cellular activity during speed transitions in fictively swimming zebrafish larvae. *Biology Open* **11,** bio059167. doi:10.1242/bio.059167 (2022).

41. Schotland, J. *et al.* Control of lamprey locomotor neurons by colocalized monoamine transmitters. *Nature* **374,** 266–268. doi:10.1038/374266a0 (1995).

42. Clemens, S., Belin-Rauscent, A., Simmers, J. & Combes, D. Opposing modulatory effects of D1- and D2-like receptor activation on a spinal central pattern generator. *Journal of Neurophysiology* **107,** 2250–2259. doi:10.1152/jn.00366.2011 (2012).

43. Humphreys, J. M. & Whelan, P. J. Dopamine exerts activation-dependent modulation of spinal locomotor circuits in the neonatal mouse. *Journal of Neurophysiology* **108,** 3370–3381. doi:10.1152/jn.00482.2012 (2012).

44. Jay, M., De Faveri, F. & McDearmid, J. R. Firing Dynamics and Modulatory Actions of Supraspinal Dopaminergic Neurons during Zebrafish Locomotor Behavior. *Current Biology* **25,** 435–444. doi:10.1016/j.cub.2014.12.033 (2015).

45. Picton, L. D. & Sillar, K. T. Mechanisms underlying the endogenous dopaminergic inhibition of spinal locomotor circuit function in Xenopus tadpoles. *Scientific Reports* **6,** 35749. doi:10.1038/srep35749 (2016).

46. Jha, U. & Thirumalai, V. Neuromodulatory Selection of Motor Neuron Recruitment Patterns in a Visuomotor Behavior Increases Speed. *Current Biology* **30,** 788–801.e3. doi:10.1016/j.cub.2019.12.064 (2020).

47. Marques, J. C., Li, M., Schaak, D., Robson, D. N. & Li, J. M. Internal state dynamics shape brainwide activity and foraging behaviour. *Nature* **577,** 239–243. doi:10.1038/s41586-019-1858-z (2020).

48. Corradi, L. & Filosa, A. Neuromodulation and Behavioral Flexibility in Larval Zebrafish: From Neurotransmitters to Circuits. *Frontiers in Molecular Neuroscience* **14,** 718951. doi:10.3389/fnmol.2021.718951 (2021).

49. Sirota, M. G., Di Prisco, G. V. & Dubuc, R. Stimulation of the mesencephalic locomotor region elicits controlled swimming in semi-intact lampreys: Brainstem-induced swimming. *European Journal of Neuroscience* **12,** 4081–4092. doi:10.1046/j.1460-9568.2000.00301.x (2000).

50. Gahtan, E. Visual Prey Capture in Larval Zebrafish Is Controlled by Identified Reticulospinal Neurons Downstream of the Tectum. *Journal of Neuroscience* **25,** 9294–9303. doi:10.1523/JNEUROSCI.2678-05.2005 (2005).

51. Sugioka, T., Tanimoto, M. & Higashijima, S.-i. Biomechanics and neural circuits for vestibular-induced fine postural control in larval zebrafish. *Nature Communications* **14,** 1217. doi:10.1038/s41467-023-36682-y (2023).

52. Hildebrand, D. G. C. *et al.* Whole-brain serial-section electron microscopy in larval zebrafish. *Nature* **545,** 345–349. doi:10.1038/nature22356 (2017).

53. Svara, F. *et al.* Automated synapse-level reconstruction of neural circuits in the larval zebrafish brain. *Nature Methods* **19,** 1357–1366. doi:10.1038/s41592-022-01621-0 (2022).

54. Vishwanathan, A. *et al.* Electron Microscopic Reconstruction of Functionally Identified Cells in a Neural Integrator. *Current Biology* **27,** 2137–2147.e3. doi:10.1016/j.cub.2017.06.028 (2017).

55. Zung, J., Tartavull, I., Lee, K. & Seung, H. S. *An Error Detection and Correction Framework for Connectomics* Version Number: 2. 2017. doi:10.48550/ARXIV.1708.02599.

56. Januszewski, M. *et al.* High-precision automated reconstruction of neurons with flood-filling networks. *Nature Methods* **15,** 605–610. doi:10.1038/s41592-018-0049-4 (2018).

57. Vishwanathan, A. *et al.* Predicting modular functions and neural coding of behavior from a synaptic wiring diagram. *Nature Neuroscience* **27,** 2443–2454. doi:10.1038/s41593-024-01784-3 (2024).

Apoio financeiro da FCT e do FSE no âmbito do Quadro Comunitário de Apoio, Bolsa nº SFRH/BD/147089/2019.

ITQB NOVA, Avenida da República, 2780-157 Oeiras, Portugal | Tel +351 214 469 100 | itqb.unl.pt